Investigating the Mechanism of Action of Sanglifehrin A

Professor Gregory L. Verdine Khian Hong Pua

Investigating the Mechanism of Action of Sanglifehrin A

Abstract

Macrocyclic natural products occupy a special niche in the small molecule chemical space. Compared with other classes of small molecules, their larger size and conformational flexibility confer a higher propensity to recognize relatively flat surfaces that are predominant in protein-protein interactions. They are also thought to be the smallest examples of biomolecules that display functional sub-domains. Examples in this class of compounds are the immunosuppressants cyclosporine A (CSA), FK506, rapamycin (RAP) and sanglifehrin A (SFA) – the subject of this dissertation.

Aside from their therapeutic use in the clinic, immunosuppressants CSA, FK506, and RAP have also been proven to be indispensable tools for interrogating signal transduction pathways at the molecular level. These natural products have significantly contributed to our understanding of T cell signal transduction pathways and the molecular events involved in T cell activation. SFA is another immunosuppressive macrocyclic natural product that is structurally distinct from CSA but which, like CSA, binds to an abundant intracellular protein, cyclophilin A (PPIA) with high affinity. Unlike CSA, neither RAP nor SFA affect calcium-dependent IL-2 production. However, distinct from RAP, SFA does not inhibit mTOR. The molecular target of SFA and the cellular events resulting from its effect are still poorly understood. This dissertation describes

efforts to identify the molecular target of SFA and tease apart its mode of action by enlisting a variety of target identification and validation approaches. Our results suggest that SFA has a mechanism of action unlike the other immunosuppressive ligands of this class. Its use as a small molecule probe has led to the discovery of a target protein implicated in cellular proliferation.

Table of Contents

Acknowledgements

This PhD has been an incredible journey – both personally and professionally – and I am deeply indebted to many people who have supported me during this transformative phase of life. First and foremost, I would like to thank my advisor, Professor Gregory Verdine for his advice, encouragement and generosity with his time and many resources. His unfettering passion and no holds barred attitude towards science, and life in general, will continue to inspire me as I move forward to my next challenge in life. I am most grateful for the opportunity to be inducted into the vibrant and thriving biotech scene in Cambridge during my time at Warp Drive Bio. My graduate school experience has been profoundly enriched as a result of this rare privilege.

I wish to thank my committee members, Professor Stuart Schreiber and Professor George Church, for their consistent support and constructive feedback during the course of my graduate work. I am especially grateful for Stuart, for our meetings outside of the GAC where he provided his sage advice and sharp insight into my project. The Harvard community has been enormously helpful for many experiments would not have been possible without their welcoming assistance.

Both the Verdine lab and Warp Drive Bio have been a tremendous source of knowledge and fun. I thank the Verdine lab members, past and present, for their unreserved willingness to offer help and advice to just about anyone who needed them. Dylan Stiles, a former post-doc who took me under his wing when I joined as a rotation student, has been a wonderful mentor and collaborator to this day. The many advances made in this thesis would not have been possible without him. Jerry Hilinski, who taught me to make my first stapled peptide, has been the one of the key pillars that kept the lab

running efficiently. He is also a friend who has showed genuine concern for me during my time in the lab. The other key pillar is our lab administrator, Lydia Carmosino, who has been a phenomenal resource and help over the past five years. I am also grateful for the friendship and collaboration with Erin May on other projects, which provided a mental respite from the frustrations I felt about my thesis work. I also thank Rahul, John, Minyun, Qian and Matt Lee for helpful research discussions. Many thanks to Jerry, Dylan, Lan, Minyun, Erin and Pam Wang for providing feedback and editing my thesis.

I also wish to thank everyone at Warp Drive Bio, past and present, for their kindness and help they have rendered along the way and most importantly, for treating me like a part of the Warp family. I thank Susan Yost and Zoe Bordenet for administrative support. Mychael Nguyen deserves special mention for always going the extra mile to help me especially during the time when my daughter was born. I thank Mat Sowa for collaborating with me on my project. I would also like to thank Jay, Chi, Linlong, Sharon, Melanie, Jean, Dan, Keith, Polina, Ping, for being great teachers and encouraging me along the way when the going got tough. I will miss the folks from the WDB “running club” – Dennis *et al.* Our 2-mile run with Greg was probably the most memorable. The friendships forged during my tenure in the lab and at Warp, I believe, will continue to make a lasting impact on my life.

This journey would have been extremely mundane and grim, if not for the many friends who have made this a lot more interesting. I would like to thank all my batch mates, friends from Highrock, HBDT and HGBC. I also thank Amit Choudhary, my undergrad mentor, for his help and advice till this day. My buddies back in Singapore have always been a constant source of support and encouragement.

Last but not least, I would like to thank my family – my parents, in-laws, brother and sisters – for their unconditional love and support all these years and for their faith in me. I owe a large part of my success to my wife Chen Li – her enduring patience, super-human understanding, sacrificial love, and unhurried attitude towards life has helped me put many things in life into perspective. I am most blessed to be able to share this experience and my life with her. My daughter, Hannah, has brought to my life joy beyond words can describe. I look forward to the reunion of our entire family in Singapore.

List of Abbreviations

adRP10	autosomal dominant retinitis pigmentosa type 10
AMP	adenosine monophosphate
AMPK	adenosine monophosphate-activated protein kinase
ATP	adenosine triphosphate
BME	β-mercaptoethanol
CBS	cystathionine beta synthase
cDNA	complementary DNA
CETSA	cellular thermal shift assay
CLC	chloride channel
CRISPR	clustered regularly interspaced short palindromic repeats
crRNA	CRISPR RNA
CSA	cyclosporine A
CyPs	cyclophilins
DAPI	4’,6-diamidino-2-phenylindole
DC	dendritic cell
DMEM	dulbecco’s modified eagle's medium
DMSO	dimethyl sulfoxide
DNA	deoxyribonucleic acid
EC_{50}	half maximal effective concentration
EMSA	electrophoretic mobility shift assay
ETDA	ethylenediaminetetraacetic acid
FACS	fluorescence-activated cell sorting
FBS	fetal bovine serum
FDA	food and drug administration
FKBP	FK506 binding protein
FPLC	fast protein liquid chromatography
GADD	growth arrest and DNA damage
GMP	guanosine monophosphate
GOI	gene of interest
GST	glutathione S-transferase
GTP	guanosine triphosphate
HDR	homology directed repair
HILIC	hydrophilic interaction chromatography
HPRT	hypoxanthine-guanine phosphoribosyltransferase
IB	immunoblotting
IC_{50}	half maximal inhibitory concentration
IMPDH	inosine monophosphate dehydrogenase
IP-MS	immunoprecipitation-mass spectrometry
IPTG	isopropyl β-D-1-thiogalactopyranoside
K_d	dissociation constant
LB	luria broth
LC-MS	liquid chromatography–mass spectrometry
MALDI-TOF	matrix-assisted laser desorption/ionization - time of flight

MEF	mouse embryonic fibroblasts
MPA	mycophenolic acid
mTOR	mammalian target of rapamycin
MWCO	molecular weight cut off
NAD	nicotinamide adenine dinucleotide
NFκB	nuclear factor kappa-light-chain-enhancer of activated B cells
NHEJ	non homologous end joining
NTA	nitrilotriacetic acid
OD	optical density
PAGE	polyacrylamide gel electrophoresis
PAM	proto adjacent motif
PBS	phosphate buffered saline
PDB	protein data bank
PFA	paraformaldehye
PLK1	polo-like kinase 1
PMSF	phenylmethylsulfonyl fluoride
PPIA	cyclophilin A
PPIase	peptidyl prolyl isomerase
PRPP	phosphoribosyl pyrophosphate
RAP	rapamycin
RISC	RNA-induced silencing complex
RNA	ribonucleic acid
RNAi	RNA interference
RT-QPCR	reverse transcription quantitative polymerase chain reaction
SAM	*S*-adenosyl methionine
SAR	structure-activity relationship
SDS	sodium dodecyl sulfate
SEC	size exclusion chromatography
SFA	sanglifehrin A
SFM	macrolide fragment of sanglifehrin A
SPR	surface plasmon resonance
TALENs	transcription activator-like effector nucleases
TAP	tandem affinity purification
TBE	tris borate EDTA
TBS	tris buffered saline
TCA	trichloroacetic acid
TCR	T-cell receptor
TEV	tobacco etch virus
TMT	tandem mass tag
TNF	tumor necrosis factor
TRIS	tris(hydroxymethyl)aminomethane
UV	ultraviolet
WT	wild-type
XMP	xanthine monophosphate
ZFNs	zinc finger nucleases

List of Figures

CHAPTER 3

CHAPTER 4

CHAPTER 5

List of Tables

CHAPTER 1

NATURAL PRODUCT MACROCYCLES AND SANGLIFEHRIN A

1.1 Natural Products – from Therapeutic Agents to Chemical Probes

Natural products are chemical substances derived from microbes, plants and animals, and they have historically been a rich and important source of therapeutic agents[1–3]. Apart from their remarkable chemical diversity, natural products are more likely than synthetic chemical libraries to have bioactivity and biochemical specificity[1]. Furthermore, they often have favorable molecular and physical properties, making them ideal drug candidates[4]. Approximately 35% of new medicines approved between 1981 and 2010 by the US Food and Drug Administration (FDA) were natural products or analogs of natural products[5,6]. While natural products have traditionally been used as anti-infective drugs, they have also found applications in a variety of therapeutic indications such as cancer, immunosuppression, cardiovascular and metabolic diseases[2,7]. Drug developers have also turned to natural products for inspiration as they provide versatile scaffolds for the development of new lead structures and drugs.

Numerous studies have been done to analyze natural products and understand the rules that dictate their desirable features as drug leads. Most notably, leads from natural sources have more complex structures with abundant stereogenic centers and greater steric complexity compared to *de novo* designed drugs or combinatorial libraries[8–10]. Natural products also contain relatively more carbon, oxygen and hydrogen, and fewer nitrogen, sulfur and other elements than their synthetic counterparts[8,10]. In addition, they have lower aromatic ring atoms to heavy atoms ratio, more solvated hydrogen-bond donors and acceptors and exhibit diverse ring systems not readily observed in synthetic libraries[1]. Finally, natural products often violate Lipinski-type descriptors – for example, high molecular weights greater than 500 daltons – while retaining desirable drug-like properties[8,11]. Given the above attributes, natural products are poised to modulate difficult screening targets, such as protein-protein interactions[12].

However, despite their impressive properties and track record as drugs, natural product research has experienced a gradual decline over the past two decades, particularly in the pharmaceutical industry, in part due to the current emphasis on high throughput screening (HTS) against selected molecular targets with “screen friendly” synthetic chemical libraries[1,3].

Aside from its therapeutic value, natural products also make good tools for interrogating biological systems[13]. Given their innate ability to modulate biomolecules, particularly proteins, often with high affinity and specificity, natural products have proven to be valuable tools as chemical probes in today’s scientific research. Mechanism of action studies of natural products have often led to powerful biological insights via the identification of key biochemical pathways and networks that would otherwise be difficult

to study using traditional genetic techniques. A classic example is the use of trapoxin, a potent cyclotetrapeptide cell cycle inhibitor as a natural product-based chemical probe to draw the connection between histone deacetylase (HDAC) inhibition, transcriptional regulation and cell cycle inhibition[14]. Consequently, this discovery led to the development of HDAC inhibitors as anti-cancer drugs[13]. The use of cyclosporin A (CSA), FK506 and rapamycin (RAP) as natural product-based chemical probes have also brought to light the pathways involved in T-cell signal transduction[15,16] (further discussed in Chapter 1.3).

1.2 Macrocyclic Natural Products

Macrocyclic natural products occupy a special niche in the small molecule chemical space. They embody the desirable characteristics aforementioned of natural products and do so in a conformationally pre-organized ring structure. This pre-organization is entropically favorable for binding to their molecular targets[17]. Compared with other classes of small molecules, macrocycles have a larger propensity to modulate relatively flat surfaces that are predominant in protein-protein interactions because of their larger size and conformational flexibility[18]. Accumulating evidence suggests that despite frequently violating Lipinski 'rule of 5', macrocycles can show drug-like characteristics, such as good solubility, lipophilicity and bioavailability and have proven to be useful in the clinic[11,17]. In fact, macrocyclic natural products are thought to be the smallest examples of biomolecules that display functional sub-domains[17].

Current macrocyclic drugs and their derivatives are almost exclusively derived from natural sources[17]. The antibiotics vancomycin and erythromycin, antifungals amphotericin B and caspofungin, antituberculosis drug rifampin as well as immunosuppressants, cyclosporin A, FK506 and rapamycin are among the many macrocyclic natural products widely used in the clinic[17]. More importantly, macrocyclic natural products have a reputation for high affinity interactions with challenging targets (notorious for their flat surfaces) that have been known to be intractable with small molecules[17,18]. For example, unlike the non-macrocyclic protein synthesis inhibitor chloramphenicol which inhibits the peptidyl transferase activity of prokaryotic ribosomes, erythromycin, also a protein synthesis inhibitor, binds to the inner surface of the ribosomal tunnel to constrict it, thereby physically blocking the exit for newly synthesized peptides from the ribosome[17,19]. Another unique feature of macrocyclic drugs is that they possess spatially organized functional domains which allow them to either self-assemble or mediate assembly of other macromolecules[17]. This is exemplified by a family of immunophilin ligands which behave like “molecular glues” that help mediate the interaction between two proteins which do not normally interact[15].

1.3 Immunophilins and their Ligands, CSA, FK506 and RAP

1.3.1 The Immunophilins – Cyclophilins and FK506 Binding Proteins

Cyclophilins (CyPs) and FK506 binding proteins (FKBPs) are two families of ubiquitous proteins that are evolutionary well conserved from prokaryotes to eukaryotes[21,27]. Collectively, they are known as immunophilins, given their ability to bind

to macrocyclic immunosuppressive drugs cyclosporin A (CSA), FK506 and rapamycin (RAP) (Figure 1.1).

Figure 1.1

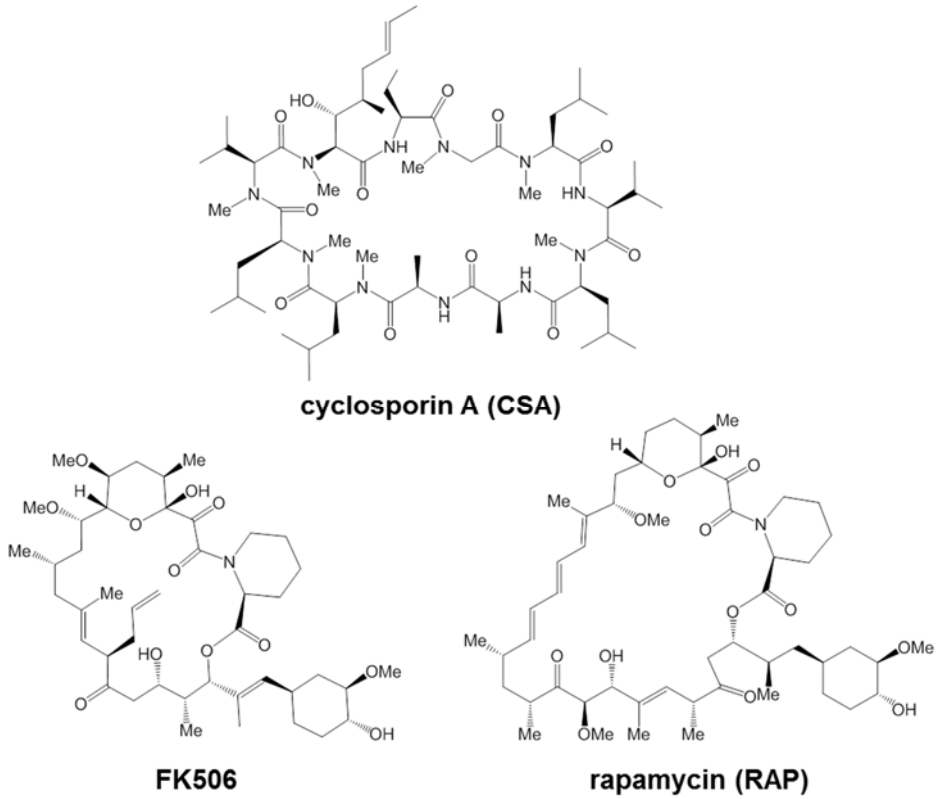

Figure 1.1 – The Structures of Immunophilin Binding Ligands Cyclosporin A, FK506 and Rapamycin. CSA, FK506 and RAP are not only clinically valuable as immunosuppressants, but also as probe reagents for dissecting T lymphocytes signal transduction pathways. FK506 and RAP exhibit structural similarity, and both bind abundant intracellular protein FKBP12 to inhibit the action of calcineurin and mTOR respectively. CSA binds another ubiquitous intracellular protein, PPIA, and also inhibits calcineurin, a phosphatase involved in early T-cell activation signaling.

Although structurally distinct, both families of proteins possess peptidyl-prolyl isomerase (PPIase) activity, which catalyzes the isomerization of peptide bonds from *trans* to *cis* at proline residues[20,21] (Figure 1.2A).

Figure 1.2

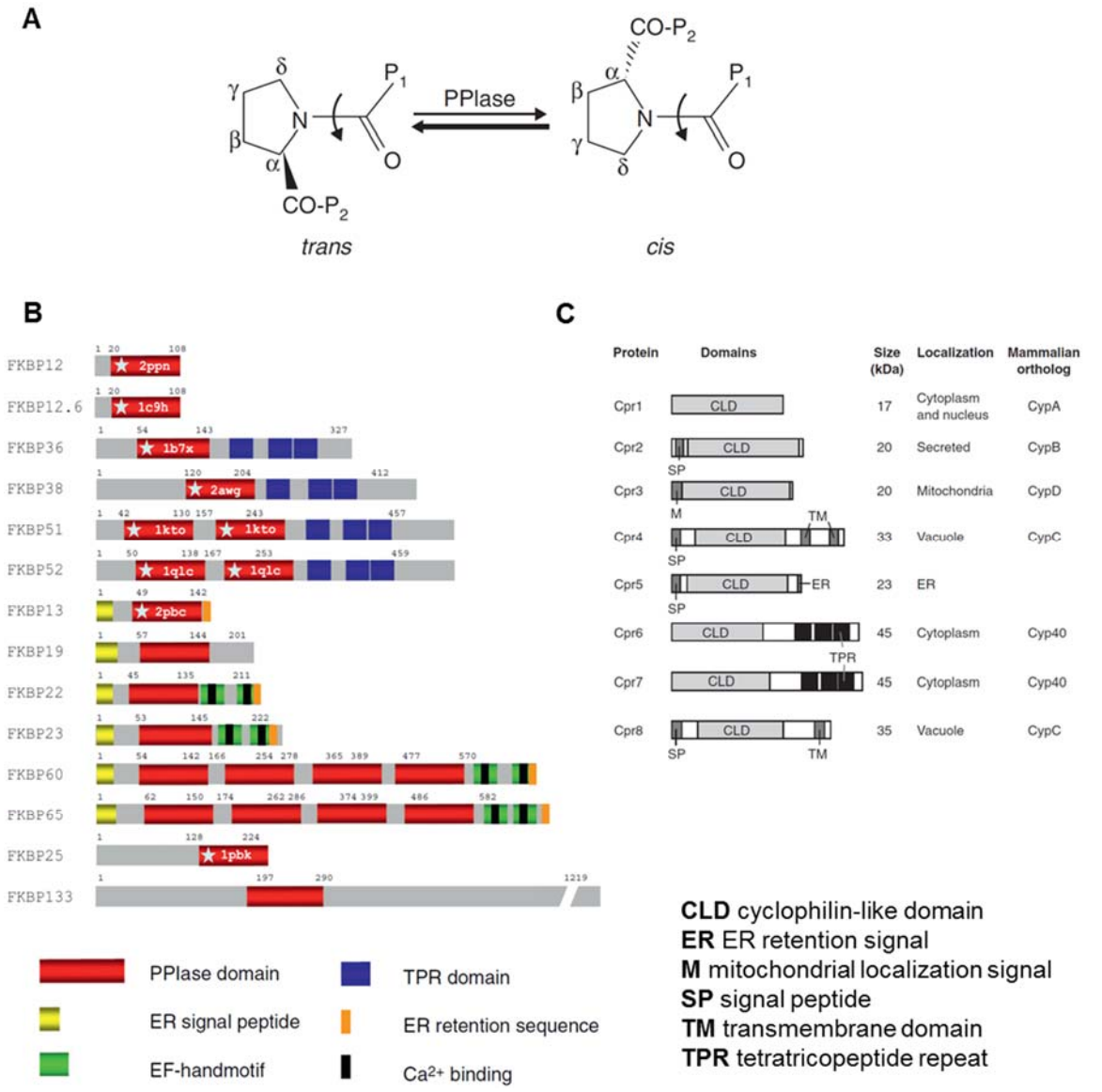

Figure 1.2 – The Structures of Immunophilins Cyclophilins and FKBPs. (A) The reaction catalyzed by peptidyl prolyl isomerases (CyPs and FKBPs). The illustration shows the interconversion between the trans and cis forms of a peptide bond. P1 and P2 are residues flanking proline in the peptide. Figure from Reference 27. (B) The domain structure of human FKBPs. All isoforms contain at least one PPIase domain (red). PDB accession code of a representative structure is indicated by a blue star preceding the PDB code. Figure from Reference 21. (C) The domain structure of *S. cerevisiae* cyclophilins with their protein size, localizations and mammalian orthologs. Figure from Reference 27.

These proteins are highly expressed in most tissues and are known to have regulatory and chaperone function[20–22]. In humans, there are about 17 naturally occurring isoforms of CyPs and 14 for FKBPs, all of which have at least one PPIase domain[21,23] (Figure 1.2B and C). Cyclophilins and FKBPs can be found in various subcellular compartments including the cytosol, mitochondria, nucleus and endoplasmic reticulum (ER)[21,24].

Interest in immunophilins in the late 1980s was fueled by the discovery that these proteins can bind to CSA, FK506 and RAP to suppress the immune system of patients that had organ transplantation[22,25]. These macrocyclic compounds bind to the active site of immunophilins and inhibit their PPIase activity[26].

Figure 1.3

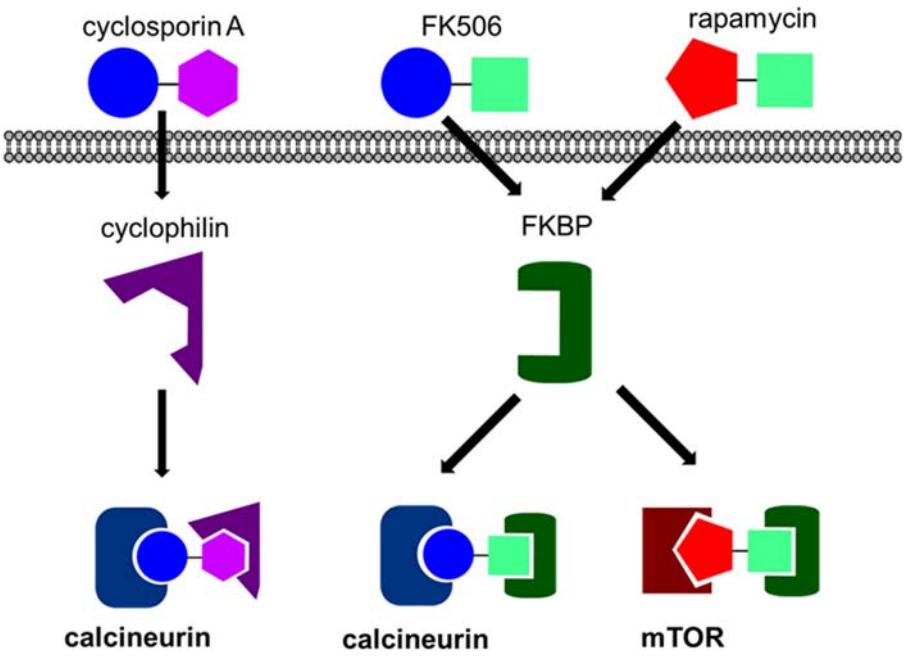

Figure 1.3 – Mode of action of CSA, FK506 and RAP. Cartoon illustration showing the mechanism of action of immunosuppressive drugs CSA, FK506 and RAP. Upon cellular penetration, these molecules engage ubiquitously expressed immunophilin proteins, cyclophilins and FKBPs to form a binary complex. The cyclophilin-CSA and FKBP-FK506 binary complexes both inhibit the same intracellular target, calcineurin, while the FKBP-RAP inhibits the action of a protein serine/threonine kinase mTOR.

Superficially, these molecules act in a similar fashion. They first bind to an immunophilin molecule to form a drug-isomerase complex. The drug-isomerase complex, which is the biologically active species, then binds to an intracellular target, giving rise to the effect of the drug[16,26] (Figure 1.3). This subject is discussed further in Chapter 1.3.4.

1.3.2 Cyclophilin A

Cyclophilin A (PPIA), the founding member of the family of CyPs, is the most abundantly expressed isoform and makes up approximately 0.5% of total cytosolic proteins[20,27]. It was identified as the primary intracellular binding protein of the immunosuppressant CSA[28]. PPIA can also be secreted from cells when subjected to inflammatory insults[29]. Both intracellular and extracellular PPIA are involved in a wide variety of cellular functions including but not limited to protein folding and trafficking, differentiation, immune response and viral infection[20,24]. More importantly, the deregulation of PPIA has been implicated in a myriad of human pathologies, such as vascular diseases, neurodegenerative disease as well as cancer[20,24].

Ppia knockout models in mice corroborated findings in prokaryotes and lower eukaryotes that PPIA (and its PPIA homologs) is not necessary for cell growth and survival[30–33]. Further, loss of *Ppia* reduced the susceptibility of ApoE deficient mice to aortic aneurysm and atherosclerosis[34,35]. Overexpression of PPIA has also been reported in diverse cancer types and is associated with poor prognosis for patients with inflammatory diseases[20,24]. Additionally, studies have demonstrated that PPIA plays a central role in HIV and HCV infectivity and replication[36–39]. For the above reasons, PPIA

represents an attractive therapeutic target in anti-cancer, anti-inflammatory and anti-viral intervention.

1.3.3 The Origins of CSA, FK506 and RAP

Cyclosporin A (CSA), FK506 and rapamycin (RAP) are microbial secondary metabolites with remarkable immunosuppressive properties that stems from selective inhibition of T-lymphocyte activation[25].

CSA, a cyclic decapeptide originally isolated from a soil fungi *Tolypocladium inflatum* in a screen for novel antibiotics, exhibits potent immunosuppressive activity *in vivo*[40,41]. Since its introduction in 1983 for the treatment of kidney transplant rejection, CSA has revolutionized the field of organ transplantation in humans[25]. The use of CSA has dramatically increased one-year graft survival to 97% in patients receiving cadaver kidneys, up from the 50% prior to CSA use[42,43]. CSA also has clinical indications in the treatment of many autoimmune diseases such as psoriasis and Behcet's disease[25]. Since then, the search for new immunosuppressants that prevent T-cell activation and proliferation has resulted in the isolation of more potent immunosuppressive natural products such as FK506 and rapamycin.

FK506 was first isolated from *Streptomyces tsukubaensis*, and demonstrated similar activity to CSA in a variety of transplantation and autoimmunity models[25]. RAP, an antifungal agent isolated from soil microbe *Streptomyces hygroscopicus* was originally described as an antibiotic[44,45]. Its use as an immunosuppressant came only after the discovery of FK506 because of the striking structural similarity between these two compounds[25] (Figure 1.1). In addition to their therapeutic value, these macrocyclic

natural products were critical probe reagents which transformed our understanding of T lymphocyte biology and were primarily responsible for the identification of calcineurin and mTOR as intermediary proteins involved in T-cell signaling[46,47].

1.3.4 The Mechanisms of Action of CSA, FK506 and RAP

The discovery that CSA binds to intracellular receptor cyclophilin A (PPIA) provided the first mechanistic insight into the immunosuppressive effects of CSA [28]. The finding that PPIA possesses isomerase activity and that CSA effectively inhibited its isomerase function logically led to the hypothesis that CSA was mediating its effects via the inhibitory action on PPIA's isomerase activity[48–50]. Further support for this model came after the discovery that other immunosuppressive agents, FK506 and rapamycin, potently inhibited FKBP, another prolyl isomerase[51,52]. Taken together, these evidence strongly suggested that the isomerase activities of FKBP and/or PPIA were essential for T cell activation.

However, several lines of evidence emerged, disproving the hypothesis of a causative link between rotamase inhibition and immunosuppression. Genetic studies in lower eukaryotes, *N. crassa* and *S. cerevisiae*, revealed that PPIA is a non-essential gene and that the cytotoxic effect of CSA is mediated by PPIA[31]. Similarly, FKBP, while not necessary for yeast survival, is required for FK506 and rapamycin-induced cytotoxicity, implying that the inhibition of immunophilins *per se* does not lead to cytotoxic effects in yeast[53,54]. Furthermore, there were analogs of CSA and FK506 that exhibited potent isomerase inhibition but were non-immunosuppressive[55].

Two plausible models were put forth to explain the apparent inconsistencies in these findings. The first model proposed some unidentified immunophilin isoform

mediating the biological effects of CSA and FK506[55]. The second model, which in retrospect was the correct model, suggested that immunophilin engagement by CSA, FK506 and rapamycin is necessary but not sufficient for their effects, and that an immunophilin-ligand complex is the active inhibitor of some unknown cellular target critical for the compounds' observed phenotype[15,16].

Both the PPIA-CSA and FKBP12-FK506 drug complexes can bind to calcineurin and inhibits its phosphatase activity, which is essential for the transcription of early T cell activation genes such as interleukin-2 (IL-2)[46,56,57]. Calcineurin plays a pivotal role in T-cell receptor (TCR) induced activation by removing several phosphate residues from N terminus of NF-ATc (cytoplasmic nuclear factor of activated T cells) proteins, resulting in the exposure of nuclear localization sequences, facilitating the translocation of the transcription factor NF-AT into the nucleus[58]. Both CSA and FK506 inhibit early T-cell receptor (TCR) induced gene activation, resulting in cell cycle blockade at the G0 to G1 phase[59]. RAP, on the other hand, blocks the G1-S phase of cell cycle progression by inhibiting IL-2 stimulated cellular proliferation[60]. The FKBP12-RAP complex inhibits mTOR, a serine/threonine protein kinase that belongs to the phosphoinosidtide 3-kinase (PI3K-related kinase family), preventing the activation of S6K1 (a substrate of mTOR) [47,61–63]. The unusual mechanism by which these natural products operate inspired the search for novel immunophilin ligands that can induce a gain of function in immunophilins. This search led to a fourth immunophilin-binding member, sanglifehrin A, which also exhibits potent immunosuppressive activity[64,65].

1.4 Sanglifehrin A (SFA) – A Novel Cyclophilin-binding Macrocycle

1.4.1 The Structure of SFA

The natural product Sanglifehrin A (SFA) was first discovered by researchers from Novartis in 1997 from screening microbial broth extracts for novel PPIA binding ligands (Figure 1.4). It was originally isolated from *Streptomyces* sp. A92-308110 [64,65]. Four sanglifehrin family members were isolated (Sanglifehrin A, B, C and D) but only sanglifehrins A and B are considered to be true natural products. Sanglifehrins C and D, acetalized cyclic versions of sanglifehrins A and B respectively, were reportedly side products formed during the isolation process[65]. Though the family of sanglifehrins exhibit remarkable affinities for cyclophilin, they are structurally distinct from cyclosporins.

Figure 1.4

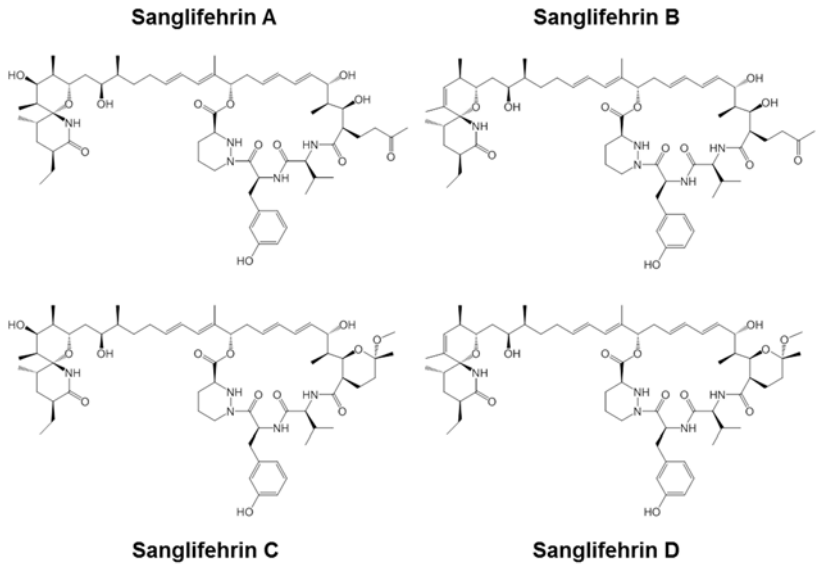

Figure 1.4 – The Structures of the Four Sanglifehrin Family Members. SFA has a unique chemical structure that consists of a 22-membered macrocycle, a linear nine-carbon tether and a highly substituted spirobicyclic moiety. The macrocycle portion contains an *E, E*-diene, a short polypropionate fragment, and a tripeptide unit composed of valine and two uncommon amino acids, meta-tyrosine and piperazic acid.

SFA has a unique chemical structure that consists of a 22-membered macrocycle, bearing in position 23 a linear nine-carbon tether terminated by a highly substituted spirobicyclic moiety (Figure 1.4). The macrocycle portion contains an *E, E*-diene, a short polypropionate fragment, and a tripeptide unit composed of valine and two unusual amino acids, meta-tyrosine and piperazic acid[65]. In contrast to other isolated piperazic acid containing natural products that use the α-nitrogen on piperazic acid for amide bond formation, SFA exclusively utilizes the β-nitrogen for amide bond linkage[66].

Because of its architectural complexity and potential therapeutic value, SFA has garnered intense synthetic interest. Nicolaou and colleagues reported the first effective and highly stereoselective total synthetic route for SFA[67]. Subsequently, several other groups reported alternative synthetic strategies for the natural product and its derivatives[68–71]. The ~100 kilo base pairs biosynthetic gene cluster leading to SFA biosynthesis has recently been sequenced and characterized[72]. This cluster consists of a mixed polyketide synthase (PKS) and non-ribosomal peptide synthetase (NRPS) pathway which utilizes (2R)-2-ethylmalonamyl-CoA as an atypical PKS starter unit[72]. Given the wealth of knowledge surrounding its synthesis – both chemically and biologically – the structure of SFA continues to inspire new SFA-like scaffolds as biological probes and therapeutic compounds.

1.4.2 The Biology of SFA

In addition to its unprecedented structural features, SFA also shows diverse and interesting biological profiles. Like other immunophilin binding ligands, SFA shows activity in MLR but the biochemical and molecular mechanisms accounting for its

immunosuppressive effect is still unclear[64]. While it is similar to CSA in that it binds cyclophilins and inhibits its isomerase activity, SFA has no effect on the calcium dependent protein phosphatase calcineurin, the biological target of CSA, suggesting a different mode of action for SFA[64]. Despite SFA's higher affinity for PPIA, its cell-permeability, as assessed by an *in cellulo* binding assay, is less than that of CSA[73]. Thus, SFA's reduced potency in MLR assay in comparison to CSA, could in part be explained by its lower cell permeability arising from the presence of multiple hydrophilic functionalities on the molecule[73].

While CSA potently suppresses IL-2 transcription and IL-2 dependent T-cell proliferation, SFA does not. Instead, SFA inhibits the proliferation of IL-2 stimulated murine and human T-cells, suggesting that SFA inhibits T-cell proliferation at a later stage after T cell activation[73,74]. In this respect, SFA behaves like RAP. Both SFA and RAP do not affect calcium-dependent IL-2 production and blocks cell cycle progression of cells at G1-S transition[73–75]. However, unlike RAP, SFA had no effect on $p70^{S6K}$ phosphorylation or its kinase activity. Taken together, results from these early studies strongly suggest that SFA has a novel, distinct mechanism of action unlike those of CSA, RAP and FK506. In addition, several groups have reported that SFA inhibits human and murine dendritic cells (DCs). Further, unlike CSA, SFA blocks bioactive IL-12 and IL-18 production and suppresses antigen uptake in DCs[76–78]. More recently, Immecke *et al.* identified SFA as a DC chemokine and migration inhibitor[79].

1.4.3 Structure Activity Relationship Studies with SFA

It is tempting to speculate that SFA acts via a mechanism similar to other known immunophilin binding immunosuppressants, CSA, FK506 and RAP. However, it remains controversial whether the biological effect of SFA is mediated by PPIA.

Several lines of evidence suggest that SFA could have a mechanism of action analogous to other immunosuppressive drugs. Elimination of the hydroxyl group on meta-tyrosine of SFA results in a substantial loss in its affinity for PPIA and immunosuppressive activity[70]. Removal of the spirolactam moiety of SFA afforded a macrocyclic fragment of SFA that retains binding to PPIA but lost immunosuppressivity, suggesting that the spirolactam moiety is essential for its bioactivity[71]. The spirolactam fragment itself also has no biological effect[71]. The crystal structure of the PPIA-SFA complex was determined at 1.6Å resolution in 2005[80]. The structure revealed that the macrocyclic portion of SFA forms hydrogen bonds with four residues on PPIA, three of which also forms contact with CSA (Figure 1.5A)[80]. The spirolactam moiety, however is free of protein contacts. The crystal structure also revealed how SFA, through its unique chemical structure, was able to promote dimerization of PPIA-SFA (Figure 1.5B)[80]. This raises the possibility that the immunosuppressive effects of SFA could be mediated by a dimer of PPIA-SFA[80].

In favor of a PPIA-independent mechanism of action for SFA, several groups have reported that that CSA and non-immunosuppressive CSA analogues failed to diminish the activity of SFA in cells[73,76,79]. However, whether PPIA is causally involved in SFA's mode of action remains to be discerned.

Figure 1.5

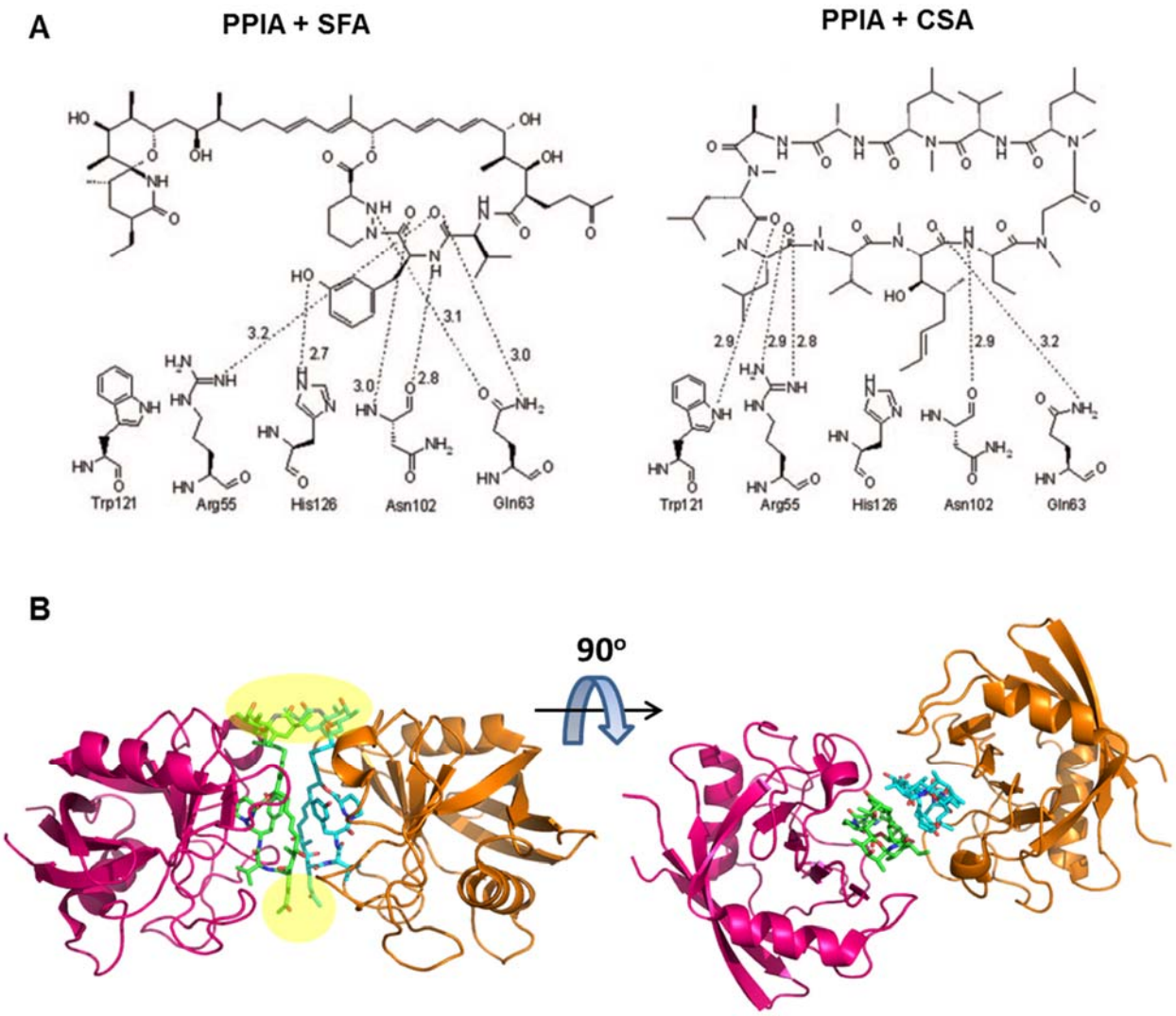

Figure 1.5 – Structure of Human Cyclophilin A in Complex with SFA. (A) A detailed view of the interactions between SFA and CSA shows SFA contacts PPIA with 6 hydrogen bonds on one face of the macrocycle. Although structurally distinct, SFA and CSA both co-opt R55, Q63 and H126 on PPIA for binding. Figure from Reference 80. (B) The structure of the dimer of PPIA-SFA complex reveals that the spirobicycle and 3-oxo-butyl side chain of SFA make limited contact with PPIA (yellow circles); (PDB 11YND).

1.5 Inosine Monophosphate Dehydrogenase (IMPDH)

1.5.1 The Biology of IMPDH

Inosine monophosphate dehydrogenase (IMPDH) catalyzes the rate limiting step in the *de novo* pathway for the synthesis of guanine nucleotides, by converting inosine monophosphate (IMP) to xanthine monophosphate (XMP) in a NAD-dependent oxidation (Figure 1.6). XMP is subsequently aminated to guanosine monophosphate (GMP), a precursor to guanosine triphosphate (GTP), by GMP synthase. Rapidly proliferating cells depend heavily on *de novo* nucleotide biosynthesis to provide the building blocks and energy requirements for cellular processes, including but not limited to DNA, RNA and protein synthesis[81]. Nucleotides can also be produced from salvage pathways. The salvage of guanine to GMP by hypoxanthine-guanine phosphoribosyltransferase (HPRT) provides an alternative source of guanine nucleotides[81]. Since IMPDH controls guanine nucleotide production, it comes as no surprise that this enzyme is frequently upregulated in tumors and rapidly growing cells, such as antigen stimulated B and T lymphocytes[81]. Its inhibition results not only in a depletion of guanine nucleotide pool, but also an imbalance between adenine and guanine nucleotides which leads to undesirable consequences in cells[81]. For these reasons, IMPDH is a clinically relevant and important target for cancer, immunosuppressive and antiviral therapy.

Figure 1.6

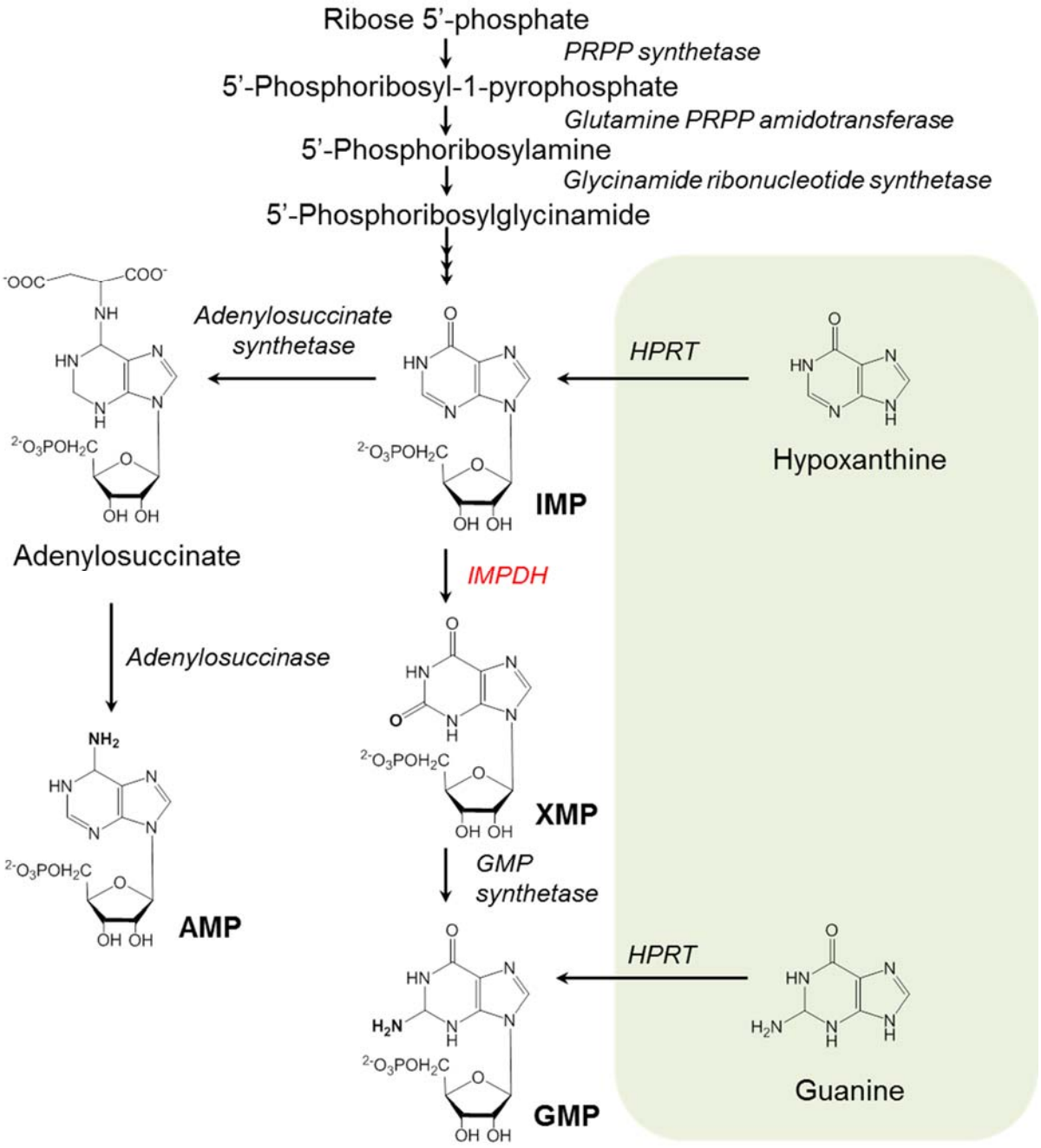

Figure 1.6 – The De Novo Synthesis of Purine Nucleotides. The initial steps in purine nucleotide biosynthesis lead to the formation of IMP, the parent purine molecule, which can ultimately be converted to AMP or GMP. IMPDH (in red) catalyzes conversion of IMP to XMP, in the de novo pathway for guanosine biosynthesis. Guanosine can also be salvaged via the action of HPRT (green box) from hypoxanthine or guanine.

Many organisms possess multiple genes encoding IMPDH. In humans, two isozymes exist – termed type 1 (IMPDH1) and type 2 (IMPDH2)[82]. The canonical hIMPDH1 and hIMPDH2 are 514 amino acids long and share 84% sequence homology at the amino acid level[81] (Figure 1.7A).

Figure 1.7

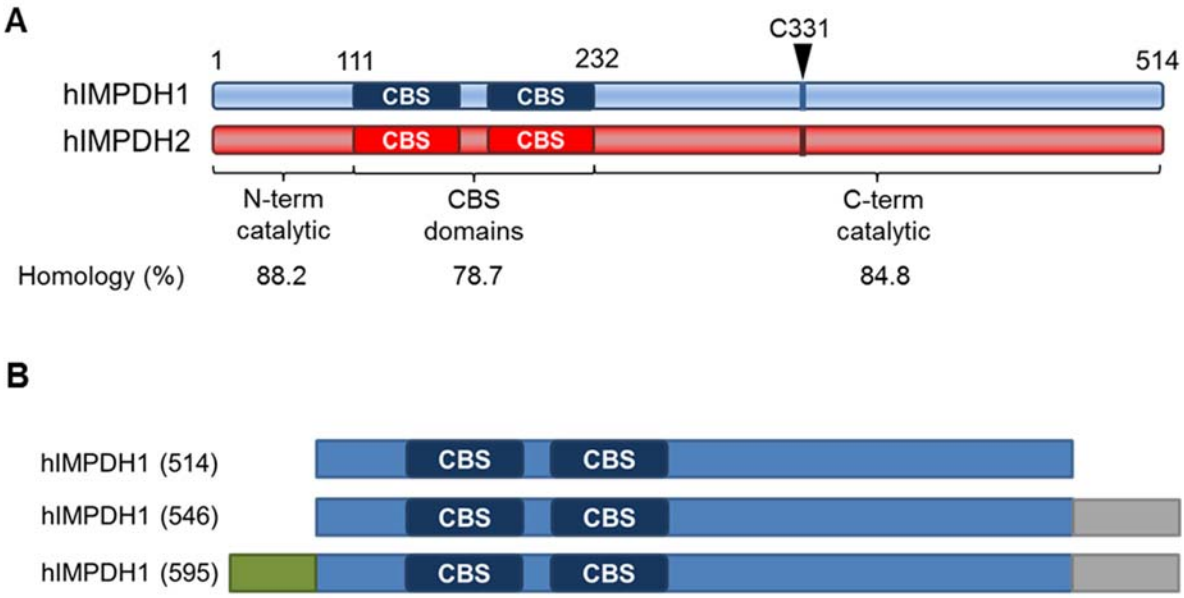

Figure 1.7 – Structure of Human IMPDHs. (A) The canonical hIMPDH1 and hIMPDH2 are 514 amino acids long and share 84% sequence homology at the amino acid level. In human IMPDHs, the catalytic cysteine residue is located at position 331. (B) Schematic showing the different hIMPDH1 splice variants. The canonical hIMPDH1 sequence is still intact in the other splice variants.

The two isozymes have very similar kinetic properties – exhibiting similar affinities for substrate IMP and cofactor NAD, and have almost identical k_{cat} values[83]. Both isoforms of IMPDH are expressed in different tissues to varying extents, although hIMPDH1 appears to be the predominating isoform in the retina, spleen and resting peripheral blood mononuclear cells[81,84]. Previous reports demonstrated that hIMPDH1 is constitutively expressed and is the main isoform in normal cells, whereas hIMPDH2 is

preferentially amplified in neoplastic and replicating cells[85]. Interestingly, despite their indistinguishable enzymatic properties, IMPDH1 versus IMPDH2 knockout in mouse exhibit very contrasting phenotypes. IMPDH1 knockout mice are viable and display progressive retinopathy whereas IMPDH2 knockout mice are embryonic lethal[86–88]. This suggests that neither isozymes is redundant, and could play additional divergent and distinct roles in cells[81]. hIMPDH1 also exists in alternative spliced versions which are longer than the canonical hIMPDH1 of 514 residues, although the significance of these variants remain poorly understood[81,84] (Figure 1.7B),.

Perhaps more intriguing is the observation that mutations of hIMPDH1 underlie an autosomal dominant form of retinitis pigmentosa (adRP10), a retinal degenerative disease which results in severe visual impairment and ultimately blindness[84,89]. The mutations responsible for the pathogenesis of adRP10 are frequently found in the cystathionine beta synthase (CBS) domains of hIMPDH1[81]. In contrast, no polymorphisms of pathogenic hIMPDH2 have been identified to date[81].

1.5.2 The Structure of IMPDH

The native IMPDH exists as a homotetramer although higher order aggregates have been described[81]. Monomeric IMPDH have not been observed *in vitro*. Each hIMPDH monomer consists of two domains – a larger catalytic core domain of about 400 residues, and a smaller accessory subdomain comprising 2 CBS domains totaling approximately 100 residues[81] (Figure 1.8).

The catalytic domain is a $(\beta/\alpha)_8$ barrel containing the active site residue Cys331 (in hIMPDH). Portions of the active site appear disordered in crystal structures of

various IMPDH enzymes[81,90]. Additionally, multiple conformations of ordered active site loop together imply a high degree of flexibility during IMPDH's catalytic cycle[81].

Figure 1.8

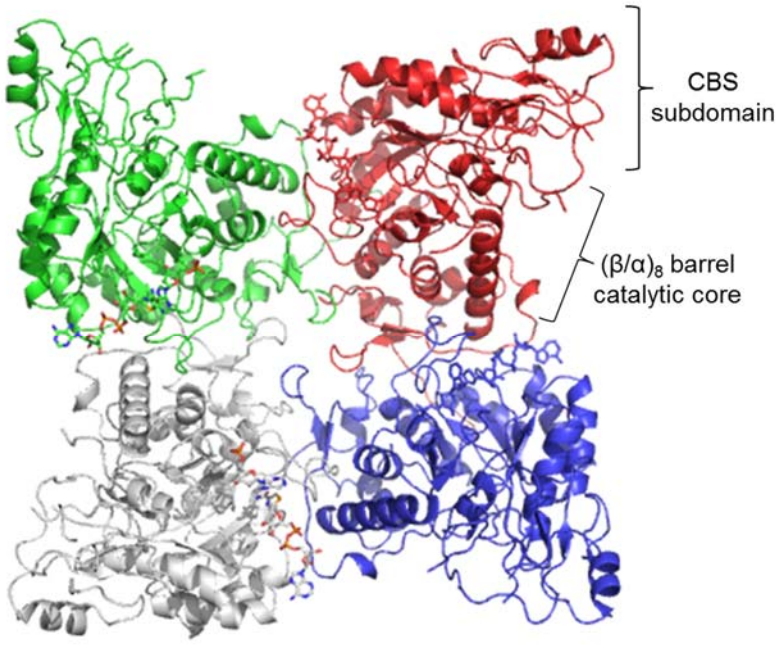

Figure 1.8 – The Structure of Human IMPDH2. The tetramer structure of *H. sapiens* IMPDH2 showing a square planar geometry. Each IMPDH2 monomer consists of two domains – a larger catalytic core domain and a smaller CBS domains subdomain (PDB 1B3O).

The CBS domains, located on the periphery of the tetrameric IMPDH structure, are not necessary for IMPDH activity and a few bacterial and protozoan IMPDH lack this subdomain[81,91,92]. The precise function of the CBS domains is unknown. CBS domains are disordered to some extent in almost all IMPDH crystal structures available[81]. The first complete structure of IMPDH from *Streptococcus pyogenes* was solved in 1999, revealing a conserved three dimensional structure similar to other CBS domain containing proteins, despite little sequence conservation[93].

1.5.3 The CBS Domains of IMPDH

While studies spanning the past few decades have focused mostly on the catalytic domain of IMPDH, less is known of its accessory CBS domains – named for the homologous domains in cystathionine beta synthase involved in cysteine metabolism. Briefly, CBS domains are found in a myriad of different proteins from all kingdoms of life, including kinases, chloride channels, transporters, and metabolic enzymes such as IMPDH[94]. First described in 1997 by Bateman, the CBS domains typically occur in pairs (also called a Bateman domain), and occasionally in quads, with each CBS domain sequence approximately 60 residues long[95] (Figure 1.9A and B). Most notably, these regions share little sequence homology yet are structurally conserved[94] (Figure 1.9C).

Mutations in the CBS domains of several human proteins are known to result in several hereditary diseases such as homocystinuria (in CBS), congenital myotonia and Bartter syndrome (in ClC), Wolff-Parkinson-White syndrome and familial cardiac hypertrophy (in AMPK)[96,97]. Specifically, mutations in CBS domains of hIMPDH1 give rise to adRP10, implying a pivotal *in vivo* function of these domains[97]. To date, the pathogenic polymorphisms giving rise to retinal degeneration are R105W, T116M, N198K, R224P, D226N, V268I and H372P[81].

Figure 1.9

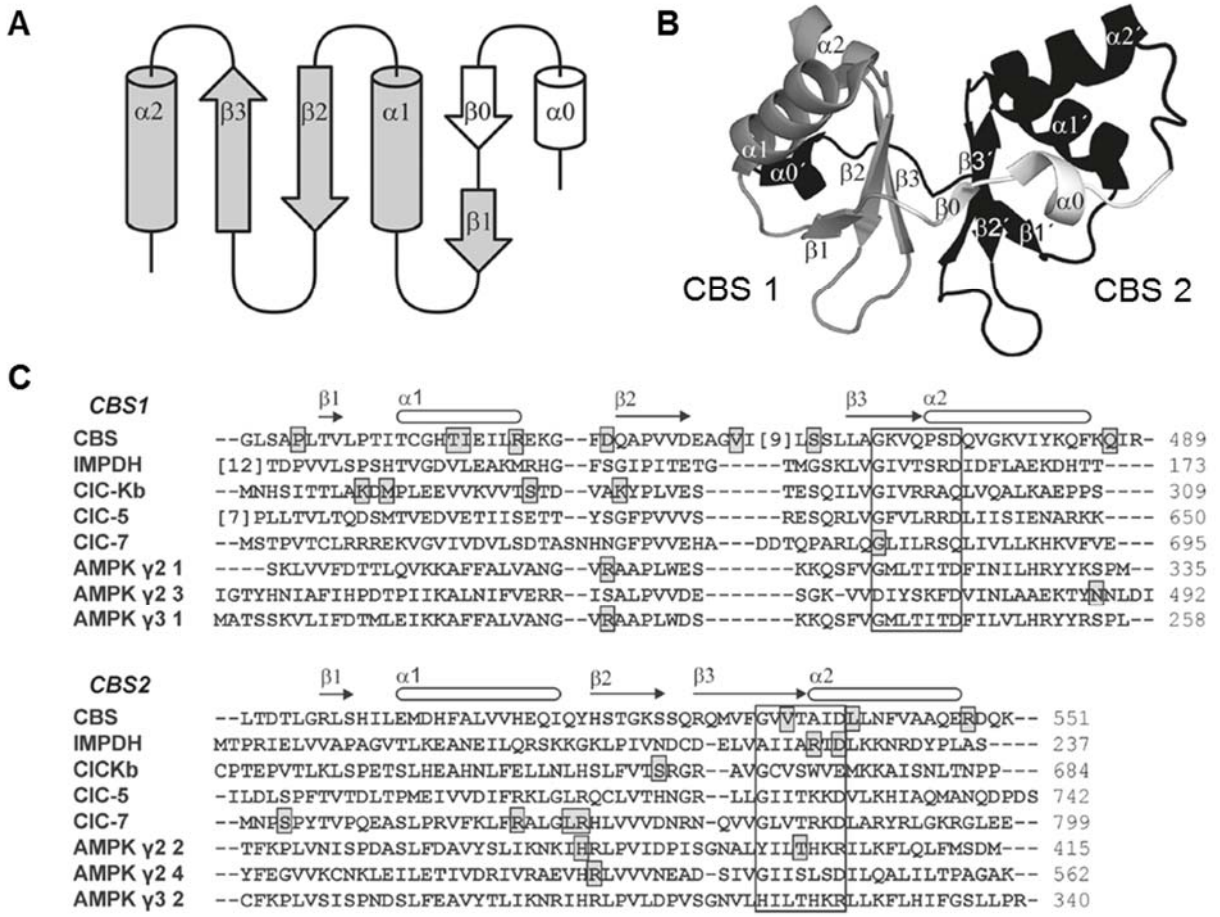

Figure 1.9 – The Topology, Structure and Sequence of CBS Domains. (A) The topology of the CBS domain showing the core in gray and common CBS linker in white. (B) Structure of the CBS domain pair from *Pyrobaculum aerophilum* (PDB 2RIF). (C) Sequence alignment of the two CBS domains of human proteins with pathogenic mutations shaded in gray with the most conserved CBS motifs boxed. Figures are from Reference 94.

Some progress has been made to elucidate the function of CBS domains, although the emerging theme seems to be that CBS domains in different proteins play different roles in cellular processes. Several lines of evidence provide support that CBS domains are regulatory units functioning as metabolic sensors by binding to a variety of adenosine containing ligands[81,98]. Scott and colleagues demonstrated that the CBS domains of AMPK, IMPDH and CLC-2 bind AMP, ATP and SAM while pathogenic

mutant CBS domains lack adenosine ligand binding capacity[98]. They also reported that ATP activates IMPDH and that the pathogenic R224P mutation obliterates ATP binding and subsequent activation of IMPDH, concluding that allosteric ATP binding to the CBS domains promotes XMP synthesis via IMPDH activation[98]. However, the CBS domains as an adenosine nucleotide binding regulator of IMPDH is a subject of debate as several research groups have failed to reproduce their findings[81]. Perhaps more interestingly, the removal of the CBS domain in IMPDH has minimal effect on its enzyme activity, suggesting that the CBS domains are not directly involved in catalysis[91,92]. CBS domains also bind metal ions (such as Mg^{2+} and Zn^{2+}) and nucleic acids[94]. There have been several studies documenting the *in vitro* and *in vivo* binding of single-stranded DNA and RNA to the CBS domains of prokaryotic IMPDH, suggesting an additional unanticipated role in nucleic acid metabolism[99–101]. IMPDH also associates with polyribosomes through its CBS domain[102].Taken together, these observations proffer the idea that IMPDH could have an alternative, previously unappreciated function aside from its catalytic activity mediated by its CBS domain.

More recently, Kozhevnikova and colleagues reported that *Drosophila* IMPDH is a DNA-binding transcriptional repressor and that the enzymatic activity of IMPDH is not necessary for DNA binding[103]. They demonstrated that nuclear IMPDH exists after DNA replication or upon cellular stress, and regulate genes involved in cell cycle progression. *E2F*, a transcription factor critical for G1/S phase transition is one of the targets modulated by IMPDH. In support of other published data, they found that adRP mutations abolished IMPDH binding to nucleic acids, specifically CT-rich single stranded DNA sequences[103]. The functional consequence of how mutants lacking

ssDNA binding ability leads to adRP is unclear, although the authors did suggest the possible impairment of transcriptional control by IMPDH as an adRP contributing mechanism[103].

Another recent study reported the aggregated fibers of octameric pathogenic hIMPDH1 in the presence of MgATP, which could provide an alternative mechanism for the onset of adRP10[104]. In contrast, while wild type hIMPDH1 polymerize in the presence of MgATP, it does not form aggregates. In addition, they described the allosteric regulation of *Pseudomonas aerugininosa* IMPDH by MgATP via the CBS subdomain[104]. It is also suggested that mutated CBS domains promote misfolding of IMPDH, leading to its aggregation[104]. Since IMPDH1 and IMPDH2 knock out mice exhibit different phenotypes, it begs the question of whether the observed phenotypes are mediated by the CBS domains of IMPDH since both isozymes are catalytically identical.

1.6 Concluding Remarks

Increasing importance is being placed on gaining a clear understanding of a drug's mode of action to boost the chance of its success upon entering clinical trials. As such, target identification and mechanism-of-action studies have become critical aspects of small molecule probe research and drug discovery in pharmaceutical companies. My doctoral thesis will describe efforts to define the mechanism of action of macrocyclic natural product Sanglifehrin A, through employing and integrating multiple target identification approaches. Through biochemical affinity purification methods, we identified IMPDH2 as a putative target for SFA (Chapter 2). This led to an in depth study

and characterization of drug-target binding through the modification of SFA and mutagenesis of IMPDH2 (Chapter 3). Chapter 4 describes efforts to validate IMPDH2 and PPIA as the targets *in vivo* with fungi and worms, as well as with RNAi and the CRISPR/Cas9 system. Last but not least, Chapter 5 describes unbiased and complementary approaches to SFA target identification, discusses the implication of our results and proposes future studies for the project.

References

1. Koehn, F. E. & Carter, G. T. The evolving role of natural products in drug discovery. *Nat. Rev. Drug Discov.* **4,** 206–220 (2005).

2. Harvey, A. L., Edrada-Ebel, R. & Quinn, R. J. The re-emergence of natural products for drug discovery in the genomics era. *Nat. Rev. Drug Discov.* **14,** 111–129 (2015).

3. Li, J. W. H. & Vederas, J. C. Drug discovery and natural products: End of era or an endless frontier? *Biomeditsinskaya Khimiya* **57,** 148–160 (2011).

4. Ajay, a., Walters, W. P. & Murcko, M. a. Can we learn to distinguish between ‘drug-like’ and ‘nondrug-like’ molecules? *J. Med. Chem.* **41,** 3314–3324 (1998).

5. Newman, D. J., Cragg, G. M. & Snader, K. M. Natural Products as Sources of New Drugs over the Period 1981-2002. *J. Nat. prof.* **66,** 1022–1037 (2003).

6. Newman, D. J. & Cragg, G. M. Natural products as sources of new drugs over the 30 years from 1981 to 2010. *J. Nat. Prod.* **75,** 311–335 (2012).

7. Harvey, A. L. Natural products in drug discovery. *Drug Discov. Today* **13,** 894–901 (2008).

8. Clardy, J. & Walsh, C. Lessons from natural molecules. *Nature* **432,** 829–837 (2004).

9. Henkel, T., Brunne, R. M., Müller, H. & Reichel, F. Statistical Investigation into the Structural Complementarity of Natural Products in comparison with Synthetic Compounds. *Angew. Chemie - Int. Ed.* **38,** 643–647 (1999).

10. Feher, M. & Schmidt, J. M. Property distributions: Differences between drugs, natural products, and molecules from combinatorial chemistry. *J. Chem. Inf. Comput. Sci.* **43,** 218–227 (2003).

11. Lipinski, C. a, Lombardo, F., Dominy, B. W. & Feeney, P. J. Experimental and computational approaches to estimate solubility and permeability in drug discovery and development settings. *Adv. Drug Deliv. Rev.* **46,** 3–26 (2001).

12. Drewry, D. H. & Macarron, R. Enhancements of screening collections to address areas of unmet medical need: an industry perspective. *Curr. Opin. Chem. Biol.* **14,** 289–298 (2010).

13. Carlson, E. E. Natural Products as Chemical Probes. *ACS Chem. Biol.* **5,** 639–653 (2010).

14. Taunton, J., Collins, J. L. & Schreiber, S. L. Synthesis of natural and modified trapoxins, useful reagents for exploring histone deacetylase function. *J. Am. Chem. Soc.* **118,** 10412–10422 (1996).

15. Schreiber, S. L. Immunophilin-sensitive protein phosphatase action in cell signaling pathways. *Cell* **70,** 365–368 (1992).

16. Kunz, J. & Hall, M. N. Cyclosporin A, FK506 and rapamycin: more than just immunosuppression. *Trends Biochem. Sci.* **18,** 334–338 (1993).

17. Driggers, E. M., Hale, S. P., Lee, J. & Terrett, N. K. The exploration of macrocycles for drug discovery--an underexploited structural class. *Nat. Rev. Drug Discov.* **7,** 608–624 (2008).

18. Kotz, J. Bringing macrocycles full circle. *Sci. Exch.* **5,** (2012).

19. Schlünzen, F. *et al.* Structural basis for the interaction of antibiotics with the peptidyl transferase centre in eubacteria. *Nature* **413,** 814–821 (2001).

20. Nigro, P., Pompilio, G. & Capogrossi, M. C. Cyclophilin A: a key player for human disease. *Cell Death Dis.* **4,** e888 (2013).

21. Blackburn, E. a. & Walkinshaw, M. D. Targeting FKBP isoforms with small-molecule ligands. *Curr. Opin. Pharmacol.* **11,** 365–371 (2011).

22. Galat, A. Functional drift of sequence attributes in the FK506-binding proteins (FKBPs). *J. Chem. Inf. Model.* **48,** 1118–1130 (2008).

23. Davis, T. L. *et al.* Structural and biochemical characterization of the human cyclophilin family of peptidyl-prolyl isomerases. *PLoS Biol.* **8,** (2010).

24. Lee, J. & Kim, S. S. An overview of cyclophilins in human cancers. *J. Int. Med. Res.* **38,** 1561–1574 (2010).

25. Sigal, N. H. & Dumont, F. J. Cyclosporin A, FK-506, and Rapamycin: Pharmacologic Probes of Lymphocyte Signal Transduction. *Annu. Rev. Immunol.* **10,** 519–560 (1992).

26. Schreiber, S. L. Chemistry and biology of the immunophilins and their immunosuppressive ligands. *Science* **251,** 283–287 (1991).

27. Wang, P. & Heitman, J. The cyclophilins. *Genome Biol.* **6,** 226 (2005).

28. Handschumacher, R. E., Harding, M. W., Rice, J., Drugge, R. J. & Speicher, D. W. Cyclophilin: A Specific Cytosolic Binding Protein for Cyclosporin A. *Science* **226,** 544–547 (1984).

29. Jin, Z. G. *et al.* Cyclophilin A is a secreted growth factor induced by oxidative stress. *Circ. Res.* **87,** 789–796 (2000).

30. Colgan, J., Asmal, M. & Luban, J. Isolation, characterization and targeted disruption of mouse ppia: cyclophilin A is not essential for mammalian cell viability. *Genomics* **68,** 167–178 (2000).

31. Tropschug, M., Barthelmess, I. B. & Neupert, W. Sensitivity to cyclosporin A is mediated by cyclophilin in Neurospora crassa and Saccharomyces cerevisiae. *Nature* **342,** 955 (1989).

32. Dolinski, K., Muir, S., Cardenas, M. & Heitman, J. All cyclophilins and FK506 binding proteins are, individually and collectively, dispensable for viability in Saccharomyces cerevisiae. *Proc. Natl. Acad. Sci. U. S. A.* **94,** 13093–13098 (1997).

33. Herrler, M., Bang, H. & Marahiel, M. a. Cloning and characterization of ppiB, a Bacillus subtilis gene which encodes a cyclosporin A-sensitive peptidyl-prolyl cis-trans isomerase. *Mol. Microbiol.* **11,** 1073–1083 (1994).

34. Nigro, P. *et al.* Cyclophilin A is an inflammatory mediator that promotes atherosclerosis in apolipoprotein E-deficient mice. *J. Exp. Med.* **208,** 53–66 (2011).

35. Satoh, K. *et al.* development of angiotensin II-induced aortic aneurysms. *Nat. Med.* **15,** 649–656 (2009).

36. Sokolskaja, E., Sayah, D. M. & Luban, J. Target Cell Cyclophilin A Modulates Human Immunodeficiency Virus Type 1 Infectivity. *Society* **78,** 12800–12808 (2004).

37. Ciesek, S. *et al.* Cyclosporine A inhibits hepatitis C virus nonstructural protein 2 through cyclophilin A. *Hepatology* **50,** 1638–1645 (2009).

38. Chatterji, U. *et al.* The isomerase active site of cyclophilin A is critical for hepatitis C virus replication. *J. Biol. Chem.* **284,** 16998–17005 (2009).

39. Yang, F. *et al.* Cyclophilin A is an essential cofactor for hepatitis C virus infection and the principal mediator of cyclosporine resistance in vitro. *J. Virol.* **82,** 5269–5278 (2008).

40. Borel, J. F., Feurer, C., Gubler, H. U. & Stähelin, H. Biological effects of cyclosporin A: A new antilymphocytic agent. *Agents Actions* **43,** 468–475 (1976).

41. Borel, J. F., Feurer, C., Magnée, C. & Stähelin, H. Effects of the new anti-lymphocytic peptide cyclosporin A in animals. *Immunology* **32,** 1017–1025 (1977).

42. Pirsch, J. D., Miller, J., Deierhoi, M. H., Vincenti, F. & Filo, R. S. A Comparison of Tacrolimus (FK506) and Cyclosporine for Immunosuppression After Cadaveric Renal Transplantation. *Transplantation* **63,** 977–983 (1997).

43. Kahan, B. D. Cyclosporine. *N. Engl. J. Med.* **321,** 1725–1738 (1989).

44. Vezina, C.Kudelski, A. & Sehgal, S. N. Rapamycin (AY-22,989), a new antifungal antibiotic: I. Taxonomy of the producing Streptomycete and isolation of the active principle. *J. Antibiot. (Tokyo).* **28,** 721–726 (1975).

45. Sehgal, S. N., Baker, H. & Vézina, C. Rapamycin (AY-22,989), a new antifungal antibiotic. II. Fermentation, isolation and characterization. *J. Antibiot. (Tokyo).* **28,** 727–732 (1975).

46. Liu, J. *et al.* Calcineurin is a common target of cyclophilin-cyclosporin A and FKBP-FK506 complexes. *Cell* **66,** 807–815 (1991).

47. Sabers, C. J. *et al.* Isolation of a Protein Target of the FKBP12-Rapamycin Complex in Mammalian Cells. *J. Biol. Chem.* **270,** 815–822 (1995).

48. Fischer, G., Wittmann-Liebold, B., Lang, K., Kiefhaber, T. & Schmid, F. X. Cyclophilin and peptidyl-prolyl cis-trans isomerase are probably identical proteins. *Nature* **337,** 476–478 (1989).

49. Takahashi, N., Hayano, T. & Suzuki, M. Takahashi_1989_Nature_PPIAcsa.pdf. *Nature* **337,** 473–475 (1989).

50. Emmel, E. a *et al.* Cyclosporin A specifically inhibits function of nuclear proteins involved in T cell activation. *Science* **246,** 1617–1620 (1989).

51. Harding, M. W., Galat, a, Uehling, D. E. & Schreiber, S. L. A receptor for the immunosuppressant FK506 is a cis-trans peptidyl-prolyl isomerase. *Nature* **341,** 758–760 (1989).

52. Siekierka, J. J., Hung, S. H., Poe, M., Lin, C. S. & Sigal, N. H. A cytosolic binding protein for the immunosuppressant FK506 has peptidyl-prolyl isomerase activity but is distinct from cyclophilin. *Nature* **341,** 755–757 (1989).

53. Koltin, Y. *et al.* Rapamycin Sensitivity in Saccharomyces cerevisiae Is Mediated by a Peptidyl-Prolyl cis-trans Isomerase Related to Human FK506-Binding Protein. *Mol. Cell. Biol.* **11,** 1718–1723 (1991).

54. Heitman, J., Movva, N. R. & Hall, M. N. Targets for cell cycle arrest by the immunosuppressant rapamycin in yeast. *Science* **253,** 905–9 (1991).

55. Sigal, N. H. *et al.* Is cyclophilin involved in the immunosuppressive and nephrotoxic mechanism of action of cyclosporin A? *J. Exp. Med.* **173,** 619–628 (1991).

56. Crabtree, G. R. Contingent genetic regulatory events in T lymphocyte activation. *Science* **243,** 355–361 (1989).

57. Flanagan, W. M., Corthésy, B., Bram, R. J. & Crabtree, G. R. Nuclear association of a T-cell transcription factor blocked by FK-506 and cyclosporin A. *Nature* **352,** 803–807 (1991).

58. Beals, C. R., Clipstone, N. a, Ho, S. N. & Crabtree, G. R. Nuclear localization of NF-ATc by a intramolecular interaction. *Genes Dev.* **4,** 824–834 (1997).

59. Schreiber, S. L. & Crabtree, G. R. The mechanism of action of cyclosporin A and FK506. *Immunol. Today* **13,** 136–142 (1992).

60. Brown, E. J. *et al.* A mammalian protein targeted by G1-arresting rapamycin-receptor complex. *Nature* **369,** 756–758 (1994).

61. Chiu, M. I., Katz, H. & Berlin, V. RAPT1, a mammalian homolog of yeast Tor, interacts with the FKBP12/rapamycin complex. *Proc. Natl. Acad. Sci. U. S. A.* **91,** 12574–8 (1994).

62. Sabatini, D. M., Erdjument-Bromage, H., Lui, M., Tempst, P. & Snyder, S. H. RAFT1: A mammalian protein that binds to FKBP12 in a rapamycin-dependent fashion and is homologous to yeast TORs. *Cell* **78,** 35–43 (1994).

63. Laplante, M. & Sabatini, D. M. MTOR signaling in growth control and disease. *Cell* **149,** 274–293 (2012).

64. Sanglier, J. *et al.* Sanglifehrins Isolated A , B , C and D , Novel Cyclophilin-binding Compounds I . Taxonomy , Fermentation , Isolation and Biological Activity. *J. Antibiot. (Tokyo).* **52,** 466–473 (1999).

65. Fehr, T., Kallen, J. & Oberer, L. Sanglifehrins Isolated A , B , C and D , Novel Cyclophilin-binding from Streptomyces Compounds II . Structure Elucidation , Stereochemistry and Physico-chemical Properties. *J. Antibiot. (Tokyo).* **52,** 474–479 (1999).

66. Oelke, A. J., France, D. J., Hofmann, T., Wuitschik, G. & Ley, S. V. Piperazic acid-containing natural products: isolation, biological relevance and total synthesis. *Nat. Prod. Rep.* **28,** 1445–1471 (2011).

67. Nicolaou, K. C. *et al.* Total synthesis of the novel immunosuppressant sanglifehrin A. *J. Am. Chem. Soc.* **122,** 3830–3838 (2000).

68. Duan, M. & Paquette, L. a. Enantioselective total synthesis of the cyclophilin-binding immunosuppressive agent sanglifehrin A. *Angew. Chemie - Int. Ed.* **40,** 3632–3636 (2001).

69. Paquette, L. a., Duan, M., Konetzki, I. & Kempmann, C. A convergent three-component total synthesis of the powerful immunosuppressant (-)-sanglifehrin A. *J. Am. Chem. Soc.* **124,** 4257–4270 (2002).

70. Bänteli, R., Wagner, J. & Zenke, G. Synthesis of derivatives of the novel cyclophilin-binding immunosuppressant sanglifehrin A with reduced numbers of polar functions. *Bioorganic Med. Chem. Lett.* **11,** 1609–1612 (2001).

71. Sedrani, R. *et al.* Sanglifehrin-cyclophilin interaction: degradation work, synthetic macrocyclic analogues, X-ray crystal structure, and binding data. *J. Am. Chem. Soc.* **125,** 3849–59 (2003).

72. Qu, X. *et al.* Cloning, sequencing and characterization of the biosynthetic gene cluster of sanglifehrin A, a potent cyclophilin inhibitor. *Mol. Biosyst.* **7,** 852 (2011).

73. Zenke, G. *et al.* Sanglifehrin A, a Novel Cyclophilin-Binding Compound Showing Immunosuppressive Activity with a New Mechanism of Action. *J. Immunol.* 7165–7171 (2001).

74. Zhang, L. & Liu, J. O. Sanglifehrin A, a Novel Cyclophilin-Binding Immunosuppressant, Inhibits IL-2-Dependent T Cell Proliferation at the G1 Phase of the Cell Cycle. *J. Immunol.* **166,** 5611–5618 (2001).

75. Zhang, L. H., Youn, H. D. & Liu, J. O. Inhibition of cell cycle progression by the novel cyclophilin ligand sanglifehrin A is mediated through the NFkappa B-dependent activation of p53. *J. Biol. Chem.* **276,** 43534–40 (2001).

76. Steinschulte, C., Taner, T., Thomson, a. W., Bein, G. & Hackstein, H. Sanglifehrin A, a Novel Cyclophilin-Binding Immunosuppressant Blocks Bioactive IL-12 Production by Human Dendritic Cells. *J. Immunol.* **171,** 542–546 (2003).

77. Woltman, A. M., Schlagwein, N., van der Kooij, S. W. & van Kooten, C. The novel cyclophilin-binding drug sanglifehrin A specifically affects antigen uptake receptor expression and endocytic capacity of human dendritic cells. *J. Immunol.* **172,** 6482–6489 (2004).

78. Ko, H. *et al.* Dentritic cell derived IL-18 production is inhibited by rapamycin and sanglifehrin A, but not cyclosporine A. *Transpl. Immunol.* **20,** 99–105 (2008).

79. Immecke, S. N. *et al.* The cyclophilin-binding agent Sanglifehrin A is a dendritic cell chemokine and migration inhibitor. *PLoS One* **6,** e18406 (2011).

80. Kallen, J., Sedrani, R., Zenke, G. & Wagner, J. Structure of human cyclophilin A in complex with the novel immunosuppressant sanglifehrin A at 1.6 A resolution. *J. Biol. Chem.* **280,** 21965–71 (2005).

81. Hedstrom, L. IMP Dehydrogenase: Structure, Mechanism and Inhibition. *Chem. Rev.* **109,** 2903–2928 (2009).

82. Natsumeda, Y. *et al.* Two distinct cDNAs for human IMP dehydrogenase. *J. Biol. Chem.* **265,** 5292–5295 (1990).

83. Carr, S. F., Papp, E., Wu, J. C. & Natsumeda, Y. Characterization of human type I and type II IMP dehydrogenases. *J. Biol. Chem.* **268,** 27286–27290 (1993).

84. Bowne, S. J. *et al.* Spectrum and frequency of mutations in IMPDH1 associated with autosomal dominant retinitis pigmentosa and leber congenital amaurosis. *Investig. Ophthalmol. Vis. Sci.* **47,** 34–42 (2006).

85. Jackson, R. C. & Weber, G. IMP dehydrogenase, an enzyme linked with proliferation and malignancy. *Nature* **256,** 331–333 (1975).

86. Gu, J. J. *et al.* Inhibition of T lymphocyte activation in mice heterozygous for loss of the IMPDH II gene. *J. Clin. Invest.* **106,** 599–606 (2000).

87. Gu, J. J. *et al.* Targeted Disruption of the Inosine 5 ′ -Monophosphate Dehydrogenase Type I Gene in Mice. *Mol. Cell. Biol.* **23,** 6702–6712 (2003).

88. Aherne, A. *et al.* On the molecular pathology of neurodegeneration in IMPDH1-based retinitis pigmentosa. *Hum. Mol. Genet.* **13,** 641–650 (2004).

89. Bowne, S. J. *et al.* Mutations in the inosine monophosphate dehydrogenase 1 gene (IMPDH1) cause the RP10 form of autosomal dominant retinitis pigmentosa. *Hum. Mol. Genet.* **11,** 559–568 (2002).

90. Colby, T. D., Vanderveen, K., Strickler, M. D., Markham, G. D. & Goldstein, B. M. Crystal structure of human type II inosine monophosphate dehydrogenase: implications for ligand binding and drug design. *Proc. Natl. Acad. Sci. U. S. A.* **96,** 3531–3536 (1999).

91. Nimmesgern, E. *et al.* Biochemical analysis of the modular enzyme inosine 5'-monophosphate dehydrogenase. *Protein Expr. Purif.* **17,** 282–289 (1999).

92. Gan, L., Petsko, G. A. & Hedstrom, L. Crystal structure of a Ternary Complex of Tritrichomonas foetus Inosine 5'-Monosphosphate Dehydrogenase: NAD+ Orients the Active Site Loop for Catalysis. *Biochemistry* 13309–13317 (2002). doi:10.1074/jbc.M208330200

93. Zhang, R. *et al.* Characteristics and crystal structure of bacterial inosine-5'-monophosphate dehydrogenase. *Biochemistry* **38,** 4691–4700 (1999).

94. Baykov, A. a., Tuominen, H. K. & Lahti, R. The CBS domain: A protein module with an emerging prominent role in regulation. *ACS Chem. Biol.* **6,** 1156–1163 (2011).

95. Bateman, A. The structure of a domain common to archaebacteria and the homocystinuria disease protein. *Trends Biochem. Sci.* **22,** 12–13 (1997).

96. Kemp, B. E. Bateman domains and adenosine derivatives form a binding contract. *J. Clin. Invest.* **113,** 182–184 (2004).

97. Ignoul, S. & Eggermont, J. CBS domains: structure, function, and pathology in human proteins. *Am. J. Physiol. Cell Physiol.* **289,** C1369–78 (2005).

98. Scott, J. W. *et al.* CBS domains form energy-sensing modules whose binding of adenosine ligands is disrupted by disease mutations. *J. Clin. Invest.* **113,** 274–284 (2004).

99. Cornuel, J.-F., Moraillon, A. & Gueron, M. Participation of yeast inosine 5'-monophosphate dehydrogenase in an in vitro complex with a fragment of the C-rich telomeric strand. *Biochimie* 279–289 (2002).

100. McLean, J. E. *et al.* Inosine 5'-monophosphate dehydrogenase binds nucleic acids in vitro and in vivo. *Biochem. J.* **379,** 243–51 (2004).

101. Mortimer, S. E. & Hedstrom, L. Autosomal dominant retinitis pigmentosa mutations in inosine 5'-monophosphate dehydrogenase type I disrupt nucleic acid binding. *Biochem. J.* **390,** 41–47 (2005).

102. Mortimer, S. E. *et al.* IMP dehydrogenase type 1 associates with polyribosomes translating rhodopsin mRNA. *J. Biol. Chem.* **283,** 36354–36360 (2008).

103. Kozhevnikova, E. N. *et al.* Metabolic enzyme IMPDH is also a transcription factor regulated by cellular state. *Mol. Cell* **47,** 133–9 (2012).

104. Labesse, G. *et al.* MgATP regulates allostery and fiber formation in IMPDHs. *Structure* **21,** 975–985 (2013).

CHAPTER 2

IDENTIFICATION OF IMPDH2 AS A CYCLOPHILIN A-SANGLIFEHRIN A BINDING PROTEIN

2.1 Biochemical Approaches to SFA Target Identification

Biochemical affinity chromatography offers the most straightforward approach in identifying targets that bind to compounds of interest[1]. This method often involves either the labeling of proteins or small molecule of interest, incubating the two populations (treated and untreated), and searching for direct binding proteins enriched after a wash procedure[2]. As this approach relies on direct physical interactions of proteins, biochemical affinity purification can reveal information on both specific molecular mechanistic effects as well as non-specific polypharmacological effects of compounds[2].

While ostensibly straightforward, the caveat to this approach is that it requires a high-affinity ligand binding to an abundant target protein[2]. Moreover, high-stringency wash procedures tend to bias identified proteins to those with very high affinities to compounds, precluding the detection of additional protein targets relevant in cellular contexts[2]. Furthermore, the preparation of immobilized affinity reagents that preserve

cellular activity can present challenges from a biochemical affinity approach as such warrants adequate and proper controls[2]. If an active small molecule is bound to a solid support, one has to be certain that the small molecule-resin attachment site does not mask the target binding surface, and hence its activity. An inactive analog attached to beads or bead-only control could serve as appropriate controls. However, these modifications are limited by the amenability of the small molecule to chemical alterations as well as the types of reactions that enable such modification to proceed at a decent yield.

In the past decade, affinity chromatography techniques have been aided by advances in protein mass spectrometry, enabling unbiased and highly sensitive platforms toward target identification[3,4]. Metabolic labeling, more commonly known as stable-isotope labeling by amino acids in cell culture (SILAC), and chemical labeling, such as isobaric tags for relative and absolute quantification (iTRAQ) and variations thereof have proven to be effective in identifying protein-small molecule interactions[2,5–7].

We sought to identify cellular targets of SFA via biochemical affinity chromatography as a first strategy. The remarkably high affinity of SFA for PPIA, coupled with the high expression levels of PPIA in cells proffer the idea that SFA exerts its biological effect via an immunophilin dependent mechanism, much like CSA, FK506 and RAP. The affinity of SFA was reported to be at least 20 fold higher than CSA[8]. Hence we would expect SFA to engage PPIA upon cellular penetration. Since inhibition of PPIA is not known to cause growth inhibition, there could potentially be another target mediating cell proliferation in a PPIA-dependent manner, analogous to the mechanism of CSA.

Structure-activity relationship studies on SFA provided evidence that the spirolactam moiety of SFA is necessary for immunosuppressive activity[9,10]. The macrolide portion of SFA, while preserving its interaction with PPIA, showed no immunosuppressive activity[10]. Importantly, the removal of the hydroxyl group on the meta-tyrosine of SFA led to a marked drop in the affinity for PPIA and consequently a loss in its immunosuppressive effect[9]. Furthermore, the crystal structure of SFA bound to PPIA showed that the macrocyclic portion of SFA forms direct hydrogen bonds with PPIA, leaving the spirolactam moiety and other parts of SFA macrolide free from other protein contacts[11]. SFA thus behaves like a bifunctional molecule, possessing a “binding domain” responsible for immunophilin engagement, and an “effector domain” that interacts with a potential target of SFA.

Although all of the above evidence provides a strong correlation between PPIA engagement and SFA bioactivity, there have been several reports that claim otherwise [8,12,13]. While the biological effect of SFA could also possibly be mediated via a PPIA-independent mechanism, an approach based on the immobilization of SFA to a solid matrix was considered impractical for two reasons. Firstly, the amount of SFA available for our study precluded the use of much material for chemical derivatization. Secondly, we would require a large amount of PPIA-depleted cell extracts for these experiments, which was a reagent that was not available during the initial efforts at SFA target identification.

Notwithstanding the foregoing, we decided to first search for cellular targets that bind to PPIA in the presence of SFA. This chapter present various biochemical approaches to isolate a direct binder to PPIA-SFA.

2.2 Assessing SFA Effect on Cell Proliferation

SFA was originally reported as a potent immunosuppressant as measured by a MLR assay (IC_{50} = 170nM). However, the action of SFA extends beyond T lymphocytes as other research groups have reported SFA activity in cancer cell lines such as human colon cancer cell line HCT 116[14]. I screened several transformed lines to determine SFA's effect on growth as assessed by CellTiter-Glo Luminescent cell viability assay (Promega). This assay quantifies the amount of ATP, which serves as proxy for the number of active and viable cells. For this initial screen, cells were exposed to SFA treatment for a 48 hour time period.

Sensitivity to SFA was observed in almost all of the cell lines screened, albeit to varying degrees, at a maximum SFA concentration of 5μM (Figure 2.1). H2122 lung adenocarcinoma line, which adheres loosely to the culture flask with some in suspension, was one of the more sensitive cell lines to SFA, with an EC_{50} of 1.25μM (Figure 2.1). SFA appears to most potently inhibit the growth of K562, a chronic myelogenous leukemia (CML) line, with an EC_{50} of 0.23μM (Figure 2.1). The cells lines which exhibited greater sensitivity to SFA, in particular, K562, H2122, Jurkat and HCT116 were selected for further target identification and validation studies.

Figure 2.1

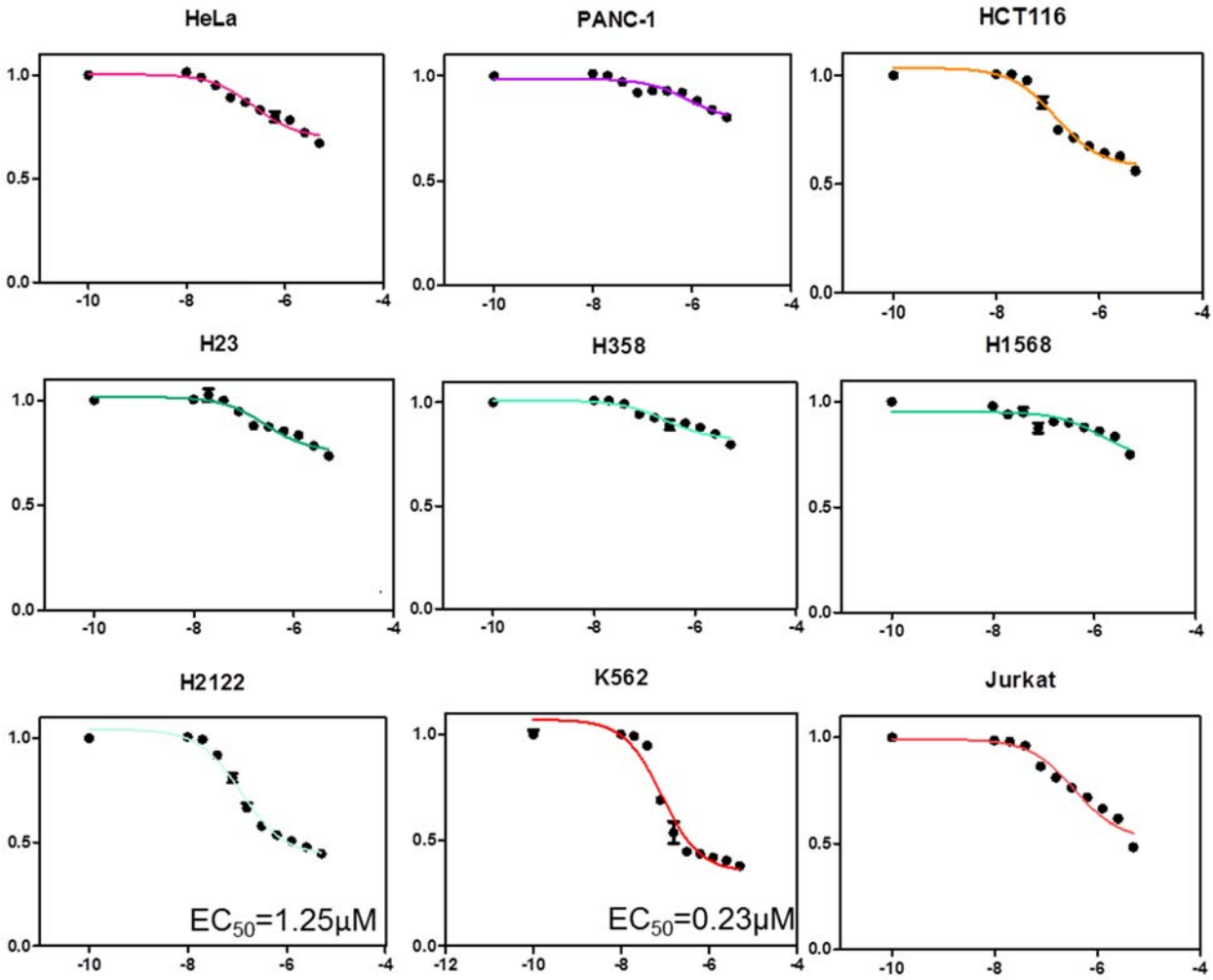

Figure 2.1 – The Effect of SFA on Cell Proliferation. A panel of cell lines was treated with SFA up to 5μM in 96-well opaque white plates for 48 hours and the relative cell amounts were quantified using the CellTiter-Glo assay (Promega). Each sample was run in triplicate and cell number was normalized relative to cells treated with DMSO only. The x axis shows the concentration of SFA to the power of 10 in M. The y axis shows growth relative to DMSO treatment. Details of the procedure are described in the Experimental Procedures section.

Aside from evaluating cell growth in multiwell plates, I also sought to develop a FACS-based assay to determine how SFA inhibits growth. I was gratified that I could largely reproduce the finding that SFA elicits cell cycle arrest at G1-S phase in HCT116 cells, although in my hands, there was a smaller proportion of cells in the G1 phase at

500nM SFA treatment[14] (Figure 2.2). Having confirmed the reported effects of SFA on cell growth, we began efforts to identify a direct molecular target of SFA.

Figure 2.2

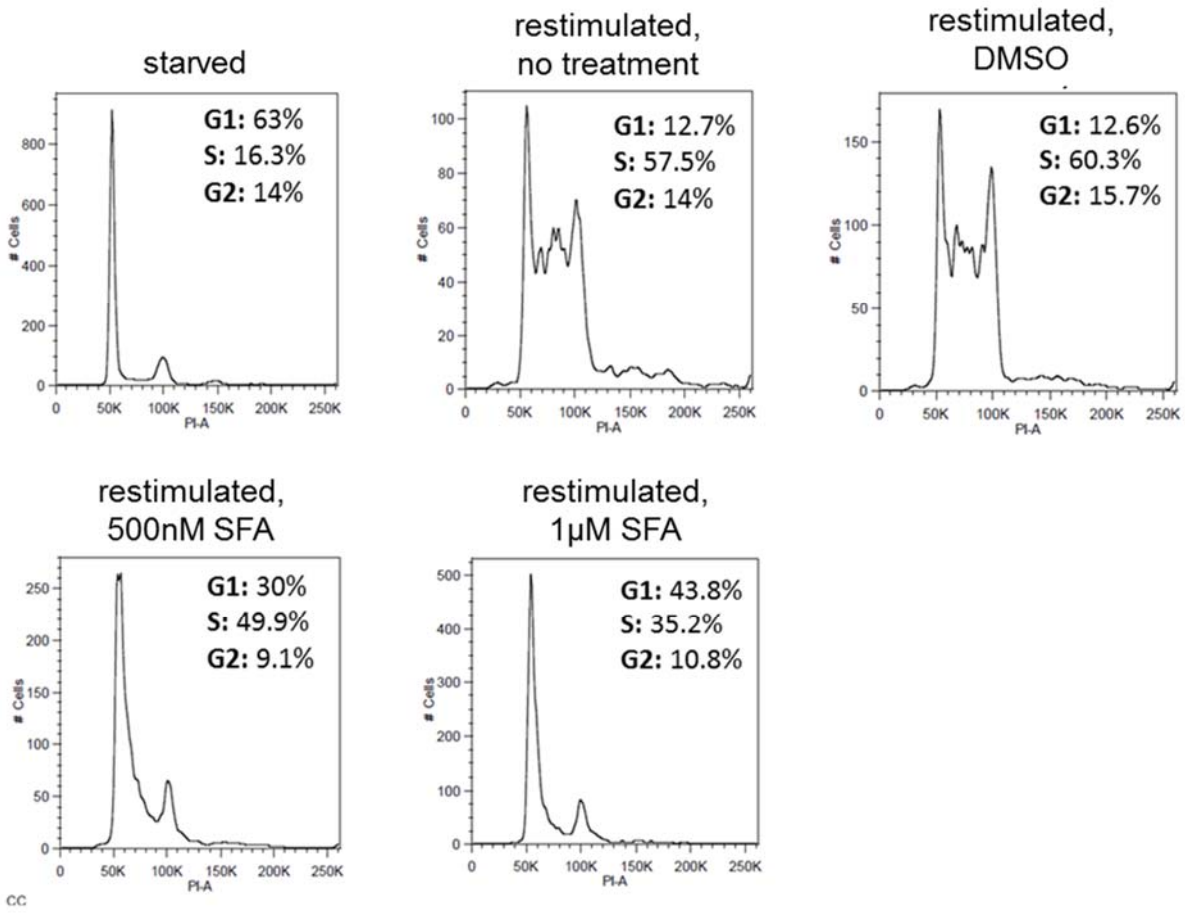

Figure 2.2 – SFA Prevents Cell Cycle Progression at G1-S Transition. Experiment was done to confirm findings by Zhang *et al.*[14]. HCT116 cells were starved in 0.1% serum for 48hrs before restimulation with full serum media in the presence or absence of SFA (500nM or 1μM) for another 12 hours. Cells were harvested, fixed, and stained with propidium iodide prior to analysis of DNA content on a flow cytometer. The percentage of cells in each phase of the cell cycle, G0/G1, S and G2/M are indicated in the figure. Details of the procedure are described in the Experimental Procedures section.

2.3 Direct Biochemical Methods to SFA Target Identification

2.3.1 Affinity Purification with GST-PPIA

To search for cellular proteins that bind specifically to the Cyclophilin A-SFA binary complex, we synthesized a glutathione S-transferase-cyclophilin A (GST-PPIA) fusion construct by cloning the cDNA encoding cyclophilin A to the C terminus of GST. This initial target identification effort was done by a former post-doc in the Verdine lab, Dr Dylan Stiles. Clarified Jurkat T cell lysate was incubated with GST-PPIA in the presence of SFA or DMSO control. A glutathione-sepharose resin was used to enrich for proteins interacting specifically with the GST-PPIA/SFA complex. Silver staining revealed two protein bands, with molecular weights of approximately 55 and 38 kDa, that were specifically retained by the GST-PPIA/SFA complex but not by GST-PPIA/DMSO (Figure 2.3A). Trypsinization and MALDI-TOF peptide mass fingerprint (PMF) analysis of the two protein bands identified inosine monophosphate dehydrogenase isoform 2 (IMPDH2) as the 55 kDa band (Figure 2.3B). The 38 kDa band was deemed to be a truncated fragment of IMPDH2, likely an artifact from degradation that occurred during the experiment. These preliminary results suggest that IMPDH2 is a putative target of SFA.

Figure 2.3

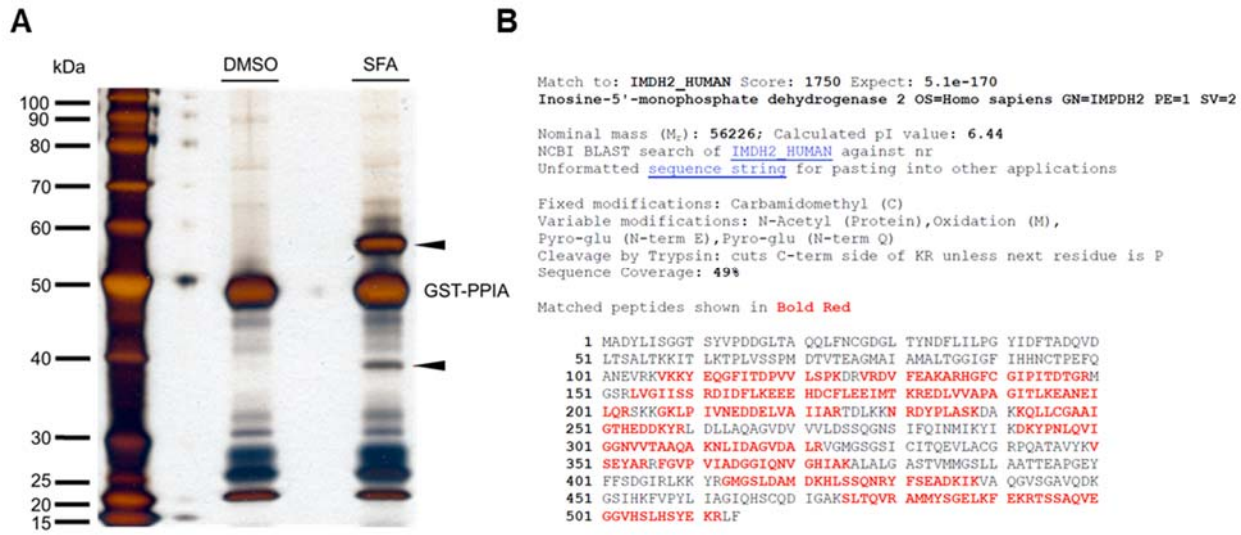

Figure 2.3 – SFA Binds to IMPDH2 in a GST-PPIA Affinity Purification Assay. (A) Silver staining of GST-PPIA pulldown with Jurkat cell lysate. (B) Results from MALDI-TOF peptide mass fingerprinting. Matched peptides are shown in red bold lettering. Figure provided by Dr Dylan Stiles.

2.3.2 Immunoprecipitation Studies with HA-PPIA

In an attempt to confirm that IMPDH2 interacts with PPIA only in the presence of SFA, we sought to utilize mass spectrometry. For this effort, we collaborated with Dr Mat Sowa from the Gygi laboratory at Harvard Medical School. An experimental overview of the IP-MS platform used to run these experiments is shown in Figure 2.4. Using Gateway cloning (Invitrogen), the gene of interest (GOI) is inserted into a pDEST-NTAP vector which has an N-terminal FLAG-HA tandem affinity purification (TAP) tag. We chose this orthogonal tag for our immunoprecipitation-mass spectrometry (IP-MS) experiments and performed the IPs in a variety of cell lysates.

Figure 2.4

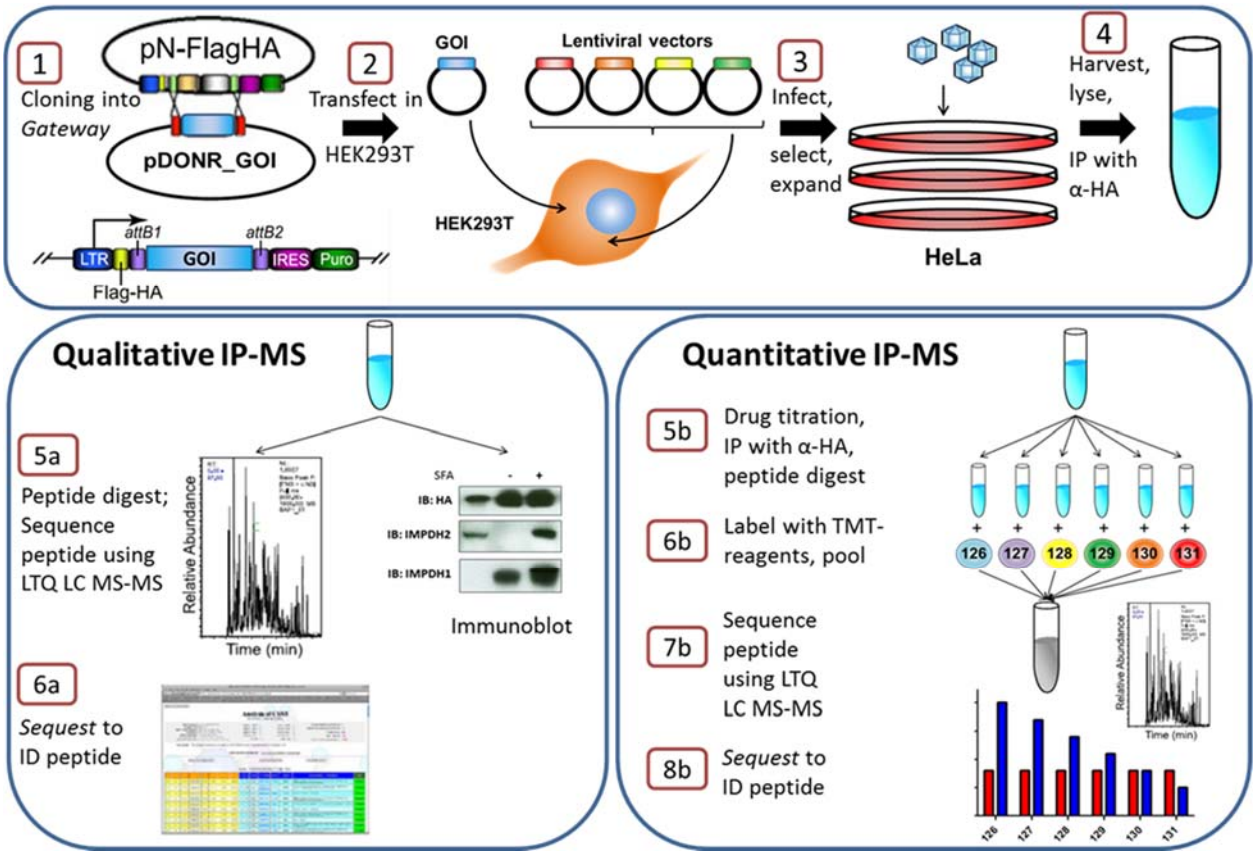

Figure 2.4 – Schematic Overview of the IP-MS Platform for Qualitative and Quantitative Target Identification. Bait proteins were cloned into a modified Gateway vector pDEST_NTAP_FLAG-HA (provided by Dr Mat Sowa) possessing an N-terminal FLAG and HA tag for tandem affinity purification. Constructs were either transiently expressed or stably transduced to make a stable line of interest. Cells overexpressing constructs of interest were expanded, harvested and lysed for immunoprecipitation. Immunoprecipitated proteins can be analyzed by western blotting or by mass spectrometry after peptide digest (qualitative). Digested peptides can also be chemically labeled with TMT-reagents for quantitative mass spectrometry analysis. Figure modified from Reference 21. Details of the procedure are described in the Experimental Procedures section.

Consistent with the above findings, we observed IMPDH enrichment in FLAG-HA-tagged PPIA overexpressing HeLa stable cell line upon SFA treatment assessed by HA immunoprecipitation followed by mass spectrometry and western blot (Figures 2.5A and B). Similar results were seen in IP-MS experiments where this construct was transiently overexpressed in HEK293 cells (data not shown). Increasing IMPDH

peptides were observed with increasing SFA dose from immunoprecipitation in TMT labeling experiments (Figure 2.5C). Although some IMPDH1 peptides were seen, this observation can be attributed to the binning of IMPDH2 peptides into IMPDH1, since a peptide fragment common to more than one isoform of a protein will be added to the isoform that occurs first alphanumerically. Our results show that IMPDH2 interacts with PPIA-SFA.

Figure 2.5

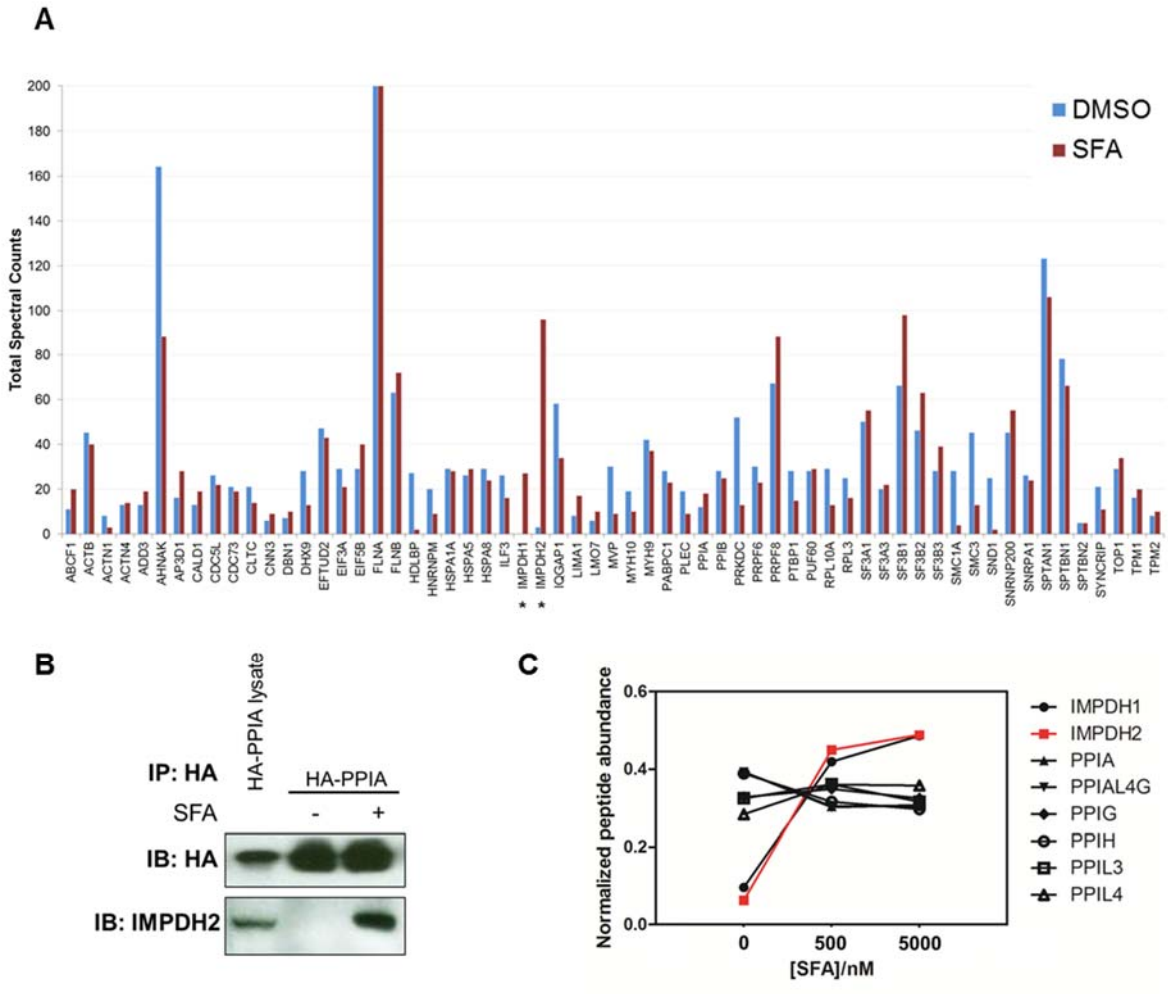

Figure 2.5 (continued) – Results from HA-immunoprecipitation of HA-tagged PPIA. (A) The total spectral counts for the top 60 proteins that were retained in HA-IP with HeLa cells overexpressing the HA-PPIA bait. Total spectral counts for each protein from the two treatment conditions, DMSO (blue) and SFA (red), are shown. IMPDH peptides were specifically enriched (see asterisks) in the SFA treated sample. (B) Immunoprecipitated proteins were directly analyzed by Western Blotting probed with IMPDH2 antibody. (C) TMT labeling experiment showing SFA dose dependent IMPDH peptide enrichment. Control proteins not affected by SFA are shown in black. The presence of IMPDH1 peptides can be attributed to the binning of IMPDH2 peptides into IMPDH1 as a peptide fragment common to more than one isoform of a protein will be added to the isoform that occurs first alphanumerically.

2.3.3 Reciprocal immunoprecipitation Studies with HA-IMPDH

IMPDH1 and IMPDH2 share 84% sequence homology at the protein level and are indistinguishable in their enzymatic function[15], thus we wondered if IMPDH1 could also bind to PPIA-SFA. Toward this end, I overexpressed FLAG-HA tagged IMPDH1 and IMPDH2 in HeLa cells and performed HA immunoprecipitation on these proteins to determine if PPIA is present only in SFA treated cell lysates. Supporting our prior finding that IMPDH2 interacts with PPIA in a SFA dependent manner, PPIA was present only in SFA treated immunoprecipitated IMPDH2 but not IMPDH1, suggesting that the interaction of PPIA-SFA to IMPDH is isoform specific (Figures 2.6A and B). This was further confirmed by Western blotting (Figure 2.6C). GST-PPIA pulldown assays with purified recombinant human IMPDH2 protein showed a SFA dose-dependent interaction with IMPDH2, strongly supporting that the interaction of PPIA with IMPDH2 is highly specific in the presence of SFA (Figure 2.7A). However, GST-PPIA pulldown assays with purified recombinant human IMPDH1 protein showed that there was modest binding of PPIA-SFA to IMPDH1 with no observed IMPDH1 binding at low nanomolar concentrations of SFA, although previous IP-MS and IP-WB experiments seemed to have suggested no interaction with this isoform (Figure 2.7B).

Figure 2.6

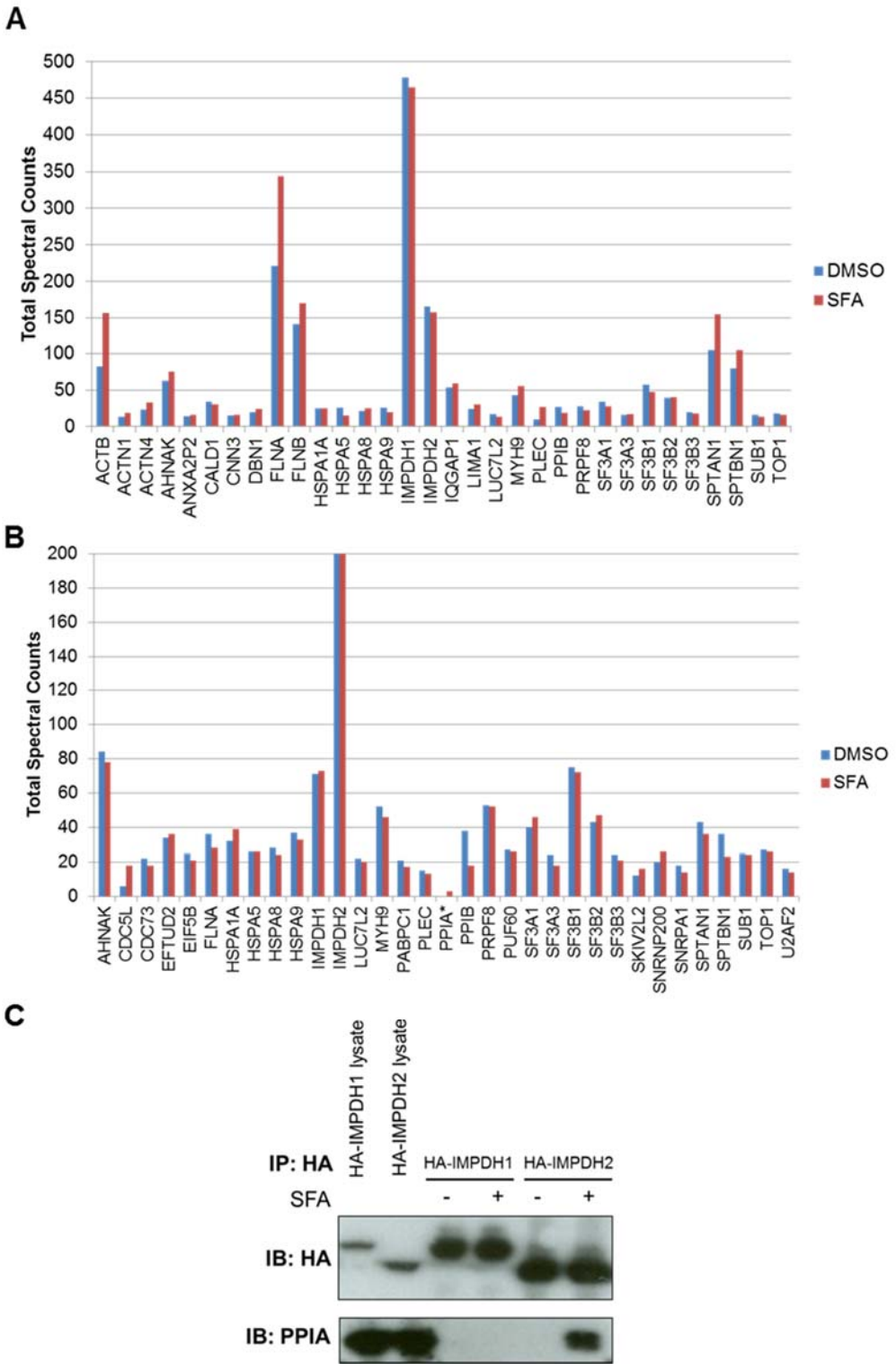
A
Total Spectral Counts
500
450
400
350
300
250
200
150
100
50
0
ACTB
ACTN1
ACTN4
AHNAK
ANXA2P2
CALD1
CNN3
DBN1
FLNA
FLNB
HSPA1A
HSPA5
HSPA8
HSPA9
IMPDH1
IMPDH2
IQGAP1
LIMA1
LUC7L2
MYH9
PLEC
PPIB
PRPF8
SF3A1
SF3A3
SF3B1
SF3B2
SF3B3
SPTAN1
SPTBN1
SUB1
TOP1
DMSO
SFA
B
Total Spectral Counts
200
180
160
140
120
100
80
60
40
20
0
AHNAK
CDC5L
CDC73
EFTUD2
EIF5B
FLNA
HSPA1A
HSPA5
HSPA8
HSPA9
IMPDH1
IMPDH2
LUC7L2
MYH9
PABPC1
PLEC
PPIA*
PPIB
PRPF8
PUF60
SF3A1
SF3A3
SF3B1
SF3B2
SF3B3
SKIV2L2
SNRNP200
SNRPA1
SPTAN1
SPTBN1
SUB1
TOP1
U2AF2
DMSO
SFA
C
HA-IMPDH1 lysate
HA-IMPDH2 lysate
IP: HA
HA-IMPDH1
HA-IMPDH2
SFA
- + - +
IB: HA
IB: PPIA

Figure 2.6 (continued) – Results from HA-immunoprecipitation of HA-tagged IMPDH. (A) Scoring results from HA-tagged IMPDH1 immunoprecipitation. The total spectral counts for the top 32 proteins that were retained in HA-IP with HeLa cells overexpressing the HA-IMPDH1 bait. Total spectral counts for each protein from the two treatment conditions, DMSO (blue) and SFA (red), are shown. No PPIA peptides were detected. (B) Scoring results from HA-tagged IMPDH2 immunoprecipitation. The total spectral counts for the top 32 proteins that were retained in HA-IMPDH1 with HeLa cells overexpressing the HA-IMPDH1 bait. Total spectral counts for each protein from the two treatment conditions, DMSO (blue) and SFA (red), are shown. Only 3 spectral counts for PPIA was detected. (C) Immunoprecipitated proteins were directly analyzed by Western Blotting probed with PPIA antibody.

Figure 2.7

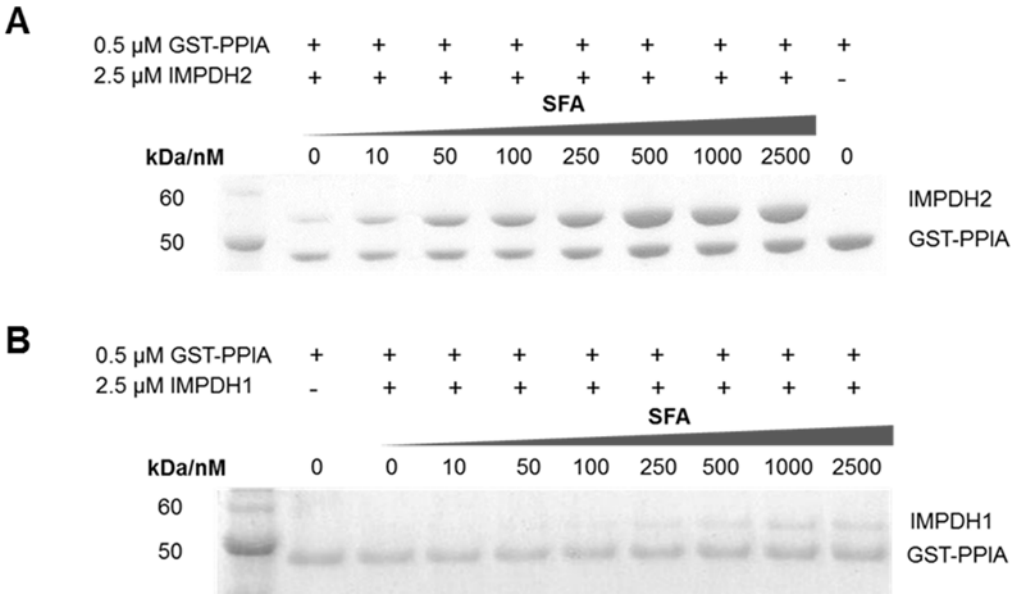

Figure 2.7 – Interaction of PPIA with IMPDH is SFA Dose-dependent. (A) Affinity purification of GST-PPIA showed SFA-dose dependent engagement of recombinantly purified IMPDH2 (B) Affinity purification of GST-PPIA showed modest IMPDH1 interaction in the presence of SFA.

2.3.4 *In vitro* Competition Experiments with CSA

Having established the interaction between PPIA, SFA and IMPDH2, I was curious to know if CSA was able to compete with SFA and disrupt the PPIA-SFA-IMPDH2 ternary complex. CSA binds to PPIA with an affinity of approximately 23nM[18]. Molar excess of CSA was added to a mix of fixed concentration of GST-PPIA, IMPDH2

and SFA (Figure 2.8). CSA was not able to disrupt the ternary complex even at 150-fold molar excess of CSA when SFA was added first (data not shown). This finding came as somewhat a surprise since PPIA-binding ligands, CSA and SFA both bind to the same catalytic cleft prior to ternary complex formation, CSA should be able to interfere with PPIA-SFA-IMPDH2 complex formation. However, when CSA was allowed to incubate with the target proteins before SFA addition, we could observe that CSA is able to prevent PPIA-SFA-IMPDH2 ternary complexation (Figure 2.8). This result reinforced the idea that a PPIA-SFA binding surface is critical for IMPDH2 engagement, and that saturating PPIA binding sites with molar excess of CSA prevented IMPDH2 interaction in the presence of SFA. For reasons not entirely clear at that point, the order of PPIA-binding ligand addition was important as CSA was not able to disrupt formed PPIA-SFA-IMPDH2 ternary complexes. Possible reasons for this observation could be that the off-rate of SFA for PPIA is very slow or that the affinity for PPIA-SFA to IMPDH2 is very high, although kinetic data would be required to validate these hypotheses.

Figure 2.8

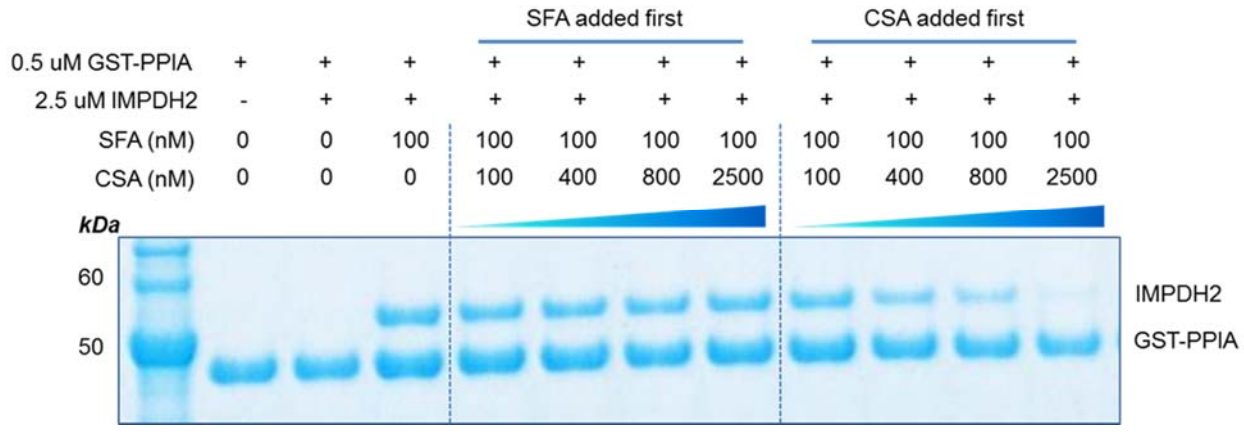

Figure 2.8 – CSA Did Not Disrupt PPIA-SFA-IMPDH2 Ternary Complex. Molar excess of CSA was added to pre-incubated PPIA-SFA-IMPDH2 complex but could not disrupt the formed complex. However, pre-incubating molar excess of CSA prior to SFA addition could prevent PPIA-SFA-IMPDH2 in a CSA dose-dependent fashion.

2.4 Studies with Other Cyclophilin Isoforms

Our collaboration with Dr Sowa has enabled us to look into protein-protein interactions at a broader, proteome-wide level. More specifically, we were interested in using this platform to study how SFA interacts with the entire family of cyclophilin proteins, which exists in about 17 distinct naturally occurring isoforms[16]. We wanted to investigate if there is an isoform other than PPIA that could be the primary interactor with IMPDH2. Additionally, we wondered if there could be other targets that interacted with other cyclophilin isoforms in a SFA dependent manner. Most of this work was done by Dr Stiles and I was assisting him with this part of the project when I joined the Verdine lab as a rotation student.

Figure 2.9

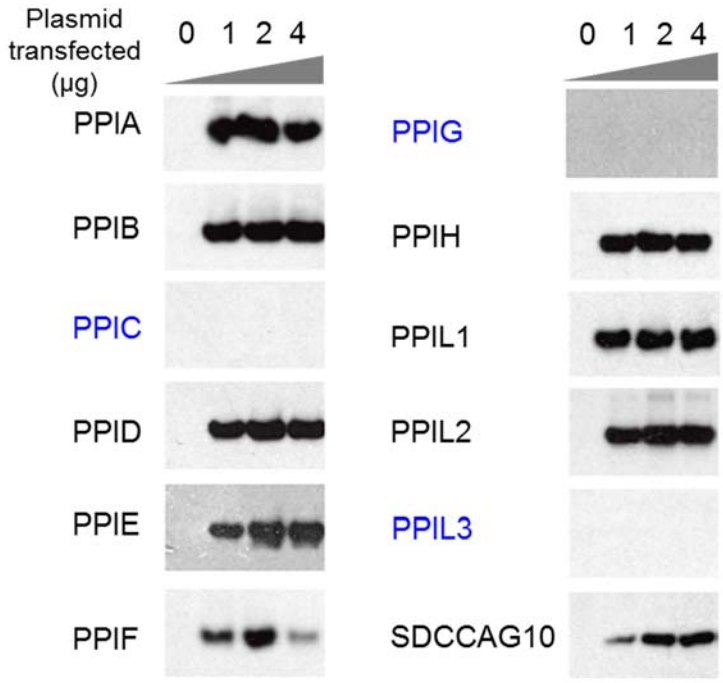

Figure 2.9 – Overexpression of Cyclophilin Isoforms in HEK293. Cyclophilin isoforms transiently overexpressed in HEK293 cells and probed with HA-antibody. Isoforms that failed to express are shown in blue. Figure adapted from Dr Dylan Stiles.

We cloned 12 of the 17 isoforms and tested their expression in HEK293 cells (Figure 2.9). This process allowed us to eliminate 3 isoforms, PPIC, PPIG and PPIL3 that failed to express, so it precluded us from further characterization of these isoforms. Subsequently, the 9 expressing constructs were individually transiently transfected in HEK293 cells. IPs with a sepharose-conjugated anti-HA antibody (Sigma-Aldrich) were performed and retained proteins were analyzed by mass spectrometry following tryptic digest. Of the 9 expressing constructs, only PPIA enriches IMPDH2 in the presence of SFA. No other cyclophilin isoforms tested showed any apparent interaction with IMPDH2 in the presence or absence of SFA. This result suggests that PPIA is likely the main interacting isoform of the 9 that were evaluated (data not shown).

2.5 Surface Plasmon Resonance Assay with SFA

2.5.1 Development of a Cyclophilin Ligand Binding SPR Assay

Initial efforts on surface plasmon resonance (SPR) were focused on developing an assay that would allow the measurement of the dissociation constants between PPIA and PPIA binding ligands. Eventually, the assay would be used to determine the dissociation constants for the formation of the ternary complexes - that is the affinity between PPIA-SFA and IMPDH2 – as an independent measure of IMPDH's interaction with PPIA-SFA.

SPR is the most frequently adopted label-free technology for the real time detection of biomolecular interactions[17]. This assay requires the immobilization of a molecule of interest (called a "ligand" in SPR terminology) to a gold layer sensor surface

attached to a prism. The partner molecule, termed “analyte” is injected over the surface as a continuous flow of solution. SPR results in a reduction of reflected light intensity at a specific angle on the surface[17]. A binding event between the analyte and the immobilized ligand will cause a the change in refractive index close to the sensor surface, which in turn alter the angle of reflected light[17]. This change of angle is directly proportional to the mass of the analyte. An interaction event is recorded as an increase in response units which can be processed to deliver equilibrium binding and kinetic rate constants. There are a variety of ways to immobilize the molecule of interest on the sensor surface either via direct covalent coupling of protein or an antibody or using affinity tags (e.g. oligohistidine, biotin). However, for the SPR assay to accurately measure binding constants, the surface immobilized molecule has to remain active and be stably attached to the sensor surface[18].

Purified hexahistadine PPIA (H6-PPIA) was targeted for capture on an nitrolotriacetic acid (NTA) sensor surface. However, the affinity of the hexahistidine tag for Ni^{2+}-NTA moiety on the sensor chip was very weak (Figure 2.10A). Once the injection phase was stopped, there was a significant and steady baseline drift attributed to the dissociation of H6-PPIA from the chip surface. Thus, the H6-PPIA surface was not suitable for the determination of binding constants of PPIA binding ligands. This problem was remedied by redesigning the PPIA construct, by including additional 6 histidine residues to the existing hexahistidine tag to afford a dodecahistidine tagged PPIA (H12-PPIA). The H12-PPIA construct was cloned, expressed and purified for use in subsequent SPR assays. The H12-PPIA surface exhibited excellent stability with no

baseline drift, even after extended wash periods with buffer post-H12-PPIA injection (Figure 2.10B).

Figure 2.10

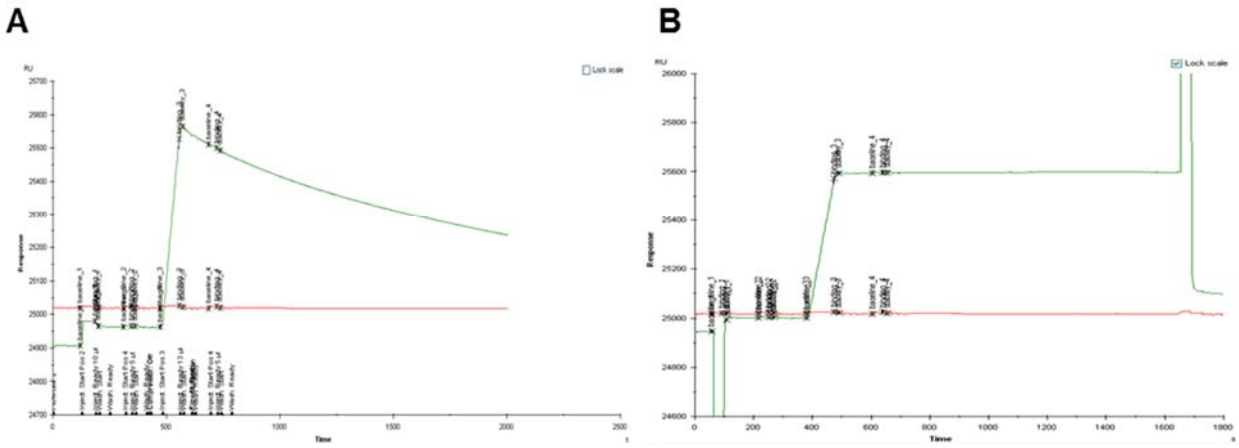

Figure 2.10 – Development of an SPR assay for SFA binding studies. (A) Sensor surface generated by hexaHis-PPIA captured on a Ni^{2+}-NTA sensor chip was not stable as seen by the baseline drift post-injection. (B) DodecaHis-PPIA captured on a Ni^{2+}-NTA sensor chip generated a highly stable surface which was used for determining the binding constants of interacting analytes.

Next, I wanted to assess the activity of the immobilized H12-PPIA on the sensor surface. This was done by using CSA as a control to determine if the K_d value reported previously can be replicated as the interaction between PPIA and CSA has been well characterized[18]. CSA binds to PPIA with a K_d of 26nM (reported K_d=23 ± 6nM), with association and dissociation constants similar to those reported by Wear and colleagues despite differences in sensor surface generation[18] (Figure 2.11A). As expected, no binding was detected with a non-PPIA binding ligand, mycophenolic acid (MPA) (Figure 2.11B).

Figure 2.11

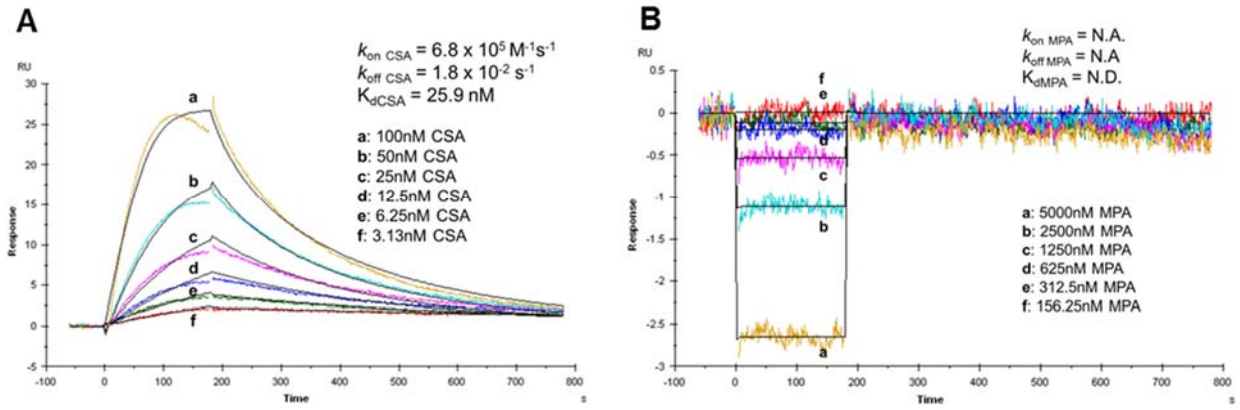

Figure 2.11 – Surface Plasmon Resonance Measurements of the PPIA and CSA/MPA Interactions. His12-PPIA was immobilized on a NTA chip and (A) CSA and (B) MPA were injected at increasing concentrations. Data was globally fitted to a model of a 1:1 complex. Details of the procedure are described in the Experimental Procedures section.

2.5.2 Determining K_d for SFA binding to PPIA

To date, the interaction between PPIA and SFA has not been characterized by SPR. Previous studies reported SFA as having an affinity for PPIA 20-60 fold higher than CSA[8]. However, those binding affinities were assessed in competitive ELISA formats and thus do not accurately reflect the true K_d of PPIA with its ligands. The active and stabilized H12-PPIA sensor surface was used to characterize the interaction between PPIA and SFA. Globally fitting a model where a 1:1 complex is formed between H12-PPIA and SFA gave excellent fits. Analysis of the data showed that SFA binds to PPIA with extremely high affinity, K_d = 0.2 ± 0.1 nM with on and off rates of 1.0 ± 0.2 × 10^6 $M^{-1}s^{-1}$ and 1.9 ± 0.8 × 10^{-4} s^{-1} respectively (Figure 2.12).

Figure 2.12

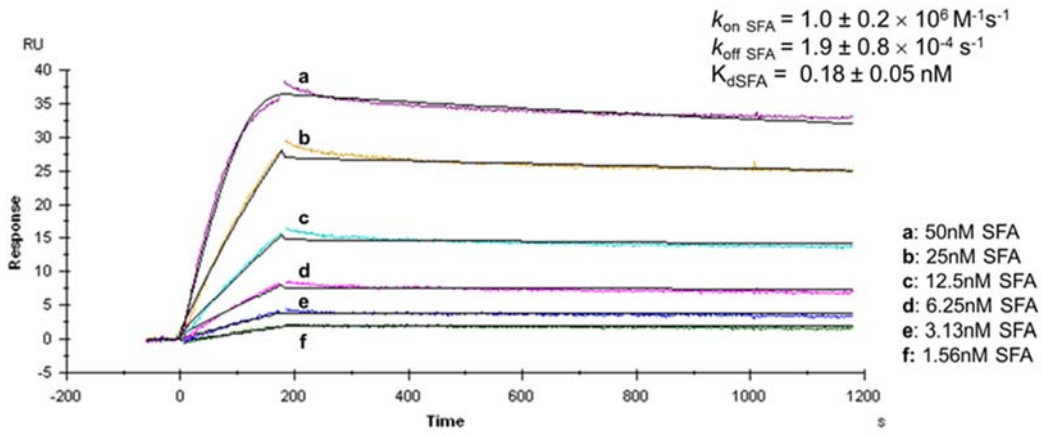

Figure 2.12 – Surface Plasmon Resonance Measurements of the PPIA and SFA Interaction. His12-PPIA was immobilized on a NTA chip and SFA was injected at increasing concentrations. Data was globally fitted to a model of a 1:1 complex. Details of the procedure are described in the Experimental Procedures section.

The exceptionally high affinity of SFA for PPIA, largely attributed by its extremely slow off rate challenges the assertion that the effect of SFA is PPIA-independent. Our prior data suggested that CSA cannot outcompete SFA once a ternary complex is formed and this finding would be expected given that SFA has an affinity to PPIA in the picomolar range. Previous reports have shown that CSA and non-immunosuppressive CSA analogues failed to diminish the activity of SFA in cells[8,12,13]. The use of CSA to saturate PPIA binding sites in cells presents two major concerns. One is that CSA itself exhibits immunosuppressive activity, and second, CSA's ability to compete with SFA for PPIA to mask SFA's effect is restricted by its affinity for PPIA, thus would undermine a conclusion asserting that SFA exerts its effect through a PPIA independent pathway. Given that SFA binds to PPIA with picomolar affinity, it would not be reasonable to expect that CSA, a much weaker ligand for PPIA (an affinity of at least 120 fold lower than SFA), would not be able to negate the effects of SFA when competed at 10-100

fold in some of the competition assays previously described[8,12,13]. Although the non-immunosuppressive analogue 4-Cs exhibits greater affinity for PPIA than CSA, it remains to be determined if 4-Cs could disrupt a PPIA-SFA-IMPDH2 complex although it reportedly does not impair SFA activity[8,13].

2.5.3 Efforts Toward Determining K_d for PPIA-SFA Binding to IMPDH2

The determination of the dissociation constant for PPIA-SFA to IMPDH2 proved to be extremely challenging. Non-specific binding was detected when purified IMPDH2 was flowed over a nickel charged NTA chip. Subsequently, it was found that the non-specific binding could be attributed to miniscule amounts of his-tagged IMPDH2 that resulted from incomplete TEV cleavage of the his-tag on the construct. Despite making several more preparations of IMPDH2 using more TEV for tag cleavage and extending the duration of TEV cleavage, IMPDH2 still attached non-specifically on the sensor surface. Reverse nickel purification of IMPDH2 to remove residual his-tagged IMPDH2 was met with little success. IMPDH2 exists as a homotetramer in solution and as a result, reverse nickel purification retained most of the IMPDH2 in the column with little tagless IMPDH2 eluting from the flow through.

In a second approach, PPIA was directly coupled to a GLC chip (Biorad) via amine coupling. While this would circumvent the problem of his-tagged IMPDH2 attaching to the NTA chip, direct coupling of PPIA to the sensor chip will not afford a homogenous binding surface. Although PPIA coupled well to generate a stable sensor surface, the surface was not amenable to the harsh regeneration conditions between each run. Further optimization would be required to figure out the regeneration

conditions suitable for this assay format, so this strategy was not pursued further. Efforts to capture GST-PPIA fusion protein using an anti-GST antibody immobilized on the chip surface is currently being explored at the time of writing.

2.6 Efforts in Obtaining a Crystal Structure of the PPIA-SFA-IMPDH2 Ternary Complex

Upon the discovery that PPIA binds to IMPDH2 in the presence of SFA, an intense amount of attention was put into obtaining an X-ray crystal structure of a ternary complex. Dr Stiles, who worked in collaboration with a former post-doc Brian Bowman, was the driving force behind this heroic crystallography effort. Their efforts yielded complex crystals with both protein components present, as evidenced by analyzing the crystal by SDS-PAGE and silver staining (data not shown). Although the crystal diffracted, no electron density was observed from PPIA nor SFA and only the core tetrameric structure of IMPDH2 could be modeled by molecular replacement (data not shown). To confirm that PPIA was indeed in the crystal, crystals were grown with selenomethionine-containing PPIA. A strong fluorescent signal was observed when these crystals were scanned with X-rays at the absorption edge of selenium (data not shown). This unambiguously confirmed the presence of PPIA in the crystal. However, only electron density from the core of IMPDH2 could be seen and modeled (data not shown).

Since efforts focused on obtaining a crystal via the mixing the components of the complex in a drop have not given a crystal that diffracted well, I sought a different strategy for our crystallization screen. I sought to first isolate a homogenous complex by

size exclusion chromatography (SEC) (discussed in more detail in Chapter 2.7) before setting up crystal trays. Prior to that, I revisited the purification protocol for IMPDH2. The original recombinant IMPDH2 purification protocol involves the Ni^{2+}-affinity chromatography of the hexahis-Trx-IMPDH2 construct, cleavage of Trx-tag with TEV and anion exchange chromatography to afford IMPDH2 for crystallography (Figure 2.13A). While previous attempts at purifying IMPDH2 by SEC was met with little success, I found that it was possible to purify IMPDH2 by SEC to obtain a purer prep of recombinant IMPDH2 that was still active (Figure 2.13B). With this revised IMPDH2 purification protocol, I sought to grow ternary complex crystals by mixing PPIA, IMPDH2 and SFA at varying molar ratios, allowing them to incubate overnight, and concentrating to approximately 5mg/ml before setting up a crystal screen. On visual inspection, two screening conditions yielded crystals that looked suitable for data collection (Figure 2.13C). These crystals were taken to Argonne National Laboratory (ANL) and were found to diffract to ~1.5Å. The data set was found to be similar to that of a dimeric PPIA-SFA complex and based on unit cell parameters, it was not possible for an asymmetric unit to accommodate a ternary complex structure. Thus, molecular replacement was not pursued.

Figure 2.13

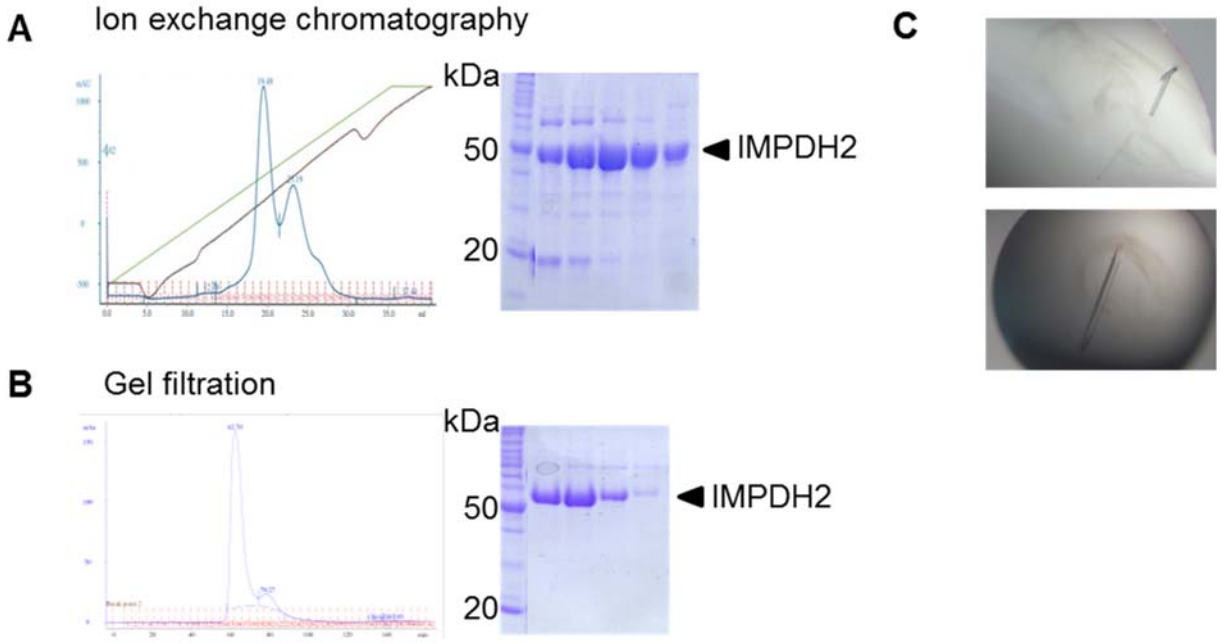

Figure 2.13 – Purification of Recombinant IMPDH2 and Complex Crystal Hits. (A) Ion exchange chromatography profile of IMPDH2 following elution from nickel resin and TEV cleavage and SDS-PAGE of IMPDH2 containing fractions from this purification step. (B) Gel filtration trace of IMPDH2 following ion exchange chromatography and SDS-PAGE of IMPDH2 fractions after gel filtration. (C) Crystals obtained when screening for conditions that would give a ternary complex.

2.7 Efforts to Isolate the PPIA-SFA-IMPDH2 Complex

In another attempt to provide independent evidence for a PPIA-SFA-IMPDH2 complex and to facilitate crystallography efforts towards solving the structure of a ternary complex, we sought to isolate a homogenous complex via SEC. Briefly, recombinant PPIA, IMPDH2 and SFA were combined to allow complex formation before running the mix through an analytical gel filtration column (10/300 Superdex 200, GE Healthcare).

In principle, injecting the pre-incubated complex through a SEC column would result in a complex peak eluting at an earlier volume and also the disappearance or

reduction in the PPIA peak. Since the binding stoichiometry of PPIA, SFA and IMPDH2 is unknown, varying ratios of each component were experimented to determine a stoichiometry that would yield a complex.

Interestingly, a complex peak was not observed but instead the appearance of a peak at 16.5ml elution volume was seen (Figure 2.14Ai). This peak turned out to be a PPIA-SFA dimer as determined by analyzing those fractions on an SDS-PAGE gel (data not shown). The retention volumes for homotetrameric IMPDH2, dimeric PPIA-SFA and monomeric PPIA were 8, 16.5 and 18.5mL respectively. Injecting PPIA alone preincubated with either DMSO or SFA showed dimer formation only in the SFA treated PPIA sample (Figure 2.14Aii and iii). Addition of two fold molar excess of SFA and overnight incubation of complex also did not yield a ternary complex peak as determined by SEC and blotting of the fractions with PPIA and IMPDH2 antibodies (Figure 2.14Aiv and B). The finding that PPIA-SFA exists as a dimer in solution has been reported[11]. Data supported by SEC, dynamic light scattering (DLS) and the X-ray crystal structure of PPIA-SFA showed an “intimate” dimer of two PPIA-SFA complexes in crystal and in solution, providing biophysical evidence suggesting that the dimeric PPIA-SFA complexes could be the active species mediating the immunosuppressive effect of SFA[11]. The inability to isolate a ternary complex via SEC could suggest that the affinity of PPIA-SFA to IMPDH2 is weak, perhaps in the μM range or higher. The dilution effect caused by the gel filtration buffer after complex sample injection, could in principle cause the complex to fall apart if the concentration of IMPDH2 in the sizing column is less than the affinity of IMPDH2 to PPIA-SFA. This could be a likely scenario, given our results from prior crystallography efforts with selenomethionine-containing crystals,

which yielded a complex crystal when components were at sufficiently high concentrations (>12mg/ml).

Figure 2.14

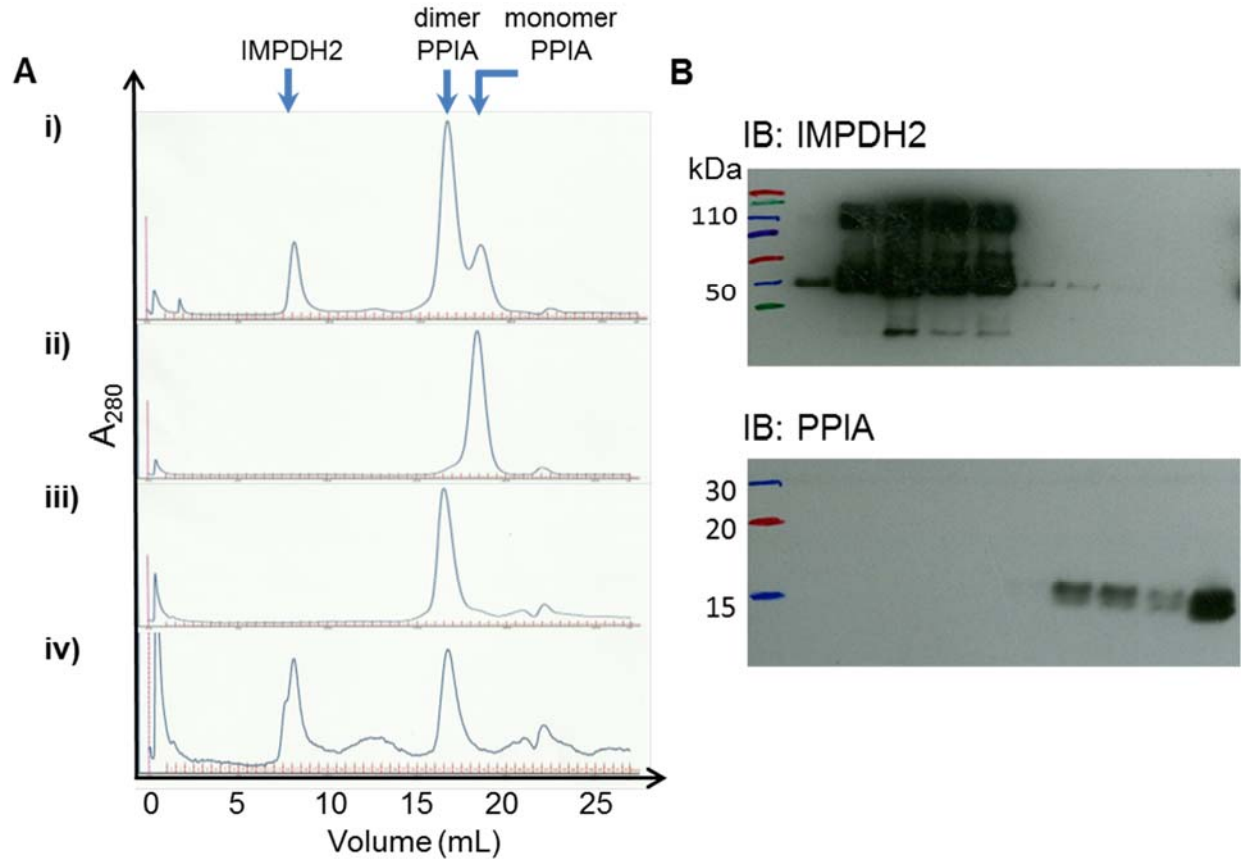

Figure 2.14 – Isolation of a PPIA-SFA-IMPDH2 Complex via Size Exclusion Chromatography. (A) Recombinant PPIA, IMPDH2 and SFA were combined to allow complex formation before running the mix through an analytical gel filtration column (i) PPIA + IMPDH2 + SFA, 1 hr (ii) PPIA + DMSO (iii) PPIA + SFA (iv) PPIA + IMPDH2 + SFA, overnight. (B) Western blot of peak fractions collected from (iv), probed with anti-IMPDH2 and anti-PPIA antibodies, showed no fractions where the two proteins coexist.

The ability of CSA to interfere with PPIA-SFA dimer formation was investigated. Previously, it was shown that CSA was not able to disrupt formed PPIA-SFA-IMPDH2 complex and data from SPR revealed a very slow SFA off rate with PPIA. Taken together, previous data would strongly predict that CSA will not be able to disrupt PPIA-

SFA dimer formation. In designing this competition assay, an optimal amount of SFA used to induce PPIA dimerization was determined by first titrating SFA into PPIA. As expected, SFA induced PPIA dimerization in a SFA dose-dependent manner (Figure 2.15A). Since a decent dimeric-PPIA A_{280} signal was observed with 12μM SFA, this fixed amount was added to PPIA to induce dimerization and up to 24 fold molar excess of CSA was added to the mix. A 6μM SFA treated PPIA was injected as a control to allow comparison between the different elution profiles. Should CSA interfere with PPIA-SFA dimer formation, a decrease in the intensity of A_{280} signal of the dimeric peak would be observed.

Figure 2.15

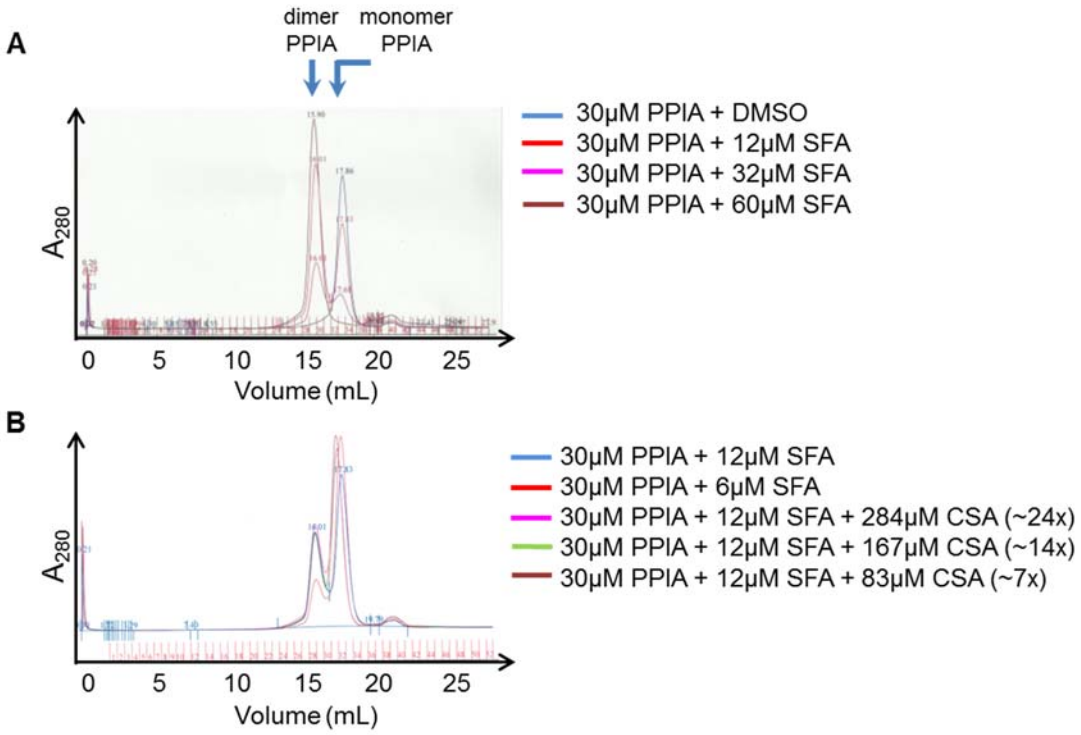

Figure 2.15 – Investigating PPIA dimerization by SFA. (A) Recombinant PPIA and varying concentrations of SFA were combined to allow complex formation before running the mix through an analytical gel filtration column. SFA promotes PPIA dimerization in a dose-dependent manner. (B) Competition experiments where molar excess of CSA was added to the PPIA-SFA mix. CSA was not able disrupt PPIA-SFA dimers at the CSA concentrations tested.

The PPIA-SFA dimer complex appeared to be resistant to disruption by CSA as dimeric PPIA-SFA peaks were superimposable regardless of the amount of CSA added to the sample, at approximately 24 fold excess of CSA (Figure 2.15B). This data indirectly challenges the notion that the immunosuppressive effect of SFA is PPIA independent and is consistent with our binding data - both with SPR and competition with CSA – which showed an exceptionally high affinity for SFA to PPIA and that CSA was neither able to abrogate PPIA-SFA dimerization nor impair the PPIA-SFA-IMPDH2 complex. Though speculative, it is not entirely inconceivable for the dimer of PPIA-SFA to mediate the immunosuppressive effects of SFA[11].

Since a complex was not observed with untagged recombinant PPIA, IMPDH2 and SFA, I wondered if I could isolate a complex with GST-PPIA, the original bait used for earlier GST-affinity purification. As with untagged PPIA, no complex peak could be observed when GST-PPIA was co-incubated with IMPDH2 and SFA. Fractions were analyzed on SDS-PAGE followed by coomassie staining showed no fractions where the two proteins coexist (data not shown). SFA still induced the dimerization of GST-PPIA (Figure 2.16).

Figure 2.16

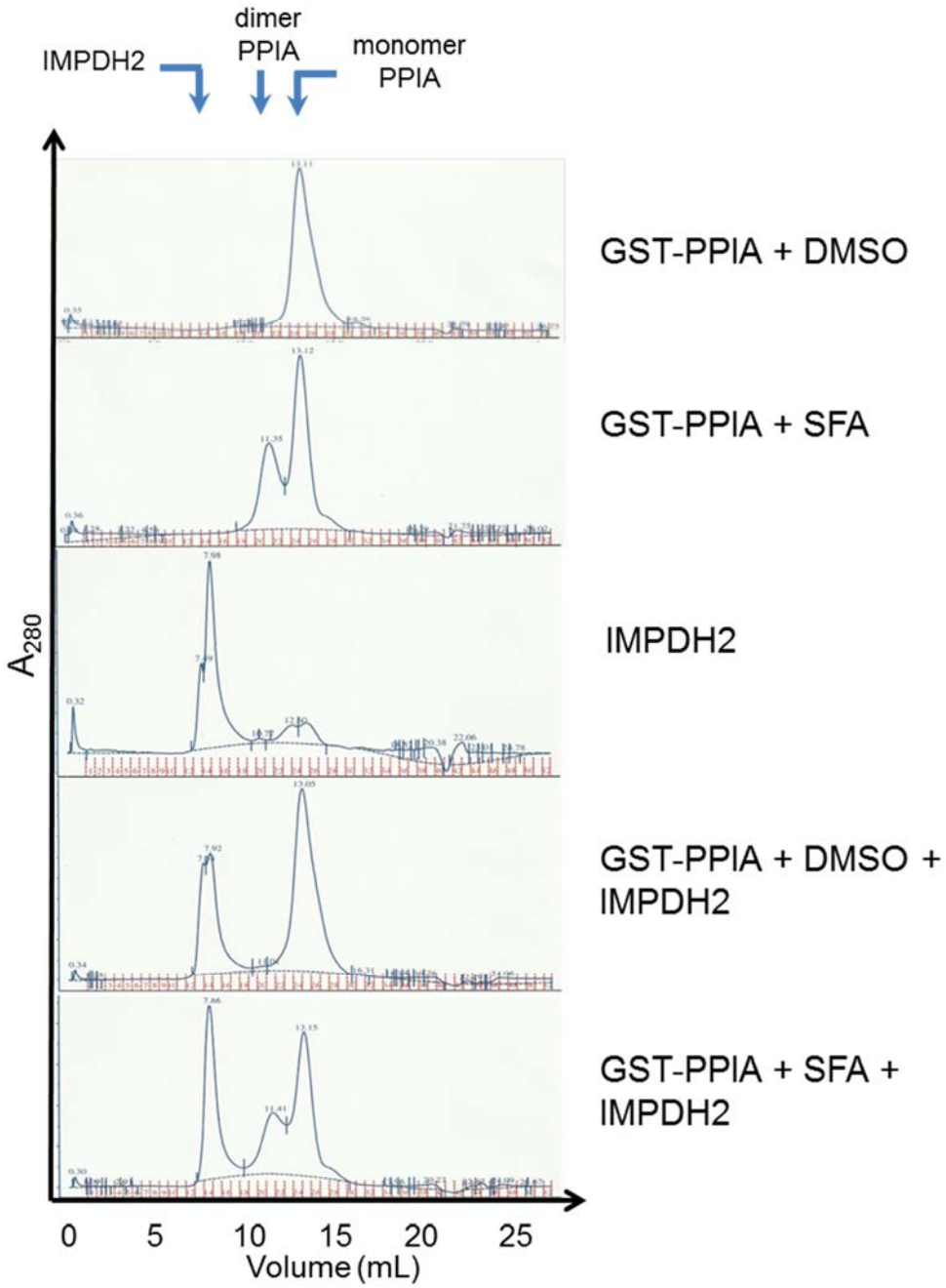

Figure 2.16 – Isolation of a GST-PPIA-SFA-IMPDH2 Complex via Size Exclusion Chromatography. Recombinant GST-PPIA and/or IMPDH2 and/or SFA/DMSO were combined to allow complex formation before running the mix through an analytical gel filtration column.

2.8 Cellular Thermal Shift Assays with SFA

Thermal shift assays are extensively used for characterization of ligand binding in structural biology and drug screening. However, such assays have been applied largely to purified proteins. Molina *et al.* recently developed a protocol, termed cellular thermal shift assay (CETSA), which is found on the basic biophysical principle that target proteins are thermally stabilized upon target engagement[19]. This method involves heating multiple aliquots of cell lysates to different temperatures, allowing them to cool and centrifuging samples to separate soluble fractions from precipitated proteins. The presence of the target protein in the soluble fraction is quantified by Western blotting[19]. More recently, CETSA has been used in combination with quantitative mass spectrometry to study the effect of drugs on the thermal profiles of cellular proteomes. This provides a novel and unbiased measure of specific and non-specific drug-target engagement, enabling the identification of targets involved in drug efficacy and toxicity[20].

While proof-of-concept studies by Molina and colleagues validated drug binding for several important clinical targets using the CETSA method, I was curious to know if this method could be extended to identify and validate targets involved in ternary interactions – such as PPIA-SFA ligand stabilizing IMPDH2. HEK293 cells were lysed and lysates were incubated with SFA, CSA, FK506 and DMSO. The lysates from each treatment were split into 9 equal fractions, with each fraction heated to a specified temperature in a thermal cycler. The heated lysates were snapped frozen, thawed and centrifuged to obtain the soluble protein fraction from each sample and probed with IMPDH2, calcineurin, PPIA and FKBP12 specific antibodies via Western blotting.

No observable stabilization of IMPDH2 and calcineurin could be seen when lysates were treated with SFA or CSA/FK506 respectively (Figure 2.17 A&B). However, SFA is found to significantly stabilize PPIA as PPIA still remained in the soluble fraction at 61^{o}C while CSA was seen to mildly stabilize PPIA compared to DMSO treatment (Figure 2.17C). It was unclear if FKBP12 was stabilized by FK506 as assessed by CETSA since FKBP12 remained soluble when heated up to 64^{o}C under all treatment conditions (Figure 2.17D). Based on the data gleaned from SFA and CSA, the CETSA method did not seem to be compatible for identifying targets involved in ternary interactions. A likely reason for this incompatibility is that at a certain high temperature, the drug-isomerase complex dissociates from its target but does not promote target unfolding and aggregation.

Figure 2.17

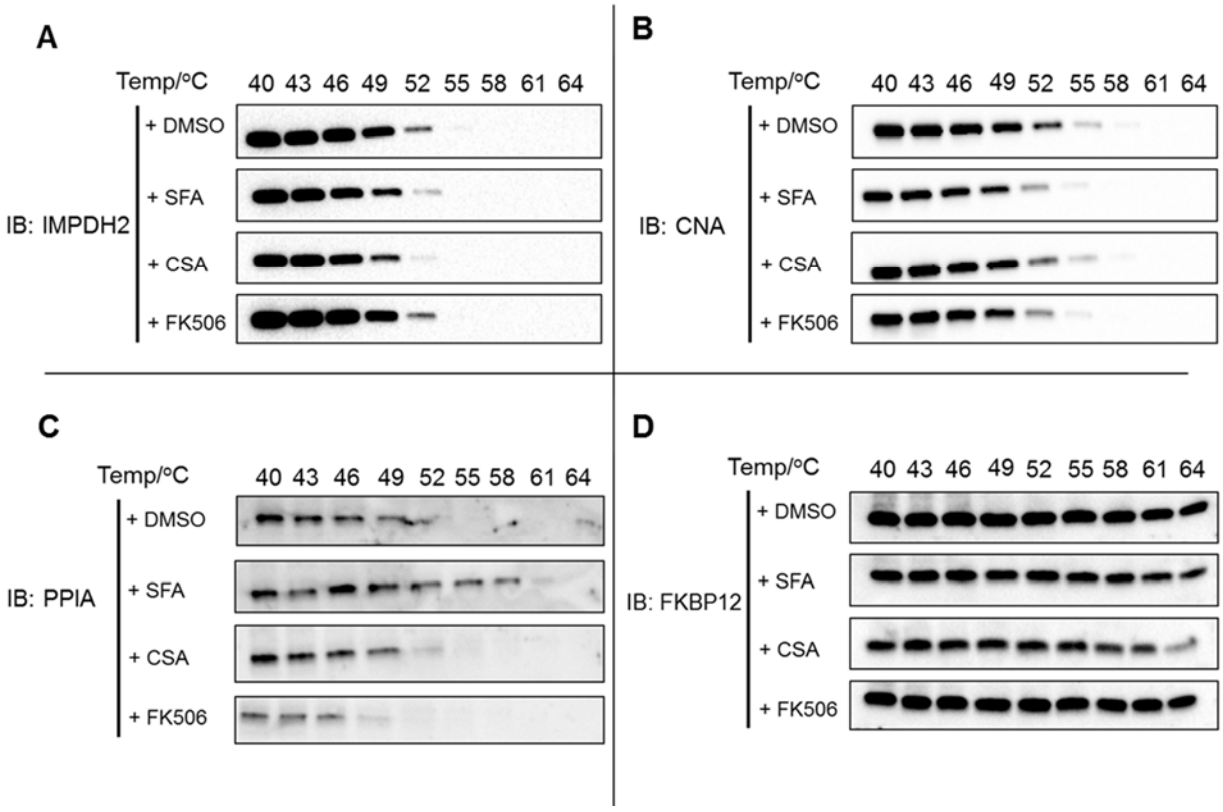

Figure 2.17 (continued) – Cellular Thermal Shift Assays with Immunophilin Binding Ligands. Compounds were incubated with HEK293 lysates and evaluated for their ability to stabilize their targets by a thermal shift assay analyzed by western blotting. (A) Lysates probed with anti-IMPDH2 antibody. (B) Lysates probed with anti-calcineurin antibody. (C) Lysates probed with anti-PPIA antibody. (D) Lysates probed with anti-FKBP12 antibody. Details of the procedure are described in the Experimental Procedures section.

2.9 Conclusions

Using direct biochemical methods, we have shown that IMPDH2 interacts with PPIA-SFA, and that this interaction is highly isoform specific. This finding was validated with qualitative and quantitative mass spectrometry. Studies with other naturally occurring cyclophilin isoforms suggest that PPIA is the primary mediator for SFA binding to IMPDH2 among those isoforms that we have evaluated. The binding constants for SFA to PPIA have been determined by SPR although attempts to elucidate the binding constants for the ternary complex have been met with technical limitations. There is substantial value to troubleshoot this assay to validate and fully characterize these interactions. Alternatively, isothermal calorimetry (ITC) can be employed obtain the binding constants for ternary complex formation. The determination of the binding constants of the ternary complex would offer an explanation the findings observed in SEC. Although we were unable to isolate a homogenous complex by SEC, we speculate that this is likely due to the weak affinity of PPIA-SFA to IMPDH2 and efforts are underway to characterize the binding constants for this ternary complex. In addition, since SEC separates biomolecules based on their size and shape, it is possible that the shape of the complex is not amenable to SEC. The remarkably high affinity of SFA for PPIA explains why CSA (at the concentrations tested) was not able to disrupt dimeric

PPIA-SFA or impair PPIA-SFA-IMPDH2 formation. A crystal structure for the ternary complex has remained elusive although we have evidence showing the presence of protein complex components in the crystal.

The following chapter discusses preliminary mechanism of action studies and more in-depth investigation of the mode of PPIA-SFA binding to IMPDH2. A section is also devoted to the structure-activity relationship of SFA.

Experimental Procedures

General Methods and Chemicals

Oligonucleotide primers were ordered from Eurofins MWG Operon or Integrated DNA Technologies. PCR was performed with Phusion High-Fidelity DNA Polymerase (Life Technologies) and purified with a PCR cleanup kit (Qiagen or Zymo Research). Absorbance measurements were performed with a NanoDrop 2000C spectrophotometer (ThermoScientific). Mini-PROTEAN® TGX Stain-Free™ polyacrylamide gels (Bio-Rad, Hercules, CA), Mini-PROTEAN Tetra cell electrophoresis chamber with Tris/Glycine/SDS running buffer (Bio-Rad, Hercules, CA) were used for protein analysis. Proteins were transferred to polyvinylidene difluoride (PVDF) membranes using Trans-Blot® Turbo™ (Bio-Rad, Hercules, CA) for blotting. SFA was a generous gift from Novartis. CSA, DMSO and polybrene were ordered from Sigma-Aldrich.

Cell Culture Information

Human cancer cell lines K562 (a kind gift from the Saghatelian lab ATCC No. CCL-243), H23 (ATCC No. CRL-5800), H358 (ATCC No. CRL-5807), H1568 (ATCC No. CRL-5876), H2122 (ATCC No. CRL-5985) and Jurkat (ATTC No. TIB-152) were cultured in RPMI-1640 medium (Gibco/Life Technologies); PANC-1 (ATCC No. CRL-1469), HEK-293 cells (ATCC No. CRL-1573), HeLa (ATCC No. CCL-2) and HCT 116 (ATCC No. CCL-243) were maintained in Dulbecco's Modified Eagle Medium (Gibco/Life Technologies). All culture media were supplemented with 10% fetal bovine serum (FBS,

Gibco/Life Technologies, Carlsbad, CA, USA), 100 units/mL penicillin and 100 units/mL streptomycin (Gibco/Life Technologies).

Western Blotting

Cells were lysed with RIPA buffer (50mM Tris pH8, 150mM NaCl, 0.1% SDS, 0.5% sodium deoxycholate, 1% NP40, 1mM EDTA and protease and phosphatase inhibitor cocktail [Roche]). For western blotting, the following antibodies were used: anti-IMPDH2 (Ab-131158, 1:1000) and anti-IMPDH1 (Ab-55297, 1:1000) were from Abcam. Anti-PPIA (CST 2175, 1:1000) and anti-calcineurin (CST 2614, 1:1000) were from Cell Signaling Technology. Anti-HA (H3663, 1:1000) was from Sigma-Aldrich.

Cell Proliferation Assays

K562 (8000 cells), Jurkat (10^4 cells), H23 (8000 cells), H358 (8000 cells), H1568 (8000 cells), H2122 (8000 cells), PANC-1 (8000 cells), HCT-116 (8000 cells) and HeLa (10^4 cells) were seeded in opaque white 96-well tissue culture plates (for CellTiter-Glo assay – Promega). Cells were placed at 37^{o}C/5% CO_2 overnight prior to compound treatment. Compounds were diluted in respective complete growth medium and serial 2-fold dilutions were prepared for dose-response experiments. Compounds were added to wells in triplicate. The plates were incubated at 37^{o}C/5% CO_2 for 48 hours and CellTiter-Glo assay was performed in accordance to manufacturer's protocol with luminescence detected by Spectromax M5. The relative cell number was calculated by normalization against wells treated with DMSO only.

Cell Cycle Analysis

Cell cycle analysis by FACS was performed in accordance to previously published protocol[14]. HCT-116 were serum starved with 0.1% FBS DMEM for 48 hours. Cells reached about 60% confluency after treatment with compounds. Cells were harvested by trypsinization and pelleted by centrifuging at 200 x *g*. Cells were fixed in 2ml of cold absolute ethanol dropwise while mixing at 4^{o}C for 1 hour. Then, the cells were washed twice with cold PBS and resuspended in 0.76ml of PBS containing 5µl of RNase (RNase stock 50µg/ml in PBS) and 20µl of propidium iodide (PI stock 2.5mg/ml in PBS). Cell suspension was incubated in the dark for 15 minutes and kept at 4^{o}C until FACS analyses. Cells were filtered through a FACS tube before propidium iodide fluorescence of individual nuclei was determined using Becton-Dickson LSR II instrument. Cell cycle distribution was analyzed with FlowJo software.

Recombinant Protein Expression and Purification

Recombinant IMPDH Expression and Purification

IMPDH constructs (Trx-His$_6$-IMPDH1, Trx-His$_6$-IMPDH2) were cloned in a pET32 bacterial overexpression vector. pET32-IMPDH was transformed into Rosetta 2 DE3 chemically competent cells (Novagen) and an overnight starter culture from a single colony was grown at 37^{o}C in LB under carbenicillin selection. 5mL of overnight starter culture was used to inoculate 1L of LB with carbenicillin, grown to OD_{600} of approximately 0.8, induced with 500µM of IPTG for 18 hours at 18^{o}C, then harvested and resuspended in 40mL IMPDH lysis buffer (500mM NaCl, 50mM sodium phosphate

pH 8.0, 10mM imidazole, 10% glycerol and 5mM BME) prior to flash freezing in liquid nitrogen and stored at -80^{o}C. To purify IMPDH constructs, cells were thawed and supplemented with 1mM PMSF. Cells were lysed using a sonicator (Virsonic) with indicated settings: power level of 6.5 for 4mins, with 10s on and 15s off cycles. Clarified lysates were obtained after centrifugation at 14,000rpm for 40 minutes at 4^{o}C. 1.5ml of Ni-NTA agarose resin (Qiagen) was added to a column with the clarified lysate and incubated for 1 hour in the cold room. The flow through was drained and the resin was washed twice with 50ml IMPDH wash buffer (300mM NaCl, 20mM sodium phosphate pH 8.0, 40mM Tris pH 8.0, 5mM imidazole, 10% glycerol and 5mM BME). The bound protein was eluted twice with 5ml of IMPDH elution buffer (300mM NaCl, 20mM sodium phosphate pH 8.0, 40mM Tris pH 8.0, 250mM imidazole, 10% glycerol and 5mM BME) and diluted two fold with a dilution buffer (20mM sodium phosphate pH 8.0, 40mM Tris pH 8.0 and 5mM BME). 1ml of TEV protease(~0.375mg/ml in 50% glycerol) was added to the diluted eluted protein and left in the cold room for overnight digestion. Another 1ml of TEV was added 24 hours later and allowed for another 24 hours of TEV digestion. Samples from nickel column purification and TEV digestion were evaluated by SDS-PAGE. The length of TEV incubation may vary depending on the efficiency of the digestion. Following cleavage of the Trx tag by TEV, the protein was purified by anion exchange chromatography using a HiTrapQ column (GE Healthcare), eluting with a gradient from 30 to 480mM NaCl with 25mM Tris pH 8.0, 10% glycerol and 5mM BME. Proteins were further purified by size exclusion chromatography on a Superdex 200 HiLoad16/600 column (GE Healthcare) into 20mM Tris pH 7.4, 200mM NaCl, 10% glycerol and 1mM BME. For long term storage, proteins were concentrated to ~1mg/ml

with a 10kDa MWCO concentrator (Millipore), snap-frozen in liquid nitrogen and stored at -80^{o}C.

Recombinant GST-PPIA Expression and Purification

PPIA was cloned into a pET41 bacterial overexpression vector to the C-terminal end of GST (in the vector backbone) via ligation independent cloning (Novagen). pET41-GST-PPIA was transformed into Rosetta 2 DE3 chemically competent cells (Novagen) and an overnight starter culture from a single colony was grown at 37^{o}C in LB under kanamycin selection. 5mL of overnight starter culture was used to inoculate 1L of LB with kanamycin, grown to OD_{600} of approximately 0.8, induced with 500μM of IPTG for 18 hours at 18^{o}C, then harvested and resuspended in 40mL lysis buffer (500mM NaCl, 20mM sodium phosphate pH 8.0, 40mM Tris pH 8.0, 10mM imidazole and 5mM BME) prior to flash freezing in liquid nitrogen and stored at -80^{o}C. To purify GST-PPIA, cells were thawed and supplemented with 1mM PMSF. Cells were lysed using a sonicator (Virsonic) with indicated settings: power level of 6.5 for 4mins, with 10s on and 15s off cycles. Clarified lysates were obtained after centrifugation at 14,000rpm for 40 minutes at 4^{o}C. 1.5ml of Ni-NTA agarose resin (Qiagen) was added to a column with the clarified lysate and incubated for 1 hour in the cold room. The flow through was drained and the resin was washed twice with 50ml wash buffer (500mM NaCl, 20mM sodium phosphate pH 8.0, 40mM Tris pH 8.0, 10mM imidazole and 5mM BME). The bound protein was eluted twice with 5ml of elution buffer (500mM NaCl, 20mM sodium phosphate pH 8.0, 40mM Tris pH 8.0, 250mM imidazole, and 5mM BME). The elutes were pooled and then purified by anion exchange chromatography using a HiTrapQ column (GE Healthcare),

eluting with a gradient from 30 to 650mM NaCl with 25mM Tris pH 8.0, and 5mM BME. Proteins were further purified by size exclusion chromatography on a Superdex 75 HiLoad16/600 column (GE Healthcare) into 25mM Tris pH 7.4, 200mM NaCl and 5mM BME. For long term storage, proteins were concentrated to ~1mg/ml with a 10kDa MWCO concentrator (Millipore), snap-frozen in liquid nitrogen and stored at -80^{o}C.

Recombinant His12-PPIA Expression and Purification

Full length PPIA was cloned into a modified pET30a vector engineered to have a His12 tag (a gift from WarpDriveBio LLC). pET30a-His12-PPIA was transformed into Rosetta 2 DE3 chemically competent cells (Novagen) and an overnight starter culture from a single colony was grown at 37^{o}C in LB under kanamycin selection. 5mL of overnight starter culture was used to inoculate 1L of LB with kanamycin and allowed to reach OD_{600} of approximately 0.8 before induction with 500μM of IPTG for 18 hours at 18^{o}C. The cells were harvested and resuspended in 40mL P300 lysis buffer (10 mM Na_2HPO_4, 2 mM KH_2PO_4, 2.7 mM KCl, 300 mM NaCl and 1mM TCEP) prior to flash freezing in liquid nitrogen and stored at -80^{o}C. For purification, cells were thawed and supplemented with 1mM PMSF. Cells were lysed using a sonicator (Virsonic) with indicated settings: power level of 6.5 for 4mins, with 10s on and 15s off cycles. Clarified lysates were obtained after centrifugation at 23,000 x g for 40 minutes at 4^{o}C. Imidazole (Boston BioProducts) was added to a final concentration of 20mM. 1.5ml of Ni-NTA agarose resin (Qiagen) was added to a column with the clarified lysate and incubated for 1 hour in the cold room. The flow through was drained and the resin was washed once with PBS + 850mM NaCl, followed by two 25ml washes with P300 + 30mM

imidazole buffer. The bound protein was eluted with 5ml of P300 containing 300mM imidazole and 1mM TCEP. Repeated elution step for a total of 10ml eluted protein. The protein was concentrated to 5ml using Centriprep YM-10 (Millipore) and purified by gel filtration on a HiLoad Superdex 75 16/600 column (GE Healthcare) into gel filtration buffer (10 mM HEPES pH 7.5, 150 mM NaCl, 1 mM TCEP). Purified His12-PPIA was concentrated to >100 μM, mixed with glycerol to 10%, and stored at -80^{o}C.

GST-pulldown Assay with Cell Lysates

A 2L culture Jurkat cells was grown, sedimented, washed with PBS, then flash frozen in liquid nitrogen and stored at -80 ºC until use. A sample containing ~1.9x10^{9} cells was thawed on ice, then 10mL of pre-cooled lysis buffer (10mM Tris pH 7.5, 5mM $MgCl_2$, 0.5% Triton X-100, 2mM BME, Sigma P8340 protease inhibitor cocktail). Cells were incubated on ice for 30 min, periodically mixing by brief vortexing. Cells were then transferred to a pre-cooled Dounce homogenizer and lysed with 30 strokes. The sample (with an approximate volume of 10mL) was transferred to a centrifuge tube, then added 1mL of 1M NaCl, 3mg $CaCl_2$•$2H_2O$, 400μL of 1M Tris pH 7.4, giving approximately 100mM NaCl, 2mM $CaCl_2$, 50mM Tris pH 7.4, 5mM $MgCl_2$, 0.5% Triton X-100, 2mM BME, protease inhibitors. Cells were centrifuged at 14000 rpm for 1 hour. At this point a Bradford assay showed the sample contained a total of approximately 66mg protein. The supernatant was transferred to a 15mL tube and 300μL of 50% glutathione sepharose slurry (in PBS) was added. The sample was placed on a rocker for 2 hours at 4^{o}C, then centrifuged at 500 rcf for 5 min. To two separate tubes, 3.3mL of the cleared lysate was added. 100μL of 12.0μM GST-PPIA, 200μL 50% glutathione

sepharose, 13µL of either DMSO or 5mM SFA was added to a clean 15ml falcon tube (giving a 3.3mL sample containing approximately 0.36µM GST-PPIA and 20µM SFA). Tubes were placed on a rocker for 2 hours. The agarose beads were pelleted by centrifuging at 500 rcf for 5 min, and the supernatant was discarded. To each tube, 4mL of wash buffer (150mM NaCl, 50mM Tris pH 7.4, 5mM $MgCl_2$, 2mM $CaCl_2$, 0.5% Triton X-100, 2mM BME, protease inhibitor cocktail) was added. The mixture was inverted several times, pelleted by centrifuging at 500 rcf for 5 min. The supernatant was discarded. The washing procedure was repeated two more times. Finally, the washed pellet was combined with an equal volume of 2X SDS-PAGE loading buffer, boiled, then analyzed by SDS-PAGE (4-12% Bis-Tris Invitrogen gel, MOPS running buffer) followed by silver staining.

GST-pulldown Assay with Purified Recombinant Proteins

60 µL glutathione magnetic beads (Pierce) was pre-incubated with 80µl of 80µM GST-PPIA in binding buffer (50mM Tris pH 7.4, 350mM NaCl, 1mM BME, 0.1% Triton-X, 1% BSA) for 1 hour at 4^{o}C. Beads were washed once with wash buffer (same as binding buffer but without BSA) and collected with a magnet to remove unbound GST-PPIA. 100 µL of wash buffer was added to prebound GST-PPIA on magnetic beads. GST-PPIA, IMPDH and SFA/DMSO were mixed in a clean microfuge tube such that the final concentration of each component was 0.5µM, 2.5µM and varied respectively. Components were rotated on a nutator in the cold room for 1 hour. The beads were collected with a magnet and washed four times with wash buffer. Proteins were eluted

from the beads in SDS loading buffer with heating for 5 minutes. The elute was collected and analyzed by SDS-PAGE and/or western blot.

HA Immunoprecipitation and Mass Spectrometry

Bait proteins bearing an N-terminal FLAG-HA tandem affinity purification (N_TAP) tag were cloned in pDEST vectors using the Gateway cloning system (Invitrogen). The pDEST backbone vector was obtained from Dr. Mat Sowa. Stable HeLa cell lines overexpression bait proteins were established using a lentivirus protocol (see following section). Stable HeLa cells lines overexpressing bait proteins of interests were expanded for IP experiments (1 x 15 cm plate for ~ 4 IPs). Cells were harvested, washed with 25mL PBS, then lysed for 30 min using 3mL MCLB lysis buffer (50mM Tris pH 7.4, 150mM NaCl, 10mM NaF, 0.5% NP40, 1x Roche complete EDTA-free protease cocktail). Clarified lysates were obtain after centrifugation at 14 000 rpm for 10 minutes. The supernatant was then filtered through 0.22µm spin filters (Millipore). DMSO or SFA (5mM stock solution) was added to lysates to give ~20µM SFA. The samples were incubated at 4 ºC using a nutator for 1h. 30µL of anti-HA resin (Sigma) was added to the samples which had been pre-equilibrated with MCLB, then incubated overnight at 4 ºC. On the following day, resin was collected by centrifugation at 3000 rpm for 10 minutes. The supernatant was discarded and the resin was washed four additional times with 1mL MCLB. The resin was then washed with four portions of PBS containing Roche protease inhibitor cocktail in order to remove detergent. The retained proteins were eluted off the resin with 3x50µL portions of 250µg/mL HA peptide (Sigma), allowing 30 minutes for each elution. To the 150µL pooled elution, 36µL of 100% TCA

was added, then vortexed briefly and placed on ice for 30 min. Precipitated proteins were pelleted by spinning at 14000 rpm for 30 minutes. The supernatant was removed and the pellet was washed with 500µL ice cold 10% TCA, followed by three additional washes with 1mL ice cold acetone. The pellet was allowed to air dry overnight. The next day, the pellet was suspended in 30µL of 100mM ammonium bicarbonate pH 8.0 with 10% acetonitrile and 750ng of trypsin and incubated at 37 ºC for 4 hours. Following stage tip purification, LC-MS/MS was performed using a Thermo Orbitrap Velos Pro mass spectrometer and analyzed using the Comparative Proteomic Analysis Software Suite (CompPASS)[21]. TMT labeling experiments was performed using the TMTsixplex™ Isobaric Mass Tagging Kit (ThermoScientific) in accordance to manufacturer's protocol.

Lentiviral Packaging and Infection Protocol

2.5 x 10^6 HEK293T cells were seeded in 6 well plates (per well) in 2mL of complete media the day before transfection. Ideally cells should be ~50-70% confluent prior to transfection. HEK293T cells were transfected using TransIT-293 transfection reagent (Mirus). For each well transfected, 12µl of Mirus TransIT-293 reagent was added to 200µl of Opti-Mem (Gibco/Life Technologies) and allowed to stand for 10 minutes. After which, 2µg of viral vector (pDEST vector obtained from Dr. Mat Sowa) and 0.5µg each of lentiviral packaging vectors (a gift from the Howley lab, HMS) was added to the transfection mix and allowed to stand for 30 minutes. Transfection mixture was added drop-wise to each well and mixed. The media of the HEK293T packaging cells was replaced with 1.5ml complete media the next day. Target cells to be infected were also seeded at 40% confluence. The following day, virus containing media is harvested from

packaging cells and filtered with a 0.45µm syringe filter to remove cellular debris. Each well was infected by adding 500µl of virus stock and 1.5µl of 10mg/ml polybrene. Infected target cells were returned to the 37^{o}C/5% CO_2 incubator for another 48 hours. After the infected cells reach desired confluency (~75% confluent), cells were expanded, grown under puromycin selection and protein overexpression was analyzed by western blot.

Surface Plasmon Resonance (SPR)

Analyses of small molecule binding kinetics were performed at 25^{o}C on a BIAcore X100 SPR instrument (GE Healthcare). The running buffer containing 10 mM HEPES (pH 7.4), 150mM NaCl, 50µM EDTA, 0.005% (v/v) Surfactant-P20 and 1% DMSO was prepared and filtered before use. The system was primed thrice with running buffer before each measurement was taken. To assess binding kinetics of cyclophilin binding ligands, pure His12-PPIA was immobilized on an NTA sensor chip to afford a highly stable and active surface suitable for kinetic measurements. The sensor chip was primed and charged with Ni^{2+}. 500nM of His12-PPIA was passed over the sensor surface at a flow rate 10µl/min for 1 min to stably immobilize ~600 RU of His12-PPIA. The ligands were injected at a concentration series (of 2 fold dilutions of analyte) over target and control flow cells with multi-cycle runs at a flow rate of 30µl/min for 3 minutes. After 600 seconds of dissociation (dissociation time was adjusted according to the small molecule analyzed), the sensor surface was regenerated with 350mM EDTA. The binding curves and kinetics data were obtained after subtracting the blank (DMSO) values and

analyzed by fitting to a 1:1 Langmuir binding model provided by the BIAcore X100 evaluation software.

Cellular Thermal Shift Assay (**CETSA)**

2 x 15cm of confluent HEK293 were harvested and washed with PBS. Cells were lysed in 3 ml MCLB (50mM Tris pH 7.4, 150mM NaCl, 10mM NaF, 0.5% beta-octyl glucoside) supplemented with EDTA-free Complete protease inhibitor cocktail (Roche) and incubated on ice for 20 minutes. The soluble fraction (lysate) was separated from the cell debris by centrifugation at 15000 x rpm for 30 minutes at 4°C. The supernatant was filtered with a 0.2uM Supor Membrane (Pall) to removed additional cellular debris. The clarified cell lysates were split into 4 aliquots, 1 mL each. Each aliquot was treated with 4ul of 5mM compound (FK506, CSA, SFA and DMSO) such that the final compound concentration is 20μM. After the samples were incubated at room temperature for 20 minutes, each treated lysates were divided into smaller 100ul aliquots (9 per sample) and heated individually at different temperatures for 3 minutes (Biorad thermal cycler) followed by flash freezing. Lysate samples were thawed in a thermal cycler at 25^{o}C and kept on ice for subsequent procedures. The heated lysates were centrifuged at 15000 x rpm for 20 minutes at 4°C in order to separate the soluble fractions from precipitates. The supernatants were transferred to new microcentrifuge tubes and analyzed by SDS-PAGE followed by western blot analysis.

References

1. Burdine, L. & Kodadek, T. Target Identification in Chemical Genetics: The (Often) Missing Link. *Chem. Biol.* **11,** 593–597 (2004).

2. Schenone, M., Dančík, V., Wagner, B. K. & Clemons, P. a. Target identification and mechanism of action in chemical biology and drug discovery. *Nat. Chem. Biol.* **9,** 232–40 (2013).

3. Aebersold, R. & Mann, M. Mass spectrometry-based proteomics. *Nature* **422,** 198–207 (2003).

4. Ong, S.-E. & Mann, M. Mass spectrometry-based proteomics turns quantitative. *Nat. Chem. Biol.* **1,** 252–262 (2005).

5. Ong, S.-E. *et al.* Identifying the proteins to which small-molecule probes and drugs bind in cells. *Proc. Natl. Acad. Sci. U. S. A.* **106,** 4617–22 (2009).

6. Ross, P. L. *et al.* Multiplexed protein quantitation in Saccharomyces cerevisiae using amine-reactive isobaric tagging reagents. *Mol. Cell. Proteomics* **3,** 1154–1169 (2004).

7. Thompson, A. *et al.* Tandem Mass Tags: A Novel Quantification\nStrategy for Comparative Analysis of Complex\nProtein Mixtures by MS/MS. *Anal. Chem.* **75,** 1895–1904 (2003).

8. Zenke, G. *et al.* Sanglifehrin A, a Novel Cyclophilin-Binding Compound Showing Immunosuppressive Activity with a New Mechanism of Action. *J. Immunol.* 7165–7171 (2001).

9. Bänteli, R., Wagner, J. & Zenke, G. Synthesis of derivatives of the novel cyclophilin-binding immunosuppressant sanglifehrin A with reduced numbers of polar functions. *Bioorganic Med. Chem. Lett.* **11,** 1609–1612 (2001).

10. Sedrani, R. *et al.* Sanglifehrin-cyclophilin interaction: degradation work, synthetic macrocyclic analogues, X-ray crystal structure, and binding data. *J. Am. Chem. Soc.* **125,** 3849–59 (2003).

11. Kallen, J., Sedrani, R., Zenke, G. & Wagner, J. Structure of human cyclophilin A in complex with the novel immunosuppressant sanglifehrin A at 1.6 A resolution. *J. Biol. Chem.* **280,** 21965–71 (2005).

12. Steinschulte, C., Taner, T., Thomson, a. W., Bein, G. & Hackstein, H. Sanglifehrin A, a Novel Cyclophilin-Binding Immunosuppressant Blocks Bioactive IL-12 Production by Human Dendritic Cells. *J. Immunol.* **171,** 542–546 (2003).

13. Immecke, S. N. *et al.* The cyclophilin-binding agent Sanglifehrin A is a dendritic cell chemokine and migration inhibitor. *PLoS One* **6,** e18406 (2011).

14. Zhang, L. H., Youn, H. D. & Liu, J. O. Inhibition of cell cycle progression by the novel cyclophilin ligand sanglifehrin A is mediated through the NFkappa B-dependent activation of p53. *J. Biol. Chem.* **276,** 43534–40 (2001).

15. Hedstrom, L. IMP Dehydrogenase: Structure, Mechanism and Inhibition. *Chem. Rev.* **109,** 2903–2928 (2009).

16. Davis, T. L. *et al.* Structural and biochemical characterization of the human cyclophilin family of peptidyl-prolyl isomerases. *PLoS Biol.* **8,** (2010).

17. Myszka, D. G. Kinetic, equilibrium, and thermodynamic analysis of macromolecular interactions with BIACORE. *Methods Enzymol.* **323,** 325–340 (2000).

18. Wear, M. a. *et al.* A surface plasmon resonance-based assay for small molecule inhibitors of human cyclophilin A. *Anal. Biochem.* **345,** 214–226 (2005).

19. Molina, D. M. *et al.* Monitoring Drug Target Engagement in Cells and Tissues Using the Cellular Thermal Shift Assay. *Science* **341,** 84–87 (2013).

20. Savitski, M. M. *et al.* Tracking Cancer Drugs in Living Cells by Thermal Profiling of the Proteome. *Science (80-.).* **346,** 55 (2014).

21. Sowa, M. E., Bennett, E. J., Gygi, S. P. & Harper, J. W. Defining the Human Deubiquitinating Enzyme Interaction Landscape. *Cell* **138,** 389–403 (2009).

CHAPTER 3

INVESTIGATION OF BINDING MODE, SAR AND MECHANISM OF ACTION STUDIES

3.1 Investigating IMPDH2 Dehydrogenase Inhibition as a Potential Mechanism of Action for SFA

Having demonstrated the interactions between PPIA, SFA and IMPDH2, we sought to determine the mechanism by which engagement of PPIA-SFA and IMPDH2 leads to cell growth inhibition. The discovery of IMPDH2 as a putative target for PPIA-SFA was important for several reasons. IMPDH catalyzes the rate limiting step in the pathway for the *de novo* synthesis of guanine nucleotides, by converting IMP to XMP in a NAD-dependent oxidation[1]. The *de novo* pathway is critical for cells that heavily rely on large nucleotide reservoirs for rapid proliferation, such as lymphocytes and cancer cells[1]. Consequently, IMPDH is a recognized target for immunosuppressive, anti-viral and anti-neoplastic chemotherapy[1]. MPA, the active inhibitor of mammalian IMPDH, is an FDA approved immunosuppressant indicated for the prevention of transplant rejection[1]. However, it carries significant gastrointestinal and bone marrow toxicity likely

resulting from its glucuronidation[2,3]. Many IMPDH inhibitor development efforts have been dedicated to isozyme specific inhibition of hIMPDH2 since this isoform is overexpressed in both cancer and proliferating T-cells[3]. However, developing isozyme specific inhibitors has been hindered by their largely indistinguishable structure and function.

Initially, we hypothesized that the PPIA-SFA complex inhibited the enzymatic function of IMPDH2. This mechanism is reminiscent of how the PPIA-CSA complex inhibits the phosphatase activity of calcineurin. Given that our biochemical data demonstrated isoform specific binding by PPIA-SFA, we wondered if the complex would also exhibit selective inhibitory action on the catalytic activity of the two hIMPDH isozymes. To test whether PPIA-SFA inhibited IMPDH2 activity, a standard inhibition assay of IMPDH2 was performed[4]. This involved incubating IMPDH2 with its substrate and cofactor, IMP and NAD respectively, and monitoring NADH formation as measured by the absorbance at 340nm over time. Interestingly, neither PPIA-SFA nor SFA alone inhibited the dehydrogenase activity of IMPDH2 (Figure 3.1). Early studies on the mechanism of action of SFA led to the conclusion that SFA does not affect targets of known immunosuppressants, such as calcineurin, dihydroorotate dehydrogenase and IMPDH[5].

Taken together, our findings and published data presented an interesting conundrum. On one hand, we have discovered IMPDH2, a well validated immunosuppressive target, which binds very specifically to PPIA-SFA. On the other hand, although we have confirmed that SFA alone does not inhibit IMPDH activity, we also found that PPIA-SFA was inactive at inhibiting IMPDH2 activity. This raises the

possibility that SFA could be modulating an alternative function of IMPDH2. Further experimental data, with IMPDH2 overexpression in cells and metabolite profiling, suggest that the inhibition of cell growth by SFA is not via the inhibition of the dehydrogenase activity of IMPDH2. Additional evidence is discussed in Chapters 4 and 5.

Figure 3.1

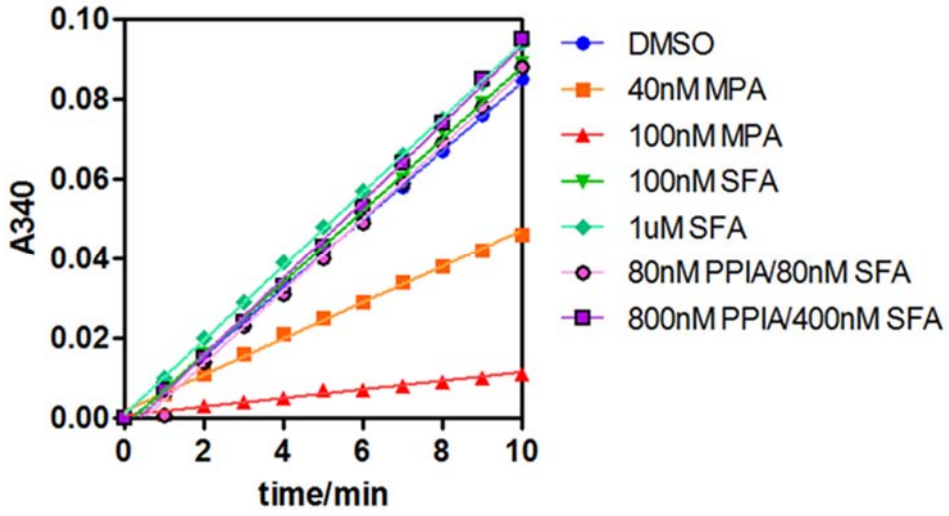

Figure 3.1 – IMPDH2 Inhibition Assay with SFA and PPIA-SFA. Enzymatic activity of IMPDH2 was performed by incubating IMPDH2 with IMP and NAD (in the absence or presence of inhibitors), and absorbance at 340nM was measured every 1 minute for 10 minutes. MPA potently inhibits IMPDH2 enzymatic activity but not SFA nor PPIA-SFA. Details of the procedure are described in the Experimental Procedures section.

3.2 Interrogating the Binding Mode of PPIA-SFA to IMPDH2

We examined the structure of IMPDH2 for other domains on IMPDH2 where PPIA-SFA could bind. Our earlier finding that IMPDH2, but not IMPDH1, binds preferentially to PPIA-SFA provided a hint that PPIA-SFA binding occurred at a site on IMPDH outside of its catalytic domain, which is highly homologous between the two isoforms (Figure 1.7A). To test the hypothesis that SFA binds to the CBS domain of IMPDH2, we created a construct of IMPDH2 with the CBS domain deleted (Figure 3.2A).

This subdomain can be removed with minimal effect on IMPDH enzyme activity *in vitro*[6,7]. The truncated IMPDH2, IMPDH2ΔCBS, while retaining wild type enzymatic activity, lost its ability to bind to PPIA-SFA (Figure 3.2B and C).

Figure 3.2

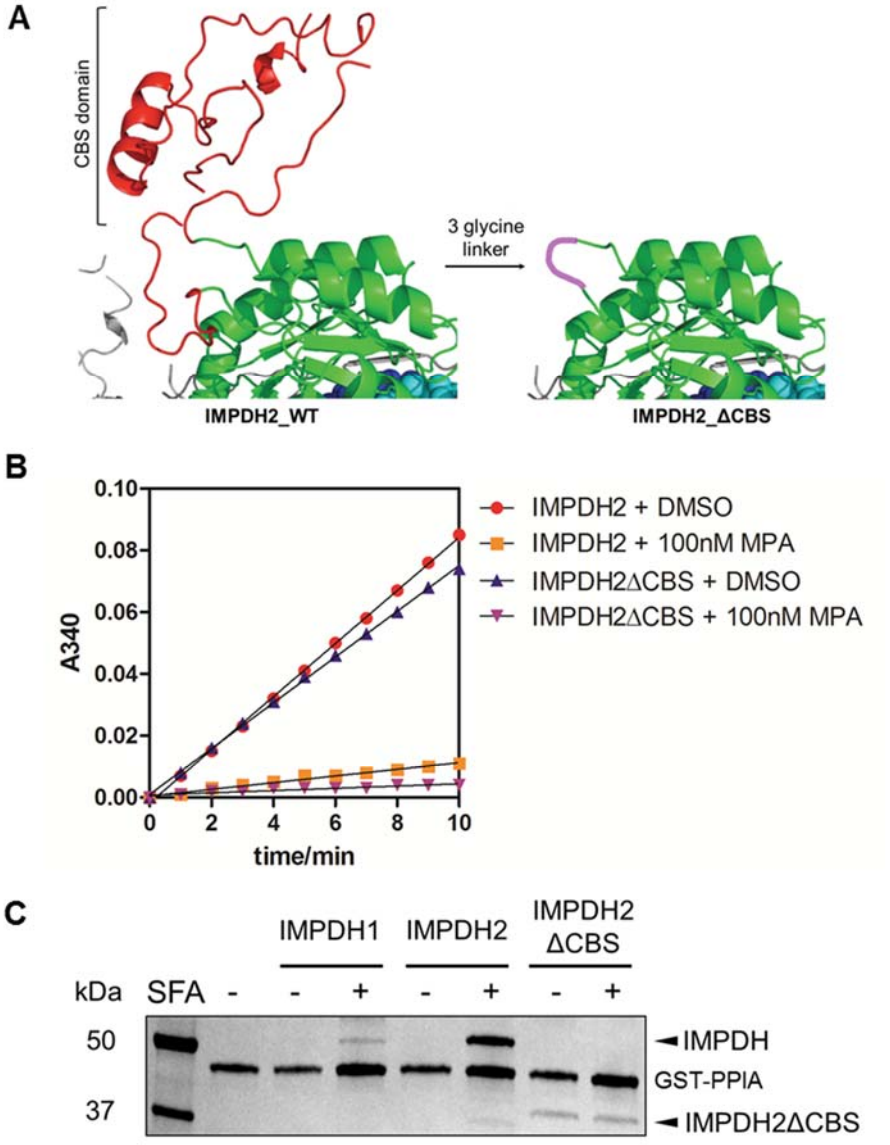

Figure 3.2 – CBS Domains are Necessary for Binding to PPIA-SFA but not for Catalytic Activity. (A) A CBS domain deleted construct was designed by replacing the CBS domains (residues 112 to 242) with a 3-glycine linker. (PDB 1B3O) (B) IMPDH2 activity assay showing that the CBS deleted construct, IMPDH2ΔCBS was equally active as full length IMPDH2. (C) GST-PPIA pulldown assay showed that IMPDH2ΔCBS was not enriched in the presence of SFA, suggesting that the CBS domain of IMPDH2 is necessary for binding to PPIA-SFA.

We next tested if the CBS domain of IMPDH2 is sufficient for binding. We designed two constructs CBS-L (CBS domain long) and CBS-S (CBS domain short) spanning residues 114 to 237 and 114 to 225 respectively. Neither of these constructs showed SFA-dependent binding to PPIA (Figure 3.3).

Figure 3.3

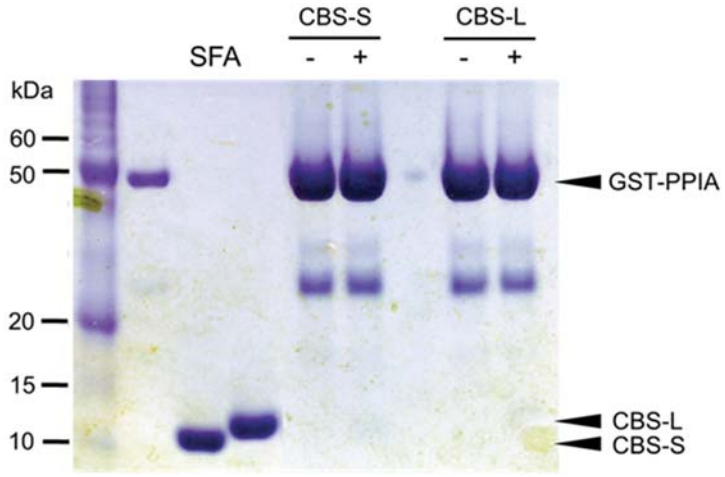

Figure 3.3 – CBS Domains Alone Do Not Bind to PPIA-SFA. GST-PPIA pulldown assay with two constructs, CBS-L (CBS domain long) and CBS-S (CBS domain short), spanning residues 114 to 237 and 114 to 225 respectively. Neither of these constructs showed SFA-dependent binding to PPIA. Figure from Dr. Dylan Stiles.

Since the CBS domains occur as an insertion within the catalytic core domain of IMPDH2, and that these domains are flexible and disordered in crystal structures, it could be possible that the CBS domain alone is not able to bind PPIA-SFA. The CBS subdomain protrudes from the core domain, and its precise function is unknown. Interestingly, CBS domains are found in a variety of proteins with diverse functions, such as protein kinases, ClC-chloride channels, and metabolic enzymes, where mutations within the CBS domains cause several hereditary diseases in humans[8]. More notably, the CBS domains of IMPDH share structural but not sequence similarity to

other CBS domain containing proteins[8]. This suggest that PPIA-SFA could potentially be modulating the CBS domains of IMPDH2

3.3 Biochemical Studies with Chimeric and Mutant IMPDHs

To further investigate the binding sufficiency of the CBS domain of IMPDH2, I created IMPDH chimeric constructs with IMPDH2 core bearing the CBS domains of IMPDH1 and vice versa (Figure 3.4).

Figure 3.4

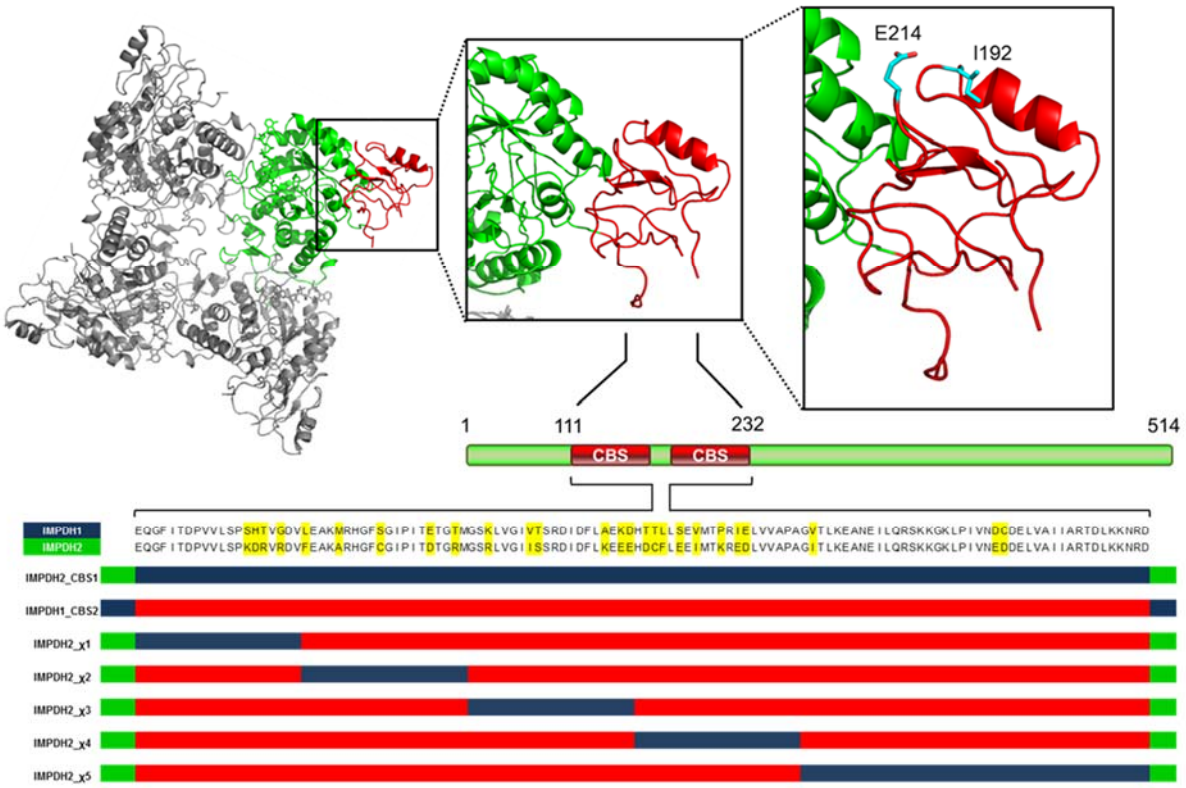

Figure 3.4 – Identifying the Sequence Determinants for the Binding of PPIA-SFA to IMPDH2 via IMPDH Chimeric Constructs. Monomeric IMPDH2 (green) with its CBS domains shown in red. IMPDH1 fragments are shown in dark blue. IMPDH chimeric constructs with IMPDH2 core bearing the CBS domains of IMPDH1 and vice versa were designed (IMPDH2_CBS1 and IMPDH1_CBS2). Five chimeric constructs where regions of the CBS domains of IMPDH1 were swapped with the corresponding regions on IMPDH2 were also designed (IMPDH2χ1 – IMPDH2χ5). Residues I192 and E214 (cyan) were identified to be critical for protein-drug interaction (inset) (PDB 1B3O).

Congruent with our hypothesis, chimeric IMPDH1 bearing the CBS domains of IMPDH2 showed binding to PPIA-SFA, but not the chimera of IMPDH2 bearing CBS domains of IMPDH1 (Figure 3.5A). To identify the sequence determinants for the binding of PPIA-SFA to IMPDH2, I designed five chimeric constructs where regions of the CBS domains of IMPDH1 were swapped with the corresponding regions on IMPDH2 (Figure 3.4). I observed that one of the chimeras, IMPDH2χ5, lost binding to PPIA-SFA (Figure 3.5B), and further inspection of that chimera's primary sequence revealed three residues, I192, E214 and D215, which appeared to be mediating protein-drug interaction.

Figure 3.5

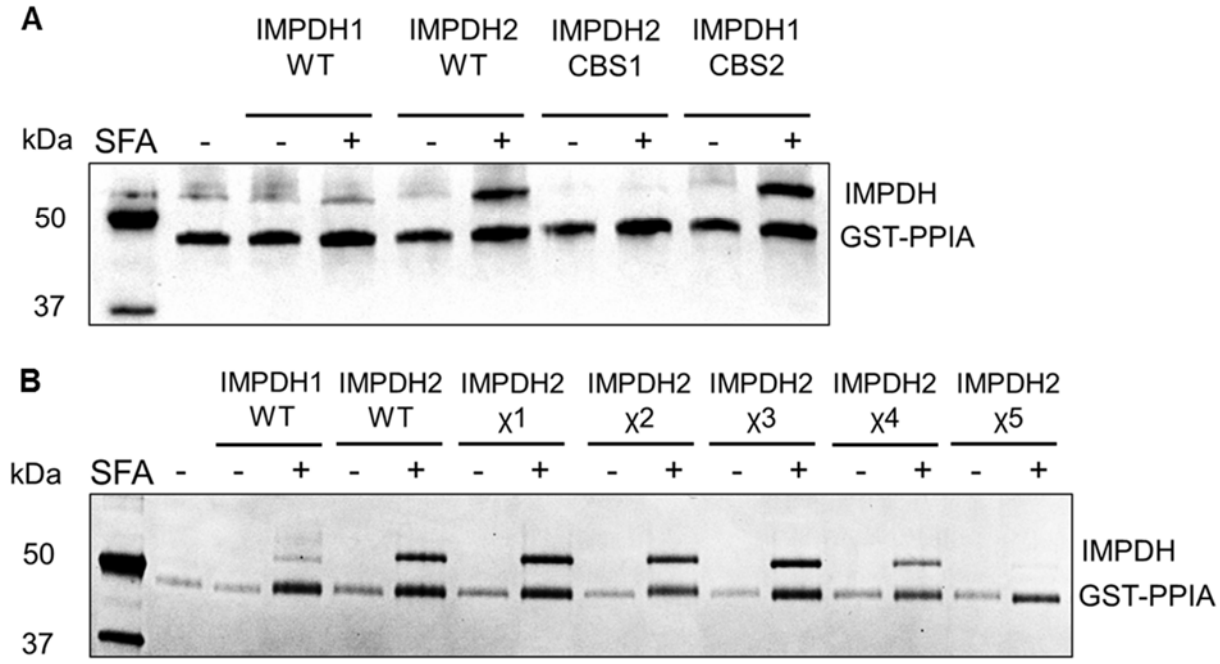

Figure 3.5 – GST-PPIA Pulldown with Chimeric Constructs. (A) GST-PPIA pulldown assays with chimeras with CBS domains completely swapped. Chimeric IMPDH1 bearing the CBS domains of IMPDH2 showed binding to PPIA-SFA, but not the chimera of IMPDH2 bearing CBS domains of IMPDH1. (B) GST-PPIA pulldown assays with chimeras with regions of the CBS domains of IMPDH1 replaced with the corresponding regions on IMPDH2. Of the five chimeras, IMPDH2χ5 appeared to have lost binding to PPIA-SFA.

IMPDH2 point mutants, I192V, E214D and D215C were made, by substituting the corresponding residue on IMPDH1. In the single I192V point mutant, I observed an almost complete loss of binding to PPIA in the presence of SFA. The E214D mutant exhibited partial loss of binding, while the D215C mutant retained binding to PPIA in the presence of SFA (Figure 3.6A).

Figure 3.6

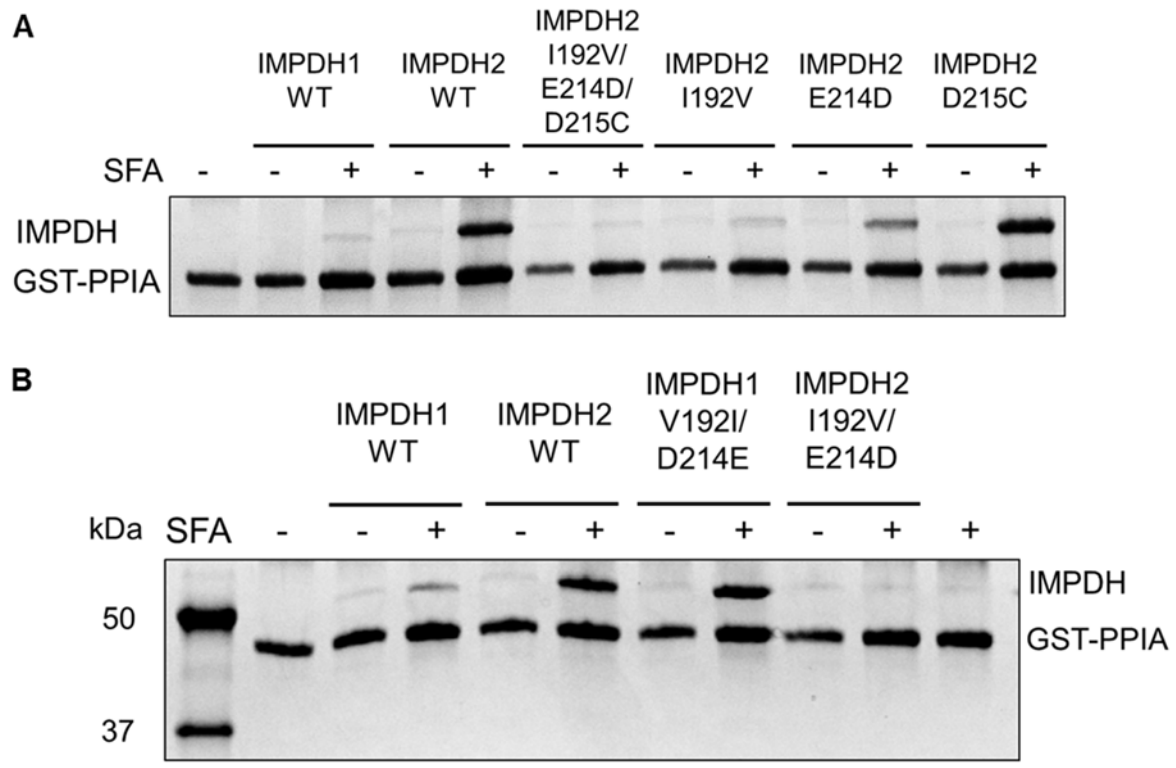

Figure 3.6 – GST-PPIA Pulldown with Mutant IMPDHs. (A) IMPDH2 point mutants, I192V, E214D and D215C, where substitutions were made by the corresponding residue on IMPDH1 were expressed and purified. In the single I192V point mutant, we observed an almost complete loss of binding to PPIA in the presence of SFA. The E214D mutant exhibited partial loss of binding. (B) The double IMPDH2 mutant, IMPDH2_I192V/E214D demonstrated impaired binding to PPIA-SFA and double IMPDH1 mutant, IMPDH1_V192I/D214E, gained the ability to bind to PPIA in a SFA-dependent fashion.

Curious to know if I could boost IMPDH1 binding to PPIA-SFA, I replaced residues V192 and D214 on IMPDH1 with the residues that corresponded to IMPDH2. I

also purified the IMPDH2 double mutant, IMPDH2_I192V/E214D which is predicted to have impaired binding to PPIA-SFA. Consistent with my prediction, the IMPDH2 double mutant lost binding to PPIA-SFA (Figure 3.6B). Surprisingly, the IMPDH1 double mutant, IMPDH1_V192I/D214E, gained the ability to bind to PPIA in a SFA-dependent fashion, suggesting that these residues are necessary for binary complex engagement (Figure 3.6B).

3.4 Structure-Activity Relationship Studies with Macrolide Fragment of SFA

An extensive study on the structure-activity relationship of SFA had been conducted by Novartis Pharmaceuticals, where they designed and synthesized a library of SFA macrolide analogues with the primary purpose of examining in detail the interaction between the macrocycle of SFA and PPIA[9]. Based off a previously published procedure that allowed the separation of the spirolactam moiety from the macrocyclic portion of SFA, Sedrani *et al.* aimed to preserve the interaction with PPIA while reducing the number of polar groups on SFA as those are known to impart poor cell penetrating properties to molecules[9–11]. They reported that neither the spirolactam nor the macrolide fragment demonstrated immunosuppressive activity despite the macrolide fragment having an affinity for PPIA almost identical to that of the parent molecule, SFA[9,12]. Installation of a variety of side chains attached to C_{23} had modest effect on PPIA-binding and does not rescue immunosuppressive activity of SFA, indicating that the spirolactam moiety of SFA is required for immunosuppressive effects and that the macrocyclic portion of SFA is critical for mediating PPIA interaction[9]. They also obtained crystal structures of the compound-isomerase complex – one of PPIA-SFA, which

turned out to be a dimer of PPIA-SFA, and another of PPIA with a macrocyclic core of SFA[9,12]. Those structures were critical in confirming the many observations made from the structure-activity relationship of SFA, specifically that the highly unique macrocyclic fragment of SFA is responsible for conferring its high affinity for PPIA.

Building upon our hypothesis that SFA's anti-proliferative effect stems from its interaction with IMPDH2 when bound to PPIA, we were curious to know if the non-immunosuppressive macrocyclic analogue of SFA would retain binding with IMPDH2. I collaborated with Dr Stiles in this effort. He synthesized a macrocyclic fragment of SFA, which we term SFM (**m**acrolide fragment of sanglifehrin A), adapting a method published previously[11]. This involved the degradation of sanglifehrin A via the oxidative cleavage of C_{26}=C_{27} olefin to afford SFM, a macrocyclic allylic aldehyde (Figure 3.7A). Consonant with previous reports, SFM retained binding to PPIA and has a K_d = 5.65 ± 1.61 nM, approximately 30 fold lower affinity than SFA[9] (Figure 3.7B). Consequently, SFM did not interact with IMPDH2 when presented by PPIA, suggesting that the spirolactam moiety of SFA is necessary for IMPDH2 engagement (Figure 3.7C). SFM also exhibited a marked lost in cell growth inhibition in K562 leukemia cell line and H2122 lung adenocarcinoma line (Figures 3.7D and E). This appears to suggest that the interaction of PPIA-SFA with IMPDH2 is necessary for the biological activity of SFA. The growth inhibitory effect seen at micromolar concentrations of SFM (in K562) could be attributed to off-target effects of the compound at high concentrations (Figure 3.7D).

Figure 3.7

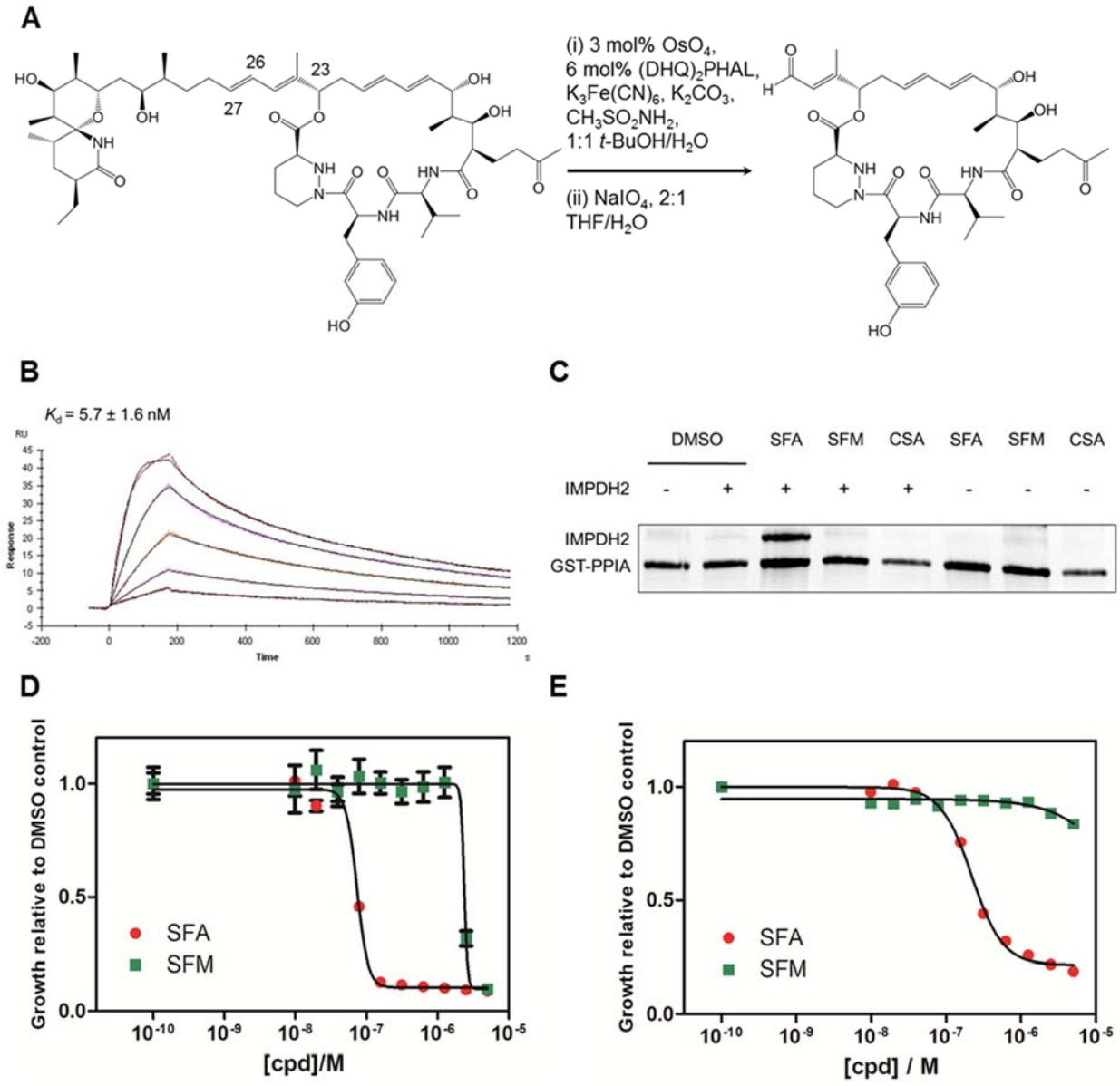

Figure 3.7 – Structure-Activity Relationship Studies with SFM. (A) Reaction scheme for the synthesis of the macrolide fragment of SFM, adapting a method published previously (citation). (B) SPR data evaluating affinity constant of SFM for PPIA. (C) GST-PPIA affinity purification with IMPDH2 in the presence and absence of SFA, SFM and CSA. Only IMPDH2 binds to PPIA in a SFA dependent manner. The removal of the spirolactam moiety of SFA resulted in the loss of PPIA-dependent IMPDH2 engagement. (D) SFM is much less potent at inhibiting cell proliferation in K562 cell lines and in (E) H2122 lung adenocarcinoma line.

3.5 Conclusions

The results described in this chapter provide further support for the molecular recognition between PPIA-SFA and IMPDH2. Through the examination of a series of chimeric IMPDHs, we identified residues I192 and E214 on the CBS domain as being necessary for PPIA-SFA interaction. Interestingly, these residues are not evolutionarily conserved (Figure 3.8).

Figure 3.8

Figure 3.8 – Sequence Alignment of a Portion of IMPDH CBS Domains Containing the Residues Critical for PPIA-SFA Binding. The residues I192 and E214 on human IMPDH2 (*) , that have been found to be necessary for PPIA-SFA interaction are not strictly conserved across IMPDH2 homologs from other organisms. Sequence numbering is shown on the right. hs = *Homo sapiens*, pt= *Pan troglodytes*, mm = *Mus musculus*, rn = *Rattus norvegicus,* dr = *Danio rerio*, dm = *Drosophila melanogaster* ce = *Caenorhabditis elegans*, sc = *Saccharomyces cerevisiae*, ec = *Escherichia coli*

While the CBS domains of IMPDH2 share sequence homology among mammals, the I192 residue on human IMPDH2, which is the residue critical for PPIA-SFA binding, is not strictly conserved. The E214 residue, surprisingly, is conserved in mammalian

IMPDH2, *Danio rerio* and *Saccharomyces cerevisiae*. The CBS domains of IMPDH2 is much less conserved in lower eukaryotes and prokaryotes, suggesting that the CBS domains could have evolved to have a different function from that in lower organisms. It would be worth investigating if IMPDH2 of other organisms can also bind to its homolog of PPIA in the presence of SFA, since the targets of CSA, FK506 and RAP are also evolutionarily conserved. SAR studies with the macrocyclic core of SFA, a much less potent cell growth inhibitor, did not engage IMPDH2 despite possessing PPIA binding activity. This provides strong evidence that the decreased potency of SFM is attributable to the inability of PPIA-SFM to bind to IMPDH2. The initial result that PPIA-SFA did not inhibit the enzymatic activity of IMPDH2, an initially hypothesized mechanism of action, made sense in light of biochemical studies showing that PPIA-SFA binds to the CBS domains of IMPDH2.

In the following chapter, efforts to genetically validate PPIA and IMPDH2 as the biological target of SFA will be discussed.

Experimental Procedures

General Methods and Chemicals

Oligonucleotide primers were ordered from Eurofins MWG Operon or Integrated DNA Technologies. PCR was performed with Q5 High-Fidelity DNA Polymerase (New England Biolabs) and purified with a PCR cleanup kit (Zymo Research). Absorbance measurements were performed with a NanoDrop 2000C spectrophotometer (ThermoScientific). Mini-PROTEAN® TGX Stain-Free™ polyacrylamide gels (Bio-Rad, Hercules, CA), Mini-PROTEAN Tetra cell electrophoresis chamber with Tris/Glycine/SDS running buffer (Bio-Rad, Hercules, CA) were used for protein analysis. Proteins were transferred to polyvinylidene difluoride (PVDF) membranes using Trans-Blot® Turbo™ (Bio-Rad, Hercules, CA) for blotting. SFA was a generous gift from Novartis. CSA, DMSO and polybrene were ordered from Sigma-Aldrich.

Cell Culture Information

Human cancer cell lines K562 (a kind gift from the Saghatelian lab ATCC No. CCL-243), H2122 (ATCC No. CRL-5985) and Jurkat (ATTC No. TIB-152) were cultured in RPMI-1640 medium (Gibco/Life Technologies); HEK-293 cells (ATCC No. CRL-1573) was maintained in Dulbecco's Modified Eagle Medium (Gibco/Life Technologies). All culture media were supplemented with 10% fetal bovine serum (FBS, Gibco/Life Technologies, Carlsbad, CA, USA), 100 units/mL penicillin and 100 units/mL streptomycin (Gibco/Life Technologies). Stable cell lines were generated as described in the Experimental Procedures section of Chapter 2.

Western Blotting

Cells were lysed with RIPA buffer (50mM Tris pH8, 150mM NaCl, 0.1% SDS, 0.5% sodium deoxycholate, 1% NP40, 1mM EDTA and protease and phosphatase inhibitor cocktail [Roche]). For western blotting, the following antibodies were used: anti-IMPDH2 (Ab-131158, 1:1000) and anti-IMPDH1 (Ab-55297, 1:1000) were from Abcam. Anti-PPIA (CST 2175, 1:1000) was from Cell Signaling Technology.

Recombinant Protein Cloning, Expression and Purification

Chimeras were cloned into pET32a vector by Gibson cloning. Gblocks were ordered from Integrated DNA Technologies. Site directed mutagenesis was performed using Quikchange (Stratagene) kit. Residues 111-232 of the CBS domains of IMPDH1 and IMPDH2 were completely swapped for IMPDH2_CBS1 and IMPDH1_CBS2 constructs. The other chimeric IMPDH2 constructs were generated by replacing the portions of IMPDH2 with sequences of IMPDH1: IMPDH2χ1 – Residues 111-130; IMPDH2χ2 – Residues 131-150; IMPDH2χ3 – Residues 151-170; IMPDH2χ4 – Residues 171-190; IMPDH2χ5 – Residues 191-232. All chimeric and mutant IMPDH proteins were purified in the same manner as described in the Experimental Procedures section of Chapter 2.

IMPDH Activity Assay

Enzymatic activity of IMPDH2 was performed by the method of Carr *et al*.[4] Briefly, in a 1mL plastic cuvette, mixed in the following order: Reaction buffer (100mM Tris pH 8.0, 100mM KCl, 3mM EDTA), 500nM IMPDH2 and 400nM NAD (freshly-prepared 10mM solution in water). Spectrophotometer was zeroed and 100nM IMP (freshly-prepared

10mM solution in water) was added. Absorbance at 340nM was measured every 1 minute. For measuring the effect of inhibitors (MPA, SFA, etc), the compound as a DMSO stock solution was added prior to adding IMP.

Synthesis of SFM

The synthesis of SFM was performed as described by Metternich *et al*.[11]

GST-pulldown Assay with chimeric and mutant IMPDH

The GST-pulldown assays were performed as described in the Experimental Procedures section of Chapter 2.

Cell Proliferation Assays

K562 (4000 cells) and H2122 (5000 cells) were seeded in black 96-well tissue culture plates (for MTT assay – Promega). Compounds were diluted in respective complete growth medium and serial 2-fold dilutions were prepared for dose-response experiments. Compounds were added to wells in triplicate. The plates were incubated at 37^{o}C/5% CO_2 for 72 hours and MTT assay performed in accordance to manufacturer's protocol absorbance at 570nm detected by a plate reader (BioTek). The relative cell number was calculated by normalization against wells treated with DMSO only.

References

1. Hedstrom, L. IMP Dehydrogenase: Structure, Mechanism and Inhibition. *Chem. Rev.* **109,** 2903–2928 (2009).

2. Franklin, T. J., Jacobs, V., Jones, G., Plã, P. & Bruneau, P. Glucuronidation Associated with Intrinsic Resistance to Mycophenolic Acid in Human Colorectal Carcinoma Cells. *Cancer Res.* **56,** 984–987 (1996).

3. Papageorgiou, C. Enterohepatic recirculation: a powerful incentive for drug discovery in the inosine monophosphate dehydrogenase field. *Mini Rev. Med. Chem.* **1,** 71–77 (2001).

4. Carr, S. F., Papp, E., Wu, J. C. & Natsumeda, Y. Characterization of human type I and type II IMP dehydrogenases. *J. Biol. Chem.* **268,** 27286–27290 (1993).

5. Zenke, G. *et al.* Sanglifehrin A, a Novel Cyclophilin-Binding Compound Showing Immunosuppressive Activity with a New Mechanism of Action. *J. Immunol.* 7165–7171 (2001).

6. Nimmesgern, E. *et al.* Biochemical analysis of the modular enzyme inosine 5'-monophosphate dehydrogenase. *Protein Expr. Purif.* **17,** 282–289 (1999).

7. Gan, L., Petsko, G. A. & Hedstrom, L. Crystal structure of a Ternary Complex of Tritrichomonas foetus Inosine 5'-Monosphosphate Dehydrogenase: NAD+ Orients the Active Site Loop for Catalysis. *Biochemistry* 13309–13317 (2002). doi:10.1074/jbc.M208330200

8. Ignoul, S. & Eggermont, J. CBS domains: structure, function, and pathology in human proteins. *Am. J. Physiol. Cell Physiol.* **289,** C1369–78 (2005).

9. Sedrani, R. *et al.* Sanglifehrin-cyclophilin interaction: degradation work, synthetic macrocyclic analogues, X-ray crystal structure, and binding data. *J. Am. Chem. Soc.* **125,** 3849–59 (2003).

10. Bänteli, R., Wagner, J. & Zenke, G. Synthesis of derivatives of the novel cyclophilin-binding immunosuppressant sanglifehrin A with reduced numbers of polar functions. *Bioorganic Med. Chem. Lett.* **11,** 1609–1612 (2001).

11. Metternich, R., Denni, D., Thai, B. & Sedrani, R. Toward a total synthesis of the immunosuppressant sanglifehrin A. Preparation of two relay compounds by degradation and their use in the reassembly of the natural product. *J. Org. Chem.* **64,** 9632–9639 (1999).

12. Kallen, J., Sedrani, R., Zenke, G. & Wagner, J. Structure of human cyclophilin A in complex with the novel immunosuppressant sanglifehrin A at 1.6 A resolution. *J. Biol. Chem.* **280,** 21965–71 (2005).

CHAPTER 4

GENETIC VALIDATION OF PPIA AND IMPDH2 AS BIOLOGICAL TARGETS OF SANGLIFEHRIN A

4.1 Genetic Approaches to Validate Targets of SFA

The identification and validation of drug targets are critical for subsequent mechanism of action studies. Genetic manipulation by target cDNA overexpression, RNAi and knock-out in whole organisms are routinely used as orthogonal strategies to identify and validate protein targets in drug discovery[1,2].These methods are based on the premise that altered target expression would alter sensitivity to the small-molecule and phenocopying a drug's effect. Advances in genomics and computational biology have enabled large-scale modifications of genomes and transcriptomes through genome-wide RNAi screens. More recently genome-scale CRISPR-Cas9 knockout screens have been used to interrogate gene function and aid the understanding of a drug's mechanism of action, albeit in a loss-of-function allele setting[2–4].

The 'gold standard' in drug target identification hinges on two criteria: (i) A mutation in the protein target confers resistance to a drug and (ii) The mutation reverses

inhibition of the target's activity by the drug[5]. Building upon our biochemical findings that IMPDH2 is a putative target of PPIA-SFA, we employed genetic approaches to validate PPIA and IMPDH2 as biological targets of SFA according to these criteria. This chapter describes *in vivo* efforts with phenotypic screens in yeasts and worms, as well as with RNAi and CRISPR/Cas9 in cell culture to validate the targets of SFA.

4.2 IMPDH2 Overexpression Studies in Cell Culture

Having demonstrated the interactions between PPIA, SFA and IMPDH2, we sought to determine the mechanism by which engagement of PPIA-SFA and IMPDH2 leads to cell growth inhibition. Intuitively, we hypothesized that the PPIA-SFA complex inhibits the enzymatic function of IMPDH2, analogous to how the PPIA-CSA complex inhibits the phosphatase activity of calcineurin. However, as demonstrated in the previous chapter, neither PPIA-SFA nor SFA alone inhibited the dehydrogenase activity of IMPDH2 (Figure 3.1). Thus, I sought evidence that overexpression of IMPDH2 would rescue SFA sensitivity, similar to how overexpression of calcineurin (the target of PPIA-CSA and FKBP12-FK506) confers greater resistance to the effects of CSA and FK506 and enhances NFAT- and NFIL2A-dependent transcription [6,7].

The cDNA encoding wild-type human IMPDH2 was cloned into a pDEST lentiviral construct and stable cell lines overexpressing IMPDH2 in K562 and Jurkat cell lines were generated (Figure 4.1A). The overexpression of IMPDH2 did not confer resistance in these cells to SFA, but did confer resistance to MPA, a reversible inhibitor of IMPDH (Figures 4.1B and C). This implies that SFA does not target the enzymatic

site of IMPDH2 and suggests that the two compounds, while engaging the same target, have distinct mechanisms of action.

Figure 4.1

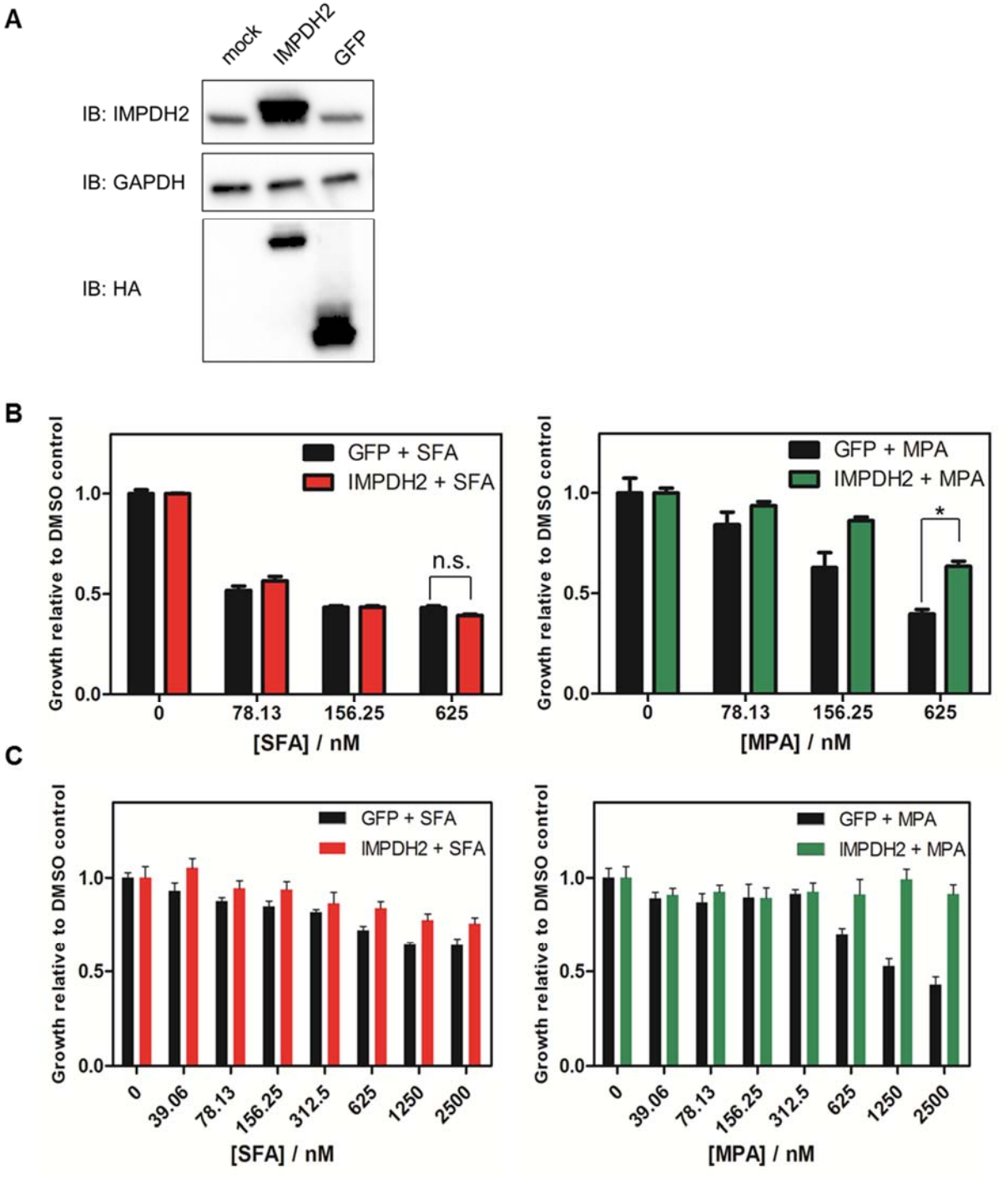

Figure 4.1 (continued) – IMPDH2 Overexpression in Cell Culture. (A) pDEST-FLAG-HA-IMPDH2 and pDEST-FLAG-HA-GFP constructs stably overexpressed in K562 chronic myelogenous leukemia line. (B) Stable IMPDH2 and GFP overexpression lines in K562 tested for sensitivity against SFA or MPA. Cells were treated for 72 hours and the relative cell numbers were assayed using the CellTiter-Glo Luminescent Cell Viability assay (Promega). (C) Stable IMPDH2 and GFP overexpression lines in Jurkat cells tested for sensitivity against SFA or MPA. Cells were treated for 48 hours and the relative cell numbers were assayed using the CellTiter-Glo Luminescent Cell Viability assay (Promega). Treatments were performed in triplicate and each data point shown is an average of replicates ± the standard deviation. Details of the experiments can be found in Experimental Procedures. *p < 0.005

I also investigated if the interaction with IMPDH2 could modulate guanine or purine nucleotide biosynthesis. However, the addition of guanosine and adenosine nucleosides to SFA-treated K562 cells also did not reverse growth inhibition (Figure 4.2). Taken together, these results suggest that inhibition of cell growth by SFA is neither via inhibition of the enzymatic function of IMPDH2 nor via the disruption of guanosine metabolism. Rather, we speculate that SFA is modulating an alternative function of IMPDH2.

Figure 4.2

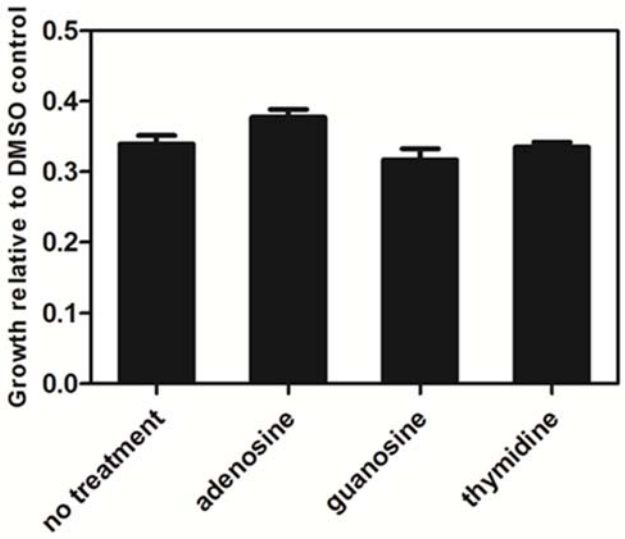

Figure 4.2 – Nucleoside Rescue Experiment with SFA Co-treatment. 10uM nucleoside was co-treated with 625nM of SFA to determine if any of these nucleosides would suppress SFA effect on K562 cells. Treatments were performed in triplicate and each data point shown is an average of replicates ± the standard deviation.

4.3 Phenotypic Screen of SFA in Fungi

4.3.1 Lessons from *Saccharomyces cerevisiae* and Lower Eukaryotes

The budding yeast *Saccharomyces cerevisiae* (*S. cerevisiae*) has been indispensable as a model organism in elucidating the mode of action for established and novel compounds *in vivo.* Given its many positive experimental attributes – such as having a well characterized genome and proteome, ease of cultivation, and genetic amenability – *S. cerevisiae* has historically been the testing ground for the development of large scale "-omics" studies in yeast[8]. The Yeast KnockOut collection paved the way for a suite of yeast genomics assays currently used in target discovery efforts. The knockout collection comprises a full set of deletion haploid and diploid strains that is barcoded with two unique 20 oligonucleotide sequences functioning as strain identifiers [9,10]. This serves as a powerful tool by allowing the competitive growth of the pooled strains to select for those that exhibit resistance under compound treated conditions. Barcodes of strains surviving drugged conditions will be enriched and can be detected and quantified by a DNA barcode microarray or next generation sequencing to identify genes implicated in survival[11]. Such assays are termed haploinsufficiency profiling (HIP) or homozygous profiling (HOP), depending on the ploidy of the strain used in the screen. In a somewhat analogous approach, commonly known as multicopy suppression profiling (MSP), genes involved in the resistance to a compound can be identified by treating a pool of yeast strains, each overexpressing different ORFs, to enrich for those encoding targets conferring resistance[12,13]. Those hypersensitive to the compound will be eliminated from drug selection relative to vehicle treated pool. As with the YKO

collection, the individual overexpression plasmids encode their unique identifiers which can be deconvoluted by microarray or sequencing techniques[12,13].

Pertinent to our studies, these lower eukaryotes were integral in confirming the role of PPIA and FKBP in mediating the effects of CSA, FK506 and RAP. The observation in *Neurospora crassa* (*N. crassa*) and *S. cerevisiae* that the loss of, or mutation in the CSA binding site of cyclophilin conferred CSA resistance in these organisms was a ground breaking one[14]. It provided the first direct evidence that cyclophilin is a *bona fide* target of CSA and that it is necessary, though not sufficient, for mediating CSA's cytotoxic effect in these organisms[14]. Additionally, the introduction of yeast cyclophilin gene to resistant strains restored CSA sensitivity[15]. Similar experiments in *S. cerevisiae* demonstrated genetically that FKBP is a target of FK506 and RAP *in vivo* [15–17]. With the identification of IMPDH2 as a cyclophilin-dependent target of SFA, we initiated studies in fungi to further validate PPIA and IMPDH2 as biologically relevant targets of SFA.

4.3.2 Screening SFA in *S. cerevisiae*

S. cerevisiae strain W303 was obtained from the O'Shea lab (Harvard MCB) and cyclophilin, FKBP and IMPDH2 (cpr1, fpr1 and imd2 are the yeast homologs respectively) knock-out strains were generated via homologous recombination of the URA3 gene at the various targeted loci. Deletion strains were selected for their ability to grow in URA- agar media and subsequently PCR screening confirmed the genomic integration of the URA3 gene in their genomes. Wild type and the deletion strains were serially diluted and spotted on YPD plates pretreated with CSA and SFA as well as RAP,

FK506 and DMSO as controls (Figure 4.3A). No apparent cytotoxicity was observed upon CSA, SFA and FK506 treatment. However, RAP exhibited potent cytotoxicity in all the W303 yeast strains, except the fpr1 deletion strain, which showed resistance to RAP's effect (Figure 4.3.1A). While this result confirms the necessity of fpr1 in mediating RAP's effect, conclusions cannot be drawn with the other compounds as the wild type strains exhibited no sensitivity to them. The yeast strains used in this study can be found in Table 4.1.

Strain	Parent strain	Genotype	Source
K42		MATa ade2 trp1 CsA^s	J. Heitman
IL993/5c		MATα p^o ilv5 CsA^s	J. Heitman
TB23	IL993/5c	MATα p^o ilv5 ura3 leu2::hisG CsA^s	J. Heitman
TB26-4	IL993/5c	MATα p^o ilv5 ura3 leu2::hisG cpr1::LEU2-1	J. Heitman
TB26-5	IL993/5c	MATα p^o ilv5 ura3 leu2::hisG cpr1::LEU2-1	J. Heitman
RDY158		MATa ura3-1 his3-11,15::cdc28VF::HIS3 leu2-3,112 trp1-1::TET-CDC20-127::TRP1 ade2-1, pdr1Δ::KAN pdr3Δ::his5ca can1-100 [linear pA24lpl (LEU2 TRP1 ARS1 CEN3)]	A. Murray
S288C		MATα SUC2 gal2 mal2 mel flo1 flo8-1 hap1 ho bio1 bio6	A. Murray, F. Winston
BY4741	S288C	MATa his3Δ1 leu2Δ0 met15Δ0 ura3Δ0	A. Murray, F. Winston
BY4743	S288C	MATa/MATα his3Δ1/his3Δ1 leu2Δ0/leu2Δ0 lys2Δ0/LYS2 met15Δ0/MET15 ura3Δ0/ura3Δ0	A. Murray, F. Winston
YDR155C	BY4741	CPR1Δ	A. Murray
YHR057C	BY4741	CPR2Δ	A. Murray
YLR432W	BY4741	IMD3Δ	A. Murray
W303		MATa/MATα {leu2-3,112 trp1-1 can1-100 ura3-1 ade2-1 his3-11,15} [phi^+]	E. O'Shea
KHP01	W303	CPR1Δ	K. Pua
KHP03	W303	FPR1Δ	K. Pua
KHP03	W303	IMD2Δ	K. Pua

Table 4.1 ─ Yeast strains used in this study

Figure 4.3

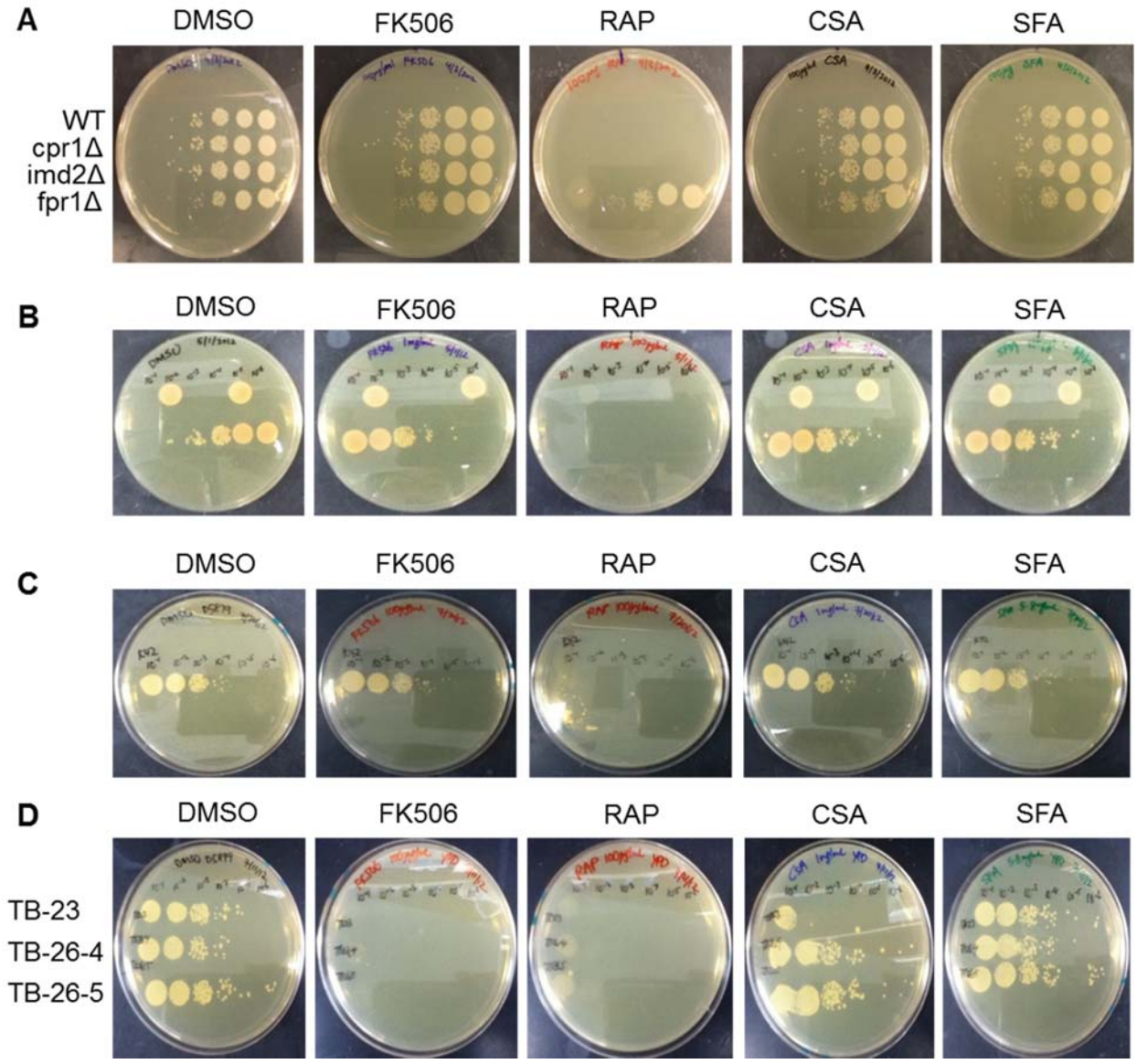

Figure 4.3 – Evaluation of Yeast Strains for Sensitivity to Compounds. Yeast cells were spotted on YPD plates pre-treated with compounds. Each row from individual plates show clonal yeast strains which have undergone six serial ten-fold dilutions. (A) Sensitivity of W303 strain to compounds. All compounds were tested at 100ug/ml. (B) Sensitivity of RDY158 strain to compounds. Ignore the top two spots on the plate. RAP was tested at 10ug/ml while other compounds were tested at 1mg/ml. (C) Sensitivity of K42 strain to compounds. Both FK506 and RAP were tested at 100ug/ml. CSA and SFA were tested at 1mg/ml and 5.8mg/ml respectively. (D) Sensitivity of TB strains to compounds. Both FK506 and RAP were tested at 100ug/ml. CSA and SFA were tested at 1mg/ml and 5.8mg/ml respectively. Details of the experiments can be found in Experimental Procedures.

The *S. cerevisiae* S288C derived strain BY4743, the strain used in the systematic deletion project was obtained from the Murray lab (Harvard MCB) and Winston lab (HMS). The wild type and cpr1 deletion strains were each tested for sensitivity to the same panel of compounds. As with the W303 strains, they were all unresponsive to CSA, SFA and FK506 (data not shown).

While yeasts have been instrumental in driving drug discovery, they are also notorious for their lack of sensitivity to many compounds. This lack of sensitivity can be attributed to their thick cell wall and active expression of drug efflux pumps which in effect lowers the intracellular concentration, and hence the effective dose of compounds[8]. In particular, CSA has been reported to be ineffective in inhibiting the growth of most yeast strains[15].

To increase the drug sensitivity of the yeasts, two strategies were pursued. The first was to test CSA and SFA sensitivity to RDY158 strain (a gift from the Murray lab). The RDY158 strain harbors the deletion of two genes pdr1 and pdr3, which are transcription factors crucial for regulating drug response in *S. cerevisiae*. This drug sensitized strain was used to identify the protein kinase Msp1, as the target of cincreasin[18]. RDY158 strain was also not sensitive to CSA, SFA and FK506 (Figure 4.3B). In a second approach, polygodial was used to render yeasts more sensitive to drugs by increasing membrane permeability: low concentrations of polygodial have been reported to decrease a drug's effective concentration without compromising membrane integrity and cell growth[19]. However, this approach did not make any of the yeast strains tested more susceptible to CSA or SFA (data not shown).

In a final attempt to screen for SFA sensitivity in *S.cerevisiae*, I acquired CSA sensitive strains, IL993/5c (TB23) and K42 from the Heitman lab (Duke University). Two isogenic IL1993/5c strains bearing the cpr1 gene deletion were also obtained for resistance testing (TB26-4, TB26-5, Table 4.1). Contrary to published reports, in our hands the K42 strain was not sensitive to CSA[15] (Figure 4.3C). I also found that strain insensitive to SFA and FK506. However, TB23 exhibited CSA sensitivity at 1mg/ml, and the isogenic strains TB26-4 and TB26-5 with cpr1 deleted were resistant to CSA at similar concentrations (Figure 4.3D). None of the TB strains showed sensitivity to SFA (Figure 4.3D).

The explanation for the apparent lack of CSA sensitivity in the K42 strain could be that multiple divisions of these strains resulted in genetic changes such as aneuploidies, suppressors, or random mutation that confer CSA resistance. The precise cause for the lack of SFA sensitivity in *S.cerevisiae* is not entirely clear to us. Given the knowledge that yeast cell walls are impermeable to many classes of small molecules and that it is unusual to find CSA-sensitive yeast strains, it is entirely conceivable that SFA lacks permeability in *S.cerevisiae* or that SFA targets other microbes of an unknown phylogenetic class. The possibility that yeasts are insensitive to SFA because they lack an intracellular target for SFA cannot be excluded, however very unlikely.

4.3.3 Screening SFA in Other Fungi

In another attempt to screen SFA in microbes, I turned to the red bread mold *Neurospora crassa* (*N. crassa*) and other wild fungi being studied in the Pringle lab (Harvard OEB). Since *N. crassa* was found to be CSA-sensitive, I considered the

possibility that it could be SFA-sensitive as well. While investigating SFA's effect in *N. crassa*, I screened in parallel other less well characterized wild fungi, *Pseudozyma aphidis*, *Rhodotorula glutinis* and *Candida glaebosa*, for sensitivity to SFA. The idea was that if any of these wild strains exhibited SFA sensitivity, I would subject the sensitive strains to mutagenesis or identify spontaneous mutants that grew under SFA selection. The wild type and resistant strains would be sequenced to identify the genes responsible for SFA resistance. Neither *N. crassa* nor any of the wild fungi showed sensitivity to SFA (Figure 4.4).

Figure 4.4

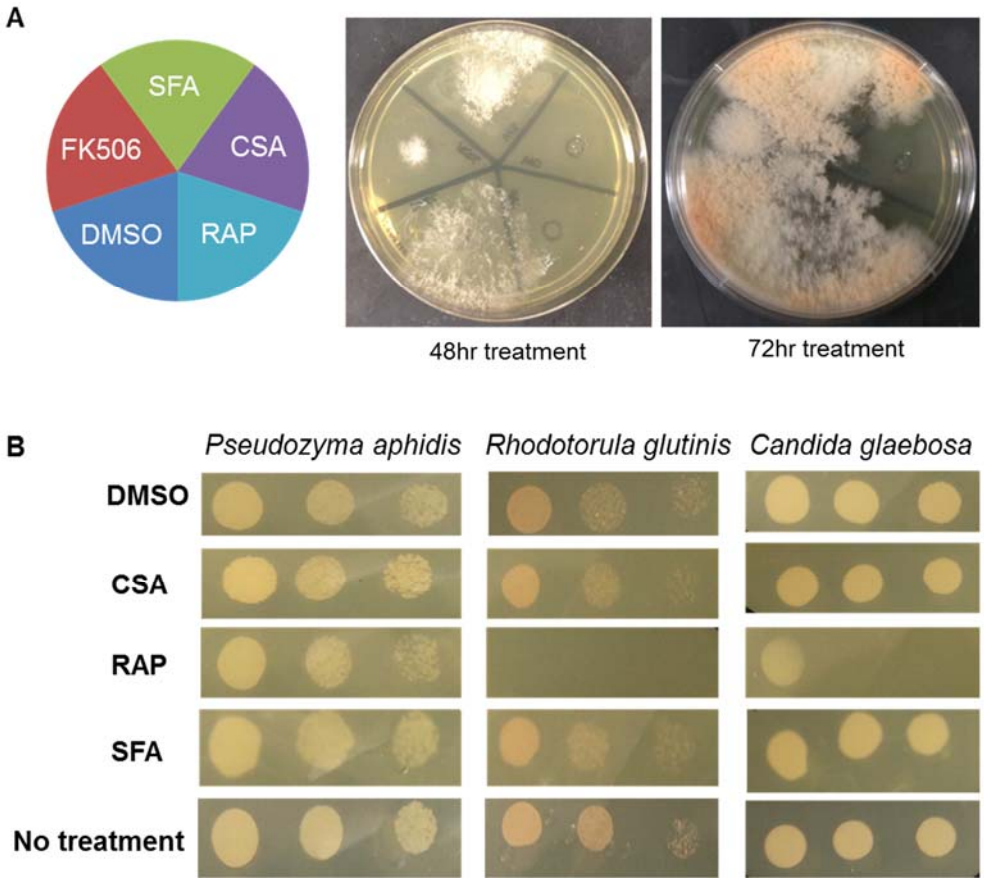

Figure 4.4 – Evaluation of *N. crassa* and Wild Fungi for Sensitivity to Compounds. All compounds were tested at 1mg/ml except for SFA, which was tested at 5.8mg/ml. (A) *N. crassa* subjected to compound treatment on a YPD plate. (B) Fungi were spotted on YPD plates pre-treated with compounds. Details of the experiments can be found in Experimental Procedures.

4.4 Phenotypic Screen of SFA in *Caenorhabditis elegans*

4.4.1 *Caenorhabditis elegans* for Drug Discovery

Caenorhabditis elegans (C. elegans) are 1mm long nematodes that have been widely used as a model organism primarily to study development and neurobiology[20]. It was also critical for mapping out key cellular processes such as apoptosis, development, aging and more recently, RNA-mediated interference (RNAi)[20–23]. Its use in biological research was popularized by Sydney Brenner, who for this work was awarded the Nobel Prize in Physiology or Medicine in 2002[24].

For a simple and tiny organism, *C. elegans* have approximately the same number of genes as humans (~20,000 in *C. elegans* and ~25,000 in humans) with 60-80% of them being homologous to human genes[25,26]. It resembles larger and more complex higher eukaryotes in fundamental ways and thus has been useful in elucidating complex biological processes with minimal technical hurdles and expense. They are inexpensive, small and easy to grow in laboratories. Most importantly, they are genetically tractable using straightforward methods to allow the facile understanding of genes and their function [25]. For these reasons, *C. elegans* have increasingly become popular as a tool for drug discovery, especially for high throughput screening and large scale target validation *in vivo*.

4.4.2 Phenotypic Screen of SFA in *C. elegans*

The motivation behind performing a phenotypic screen with C. elegans was twofold. First, I wanted to study the effect of SFA *in vivo*, and since previous studies with yeasts and fungi were unilluminating, *C. elegans* became the next simplest model

organism available for *in vivo* target validation studies. Secondly, if SFA treated worms exhibited a phenotype, I could directly use RNAi targeting the *C. elegans* homolog of PPIA or IMPDH2 to genetically validate these genes as the targets of SFA.

Annie Conery, a post-doc in Dr Frederick Ausubel's lab at MGH, was instrumental with the set-up of the preliminary screen in *C.elegans*. Since there were no reports documenting the treatment of worms with SFA and we were unsure of the phenotype that we would observe, the goal of this initial study was to observe the effect on worm growth and viability, extrapolating from the knowledge that SFA exhibits potent anti-proliferative effects in a variety of human cell lines. Briefly, worms were treated with vehicle (DMSO) or compounds (MPA, CSA, SFA, ANT) up to 100μM, in liquid S basal media in a 96 well format. Worm viability and growth were visually inspected under a microscope every 24 hours for the next 3 days, and on day 3, wells were imaged with a high-content imager where an entire well is captured in one field. The worms did not exhibit any gross morphological changes nor were they non-viable upon 72 hours SFA treatment (Figure 4.5A). Their sizes were scored with an open-source, image analysis software, CellProfiler, which showed no significant change in worm size between compound and vehicle treatment (Figure 4.5B).

Figure 4.5

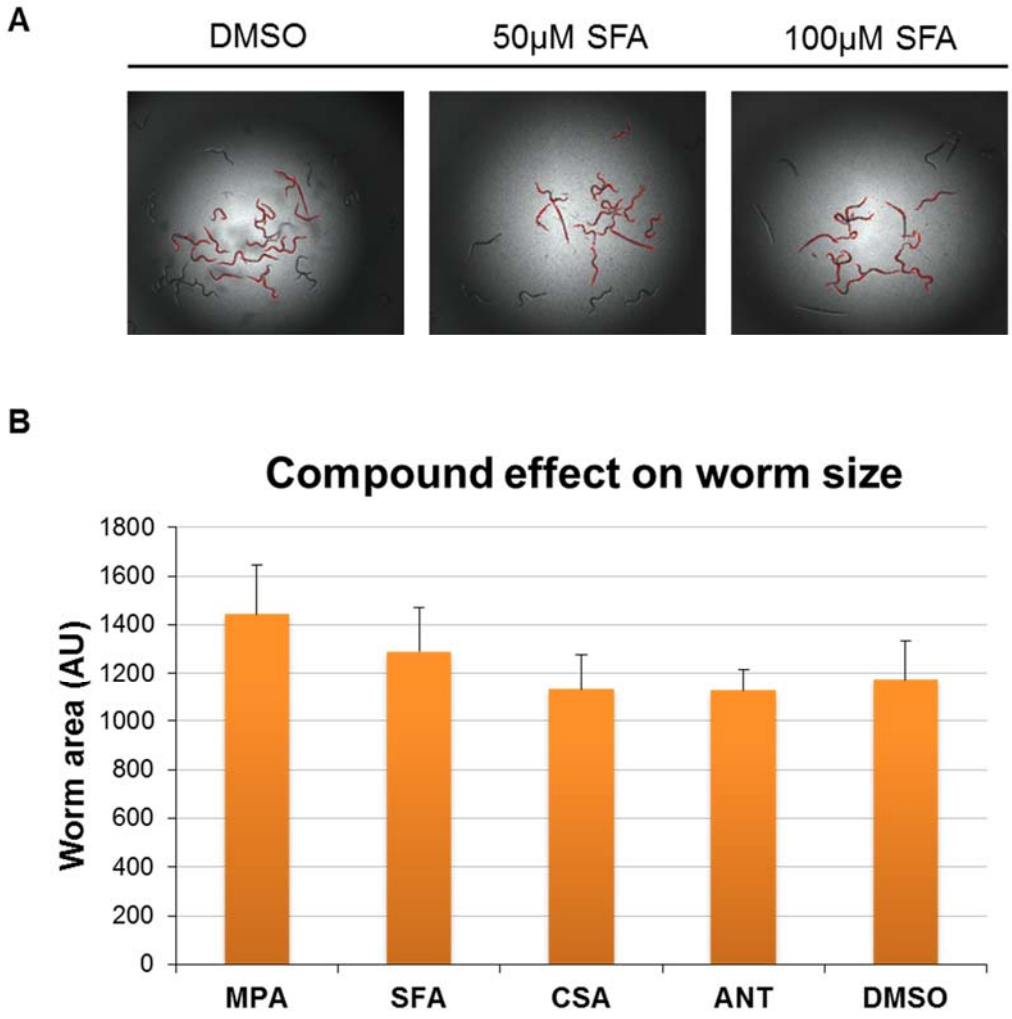

Figure 4.5 – Investigating SFA's Effect on *C. elegans* Grown in Liquid Media. Worms were treated with 0.78uM to 100uM of compound for 3 days with treatments performed in triplicate. (A) Worms were imaged in one field to observe for loss of viability or any gross morphological changes. There is no apparent loss of viability at up to 100uM SFA treatment. (B) Worm sizes from each treatment condition were scored with an open-source image analysis software, CellProfiler after a 3 day treatment. Average worm size was determined by dividing the total worm area in one field by the total number of worms in that same field (outlined in red). Details of the experiments can be found in Experimental Procedures.

While the ease of generating and manipulating a large population of worms makes *C. elegans* attractive for high-throughput screening, its use is not without caveats. As with most organisms, bioavailability remains a chief concern that first needs to be

overcome – that is, compounds need to reach potential targets within the worm. The cuticle and intestinal linings of *C. elegans* pose a major barrier for drugs to access their intended targets[25]. Additionally, the live *E. coli* (OP50) added as a food source could possibly lower effective doses of compounds either by metabolizing or degrading them[26]. Another drawback of screening worms in liquid media is the difficulty of scoring complex phenotypes particularly those involved in behavior, locomotion or subtle morphological changes[26].

Another attempt was made to drug *C. elegans* with SFA on solid nematode growth media. Chi Zhang, a scientist at Warp Drive Bio, provided invaluable assistance with this effort. For this screen, we focused on phenotypes such as sterility, embryonic lethality, larval arrest, changes in brood size, high male incidence, locomotive defects and abnormal body shapes. None of the phenotypes described above was observed with worms that were treated with SFA (Figure 4.6).

Figure 4.6

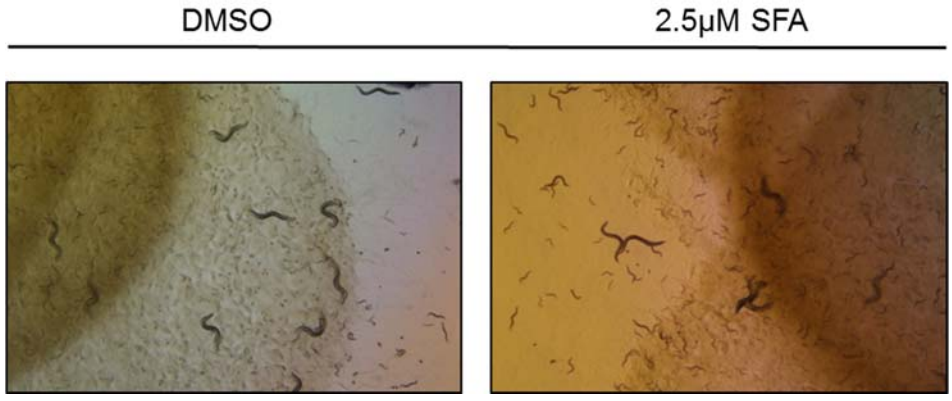

Figure 4.6 – Investigating SFA's Effect on *C. elegans* Grown on Solid Nematode Growth Media. 1 L4 larval worm was treated with DMSO or SFA 5.8mg/ml with fresh compound added to plates daily.

4.5 Using Sequencing to Validate the Targets of SFA

4.5.1 Transcriptome Sequencing to Identify Mechanisms of Drug Action

Given the challenges of target identification, Wacker and colleagues recently demonstrated a novel and alternative approach to ascertain a drug's biological target[5]. Their strategy involves the isolation of multiple-drug-resistant clones and subsequent transcriptome sequencing of these clones to identify mutations in target genes. The rationale behind this approach was that protein mutations of the drug target would confer resistance to that drug[5]. In their proof-of-concept studies with anticancer compounds BI 2536 and bortezomib, they successfully utilized this method to identify Polo-like kinase 1 (PLK1) and proteasomal subunit PSMB5 as the respective targets for these drugs[5]. Another advantage of this target identification strategy is that it does not depend on chemical modifications of compounds, which can potentially affect a compound's mechanism of action[5].

4.5.2 Targeted Sequencing of "resistant" HCT116 Clones

To determine whether PPIA and IMPDH2 are mediating SFA's anti-proliferative effect, I sought to isolate SFA resistant clones from mutagenized HCT116 colon cancer cell line. This cell line was used in the above study by Wacker *et al.* as it has not only defective mismatch repair mechanisms, but also modest expression of multidrug resistant pumps – features ideal for the rapid generation and isolation of clones conferring target specific drug resistance[5]. A schematic illustrating our strategy for SFA resistant clonal selection is shown in Figure 4.7.

Figure 4.7

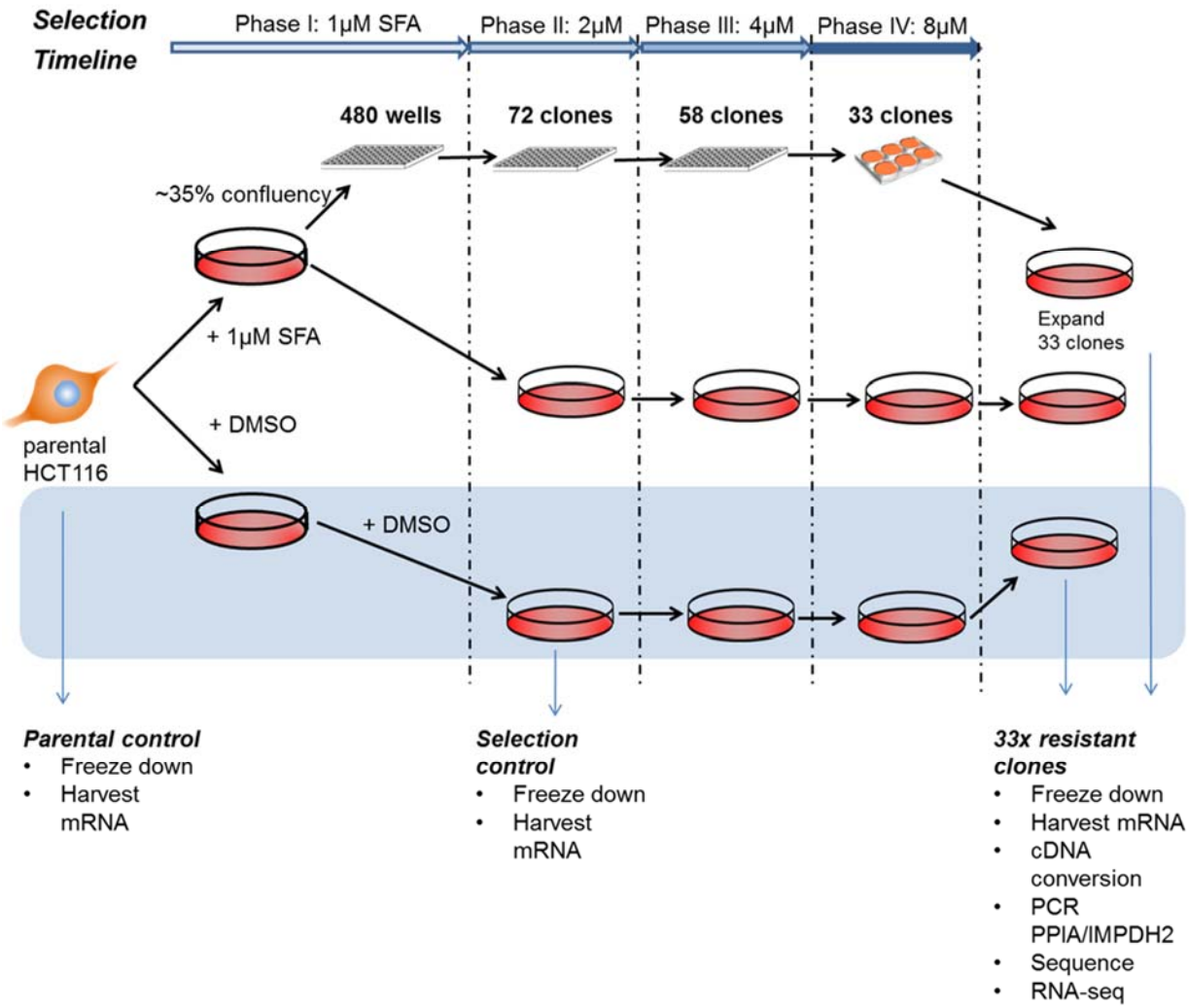

Figure 4.7 – Schematic Illustration of the Strategy for Selecting SFA Resistant HCT116 Clones. Cells were subjected to increasing doses of SFA or DMSO after every passage/phase of selection, starting at 1μM SFA up to 8μM SFA. Cells were split via limiting dilution to obtain single clones for transcriptome analysis. 33 clones that remained viable under 8μM SFA were isolated. The blue box indicates parental line that had undergone a parallel selection process with DMSO.

Since SFA exhibited a potent anti-proliferative effect at 1μM, HCT116 was treated with 1μM SFA or volume matched DMSO as a control (Figure 4.8A). Cells were subjected to increasing doses of SFA or DMSO after every passage, up to 8μM SFA. Cells were split via limiting dilution to obtain single clones for transcriptome analysis. 33

clones that remained viable under 8μM SFA were isolated, and together with the parental line, their mRNA were harvested, converted to cDNA, amplified with PPIA and IMPDH2 specific primers via PCR, and sequenced to determine if there are mutations observed in these putative targets of SFA. Specifically, I was interested to find mutations that lie within the CBS domain of IMPDH2 and/or catalytic residues of PPIA.

Figure 4.8

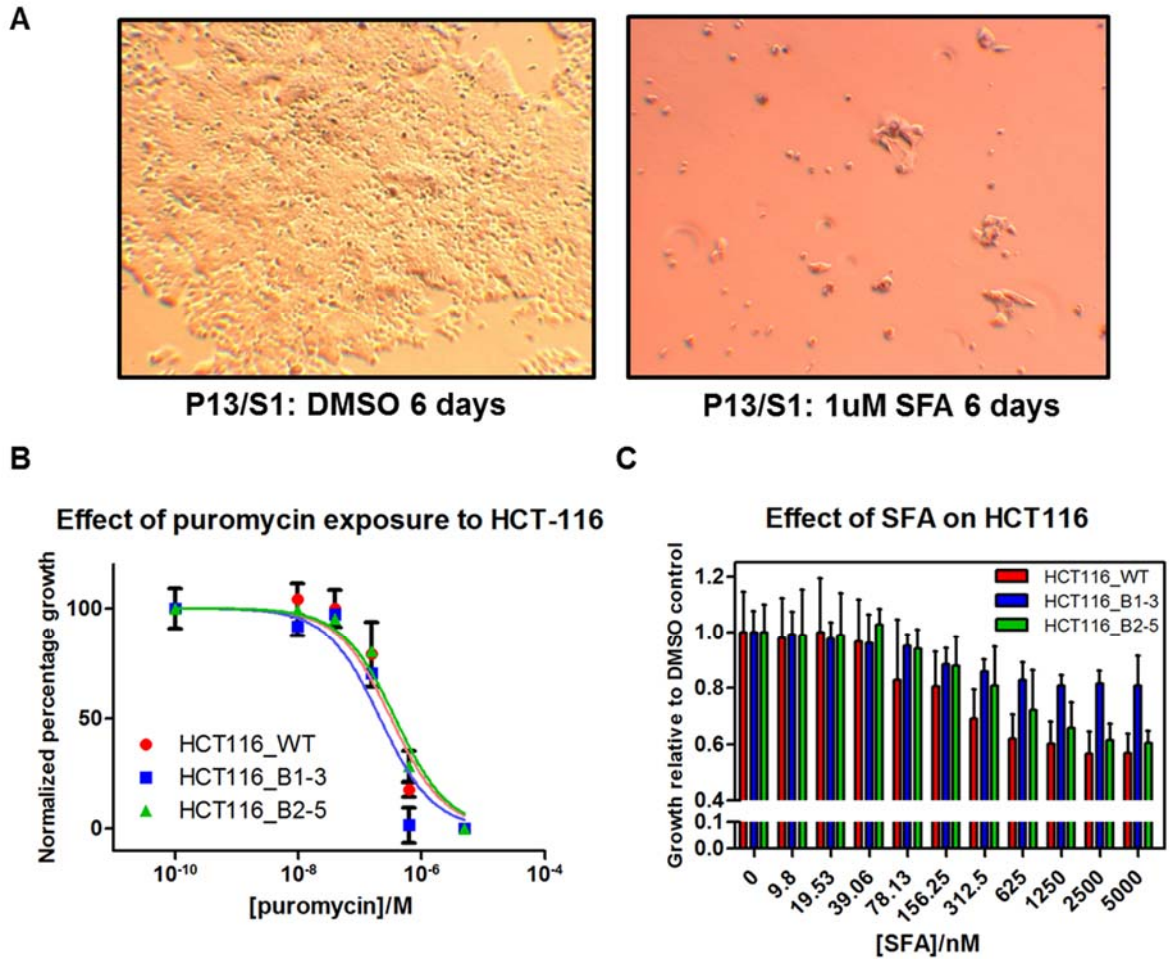

Figure 4.8 – Selecting HCT116 SFA Resistant Clones. (A) HCT116 cells treated with DMSO or SFA for 6 days. Same amount of cells were seeded for each treatment condition. (B) Effect of puromycin on parental and SFA resistant clones, B1-3 and B2-5. Puromycin appeared to be equally potent in all the cell lines. (C) B1-3 and B2-5, isolated clones that have undergone SFA selection were tested for their sensitivity to SFA. These clones did not seem to exhibit significant sensitivity to SFA. Treatments were performed in triplicate and each data point shown is an average of replicates ± the standard deviation.

Resistance to SFA, or any compound for that matter, can also occur through non-target specific mechanisms such as the upregulation of drug efflux pumps (Wacker 2012). Multidrug resistance clones can be identified by reduced sensitivity to unrelated compounds such as puromycin. To determine if clones acquired multidrug resistance, clones were randomly picked and evaluated for their sensitivity to puromycin. Parental HCT116 should be equally sensitive to puromycin as clones that have undergone repeated rounds of SFA selection, if the clones are resistant only to SFA. Two of the clones screened, B1-3 and B2-5, showed similar sensitivity to puromycin as the parental HCT116 line, with an EC_{50} of approximately 30nM (Figure 4.8B). However, the same two clones did not show significant resistance to SFA given that those clones had undergone selection at 8μM SFA (Figure 4.8C). Nonetheless, I went ahead with sequencing the PPIA and IMPDH2 loci of all 33 clones. Although PPIA mutations were observed in some of the clones, those mutations did not occur at the CSA binding site and could have arisen as a PCR or sequencing artifact as the mutations that came up in the disparate clones were similar. No mutations were observed in IMPDH2 (data not shown).

While the examination of compound-resistant clones of cells allows for rapid identification of physiologically relevant targets in mammalian cells, it is not without limitations. This approach is currently restricted to analysis of compounds that are highly cytotoxic although efforts are underway to expand this method to assess phenotypes other than cell viability [2,5]. Since SFA is not strongly cytotoxic, it would be difficult to isolate clones that are truly resistant to SFA. In retrospect, this was not a robust method to identify the target of SFA and this strategy was not pursued further.

4.6 Using RNAi to Validate the Targets of SFA

4.6.1 A Primer on RNAi

Since the landmark publication by Fire et al on the genetic interference of double stranded RNA in *C. elegans*, RNA interference (RNAi) has been extensively used to investigate gene function through the generation of loss-of-function phenotypes by targeting its corresponding transcript[23,27]. Both short hairpin RNA (shRNA) and small interfering RNA (siRNA) genome wide screens have been used to search for new therapeutic targets in a myriad of human disease. Besides being a tool for functional genomics, RNAi also opens the possibility for the development of therapeutic gene silencing.

RNAi is an endogenous cellular process by which messenger RNAs (mRNAs) are targeted for degradation by double-stranded RNA (dsRNA) of identical sequences, which results in gene silencing. Briefly, this silencing is initiated by the RNaseIII enzyme Dicer, which processes dsRNA into small RNAs that are approximately 20 nucleotides long. When integrated into a multi-protein silencing-effector complex termed ribonuclease-containing RNA-induced silencing complex (RISC), the small RNAs direct RISC to complementary mRNA for subsequent mRNA cleavage by Argonaute, the nuclease component of the complex[28,29]. The result is reduced target transcript resulting in reduced target protein levels. Thus RNAi has been valuable as a genomic tool to interrogate gene function.

4.6.2 Studies on PPIA and IMPDH2 Knockdown in Cell Culture

In another approach to genetic target validation, I sought RNAi experiments in mammalian cell lines to confirm that PPIA and IMPDH2 are relevant targets for the growth suppressive phenotype observed upon SFA treatment. Unlike fungi, which appeared resistant to SFA, we observed significant anti-proliferative effect by SFA in certain mammalian cell lines. In addition, the delivery of short-hairpin RNA (shRNA) expression constructs into cell lines can be accomplished using readily available commercial lentiviral pLKO vectors (ThermoScientific). I reasoned that the knockdown of PPIA in cells should produce SFA resistance based on the hypothesis that the biological effect of SFA is contingent on PPIA. Most of the genetic evidence pointing to PPIA as a relevant biological target of CSA were obtained in lower eukaryotes[14–16] and none was published on SFA. A study published by Colgan *et al.* in 2005, demonstrated for the first time in mammals that PPIA knock-out mice are resistant to immunosuppression by CSA[30].

Constructs expressing shRNAs targeting PPIA were chosen over synthetic PPIA siRNAs as we desired to make stable PPIA knockdown lines for permanent silencing of PPIA as a tool for downstream studies. PPIA knockdown shRNA constructs were ordered from ThermoScientific and screened for knockdown efficiencies in HEK293 cell lines. Two PPIA shRNA constructs screened, shPPIA-168 and shPPIA-232, exhibited greater than 90% knockdown efficiency as assessed by western blotting (Figure 4.9A). These two PPIA knockdown constructs were used to further generate stable PPIA knockdown cell lines in Jurkat, HeLa, K562 and KBM7 lines (Figure 4.9B-D).

Figure 4.9

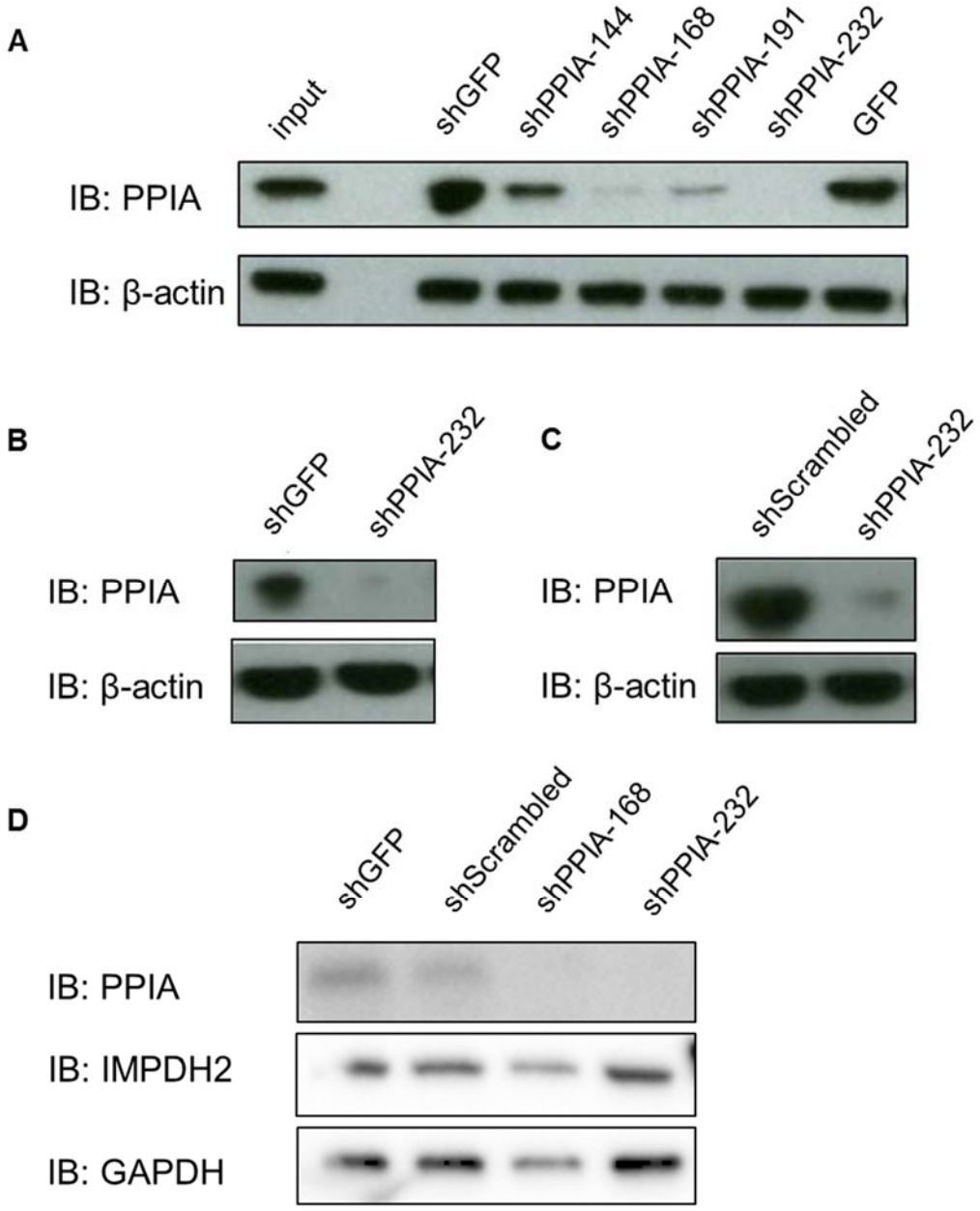

Figure 4.9 – Knockdown of PPIA in Mammalian Cells. (A) PPIA knockdown shRNA constructs were ordered from ThermoScientific and screened for knockdown efficiencies in HEK293. shPPIA-168 and shPPIA-232 constructs were effective at depleting endogenous PPIA and were used to make stable PPIA knockdown mammalian lines. (B) Assessing PPIA knockdown efficiency in stable PPIA knockdown HeLa line. (C) Assessing PPIA knockdown efficiency in stable PPIA knockdown Jurkat line. (D) Assessing PPIA knockdown efficiency in stable PPIA knockdown K562 line. Details of the experiments can be found in Experimental Procedures.

The PPIA knockdown cell lines were then tested to determine if they show resistance to SFA compared to mock knockdown cell lines. PPIA depletion in these cell lines did not afford SFA resistance relative to control (Figure 4.10).

While these results potentially suggest that the effect of SFA is independent of PPIA, there are several reasons why this could be otherwise. The most obvious reasons derive from the limitations of RNAi technology, namely inherent partial target depletion and confounding off-target effects[31,32]. The former limitation is of particular importance based on our PPIA gain-of-function hypothesis since incomplete knockdown may fail to produce a measurable resistance to SFA's anti-proliferative effect. This notion is further supported by evidence demonstrating that heterozygous PPIA +/- splenocytes were as sensitive to CSA as homozygous PPIA +/+ wild-type splenocytes showing no PPIA dosage sensitivity to CSA[30]. Interestingly, homozygous PPIA -/- knockout splenocytes exhibited resistance to CSA up to approximately 100nM and showed CSA dose dependent sensitivity at concentrations above 250nM[30]. This was attributed to other cyclophilin isoforms mediating calcineurin inhibition. Additionally, since PPIA is ubiquitously expressed, it is possible that the suppressed PPIA levels are sufficient to mediate the growth inhibitory effects of SFA.

Figure 4.10

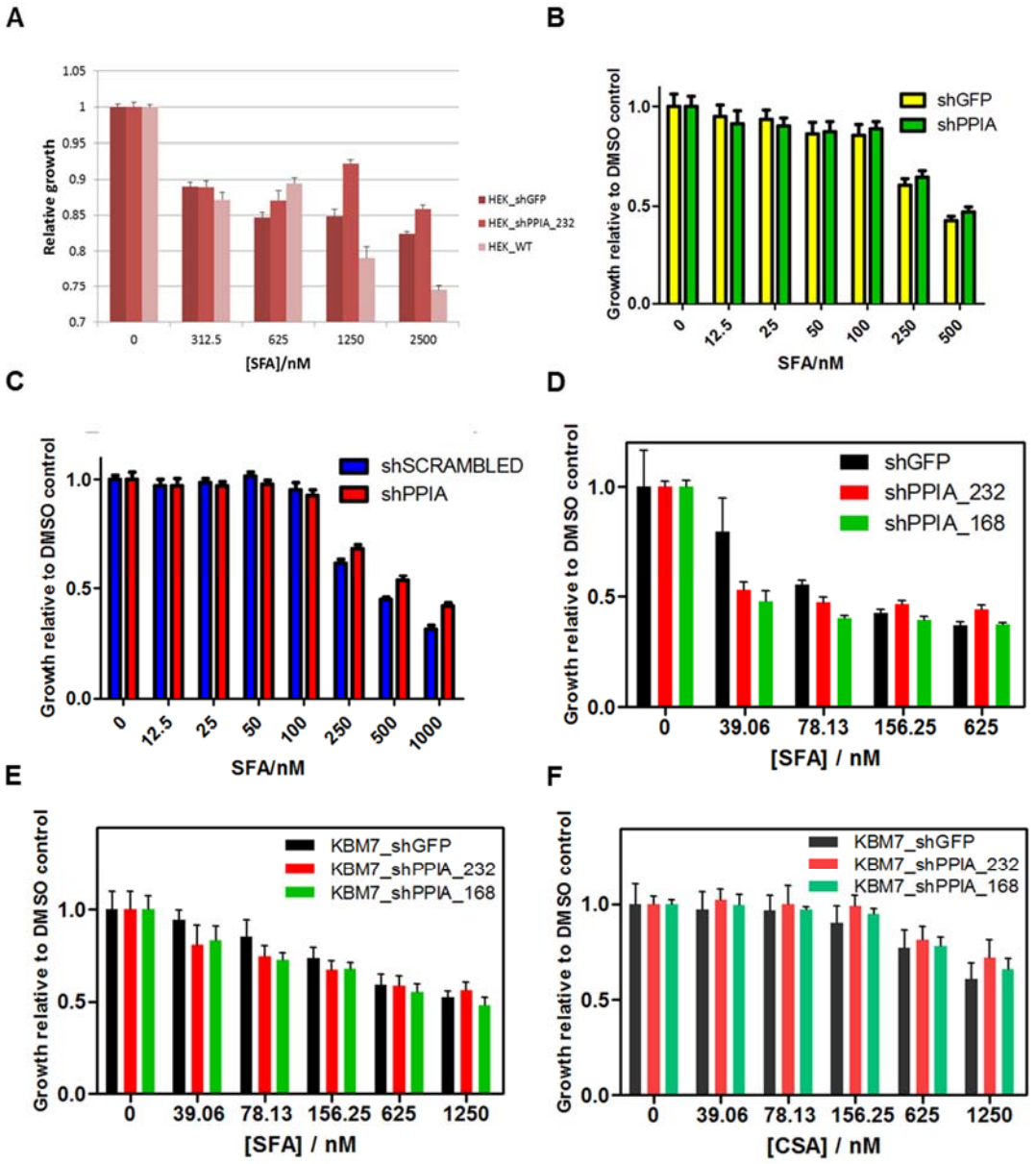

Figure 4.10 – Evaluation of SFA Sensitivity in Stable PPIA Knockdown Cell Lines. (A) Stable HEK293 cells were subjected to SFA treatment for 3 days. (B) Stable Jurkat cells were treated with SFA for 4 days. (C) Stable HeLa lines were subjected to SFA treatment for 4 days and the relative cell numbers were assayed using crystal violet staining assay. (D) Stable K562 cells were subjected to SFA treatment for 3 days. (E) Stable KBM7 cells were treated with SFA for 3 days. (F) Stable KBM7 cells were treated with CSA for 3 days. Treatments were performed in triplicate and each data point shown is an average of replicates ± the standard deviation. shPPIA refers to shPPIA-232 construct unless otherwise stated. The relative cell numbers were assayed using the CellTiter-Glo Luminescent Cell Viability assay (Promega) unless otherwise stated. Details of the experiments can be found in Experimental Procedures.

Efforts were made to obtain PPIA -/- knockout MEFs or splenocytes from the Luban lab that created this knockout mouse, but they had stopped working with these mice at the time of contact. Another faculty at University of California Los Angeles, Robert Chiu, who is working with these mice, was not able to provide us with the materials.

To achieve stable IMPDH2 knockdown in cells, a similar approach was followed. IMPDH2 knockdown shRNA constructs were ordered from ThermoScientific and screened for knockdown efficiencies in Jurkat cell lines. While the PPIA knockdown constructs resulted in a significant loss in endogenous PPIA, the IMPDH2 knockdown constructs did not effectively deplete endogenous IMPDH2 (Figure 4.11). As such, we turned to CRISPR/Cas9 gene editing technology to knockout PPIA and IMPDH2.

Figure 4.11

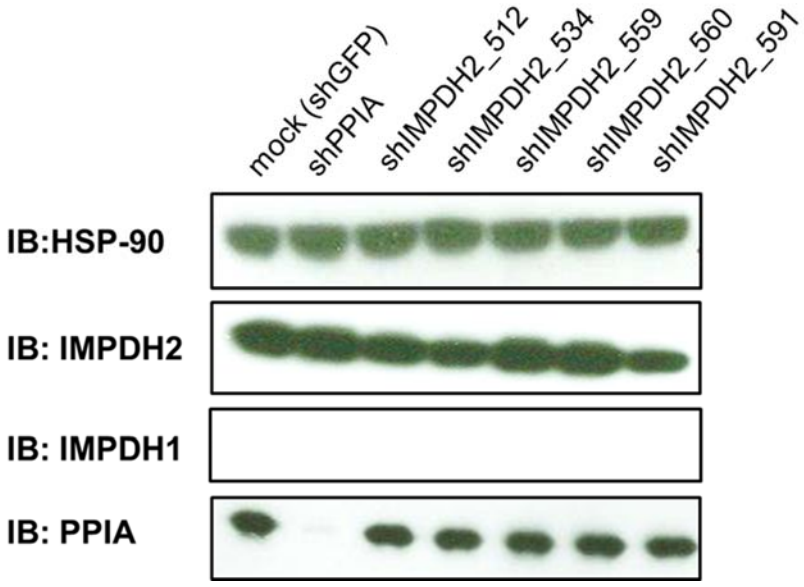

Figure 4.11 – Knockdown of IMPDH2 in Jurkat Cells. IMPDH2 knockdown shRNA constructs were ordered from ThermoScientific and screened for knockdown efficiencies. None of these constructs tested seemed to be effective at depleting endogenous IMPDH2.

4.7 Using CRISPR/Cas9 to Knockout SFA Targets in Cells

4.7.1 The CRISPR/Cas9 System

Clustered regularly interspaced short palindromic repeats, or CRISPR, are loci found within prokaryotic and archaeal genomes that provide acquired immunity against attacking foreign DNA through RNA-mediated DNA cleavage by Cas9 nucleases[33,34]. Briefly, short segments of foreign DNA are integrated into the CRISPR loci as 'spacers', transcribed and processed to mature CRISPR RNAs (crRNAs) that guide Cas9 nucleases to home-in and cleave DNA complementary to the spacer sequence. The CRISPR/Cas9 system is actively being employed by scientists to target specific genes in cells from all kingdoms and has since become an efficient and versatile method to manipulate target DNA sequences and genes, both *in vitro* and *in vivo* [35–37].

Prior gene editing technologies such as zinc finger nucleases (ZFNs) and transcription activator-like effector nucleases (TALENs) rely on custom protein design and engineering to precisely target genomic areas of interest, which itself is a technical hurdle[38]. The CRISPR-Cas9 system bypasses the need for customized nuclease engineering since Cas9 facilitates DNA targeting via a programmability that is dictated by easily designed RNA molecules [35,36,39]. Hence Cas9 is the "single unifying factor capable of colocalizing RNA, DNA and protein" that has revolutionized the field of genetic editing[37].

Early Cas-9 based gene editing platforms required two short RNAs for specific targeting by *Streptococcus pyogene's* Cas9 but has since been replaced by a single guide RNA (sgRNA) for targeting[35,36,39]. The co-expression of Cas9 tagged with nuclear

localization signals and custom designed sgRNA forms a DNA targeting recognition and cleavage complex that specifically cuts DNA that complements the sgRNA sequence a few base pairs upstream of a required NGG protospacer adjacent motif (PAM)[35,36]. This complex induces targeted double stranded breaks in DNA that stimulate both homology-directed repair (HDR) and non-homologous end joining (NHEJ) repair mechanisms. Repair by NHEJ often leads to small insertions and deletions (indels) that result in frameshift mutations[40]. Furthermore, the engineering of nuclease-dead and nicked version of Cas9 (Cas9-D10A) has expanded a scientist's genomic toolkit to generate knock-ins and modulate gene expression through Cas9 fusion with transcriptional activators and repressors[37,40]. Looking forward, the CRISPR/Cas9 editing technology will enable the discovery of new therapeutic targets and facilitate target identification and validation efforts in drug discovery.

4.7.2 IMPDH2 Knockout with CRISPR/Cas9

Since knockdown of IMPDH2 by shRNA was incomplete and that of PPIA yielded inconclusive results, I sought orthogonal approaches that would enable the study of how modulating PPIA and IMPDH2 would influence the cellular phenotype upon treatment with SFA. The relative ease of using the CRISPR/Cas9 system via a sgRNA to perturb gene function makes this a powerful tool for creating PPIA and IMPDH2 knockout cell lines. sgRNAs targeting exon 1 of PPIA and IMPDH2 were designed and checked for off-sequence targeting with the CRISPR design tool developed by the Zhang lab (MIT) (Figure 4.12A). The K562 cell line, which appeared to be the most sensitive cell line to SFA, was used to generate PPIA and IMPDH2 knockout clonal lines. The sgRNA

targeting IMPDH2 had a targeting efficiency of ~19% as assessed by sequencing (Figure 4.12B). However, sgRNA targeting of PPIA did not yield any clones that harbored a frameshift in PPIA as determined by sequencing (Figure 4.12C). The likely reason for the unsuccessful targeting of PPIA can be attributed to the difficulty in designing highly specific PPIA sgRNAs at the desired genomic loci due to homology to PPIA pseudogenes and other cyclophilin isoforms. This problem can potentially be circumvented by creating multiple double stranded breaks at the PPIA loci of interest by targeting it with two or more sgRNAs.

Figure 4.12

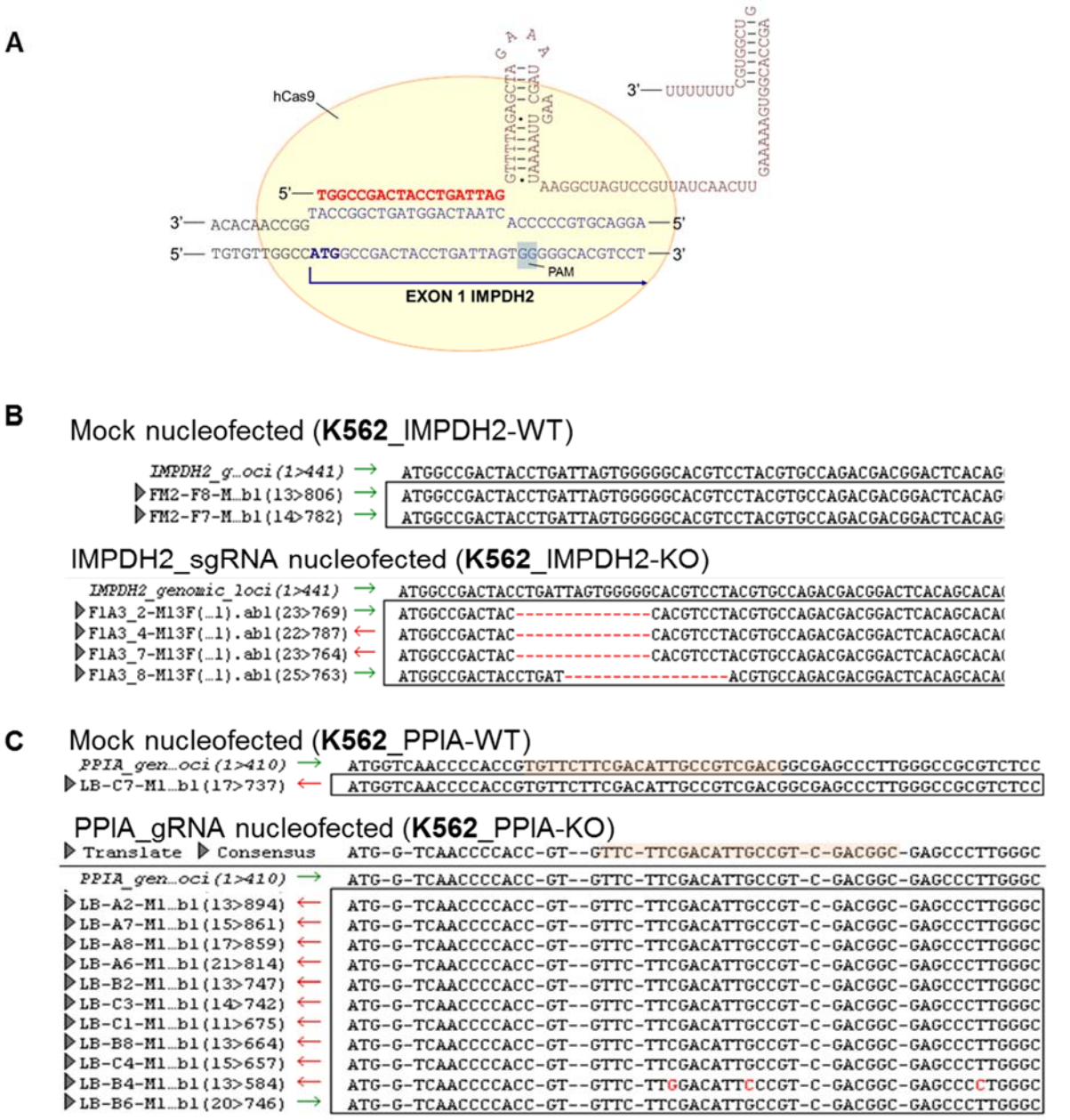

Figure 4.12 – IMPDH2 and PPIA gene inactivation by CRISPR/Cas9. (A) Cartoon showing Cas9 nuclease (yellow) complexed with sgRNA (red/deep red) targeting exon 1 of IMPDH2 (blue). (B) Successful targeting of IMPDH2 loci as shown by the deletions in the genome from sequencing. Mock nucleofected K562 cells showed wild type sequence at exon 1 of IMPDH2 loci (top) but A3 knockout clonal line had deletions at exon 1 of IMPDH2 loci (bottom). These deletions led to a frameshift which results in IMPDH2 gene inactivation. (C) Targeting of PPIA was not successful as targeting efficiency was extremely low. None of the colonies screen harbored any indels at exon 1 of PPIA. Details of the experiments can be found in Experimental Procedures.

sgRNA targeting IMPDH2 was co-transfected with a hCas9 construct, and cells were split via limiting dilution to obtain single clones. Several clonal cell lines that harbored IMPDH2 deletion were isolated. In particular, the A3 clone, with IMPDH2 completely knocked out, and the B7 clone which was a control clonal line that escaped CRISPR targeting and has endogenous IMPDH2 expression, were characterized for IMPDH2 expression level, growth rate and sensitivity to SFA (Figures 4.13A-C). Although cells were viable, A3 cells were growing significantly slower than the control B7 cells as would be expected of SFA treated K562 cells. When treated with 100nM SFA for 3 days. A3 exhibited less sensitivity than the B7 or WT lines (Figure 4.13B). Nonetheless, this method does not solely assess the specific role of the CBS domains of IMPDH2 in cell proliferation as the enzymatic function of IMPDH2 is also perturbed: inhibition of the enzymatic function of IMPDH with inhibitor MPA also results in decreased cell proliferation[41]. Further complication came to light with the discovery that IMPDH2 knockout in K562 cells induced their differentiation to hemoglobin producing erythroid cells as determined by the pinkish coloration of cell pellet and further confirmed by benzidine staining[41] (Figure 4.14). These differentiated cells show restricted potential for proliferation relative to undifferentiated precursors, which complicates the comparison of the effect of SFA on the wild type and knockout IMPDH2 lines[41].

Figure 4.13

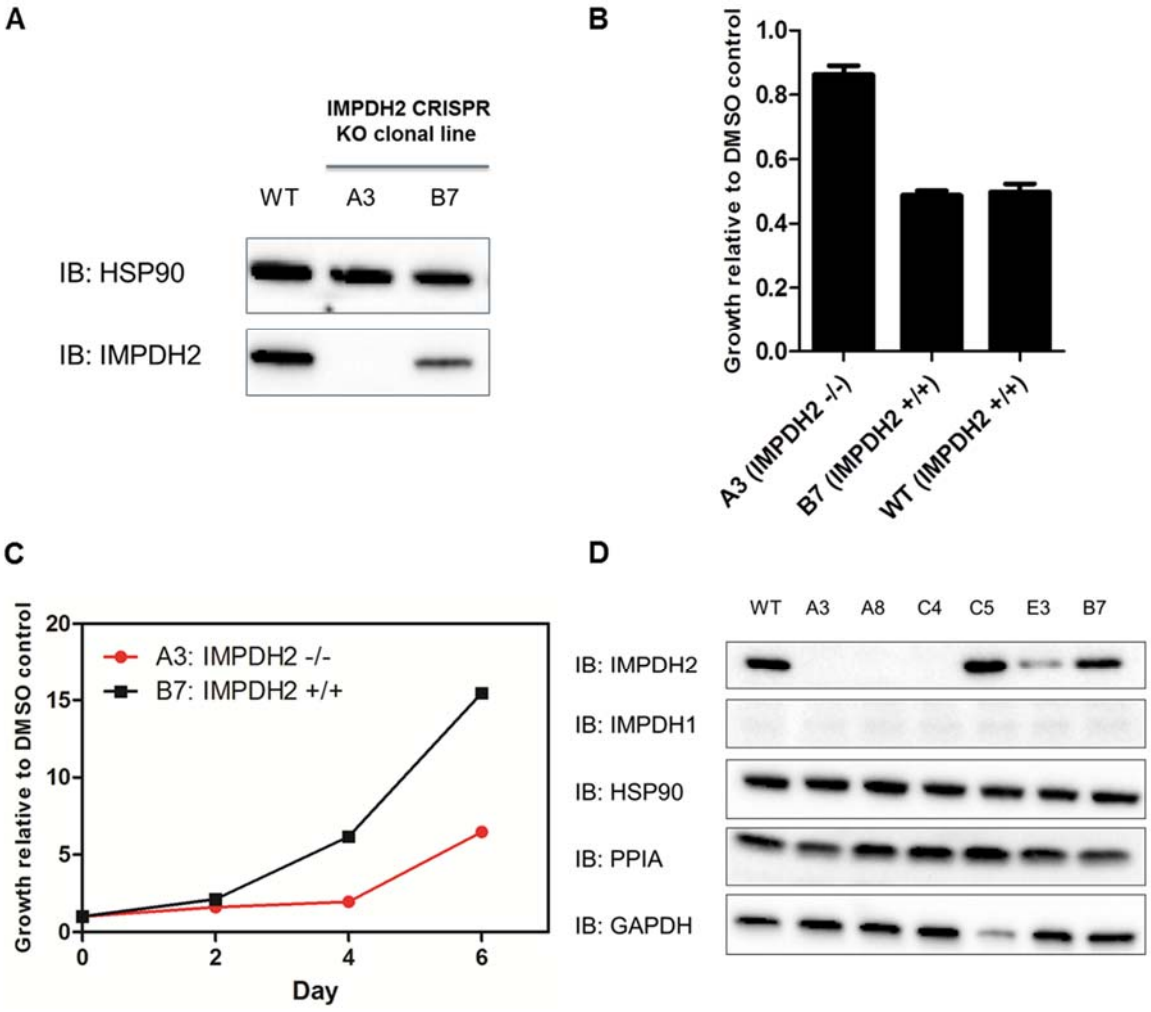

Figure 4.13 – Characterization of CRISPR Knockout Lines. (A) Western blot showing IMPDH2 expression was completely eliminated in A3 knockout clonal line. B7, a clonal line which escaped CRISPR targeting, presumably through faithful DNA repair, showed endogenous levels of IMPDH2. (B) A3 clonal line (IMPDH2 knockout) and B7 and wild-type (WT) K562 cells were treated with 100nM SFA for 3 days and the relative cell numbers were measured using the CellTiter-Glo Luminescent Cell Viability assay (Promega) (C) Cell growth for A3 and B7 clonal lines were monitored over a period of 6 days. The relative cell numbers were measured using an MTT assay (Promega). Treatments were performed in triplicate and each data point shown is an average of replicates ± the standard deviation. (D) Evaluation of IMPDH2 levels of isolated clones from CRISPR targeting by Western Blotting.

Figure 4.14

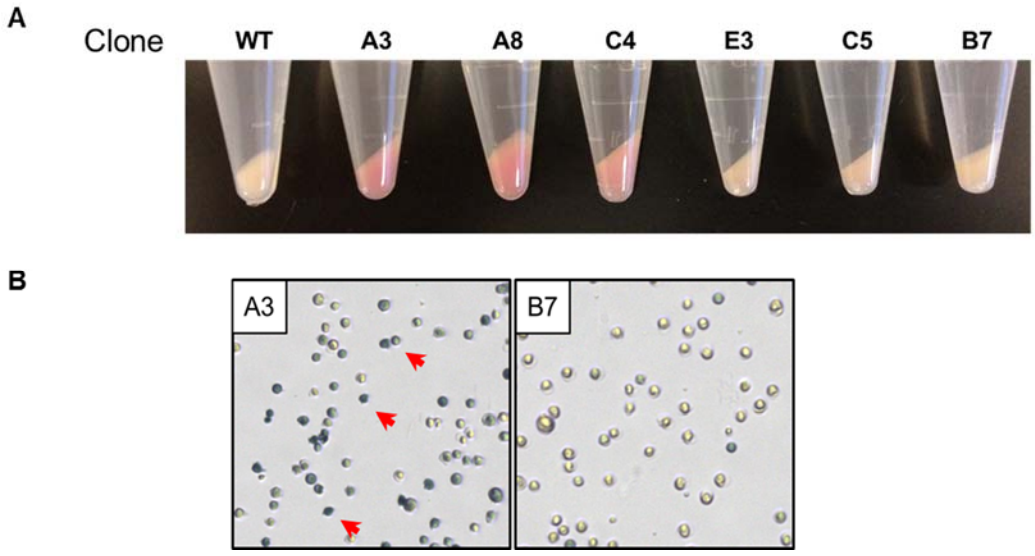

Figure 4.14 – Induction of Differentiation to Hemoglobin Producing Erythroid Cells. (A) Cell pellets for isolated CRISPR clonal lines were obtained by centrifuging 10ml of cells followed by a wash with PBS. Clonal cells with IMPDH2 knocked out appeared pink (clones A3, A8 and C4) (B) Benzidine staining of A3 and B7 clonal lines. Hemoglobin producing cells are stained blue (indicated by red arrows). Details of the experiments can be found in Experimental Procedures.

Since the A3 clones still exhibited sensitivity to SFA at higher concentrations, I wondered if there could be other biologically relevant, low affinity, low abundance targets of PPIA-SFA that perhaps got masked in the IP-MS assay by the presence of IMPDH2. Toward this end, I revisited the IP-MS assay using A3 cells as a source of IMPDH2 depleted protein lysate. In CSA treated lysate samples, we consistently found HERC2 and NEURL4 proteins being enriched indicating that the affinity purification assay produced reliable results (Figure 4.15A). These proteins have been shown to interact very specifically with PPIA-CSA in IP-MS experiments performed in a variety of cells lines (personal communications). However, there was not a single enriched target that appeared consistently in all SFA treated lysate samples (Figure 4.15B). PKM2,

FASN, GPI and PGK1 showed up as putative targets in some but not all SFA treated samples, but also showed up in CSA and MPA negative control samples. This lack of consistency led us to conclude that the interactions with these other targets are likely non-specific, and that it is more reasonable to suggest that a direct molecular target of SFA could be eliciting SFA's effect in these knockout lines.

Figure 4.15

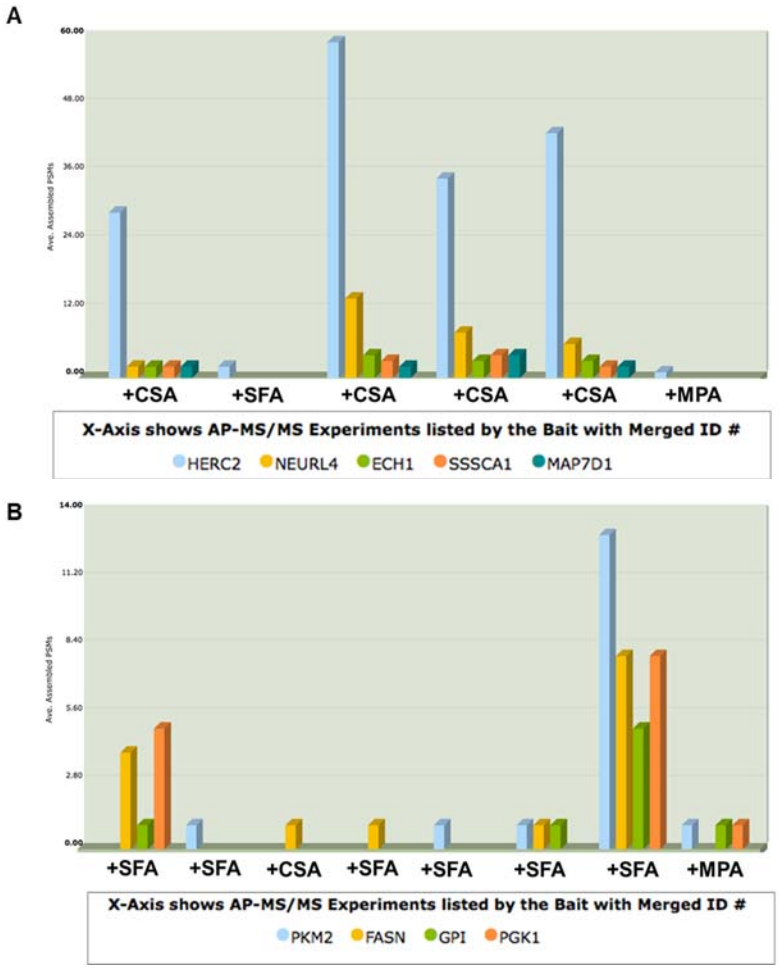

Figure 4.15 – Results from HA-immunoprecipitation of HA-tagged PPIA Using A3 cells as Lysate Source. (A) IP performed in the presence of CSA showed consistent enrichment of HERC2, NEURL4, ECH1, SSSCA1 and MAP7D1 but not in other compound treatment. (B) IP done in the presence of SFA. None of the protein targets were consistently enriched. Each set of bar graphs represent one IP experiment done with one compound treatment as indicated on the x-axis. Total spectral counts are represented on the y-axis. Details of the experiments can be found in Experimental Procedures.

4.7.3 Investigating Rescue with IMPDH Overexpression Constructs

To disentangle the enzymatic and CBS domain effect on cell proliferation, I introduced expression vectors encoding IMPDH2 cDNA that would restore the enzymatic function of IMPDH2. The discovery of the I192V/E214D IMPDH2 double mutant which lost binding to PPIA-SFA (see Chapter 3.3) provided an excellent negative control for SFA sensitivity experiments because in principle, we would expect this mutant to not only rescue the enzymatic function but show resistance to SFA's effect. Prior to that discovery, I worked with IMPDH1, a null binder to PPIA-SFA at 100nM as a surrogate negative control.

Stable cell lines overexpressing wild-type IMPDH2 and IMPDH1, CBS deleted IMPDH2 and GFP control were made using A3 clones as the parental line (Figure 4.16A). The cells were then tested for sensitivity to SFA. Cells overexpressing IMPDH1 did not appear to be significantly resistant to SFA when tested at 100nM, while the IMPDH2 overexpressing A3 cells were the most sensitive (Figure 4.16B). This rescue of SFA sensitivity via the overexpression of IMPDH2 in A3 further confirms the specificity of the target. Although the introduction of CBS deleted IMPDH2 did not seem to rescue SFA sensitivity, this analysis was confounded by the differences in the growth rate relative to wild-type observed in these cell lines in the absence of the drug. Despite restoring the enzymatic activity of IMPDH2 in the cells, I could not rescue the defect in proliferation in the A3 line. This suggests that the CBS domain in the context of the IMPDH2 core domain has a previously unappreciated function involved in cellular proliferation.

Figure 4.16

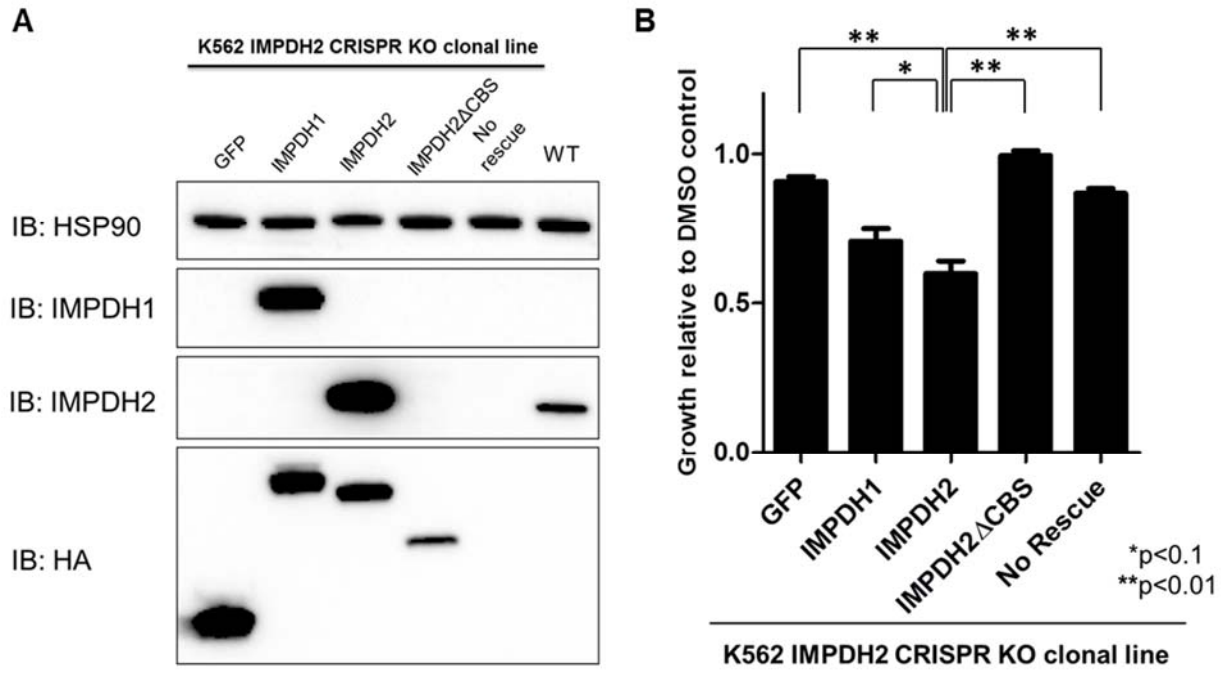

Figure 4.16 – Investigating the Effect of Rescue Constructs on SFA Sensitivity in A3 Cells. Overexpression constructs of IMPDH were introduced to A3 clonal cells (IMPDH2 null) (A) Western blot showing the overexpression of rescue constructs in IMPDH2 knock out A3 parental line. (B) Rescue cell lines were tested for their sensitivity to SFA. Rescue with wild type IMPDH2 restored SFA sensitivity. Rescue cell lines were treated with 100nM SFA for 3 days and the relative cell numbers were measured using the CellTiter-Glo Luminescent Cell Viability assay (Promega). Treatments were performed in triplicate and each data point shown is an average of replicates ± the standard deviation.

In another independent attempt to investigate the different sensitivities of IMPDH2 overexpression in A3 clonal lines, stable cell lines overexpressing wild-type, double mutant I192V/E214D, CBS deleted IMPDH2 and GFP control were made using A3 clones as the parental line (Figure 4.17A) and their growth rates under normal conditions were evaluated. There was no significant difference between the growth rates of the wild-type and double mutant rescue lines, indicating that the mutations did not affect the function of the CBS domains (Figure 4.17B). I then evaluated the effect of SFA on these rescue cell lines. While the wild type rescue line showed sensitivity to

SFA at EC_{50} of 100nM, there was no significant effect of SFA on the double mutant rescue line (Figure 4.17C). These findings suggest that the CBS domains of IMPDH2 could be implicated in cell proliferation and that SFA, by co-opting PPIA, interferes with this domain function.

Figure 4.17

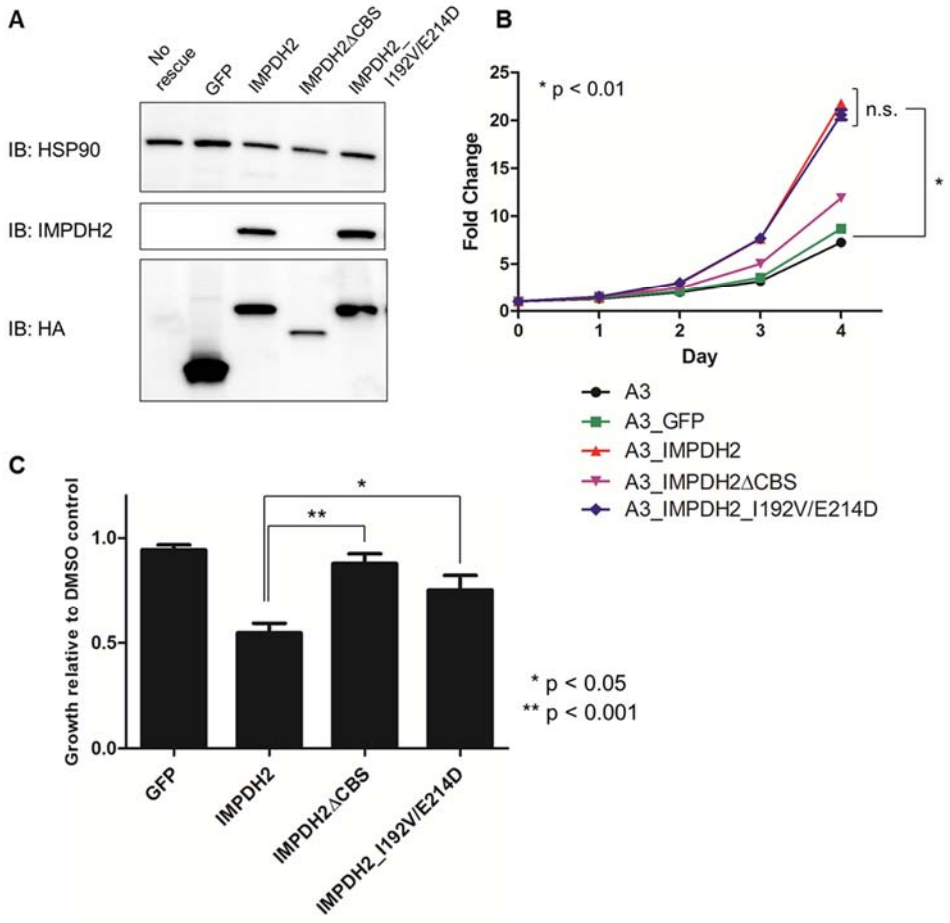

Figure 4.17 – Reinvestigating the Effect of Rescue Constructs on SFA Sensitivity in A3 cells. Overexpression constructs of IMPDH2 were introduced to A3 clonal cells (IMPDH2 null) (A) Western blot showing the overexpression of rescue constructs in IMPDH2 knock out A3 parental line. (B) Cell growth for the rescue lines were monitored over a period of 4 days. The relative cell numbers were measured using an MTT assay (Promega). (C) Rescue cell lines were tested for their sensitivity to SFA. Rescue with wild type IMPDH2 restored SFA sensitivity, whereas rescue with IMPDH2_I192V/E214D mutant conferred resistance to SFA. Rescue cell lines were treated with 100nM SFA for 3 days and the relative cell numbers were measured using an MTT assay (Promega). Treatments were performed in triplicate and each data point shown is an average of replicates ± the standard deviation.

4.8 Conclusions

In this chapter, we examined a variety of approaches towards genetically validating PPIA and IMPDH2 as biologically relevant targets of SFA. Inspired by the lessons gleaned from CSA, FK506 and RAP in yeast genetic studies, we made attempts to validate PPIA and IMPDH2 as targets of SFA in yeast. Furthermore, to date, there have been no published data on SFA's effect in yeast. However, *in vivo* studies with fungi and worms, showed no observable phenotype when these organisms were treated with SFA. Screening for a microbe which exhibits SFA sensitivity would be an effort worth pursuing moving forward, although this would require collaboration with a lab possessing a vast collection of microbial strains amenable for high throughput screening.

Although examination of drug-resistant clones has proven utility in target identification endeavors, this approach is not well suited for a compound like SFA since cell viability remains the primary phenotype for the success of such an approach. In another approach, we sought to modulate target expression either by overexpressing IMPDH2 or by knocking down PPIA and IMPDH2 in the hope that altered target levels would alter SFA sensitivity. Overexpressing IMPDH2 did not confer resistance to SFA suggesting that the mechanism of growth inhibition was not likely to involve the loss of IMPDH2 function. Rather, it could be a gain of function of IMPDH2 or that the ternary complex forms a toxic species in cells. Our results also imply that SFA does not modulate guanosine biosynthesis. Knocking down PPIA in mammalian cells did not provide insight into whether PPIA is required for SFA's action. Knock out studies in mice have previously shown that haploinsufficiency of PPIA does not confer resistance to

CSA suggesting that intermediate PPIA levels would still show complete sensitivity to CSA, and quite possibly to SFA. This was observed with our data as well, as a near complete knockdown of PPIA still did not produce the phenotype we had expected.

Finally, we turned to the CRISPR/Cas9 gene editing platform to inactivate PPIA and IMPDH2. We had no success with targeting PPIA but efforts in this area are still ongoing. Hence, whether PPIA is causally involved in SFA's action remains to be firmly established. While CRISPR/Cas9 inactivation of IMPDH2 was successful in K562 cells, it was difficult to obtain actionable data from testing the sensitivity of knockout clones to SFA largely because the loss of IMPDH2 also affected the enzymatic function of IMPDH2, which is known to be critical for cell proliferation. In K562, inhibition of the enzymatic function induced these cells to differentiate into hemoglobin producing erythroid cells which showed restricted potential for growth[41]. In an attempt to deconvolute the enzymatic and CBS functions of IMPDH2, we added back expression vectors encoding wild-type, double mutant I192V/E214D and CBS deleted IMPDH2 to reinstate the enzymatic function of IMPDH2. Cells with wild-type and double mutant I192V/E214D IMPDH2 introduced regained their ability to proliferate quickly, but not cells introduced with the CBS deleted IMPDH2 construct. When tested with SFA, the wild type cells were significantly more sensitive to SFA than the double mutant cells at 100nM, although the difference in EC_{50} of these two lines was only approximately 2 fold. Nonetheless, this does suggest that the CBS domain of IMPDH2 could have a previously unappreciated role in cell proliferation that is modulated by PPIA-SFA. It was initially surprising to observe that the CBS deleted IMPDH2 did not restore growth to a similar extent as full length IMPDH2. This, however, is consistent with previous

observations that have been made on the role of this domain as a regulatory element in adenylate nucleotide biosynthesis[42].

In the final chapter of my thesis, other hypothesis guided mechanism-of-action studies will be discussed as well as unbiased approaches toward SFA target identification.

Experimental Procedures

General Methods and Chemicals

Oligonucleotide primers were ordered from Eurofins MWG Operon or Integrated DNA Technologies. PCR was performed with Phusion High-Fidelity DNA Polymerase (Life Technologies) and purified with a PCR cleanup kit (Qiagen or Zymo Research). Absorbance measurements were performed with a NanoDrop 2000C spectrophotometer (ThermoScientific). Mini-PROTEAN® TGX Stain-Free™ polyacrylamide gels (Bio-Rad, Hercules, CA), Mini-PROTEAN Tetra cell electrophoresis chamber with Tris/Glycine/SDS running buffer (Bio-Rad, Hercules, CA) were used for protein analysis. Proteins were transferred to polyvinylidene difluoride (PVDF) membranes using Trans-Blot® Turbo™ (Bio-Rad, Hercules, CA) for blotting. SFA was a generous gift from Novartis. CSA, DMSO, puromycin, adenosine, thymidine and guanosine were ordered from Sigma-Aldrich. Polygodial was ordered from Santa Cruz.

Fungi Culture Information

S. cerevisiae strains used in experiments were a kind gift from various laboratories. Strain information and sources can be found in Table 4.1. Yeasts were grown in YPD media at 30^{o}C. For yeast spotting experiments, yeasts were grown in YPD media overnight and the next day, cells were diluted to give an OD_{600} of 0.8 in 5ml of YPD media. Cells were centrifuged at 5 minutes at 2000 rpm in a table top centrifuge. Pellet was transferred into a microcentrifuge tube using 1.2ml of milliQ water. Cells were centrifuged briefly at 10000 rpm and pellet was resuspended in 1ml milliQ water. Yeast was spotted after 1 to 6 ten-fold dilutions on a YPD plate pre-treated with compound.

Dilutions were done in a 96 well plate. For polygodial treatment, a 100µg/ml stock (in ethanol) was mixed with tested compound to give a final polygodial concentration of 0.4µg/ml. *N. crassa, P. aphidis*, *R. glutinis* and *C. glaebosa* were a kind gift from Anne Pringle (Harvard OEB). These were grown on YPD agar at room temperature.

Cell Culture Information

Human cancer cell lines K562 (a kind gift from the Saghatelian lab ATCC No. CCL-243), KBM7 (a kind gift from the Brummelkamp lab) and Jurkat (ATTC No. TIB-152) were cultured in RPMI-1640 medium (Gibco/Life Technologies); HEK-293 cells (ATCC No. CRL-1573), HeLa (ATCC No. CCL-2) and HCT 116 (ATCC No. CCL-243) were maintained in Dulbecco's Modified Eagle Medium (Gibco/Life Technologies). All culture media were supplemented with 10% fetal bovine serum (FBS, Gibco/Life Technologies, Carlsbad, CA, USA), 100 units/mL penicillin and 100 units/mL streptomycin (Gibco/Life Technologies).

Western Blotting

Cells were lysed with RIPA buffer (50mM Tris pH8, 150mM NaCl, 0.1% SDS, 0.5% sodium deoxycholate, 1% NP40, 1mM EDTA and protease and phosphatase inhibitor cocktail [Roche]). For western blotting, the following antibodies were used: anti-IMPDH2 (Ab-131158, 1:1000) and anti-IMPDH1 (Ab-55297, 1:1000) were from Abcam. Anti-PPIA (CST 2175, 1:1000) and anti-GAPDH (CST 2118, 1:1000) were from Cell Signaling Technology. Anti-HSP90 (610419, 1:3000) was from BD Biosciences. Anti-HA (H3663, 1:1000) and anti-β-actin (A3853, 1:5000) were from Sigma-Aldrich.

Screening *C. elegans* in Liquid Media

N2 *C. elegans* stock plates containing many gravid hermaphrodites were used for egg prep. For each 6cm plate, pipetted 1 ml of M9 buffer (3 g KH_2PO_4, 6 g Na_2HPO_4, 5 g NaCl, 1 ml 1M Mg_2SO_4, H_2O to 1 liter. Buffer was sterilized by autoclaving) onto the plate, gently rocked and poured worms into 15 ml conical tube. The worms were brought up to a volume of 7mls with M9 buffer. The worm suspension was treated with 1 ml 5 N NaOH and 2 mls household bleach to give a total of 10ml suspension. The conical tube was shaken vigorously for about 30 seconds, and after 2 minutes, the status of the worms was checked with a dissecting scope. When half the worms have cracked open (~4 minutes), 5 mls of M9 buffer was added and the suspension was centrifuged for 30 seconds (< 1300 x *g*) using a clinical centrifuge. The supernatant was aspirated and 5 mls of M9 buffer was added. The tube was vortexed for a few seconds and another 10 mls of M9 was added to the tube. The pellet of embryos were washed for three additional times and resuspended in final volume of 5 mls M9 buffer. The embryos were allowed to hatch overnight on a rotator at room temperature. The next day, serial dilutions (2 fold) of compounds were prepared with S Basal complete media (100 ml S basal complete medium = 100ml S basal medium + 1ml 5mg/ml cholesterol, 1ml trace metal, 1 ml potassium citrate pH 6, 0.3ml 1M $CaCl_2$ and 0.3ml Mg_2SO_4) in v-bottom 96-well PCR plates (Corning). Each dilution was 4x the intended concentration in the final assay sample. Compound stocks were all at 10mM. The highest concentration of compounds tested was 100µM. 50ml of overnight OP50 *E. coli* culture was centrifuged and resuspended in 50ml S Basal complete media. Worms were counted and diluted with S basal complete media until there was about 1 worm/µl media.

Black clear bottom 96-well plate (Corning) was used to prepare the assay. To each well, 50µl of OP50 in S basal complete, 25µl of worms in M9 and 25µl compounds were added. After compound treatment, assay plate was incubated in a shaking incubator at 20^{o}C. The worms were visually inspected with a dissecting scope every 24 hours, and at 72 hours, the wells were imaged with ImageXpress Micro High-Content Analysis System (Molecular Devices).

Screening *C. elegans* in Solid Nematode Growth Media (NGM)

Compounds were diluted in 200µl M9 buffer (as previously described) and mixed with OP50 *E. coli* culture. SFA was tested at a final concentration of 2.5µM. Volume matched DMSO sample was used as a negative control. Compound/OP50 mixture was seeded on an NGM plate (Teknova) and allowed to dry in a hood. 1 L4 larval worm (P0 generation – picked by observing the presence of white crescent shape vulva) was transferred to each compound treated NGM plate and fresh compound was added to existing plates daily for the next 3 days. Potential phenotypes (sterility, embryonic lethality, larval arrest, changes in brood size, high male incidence, locomotive defects and abnormal body shapes) were inspected under a dissecting scope every 24 hours.

Selection of Resistant HCT-116 Clones

Resistant clones were generated by plating 0.5 x 10^6 HCT-116 cells in 10cm culture dishes with media containing 1µM SFA or DMSO. Media containing compounds was changed every 3 days, and cells were split when they become ~80% confluent. Cells were subjected to increasing doses of SFA or DMSO after every passage, up to 8µM

SFA. Cells were split via limiting dilution into 96-well culture plates (Corning) to obtain single clones for transcriptome analysis. The resistant clones were expanded in 10cm culture dishes before harvesting. Total RNA was purified from cell lines using the RNeasy Mini Kit (Qiagen) and was reversed transcribed into cDNA using the High Capacity cDNA Reverse Transcription Kit (Applied Biosystems) according to the manufacturer's protocol. IMPDH2 and PPIA loci were amplified with the following primers:

Primer name	Sequence (5' - 3')
AttB1_IMPDH2_F	GGGGACAACTTTGTACAAAAAAGTTGGCATGGCCGACTACCTGATTAGTGGGGGCACGTCCTACGTGCCAGACGACGGACTCACAG
AttB2_IMPDH2_R	GGGGACAACTTTGTACAAGAAAGTTGGGCATCAGAAAAGCCGCTTCTCATACGAATGGAGGCTATGGACGCCACCTTCCACCTGGGCT
AttB1_PPIA_F	GGGGACAACTTTGTACAAAAAAGTTGGCATGGTCAACCCCACCGTGTTCTTCGACATTGCCGTCGACGGCGAGCCCTTGG
AttB2_PPIA_R	GGGGACAACTTTGTACAAGAAAGTTGGGTATTATTCGAGTTGTCCACAGTCAGCAATGGTGATCTTCTTGCTGGTCTTGCCATTCCTG

The PCR products were purified (Qiagen) and sequenced (Genewiz).

Cell Proliferation Assays

K562 (4000 cells), Jurkat (8000 cells), KBM7 (8000 cells), HeLa (10^4 cells), HEK293 (10^4 cells) were seeded in opaque white 96-well tissue culture plates (for CellTiter-Glo assay – Promega) or in clear bottom black 96-well tissue culture plates (for MTT assay – Promega). Adherent lines were placed at 37^{o}C/5% CO_2 overnight prior to compound

treatment. Suspension lines were treated with compounds after seeding. Compounds were diluted in respective complete growth medium and serial 2-fold dilutions were prepared for dose-response experiments. Compounds were added to wells in triplicate. The plates were incubated at 37°C/5% CO_2 for 72 hours and CellTiter-Glo or MTT assay was performed in accordance to manufacturer's protocol with luminescence or absorbance at 570nm detected by Spectromax M5. The relative cell number was calculated by normalization against wells treated with DMSO only.

Generation of Stable Knockdown Cell Lines with shRNA

pLKO.1 lentiviral vectors targeting PPIA and IMPDH2 were ordered from ThermoScientific. pLKO.1 lentiviral vectors containing scrambled and GFP target sequences were a kind gift from the Pandolfi laboratory (Harvard Medical School). The generation of stable lines was described in the Experimental Procedures of Chapter 2.

Generation of Knockout K562 Cell Line with CRISPR

The human codon-optimized Cas9 (hCas9) expressing vector was a kind gift from the Church Lab (Harvard Medical School). The target sequences used are TTCTTCGACATTGCCGTCGACGG and ATGGCCGACTACCTGATTAGTGG for PPIA and IMPDH2 respectively. sgRNA was cloned into pCR-BluntII-TOPO vector (Life Technologies) as a gblock fragment following Mali's protocol. Knockout K562 cell lines of IMPDH2 were generated by co-transfecting 1µg of IMPDH2 gRNA-expressing plasmid and 1µg of hCas9 plasmid via nucleofection (Lonza) with 1 x 10^6 K562 cells as per manufacturer's instruction. Half of the nucleofected cells were set aside, allowed to

recover and grow for population analysis while the other half were seeded in 96 well plates via limiting dilution to obtain single clones. To screen population for CRISPR knockout efficiency, genomic DNA from nucleofected K562 cells was extracted using QuickExtract DNA solution (Epicenter) and primers flanking the targeted region were used in PCR to obtain amplicons that are subsequently subcloned into pCR-BluntII-TOPO vector (Life Technologies). The amplicons were checked by sequencing to assess the efficiency of sgRNA targeting of PPIA or IMPDH2. The sequences of primers used are:

PPIA_Grna1_F: CCGTCTATAGGCCAGATGCAC

PPIA_Grna1_R: TCGCGGACCTCCCAAAATG

IMPDH2_Grna1_F: CTGTTTCTTCAGCGCCAGC

IMPDH2_Grna1_R: ATGTCTCAAAGTGAGCCCCG

K562 clonal cells possessing the desired gene knockout were checked by sequencing and confirmed via western blot with the corresponding antibodies.

Benzidine Staining

Benzidine staining of hemoglobins was performed as described by Fibach *et al.*[43]. Briefly, benzidine stock solution was made by adding 1 g benzidine dihydrochloride (Sigma-Aldrich) to 14.6 ml glacial acetic acid (Sigma-Aldrich) and 485.4 ml milliQ water and mixed for a few hours until benzidine completely dissolved. 1ml of benzidine stock solution was mixed with 20µl of 33% H_2O_2 to prepare the working solution. Cells were mixed with benzidine working solution at a 1:1 (v/v) ratio and allowed to stand for 2 minutes. Blue cells were scored by imaging with Cellometer (Nexcelom).

Statistical Analysis

For quantitative data, data sets were analyzed using the unpaired, two-tailed Student's t tests (GraphPad Prism, GraphPad Software). $p<0.05$ was considered significant. Graphs were plotted with Graphpad Prism and fitted using Sigmoidal dose-response (variable slope).

References

1. Zheng, X., Chan, T. & Zhou, H. H. Genetic and genomic approaches to identify and study the targets of bioactive small molecules. *Chem. Biol.* **11,** 609–618 (2004).

2. Schenone, M., Dančík, V., Wagner, B. K. & Clemons, P. a. Target identification and mechanism of action in chemical biology and drug discovery. *Nat. Chem. Biol.* **9,** 232–40 (2013).

3. Wang, T., Wei, J. J., Sabatini, D. M. & Lander, E. S. Genetic screens in human cells using the CRISPR-Cas9 system. *Science* **343,** 80–84 (2014).

4. Shalem, O. *et al.* Genome-Scale CRISPR-Cas9 Knockout. *Science* **343,** 84–88 (2014).

5. Wacker, S. A., Houghtaling, B. R., Elemento, O. & Kapoor, T. M. Using transcriptome sequencing to identify mechanisms of drug action and resistance. *Nat. Chem. Biol.* **8,** 235–237 (2012).

6. Clipstone, N. A. & Crabtree, G. R. Identification of calcineurin as a key signalling enzyme in T-lymphocyte activation. *Nature* **356,** 695–697 (1992).

7. O'Keefe, S. J., Tamura, J., Kincaid, R. L., Tocci, M. J. & O'Neill, E. A. FK-506- and CSA-sensitive activation of the interleukin-2 promoter by calcineurin. *Nature* **357,** 693–694 (1992).

8. Smith, A. M. et al. A survey of yeast genomic assays for drug and target discovery. *Pharmacol. Ther.* **127,** 156–164 (2010).

9. Winzeler, E. a *et al.* Functional characterization of the S. cerevisiae genome by gene deletion and parallel analysis. *Science* **285,** 901–906 (1999).

10. Giaever, E. A. Functional profiling of the Saccharomyces cerevisiae genome. *Nature* **418,** 387–91 (2002).

11. Giaever, G. *et al.* Genomic profiling of drug sensitivities via induced haploinsufficiency. *Nat. Genet.* **21,** 278–283 (1999).

12. Butcher, R. a *et al.* Microarray-based method for monitoring yeast overexpression strains reveals small-molecule targets in TOR pathway. *Nat. Chem. Biol.* **2,** 103–9 (2006).

13. Hoon, S. *et al.* An integrated platform of genomic assays reveals small-molecule bioactivities. *Nat. Chem. Biol.* **4,** 498–506 (2008).

14. Tropschug, M., Barthelmess, I. B. & Neupert, W. Sensitivity to cyclosporin A is mediated by cyclophilin in Neurospora crassa and Saccharomyces cerevisiae. *Nature* **342,** 955 (1989).

15. Breuder, T., Hemenway, C. S., Movva, N. R., Cardenas, M. E. & Heitman, J. Calcineurin is essential in cyclosporin A- and FK506-sensitive yeast strains. *Proc. Natl. Acad. Sci. U. S. A.* **91,** 5372–6 (1994).

16. Heitman, J., Movva, N. R., Hiestand, P. C. & Hall, M. N. FK 506-binding protein proline rotamase is a target for the immunosuppressive agent FK 506 in Saccharomyces cerevisiae. *Proc. Natl. Acad. Sci. U. S. A.* **88,** 1948–52 (1991).

17. Heitman, J., Movva, N. R. & Hall, M. N. Targets for cell cycle arrest by the immunosuppressant rapamycin in yeast. *Science* **253,** 905–9 (1991).

18. Dorer, R. K. *et al.* A small-molecule inhibitor of Mps1 blocks the spindle-checkpoint response to a lack of tension on mitotic chromosomes. *Curr. Biol.* **15,** 1070–1076 (2005).

19. Mayan, M. D. Drug-induced permeabilization of S. cerevisiae. *Curr. Protoc. Mol. Biol.* 1–4 (2010). doi:10.1002/0471142727.mb1302bs92

20. Brenner, S. The Genetics of Caenorhabditis elegans. *Genetics* **77,** 71–94 (1974).

21. Hengartner, M. O. & Horvitz, H. R. Programmed cell death in Caenorhabditis elegans. *Curr. Opin. Genet. Dev.* **4,** 581–586 (1994).

22. Kenyon, C., Chang, J., Gensch, E., Rudner, a & Tabtiang, R. A C. elegans mutant that lives twice as long as wild type. *Nature* **366,** 461–464 (1993).

23. Fire, A. *et al.* Potent and specific genetic interference by double-stranded RNA in Caenorhabditis elegans. *Nature* **391,** 806–811 (1998).

24. Brenner, S. Nature's gift to science (Nobel lecture). *ChemBioChem* **4,** 683–687 (2003).

25. Hulme, S. E. & Whitesides, G. M. Chemistry and the worm: Caenorhabditis elegans as a platform for integrating chemical and biological research. *Angew. Chemie - Int. Ed.* **50,** 4774–4807 (2011).

26. O'Reilly, L. P., Luke, C. J., Perlmutter, D. H., Silverman, G. a. & Pak, S. C. C. elegans in high-throughput drug discovery. *Adv. Drug Deliv. Rev.* **69-70,** 247–253 (2014).

27. Boutros, M. & Ahringer, J. The art and design of genetic screens: RNA interference. *Nat. Rev. Genet.* **9,** 554–566 (2008).

28. Meister, G. *et al.* Human Argonaute2 mediates RNA cleavage targeted by miRNAs and siRNAs. *Mol. Cell* **15,** 185–197 (2004).

29. Matzke, M. a & Birchler, J. a. RNAi-mediated pathways in the nucleus. *Nat. Rev. Genet.* **6,** 24–35 (2005).

30. Colgan, J., Asmal, M., Yu, B. & Luban, J. Cyclophilin A-deficient mice are resistant to immunosuppression by cyclosporine. *J. Immunol.* **174,** 6030–6038 (2005).

31. Jackson, A. L. *et al.* Widespread siRNA 'off-target' transcript silencing mediated by seed region sequence complementarity. *RNA* **12,** 1179–1187 (2006).

32. Echeverri, C. J. *et al.* Minimizing the risk of reporting false positives in large-scale RNAi screens. *Nat. Methods* **3,** 777–779 (2006).

33. Horvath, P. & Barrangou, R. CRISPR/Cas, the immune system of bacteria and archaea. *Science* **327,** 167–170 (2010).

34. Wiedenheft, B., Sternberg, S. H. & Doudna, J. a. RNA-guided genetic silencing systems in bacteria and archaea. *Nature* **482,** 331–338 (2012).

35. Prashant, M. *et al.* RNA-Guided Human Genome Engineering via Cas9. *Science* 823–827 (2013).

36. Cong, L. *et al.* Multiplex Genome Engineering Using CRISPR/Cas Systems. *Science* **339,** 819–824 (2013).

37. Mali, P., Esvelt, K. M. & Church, G. M. Cas9 as a versatile tool for engineering biology. *Nat Methods* **10,** 957–963 (2013).

38. Gaj, T., Gersbach, C. a. & Barbas, C. F. ZFN, TALEN, and CRISPR/Cas-based methods for genome engineering. *Trends Biotechnol.* **31,** 397–405 (2013).

39. Jinek, M. *et al.* A Programmable Dual-RNA – Guided DNA Endonuclease in Adaptive Bacterial Immunity. *Science* **337,** 816–822 (2012).

40. Moore, J. D. The impact of CRISPR–Cas9 on target identification and validation. *Drug Discov. Today* **00,** (2015).

41. Yu, J., Lemas, V., Page, T., Connor, J. D. & Yu, a. L. Induction of erythroid differentiation in K562 cells by inhibitors of inosine monophosphate dehydrogenase. *Cancer Res.* **49,** 5555–5560 (1989).

42. Pimkin, M., Pimkina, J. & Markham, G. D. A regulatory role of the Bateman domain of IMP dehydrogenase in adenylate nucleotide biosynthesis. *J. Biol. Chem.* **284,** 7960–7969 (2009).

43. Fibach, E. & Prus, E. Differentiation of human erythroid cells in culture. *Curr. Protoc. Immunol.* **Chapter 22,** Unit 22F.7 (2005).

CHAPTER 5

OTHER APPROACHES TO SFA TARGET IDENTIFICATION AND FURTHER MECHANISM OF ACTION STUDIES

5.1 Modulating the DNA Binding Function of IMPDH2 as a Potential Mechanism of Action for SFA

Our previous findings have demonstrated the interaction of IMPDH2 with PPIA in the presence of SFA. However the biological implications of this interaction are unclear, especially since PPIA-SFA was interacting with the CBS domains of IMPDH2, which are not well understood.

Recently, Kozhevnikova *et al.* showed that *drosophila* IMPDH (dmIMPDH) functions as a sequence-specific DNA-binding transcriptional repressor and this unappreciated function is mediated by the CBS domains of IMPDH[1]. In light of this finding, we speculated that PPIA-SFA could be modulating a transcription factor role of IMPDH2, thus giving rise to the biological activity of SFA. Although direct evidence showing human IMPDH2 (or IMPDH1 for that matter) as a transcription factor is lacking, it does proffer the interesting notion that PPIA-SFA could be interfering with a yet-to-be-

characterized transcriptional role of human IMPDH2. To address this hypothesis, we sought evidence to show that (i) PPIA-SFA could interfere with hIMPDH2's nucleic acid binding ability (ii) hIMPDH2 is localized in the nucleus (iii) SFA could modulate IMPDH target gene expression.

5.1.1 Interrogating the Nucleic-acid Binding Ability of hIMPDH2

ChIP-chip using *Drosophila* tiling arrays revealed that dmIMPDH binds chromatin and represses its target genes[1]. Selected targets of dmIMPDH, such as *E2f*, histone genes, *Mlc2* are validated by ChIP-qPCR[1]. We wanted to determine if hIMPDH2 could also bind to these genomic sequences. Of all the dmIMPDH target genes, E2f caught our attention because it encodes a critical transcription factor for G1-S phase of the cell cycle[2]. In light of the discovery that SFA also inhibits G1-S phase in cell cycle progression, we wanted to examine if there was any connection between E2f target repression, possibly through a PPIA-SFA-IMPDH2 complex, and SFA's anti-proliferative effect.

To test whether hIMPDH2 could bind to target specific DNA, I performed an electrophoretic mobility shift assay (EMSA) of hIMPDH2 with biotinylated oligonucleotides. I tested hIMPDH2 binding to *Drosophila Mlc2* promoter sequence, instead of *E2f* , since only the *Mlc2* probe sequence was published in the supplementary materials of Kozhevnikova's paper[1]. The sequences used in this EMSA assay are described in the Experimental Procedures section[1]. The *Mlc2* single stranded oligonucleotide probes were biotinylated at the 5' end. Two biotinylated *Mlc2* probes were synthesized – one has a CT rich sequence, and the other is AG rich – the

complement strand of the former. For reasons that remain unclear, dmIMPDH binds only to CT-rich single stranded DNA elements[1].

Figure 5.1

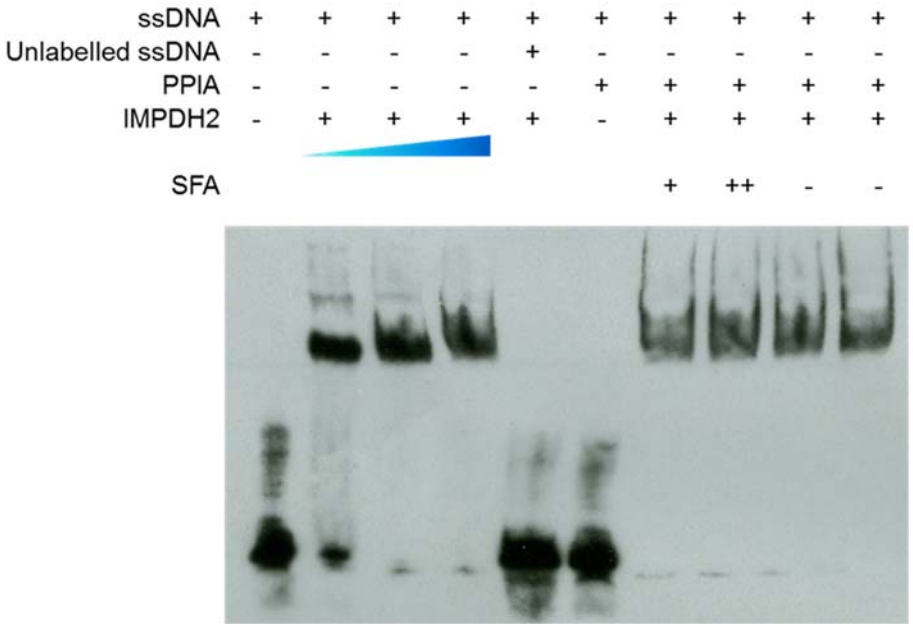

Figure 5.1 – Investigation of the Specificity of IMPDH2 to ssDNA. IMPDH2, but not PPIA, binds to single stranded drosophila Mlc2 sequence. However, PPIA-SFA did not seem to antagonize IMPDH2's interaction with ssDNA. The concentrations of SFA in this experiment were 25μM (+) and 250μM (++).

To perform the EMSA, recombinant hIMPDH2 was mixed with biotinylated single stranded oligos. After incubation, the IMPDH2/ssDNA complexes were separated from unbound DNA by native PAGE and transferred to a nylon membrane. The two species were visualized via the detection of biotin-labelled DNA by chemiluminescence. I was gratified to observe that hIMPDH2, like dmIMPDH, also bound to single stranded *Mlc2* CT rich sequence (Figure 5.1). This DNA binding event is hIMPDH2 concentration dependent (Figure 5.1). Consistent with previous reports, hIMPDH2 showed negative binding to the complementary single stranded *Mlc2* AG rich sequence (data not shown).

Addition of 1000 fold excess of unlabeled *Mlc2* CT rich oligo was able to outcompete hIMPDH2 binding to labelled oligos, suggesting the specificity of the IMPDH2/ssDNA interaction (Figure 5.1). As might have been predicted, PPIA did not show binding to ssDNA (Figure 5.1).

Next, I wondered if PPIA-SFA could antagonize the DNA binding activity of IMPDH2. Briefly, 15μM recombinant IMPDH2 and PPIA were combined with 25μM and 250μM SFA or volume matched DMSO, in the presence of 10nM labelled DNA. Addition of PPIA-SFA did not appear to prevent IMPDH2 from binding to DNA. This result could stem from the differences in affinity of ssDNA and PPIA-SFA for IMPDH2, with ssDNA exhibiting a higher affinity for IMPDH2 than PPIA-SFA. Experimental binding data would be required to confirm this reasoning.

5.1.2 hIMPDH2 Nuclear Localization Studies

In another approach to seek evidence showing that IMPDH2 is a transcription factor, I performed a series of immunofluorescence (IF) experiments to examine the subcellular localization of IMPDH2. One possible scenario is that the subcellular localization of IMPDH2 would change upon PPIA-SFA engagement. Although IMPDH is mainly cytosolic, it has also been found in the nucleus of K562, PC-3 and HeLa cells[3]. In addition, IMPDH is able to bind single stranded DNA and RNA molecules independent of its catalytic activity[3]. More recently, IMPDH is found to associate with polyribosomes mediated by its CBS subdomain[4]. Taken together, these data suggest that IMPDH could have a role in transcriptional or translational regulation[3,4].

In *Drosophila* S2 cells, nuclear dmIMPDH is cell cycle regulated[1]. In most of these cells, IMPDH is absent in the nucleus. However, cells possessing nuclear IMPDH coincide with those expressing high levels of cyclin A and cyclin B, implying that nuclear IMPDH only exists in certain phases of cell cycle, namely late S and G2 phase [1]. While hoping to confirm hIMPDH2 localization to the nucleus, I was were also interested to know if SFA could modulate the subcellular localization of IMPDH2.

First, I assessed subcellular localization of IMPDH2 and PPIA in Jurkat cells by IF. Jurkat cells were plated on coverslips that were pre-treated with poly-L-lysine, fixed and permeabilized with 4% PFA. Subsequently, the fixed cells were co-incubated with IMPDH2 and PPIA specific primary antibodies (raised in rabbit and mouse respectively) followed by the addition of Alexa-Fluor 488 and 594 conjugated goat monoclonal antibodies raised against rabbit and mouse IgG. After addition of mounting media containing DAPI, cells were viewed under an MS-18 Olympus FV300 Laser Scanning Confocal Microscope.

I found that both IMPDH2 and PPIA were predominantly localized to the cytoplasm (Figure 5.2A). From the many views imaged, I could not detect a population of cells showing predominant nuclear IMPDH localization at steady state, despite the relative low background of the images. Since it was reported that oxidative stress could promote nuclear dmIMPDH localization, I treated cells with H_2O_2 to see if we could recapitulate previous findings. However, I did not observe an increase in nuclear IMPDH2. Instead, Jurkat cells treated with H_2O_2 under same treatment concentration and duration seem to appear less healthy compared to DMSO control treatment (Figure 5.2B). The edges of the cells seem less defined, and the appearance of blebs

suggested that cells were undergoing apoptosis under treatment conditions. Treatment of Jurkat cells with SFA also did not seem to have any influence on IMPDH2 subcellular localization (Figure 5.2B).

Figure 5.2

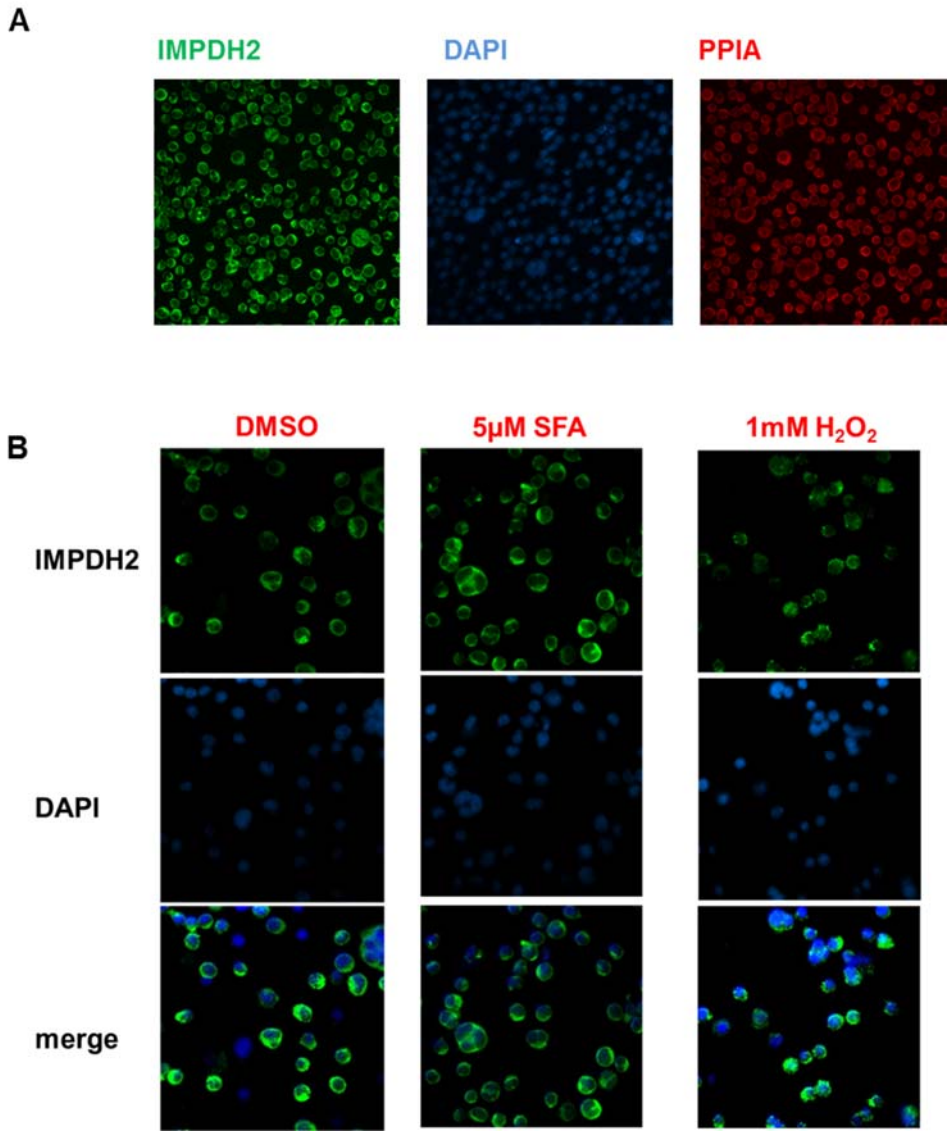

Figure 5.2 – Determining IMPDH2 Localization in Jurkat. (A) Steady state subcellular distribution of IMPDH and PPIA. IMPDH2 seemed to be exclusively localized in the cytoplasm. Jurkat cells were stained with antibodies against IMPDH2 (green), PPIA (red) and nuclei were visualized by DAPI staining of DNA (blue). (B) Subcellular localization of IMPDH2 upon SFA or H_2O_2 treatment. IMPDH2 appeared to be excluded from the nucleus regardless of the treatment condition. Details of the experiments can be found in Experimental Procedures.

The reasons that underlie the differences observed in IMPDH nuclear localization remain unclear. By extrapolating findings in *Drosophila*, we had hypothesized that human IMPDH2 could also be present in the nucleus of human cells at steady state and also under specific stimuli. However, it is likely that the conditions resulting in IMPDH2 nuclear localization are different in human cells although it remains to be seen if nuclear IMPDH2 could be present under certain metabolic state or stress in other cell lines (e.g. K562, PC-3, HeLa) since nuclear IMPDH2 has been observed in those cell lines at steady state[3]. It would have been helpful to know the distribution of cells that had predominantly cytoplasmic or nuclear hIMPDH.

5.1.3 Investigating SFA's Effect on IMPDH2 Target Gene Expression

We also wanted to test SFA's effect on IMPDH2 target gene expression. As mentioned previously, one of the IMPDH target genes (in *Drosophila*) is the *E2f* gene, which encodes for a transcription factor important for cell cycle regulation[1,2]. The E2F family of transcription factors regulates the expression of a wide variety of genes implicated in cell-cycle progression, cell proliferation, differentiation and apoptosis[5]. Although the fundamental E2F/RB pathway is evolutionary conserved, the picture is much more complicated in mammals as there are 8 mammalian E2F genes (*E2f1-E2f8*)[5]. Each member of this family is classically thought to behave uniquely as either a transcriptional activator or repressor, although a growing body of work, primarily motivated by efforts to understand this complex network of proteins involved in tumorigenesis, shows that individual E2F can play both activating and repressive roles in transcription depending on the cellular context [5,6]. There are two E2f genes in

Drosophila – dm*E2f1*, which functions as a transcriptional activator and dm*E2f2*, a transcriptional repressor[2]. Although it was not explicitly mentioned which E2f gene is targeted by dmIMPDH, the notion that IMPDH could transcriptionally regulate another master regulator of cell proliferation is scientifically exciting, especially in the context of G1/S phase arrest upon SFA treatment and human IMPDH2 interaction with SFA[1].

We hypothesized that PPIA-SFA could block IMPDH2 binding to its target genes, such as E2f1, modulating its expression and hence resulting in cell growth inhibition. As an initial test, we chose to examine the expression levels of E2f1 as it is pro-proliferative (E2f1, E2f2 and E2f3 are under this subset) and its loss impairs cell cycle progression in activated T cells[6,7]. After treating K562 cells with SFA for different lengths of time, E2f1 mRNA expression was quantified by real-time RT-qPCR to determine how E2f1 transcript abundance would change upon SFA treatment. The results demonstrated a strong suppression of E2f1 transcript upon SFA treatment in K562 cells. After a 3 hour treatment with 1μM SFA, there was an approximate 5 fold decrease in E2f1 transcript level (Figure 5.3A, middle panel). By 6 hours, SFA down regulated E2f1 expression by almost 10 fold (Figure 5.3A, bottom panel) relative to DMSO control. I also evaluated RB transcript level since RB, a tumor suppressor protein, is a critical player in regulating cell cycle progression as it binds to E2f1 preventing it from activating its target genes. E2f1 and RB transcript levels were normalized to both HPRT and GAPDH levels, yielding similar changes in levels (Figure 5.3A). Although transcript level of RB was not affected after 3 hr SFA treatment, there was a 2 fold reduction in RB after a 6 hour exposure to SFA, relative to DMSO (Figure 5.3A, middle and bottom panel). The down

regulation of RB is counter-intuitive for I would have expected RB transcript level to increase since RB acts to prevent cell cycle from progressing.

Figure 5.3

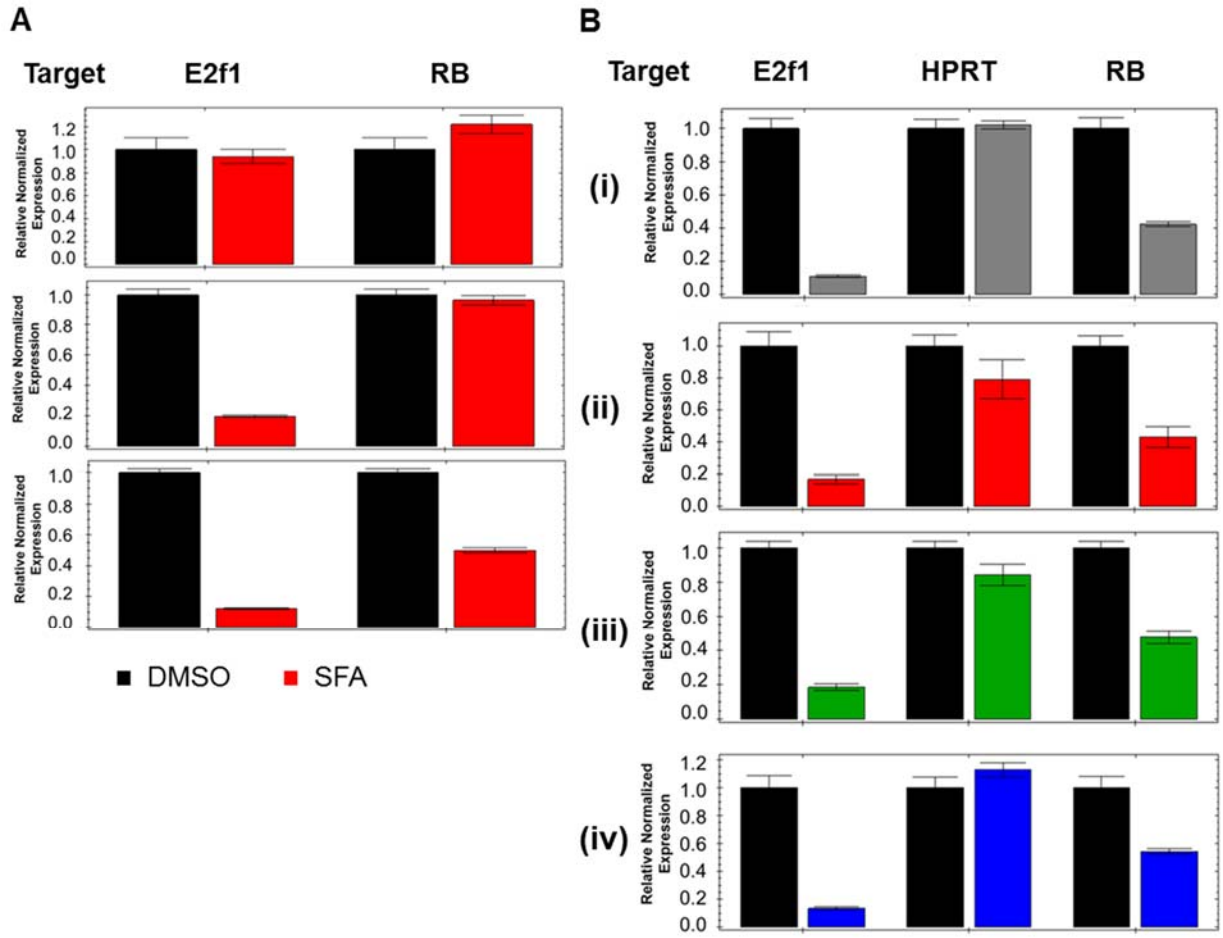

Figure 5.3 – Evaluating E2f1 and RB Transcript Levels Upon Treatment with SFA. (A) K562 chronic myelogenous leukemia line was treated with 1μM SFA for 0 (top), 3 (middle) and 6 (bottom) hours and E2f1 and RB transcript levels were quantified by RT-qPCR. (B) E2f1 and RB transcripts levels were assessed in K562 rescue lines (i) wild type (ii) A3_IMPDH2 (iii) A3_IMPDH2ΔCBS (iv) A3_IMPDH2_I192V/E214D. Cells were treated with 1μM SFA for 6 hours and E2f1 and RB transcript levels were quantified by RT-qPCR). Relative mRNA quantification for E2f1 and RB are shown after normalization to the endogenous control GAPDH. Details of the experiments can be found in Experimental Procedures.

Next, I investigated whether the rescue K562 lines (see Chapter 4.7.3) would have altered levels of E2f1 transcript upon SFA treatment. All the rescue lines showed

similar levels of E2f1 and RB transcript suppression 6 hours after treatment with 1μM SFA (Figure 5.3B). This result demonstrates that there is an IMPDH2-independent effect by SFA which modulates E2f1 and RB transcript levels, suggesting that there could be another molecular target of SFA mediating this effect. It is also worth investigating how the transcript levels of other E2f family members change upon SFA treatment.

5.2 Using Gene Expression Profiling to Determine the Mechanism of Action of SFA

I turned to gene expression profiling as an unbiased approach to generate hypotheses regarding the mechanism of action of SFA. Genomewide expression analysis with DNA microarray or more recently, with RNA-seq, have increasingly gained importance as a tool to investigate the effects of small molecules on cells. The challenge however, lies in interpreting the results to gain meaningful biological insights[8]. Although it is typically not feasible to identify the molecular target of a compound based off analyses from its transcriptome, gene expression profiling could aid in the understanding of a compound's mechanism of action by identifying pathways and processes relevant to small molecule action[8,9]. In addition, transcription profiling data of small molecule of interest can be analyzed in databases such as the Connectivity Map (cmap) – a platform that compares profiles from compounds with known molecular targets to find connections with compounds that share similar mechanism of action[10].

5.2.1 Studies on Gene Expression Profiling

To gain insight into the molecular mechanism of SFA, I conducted gene expression profiling of SFA and DMSO treatment for 3 cell lines – HeLa, Jurkat and K562. Briefly, cells were treated with 1μM SFA or DMSO for 16 hours and their mRNA were harvested (Qiagen) and quantified. The mRNA samples were submitted to the Microarray Core Facility at Dana Farber Cancer Institute where the samples were examined for degradation by a bioanalyzer (Agilent 2100) and processed on a 3' IVT HG-U133 plus 2.0 Affymetrix array. The data was then analyzed on the software, GenePattern that was developed by the Broad Institute. The dataset was analyzed by (i) comparative marker selection (ii) gene set enrichment analysis (GSEA) (ii) leading edge analysis.

Comparative marker selection analysis find genes that are significantly differentially expressed between compound and control treated samples. The top 40-50 genes differentially expressed in SFA treated cells can be found in Tables 5.1 – 5.3. Based on these lists, it was difficult to extract any meaningful insight into the mechanism of action of SFA.

	Description	ES	FC
1	ribosomal protein L37a, RPL37A	-269.39	9.53
2	RNA binding motif protein 18, RBM18	-261.63	3.06
3	mediator complex subunit 21, MED21	-254.20	2.85
4	zinc finger protein 394, ZNF394	-182.33	4.07
5	lines homolog (Drosophila), LINS	-145.31	4.34
6	KIAA1984, KIAA1984	-143.77	4.54
7	chromosome 1 open reading frame 63, C1orf63	-137.53	3.22
8	RRS1 ribosome biogenesis regulator homolog (S. cerevisiae), RRS1	-131.16	2.09
9	WD repeat domain 33, WDR33	-130.33	12.38
10	Chromosome 20 open reading frame 111, C20orf111	-128.09	3.80
11	WD repeat domain, phosphoinositide interacting 2, WIPI2	-124.97	2.42
12	TATA box binding protein (TBP)-associated factor, RNA polymerase I, D, 41kDa, TAF1D	-122.92	12.95
13	Proteasome (prosome, macropain) 26S subunit, non-ATPase, 7, PSMD7	-113.03	5.58
14	nuclear transcription factor Y, alpha, NFYA	-112.46	6.44
15	zinc finger protein 420, ZNF420	-112.34	2.96
16	kelch domain containing 10, KLHDC10	-106.59	4.08
17	RIO kinase 2 (yeast), RIOK2	-104.95	2.17
18	SET domain containing 4, SETD4	-104.70	5.97
19	CLP1, cleavage and polyadenylation factor I subunit, homolog (S. cerevisiae), CLP1	-99.77	3.04
20	general transcription factor IIIC, polypeptide 4, 90kDa, GTF3C4	-98.72	3.63
21	ubiquitin specific peptidase 42, USP42	-97.06	2.15
22	myosin regulatory light chain interacting protein, MYLIP	-93.94	3.96
23	COP9 constitutive photomorphogenic homolog subunit 2 (Arabidopsis), COPS2	-92.86	1.45
24	family with sequence similarity 133, member B	-91.71	2.28
25	solute carrier family 25, member 36, SLC25A36	-91.06	2.68
26	BTG3 associated nuclear protein, BANP	-90.63	2.46
27	zinc finger, matrin-type 3, ZMAT3	-90.46	2.62
28	ribosomal protein L10a, RPL10A	-88.28	5.87
29	mediator complex subunit 13, MED13	-87.47	3.96
30	KIAA0317, KIAA0317	-86.84	39.52
31	platelet-activating factor acetylhydrolase 1b, catalytic subunit 2 (30kDa), PAFAH1B2	-86.29	1.68
32	translocase of inner mitochondrial membrane 23 homolog (yeast), TIMM23	-85.78	4.58
33	zinc finger with KRAB and SCAN domains 5, ZKSCAN5	-83.82	3.12
34	zinc finger protein 26-like /// zinc finger protein 26, LOC100287515 /// ZNF26	-83.79	6.13
35	Topoisomerase (DNA) II alpha 170kDa, TOP2A	-83.39	11.94
36	zinc finger protein 266, ZNF266	-82.45	2.96
37	myosin regulatory light chain interacting protein, MYLIP	-81.30	4.04
38	thyroid adenoma associated, THADA	-80.40	1.81
39	hypothetical LOC388796, LOC388796	-77.57	6.38
40	PRP3 pre-mRNA processing factor 3 homolog (S. cerevisiae), PRPF3	-76.80	3.92
41	zinc finger protein 202, ZNF202	-74.36	4.11
42	Holliday junction recognition protein, HJURP	-74.34	3.98
43	ATPase, class VI, type 11B, ATP11B	-73.38	4.45
44	craniofacial development protein 1, CFDP1	-72.24	1.93
45	F-box and WD repeat domain containing 4 pseudogene 1, FBXW4P1	-72.18	9.90
46	zinc finger, X-linked, duplicated B, ZXDB	-71.01	2.54
47	Kruppel-like factor 6, KLF6	-70.76	4.79
48	zinc finger protein, X-linked, ZFX	-70.44	3.98
49	thymopoietin, TMPO	-70.15	28.61
50	zinc finger and SCAN domain containing 12, ZSCAN12	-69.93	3.30

Table 5.1 - Top 50 genes differentially expressed in SFA treated K562 by Comparative Marker Selection analysis.

	Description	ES	FC
1	zyg-11 homolog B (C. elegans), ZYG11B	-56.69	1.20
2	TAF9 RNA polymerase II, TATA box binding protein (TBP)-associated factor, 32kDa, TAF9	-46.02	1.18
3	death inducer-obliterator 1, DIDO1	-44.56	1.98
4	nuclear cap binding protein subunit 2, 20kDa, NCBP2	-38.36	1.25
5	family with sequence similarity 169, member A, FAM169A	-38.08	1.14
6	zinc finger, C3H1-type containing, ZFC3H1	-36.29	1.54
7	BRCA2 and CDKN1A interacting protein, BCCIP	-35.19	1.50
8	hypothetical protein LOC286437, LOC286437	-32.39	1.30
9	SMEK homolog 2, suppressor of mek1 (Dictyostelium), SMEK2	-29.86	1.30
10	RPTOR independent companion of MTOR, complex 2, RICTOR	-29.40	1.35
11	ankyrin repeat domain 11, ANKRD11	-28.77	1.81
12	nucleobindin 2, NUCB2	-28.67	1.59
13	dpy-19-like 4 (C. elegans), DPY19L4	-27.72	2.38
14	golgi SNAP receptor complex member 1, GOSR1	-27.33	1.35
15	dipeptidyl-peptidase 8, DPP8	-26.84	1.24
16	CTTNBP2 N-terminal like, CTTNBP2NL	-25.99	1.24
17	acidic repeat containing, ACRC	-25.29	2.32
18	zinc finger, HIT-type containing 6, ZNHIT6	-24.84	1.35
19	ribosomal protein L37, RPL37	-23.97	2.30
20	ribosomal L1 domain containing 1, RSL1D1	-23.91	1.69
21	solute carrier family 7, (cationic amino acid transporter, y+ system) member 11, SLC7A11	-23.72	2.95
22	ubiquitin specific peptidase 16, USP16	-23.58	1.18
23	Nedd4 family interacting protein 2, NDFIP2	-23.33	1.81
24	ribosomal protein L37, RPL37	-23.05	2.22
25	hypothetical LOC100129637, LOC100129637	-22.97	1.28
26	carbohydrate kinase domain containing, CARKD	-22.97	1.42
27	ribosomal protein L13, RPL13	-22.49	1.06
28	zinc finger and BTB domain containing 40, ZBTB40	-22.24	1.58
29	coiled-coil domain containing 101, CCDC101	-22.07	1.43
30	paraspeckle component 1, PSPC1	-21.76	1.70
31	membrane protein, palmitoylated 5 (MAGUK p55 subfamily member 5), MPP5	-21.73	1.30
32	COP9 constitutive photomorphogenic homolog subunit 2 (Arabidopsis), COPS2	-20.96	1.22
33	sirtuin 7, SIRT7	-20.87	1.43
34	SEC62 homolog (S. cerevisiae), SEC62	-20.78	1.19
35	RAE1 RNA export 1 homolog (S. pombe), RAE1	-20.67	1.31
36	leucine rich repeat containing 36, LRRC36	-20.59	1.22
37	Cell cycle associated protein 1, CAPRIN1	-20.33	2.00
38	leucine rich repeat containing 8 family, member D, LRRC8D	-20.26	1.24
39	A kinase (PRKA) anchor protein 1, AKAP1	-20.20	1.37
40	KIAA2022, KIAA2022	-20.20	1.49

Table 5.2 - Top 40 genes differentially expressed in SFA treated Jurkat by Comparative Marker Selection analysis.

	Description	ES	FC
1	serpin peptidase inhibitor, clade E (nexin, plasminogen activator inhibitor type 1) SERPINE1	-131.32	1.43
2	low density lipoprotein receptor, LDLR	-77.19	1.55
3	IMP4, U3 small nucleolar ribonucleoprotein, homolog (yeast), IMP4	-70.10	1.45
4	ribosomal protein L37, RPL37	-66.34	1.76
5	PRP4 pre-mRNA processing factor 4 homolog (yeast), PRPF4	-63.97	1.49
6	Dipeptidyl-peptidase 7, DPP7	-58.36	1.48
7	ribosomal protein L22-like 1, RPL22L1	-57.68	1.98
8	WD repeat domain 75, WDR75	-56.88	1.29
9	GTP binding protein 4, GTPBP4	-53.52	1.47
10	cytokine induced apoptosis inhibitor 1, CIAPIN1	-52.43	1.30
11	mediator complex subunit 10, MED10	-51.47	1.65
12	ribose 5-phosphate isomerase A, RPIA	-51.35	1.64
13	solute carrier family 7, member 6 opposite strand, SLC7A6OS	-49.62	2.34
14	selenoprotein K, SELK	-48.79	1.09
15	BCL2-associated athanogene 4, BAG4	-47.97	1.82
16	FERM domain containing 8, FRMD8	-47.16	1.39
17	selenoprotein S, SELS	-46.87	1.52
18	small nucleolar RNA host gene 7 (non-protein coding), SNHG7	-45.84	1.77
19	ribosomal protein L37, RPL37	-44.39	1.83
20	RAE1 RNA export 1 homolog (S. pombe), RAE1	-43.99	1.47
21	casein kinase 1, alpha 1, CSNK1A1	-43.70	1.26
22	cleavage stimulation factor, 3' pre-RNA, subunit 3, 77kDa, CSTF3	-43.61	1.67
23	nucleophosmin (nucleolar phosphoprotein B23, numatrin), NPM1	-43.52	1.05
24	mRNA turnover 4 homolog (S. cerevisiae), MRTO4	-42.43	1.33
25	phosphatidylcholine transfer protein, PCTP	-42.15	1.17
26	Smith-Magenis syndrome chromosome region, candidate 7-like, SMCR7L	-41.06	1.54
27	TM2 domain containing 3, TM2D3	-40.84	1.40
28	pinin, desmosome associated protein, PNN	-40.65	2.12
29	F-box protein 31, FBXO31	-40.54	1.53
30	hypothetical LOC151009, LOC151009	-39.81	1.61
31	glutamate-cysteine ligase, catalytic subunit, GCLC	-39.75	1.79
32	pinin, desmosome associated protein, PNN	-39.52	1.76
33	splicing factor proline/glutamine-rich, SFPQ	-39.45	1.34
34	scaffold attachment factor B, SAFB	-39.36	1.46
35	natriuretic peptide receptor C/guanylate cyclase C (atrionatriuretic peptide receptor C), NPR3	-38.75	1.31
36	proteasome (prosome, macropain) 26S subunit, non-ATPase, 11, PSMD11	-38.74	1.34
37	methyl-CpG binding domain protein 1, MBD1	-38.42	1.38
38	RAE1 RNA export 1 homolog (S. pombe), RAE1	-38.24	1.46
39	mitochondrial ribosomal protein S25, MRPS25	-37.86	2.23
40	p53 and DNA-damage regulated 1, PDRG1	-37.62	2.32
41	Ras homolog enriched in brain, RHEB	-37.31	1.15
42	Smg-5 homolog, nonsense mediated mRNA decay factor (C. elegans), SMG5	-37.28	1.55
43	ADP-ribosylhydrolase like 2, ADPRHL2	-37.00	1.51
44	DIS3 mitotic control homolog (S. cerevisiae), DIS3	-36.93	1.30
45	heat shock protein 70kDa family, member 13, HSPA13	-36.72	1.28
46	adaptor-related protein complex 3, sigma 2 subunit, AP3S2	-36.55	1.41
47	RNA binding motif protein 5, RBM5	-36.32	1.34
48	chromosome 10 open reading frame 2, C10orf2	-36.10	1.66
49	glutaminase, GLS	-36.03	2.47
50	hexamethylene bis-acetamide inducible 1, HEXIM1	-35.97	1.37

Table 5.3 - Top 50 genes differentially expressed in SFA treated HeLa by Comparative Marker Selection analysis.

I next analyzed our data with GSEA and leading edge analysis. GSEA allows the interpretation of large scale data by identifying pathways and processes resulting from changes in a group of genes acting in concert[8]. Gene sets that are enriched upon SFA treatment can be found in Tables 5.4 – 5.6. I was specifically interested in common gene sets that were enriched in the three cell lines when treated with SFA. However, there were not many gene sets that were commonly enriched in the three cell lines. The HOXA5 targets and response to oxidized phospholipids gene set, while appearing as two of the top ranked gene sets across all three cell lines, are relatively large gene sets (represented by 183 and 110 genes respectively) and thus, it was difficult to investigate which genes in those gene sets are important in SFA's effect. The NFκB and TNF pathways also appeared in the top 20 enriched gene sets. Zhang *et al.* previously showed that SFA activated p53 transcription by activating the transcription factor NFκB in HCT 116 cells although the exact mechanism of IκB kinase activation of NFκB is still poorly understood[11].

	GS MSigDB	SIZE	ES	NES	NOM p-val	FDR q-val	FWER p-val	RANK AT MAX
1	ENK_UV_RESPONSE_EPIDERMIS_DN	467	-0.21			1	0	2256
2	PICCALUGA_ANGIOIMMUNOBLASTIC_LYMPHOMA_DN	111	-0.6	-2.68	0	0	0	1610
3	REACTOME_GENERIC_TRANSCRIPTION_PATHWAY	305	-0.51	-2.53	0	0	0	2168
4	CHEN_HOXA5_TARGETS_9HR_UP	183	-0.53	-2.53	0	0	0	1619
5	NAGASHIMA_EGF_SIGNALING_UP	52	-0.66	-2.51	0	0	0	3219
6	RASHI_NFKB1_TARGETS	18	-0.8	-2.47	0	0	0.002	1786
7	PLASARI_TGFB1_TARGETS_1HR_UP	30	-0.73	-2.43	0	0.001	0.003	1795
8	PHONG_TNF_TARGETS_UP	59	-0.58	-2.35	0	0.001	0.004	2001
9	GESERICK_TERT_TARGETS_DN	20	-0.75	-2.35	0	0.001	0.004	1649
10	GARGALOVIC_RESPONSE_TO_OXIDIZED_PHOSPHOLIPIDS_BLUE_UP	110	-0.53	-2.31	0	0.001	0.004	1730
11	AMIT_SERUM_RESPONSE_40_MCF10A	28	-0.68	-2.25	0	0.001	0.01	1649
12	AMIT_DELAYED_EARLY_GENES	17	-0.76	-2.24	0	0.001	0.01	3219
13	BURTON_ADIPOGENESIS_1	31	-0.64	-2.21	0	0.001	0.013	1742
14	NIKOLSKY_BREAST_CANCER_19Q13.1_AMPLICON	19	-0.72	-2.21	0	0.001	0.013	2757
15	BURTON_ADIPOGENESIS_PEAK_AT_2HR	48	-0.57	-2.14	0	0.003	0.037	1649
16	NOJIMA_SFRP2_TARGETS_UP	29	-0.65	-2.14	0	0.003	0.038	1472
17	AMIT_EGF_RESPONSE_40_HELA	38	-0.58	-2.11	0	0.005	0.063	1795
18	UZONYI_RESPONSE_TO_LEUKOTRIENE_AND_THROMBIN	34	-0.6	-2.1	0	0.005	0.067	3018
19	NAKAYAMA_FRA2_TARGETS	38	-0.59	-2.09	0	0.006	0.087	1953
20	SMIRNOV_RESPONSE_TO_IR_2HR_UP	44	-0.53	-2.06	0	0.008	0.118	1610

Table 5.4 - Gene sets (from MSigDB) enriched in SFA treated K562.

	GS MSigDB	SIZE	ES	NES	NOM p-val	FDR q-val	FWER p-val	RANK AT MAX
1	CHEN_HOXA5_TARGETS_9HR_UP	183	-0.61	-2.67	0	0	0	3916
2	SMIRNOV_RESPONSE_TO_IR_2HR_UP	44	-0.68	-2.35	0	0	0	2220
3	GARGALOVIC_RESPONSE_TO_OXIDIZED_PHOSPHOLIPIDS_BLUE_UP	110	-0.54	-2.19	0	0.002	0.007	2570
4	KRIGE_AMINO_ACID_DEPRIVATION	28	-0.68	-2.11	0	0.004	0.02	2169
5	PACHER_TARGETS_OF_IGF1_AND_IGF2_UP	31	-0.64	-2.09	0	0.005	0.034	1669
6	MITSIADES_RESPONSE_TO_APLIDIN_UP	369	-0.43	-2.06	0	0.007	0.056	3707
7	REACTOME_GENERIC_TRANSCRIPTION_PATHWAY	305	-0.44	-2.05	0	0.007	0.07	4079
8	MAHADEVAN_RESPONSE_TO_MP470_DN	18	-0.71	-2.01	0	0.014	0.151	2087
9	SUH_COEXPRESSED_WITH_ID1_AND_ID2_UP	18	-0.71	-2	0.002	0.016	0.186	1834
10	PRAMOONJAGO_SOX4_TARGETS_UP	46	-0.58	-1.99	0	0.017	0.215	2463
11	PHONG_TNF_TARGETS_UP	59	-0.53	-1.97	0	0.021	0.289	3328
12	GAUSSMANN_MLL_AF4_FUSION_TARGETS_C_DN	17	-0.7	-1.96	0.004	0.022	0.322	2415
13	RASHI_NFKB1_TARGETS	18	-0.67	-1.93	0.002	0.028	0.401	4680
14	DUTTA_APOPTOSIS_VIA_NFKB	31	-0.59	-1.9	0	0.042	0.552	1257
15	SARTIPY_BLUNTED_BY_INSULIN_RESISTANCE_DN	15	-0.69	-1.87	0.004	0.058	0.704	4034
16	KEGG_SPLICEOSOME	96	-0.47	-1.85	0	0.068	0.786	2365
17	CERIBELLI_GENES_INACTIVE_AND_BOUND_BY_NFY	30	-0.6	-1.85	0.006	0.065	0.789	1608
18	DEBIASI_APOPTOSIS_BY_REOVIRUS_INFECTION_UP	275	-0.4	-1.82	0	0.087	0.889	3141
19	GARGALOVIC_RESPONSE_TO_OXIDIZED_PHOSPHOLIPIDS_MAGENTA_U	23	-0.62	-1.82	0.002	0.084	0.894	2694
20	DAZARD_UV_RESPONSE_CLUSTER_G28	20	-0.63	-1.82	0.002	0.081	0.898	1257

Table 5.5 - Gene sets (from MSigDB) enriched in SFA treated Jurkat.

	GS MSigDB	SIZE	ES	NES	NOM p-val	FDR q-val	FWER p-val	RANK AT MAX
1	GARGALOVIC_RESPONSE_TO_OXIDIZED_PHOSPHOLIPIDS_BLUE_UP	110	-0.68	-2.86	0	0	0	2497
2	CHEN_HOXA5_TARGETS_9HR_UP	183	-0.62	-2.76	0	0	0	3143
3	DAZARD_RESPONSE_TO_UV_SCC_DN	108	-0.59	-2.45	0	0	0	3136
4	SARTIPY_NORMAL_AT_INSULIN_RESISTANCE_UP	29	-0.73	-2.34	0	0	0	3108
5	REACTOME_GENERIC_TRANSCRIPTION_PATHWAY	305	-0.5	-2.31	0	0	0.001	4216
6	AMIT_EGF_RESPONSE_120_HELA	62	-0.62	-2.3	0	0	0.001	2960
7	GENTILE_UV_HIGH_DOSE_DN	279	-0.5	-2.28	0	0	0.002	3843
8	DAZARD_RESPONSE_TO_UV_NHEK_DN	271	-0.49	-2.27	0	0	0.002	3565
9	SMIRNOV_RESPONSE_TO_IR_2HR_UP	44	-0.66	-2.25	0	0	0.003	2046
10	WANG_METHYLATED_IN_BREAST_CANCER	35	-0.67	-2.24	0	0	0.003	1447
11	DAZARD_UV_RESPONSE_CLUSTER_G2	27	-0.7	-2.23	0	0	0.003	1648
12	KOBAYASHI_EGFR_SIGNALING_6HR_DN	17	-0.83	-2.23	0	0	0.003	842
13	PHONG_TNF_RESPONSE_VIA_P38_PARTIAL	150	-0.51	-2.23	0	0	0.003	3698
14	DAZARD_UV_RESPONSE_CLUSTER_G28	20	-0.76	-2.22	0	0	0.003	1440
15	GARGALOVIC_RESPONSE_TO_OXIDIZED_PHOSPHOLIPIDS_MAGENTA_UP	23	-0.73	-2.21	0	0	0.004	2291
16	GARGALOVIC_RESPONSE_TO_OXIDIZED_PHOSPHOLIPIDS_RED_UP	15	-0.83	-2.2	0	0	0.004	2534
17	KEGG_SPLICEOSOME	96	-0.55	-2.2	0	0	0.004	4793
18	GARGALOVIC_RESPONSE_TO_OXIDIZED_PHOSPHOLIPIDS_TURQUOISE_UP	70	-0.58	-2.2	0	0	0.004	3657
19	PHONG_TNF_TARGETS_UP	59	-0.59	-2.19	0	0	0.004	3132
20	SCHOEN_NFKB_SIGNALING	31	-0.68	-2.17	0	0	0.006	2717

Table 5.6 - Gene sets (from MSigDB) enriched in SFA treated HeLa.

Identifying genes in the leading edge subsets common within the gene sets could help to focus our attention on genes that will be most relevant to the SFA phenotype. To search for genes that overlap within the gene sets, we performed leading edge analysis on the enriched gene sets for each of the 3 lines. The results are tabulated in Table 5.7. There were several genes that appeared to be modulated by SFA treatment across all three cell lines, namely GADD45, IER3, ATF3 and DUSP6. IER3 and ATF3 were not chosen for further characterization as these genes have been reported to be modulated in most treatment conditions (personal communications). GADD45 and DUSP6 are currently being investigated though preliminary data suggest the upregulation of GADD45 genes upon SFA treatment (data not shown). In our hands, SFA did not induce p53 at the level of transcription in K562 cells, the most sensitive cell line to SFA, raising the possibility of whether SFA acts via the same mechanism across different cell lines (data not shown).

	K562		JURKAT		HELA	
	LEADING EDGE ANALYSIS		LEADING EDGE ANALYSIS		LEADING EDGE ANALYSIS	
No.	Gene	No. of subsets	Gene	No. of subsets	Gene	No. of subsets
1	JUN	4	DDIT3	6	IL8	8
2	KLF6	4	ATF3	6	ATF3	7
3	GADD45B	4	GADD45B	5	PMAIP1	7
4	HBEGF	4	NFKBIA	5	MAFF	7
5	TNFAIP3	4	ZNF222	5	IER3	7
6	NR4A1	4	TNFRSF10B	5	FOSL1	6
7	ATF3	4	GADD45A	5	TNFRSF10B	6
8	IER3	4	BIRC3	5	GADD45A	6
9	NFKBIA	3	TNFAIP3	5	CXCL2	6
10	ZNF222	3	MAFF	5	MCL1	6
11	ZNF468	3	IER3	5	CTGF	5
12	DUSP6	3	CCNL1	5	F3	5
13	BCL10	3	SLC7A11	5	NCOA3	5
14	NR4A2	3	ASNS	5	CXCL3	5
15	IER2	3	ZNF394	4	THBS1	5
16	IER5	3	STC2	4	TLK2	4
17	FOS	3	NRBF2	4	MYC	4
18	NFIL3	3	RYBP	4	ADNP	4
19	CCNL1	3	CCNT2	4	ZNF264	4
20	TIPARP	3	SLC3A2	4	DUSP5	4
21	RORA	2	ZNF274	4	HBEGF	4
22	CLK1	2	BIRC2	4	DUSP6	4
23	MAP3K8	2	DUSP6	4	DDIT4	4
24	SERPINE1	2	PMAIP1	4	SAT1	4
25	ZNF394	2	CHAC1	4	HMGA2	4
26	-	-	SESN2	4	ID1	4
27	-	-	HERPUD1	4	GDF15	4
28	-	-	CEBPB	4	EIF2C2	4
29	-	-	ID2	4	KLF6	4
30	-	-	CLK4	3	RYBP	4
31	-	-	FAM53C	3	-	-
32	-	-	ZNF45	3	-	-

Table 5.7 - **Leading Edge Analysis showing genes that overlap in each gene set for all three cell lines.** The number of subsets these genes appearing in each gene set is shown in the column to the right of the gene. Genes that appear in all three cell lines are shown in red and those that appear in at least two are shown in orange.

The gene expression profiling data provided subtle hints into the mechanism of action of SFA, although efforts to fully mine and validate this dataset are still on-going. The analysis was also frustrated by the absence of a gene set that provided clear mechanistic insight into the biology of SFA. It was suggested that additional gene expression profiling experiments be done with different SFA dose and/or with different treatment periods to further validate and substantiate the findings from this current profiling experiment.

5.2.2 Analysis of SFA gene expression signatures with cmap

To gain further insight into the gene expression signatures from the microarray dataset above, we used cmap to help identify other drugs that may have a common mechanism of action as SFA. Interestingly, the genomic signatures from SFA treated K562 appeared to point to a mechanism of action that is similar to compounds classed as cardiac glycosides (e.g. proscillaridin, digoxin, helveticoside, ouabain, lanatoside C and digitoxigenin) (Table 5.8). Briefly, cardiac glycosides are potent inhibitors of a ubiquitous membrane protein, Na^+/K^+-ATPase[12]. Inhibition of this membrane protein leads to the rise in sodium ion levels in cardiac myocytes, which in turn elevates calcium ion levels and enhances cardiac contractile force[12]. As such, cardiac glycosides have been used to treat heart failures and atrial arrhythmias[12]. While this potentially suggests that SFA could be modulating sodium ion levels by inhibiting Na^+/K^+-ATPase, it is puzzling that was only observed in K562 cells. Moreover, the connection between cellular growth inhibition and the blockade of Na^+/K^+-ATPase remains poorly understood, although it has been recently reported that ouabain induces cell death and impairs K+

homeostasis in glioblastoma cell lines[13]. It would be interesting to see if the genetic knockdown of Na^+/K^+-ATPase α1 subunit would make cells less sensitive to SFA. Inhibitors of protein synthesis (e.g. puromycin and anisomycin) appeared in all three cell lines but this did not provide any meaningful insight into the mechanism of action of SFA, aside from the fact that it could modulate a pathway that inhibits protein synthesis (Table 5.8).

Cell line	Rank	CMAP Name	mean	n	enrichment	p	specificity	percent non-null
K562	1	proscillaridin	0.883	3	0.997	0	0	100
	2	digoxin	0.835	4	0.994	0	0	100
	3	helveticoside	0.806	6	0.994	0	0	100
	4	ouabain	0.833	4	0.991	0	0	100
	5	lanatoside C	0.8	6	0.99	0	0.0046	100
	6	digitoxigenin	0.867	4	0.988	0	0	100
	7	anisomycin	0.738	4	0.974	0	0.0155	100
	8	phenoxybenzamine	0.658	4	0.972	0	0.0891	100
	9	securinine	0.657	4	0.97	0	0	100
	10	puromycin	0.613	4	0.949	0	0.0449	100
Jurkat	1	GW-8510	-0.806	4	-0.999	0	0	100
	2	MG-262	0.86	3	0.996	0	0	100
	3	cephaeline	0.807	5	0.99	0	0.0069	100
	4	emetine	0.822	4	0.985	0	0.007	100
	5	puromycin	0.807	4	0.983	0	0.0169	100
	6	anisomycin	0.85	4	0.983	0	0.0155	100
	7	phenoxybenzamine	0.695	4	0.967	0	0.099	100
	8	parthenolide	0.637	4	0.966	0	0.018	100
	9	15-delta prostaglandin J2	0.528	15	0.651	0	0.0894	73
	10	vorinostat	-0.277	12	-0.625	0	0.2389	50
HeLa	1	mycophenolic acid	-0.662	3	-0.985	0	0	100
	2	anisomycin	0.692	4	0.976	0	0.0155	100
	3	parthenolide	0.524	4	0.959	0	0.024	100
	4	helveticoside	0.578	6	0.955	0	0.0085	100
	5	puromycin	0.564	4	0.946	0	0.0449	100
	6	15-delta prostaglandin J2	0.458	15	0.699	0	0.0447	73
	7	trichostatin A	-0.282	182	-0.485	0	0.198	52
	8	5182598	0.738	2	0.996	2E-05	0.0065	100
	9	MG-262	0.739	3	0.995	2E-05	0.0054	100
	10	withaferin A	0.473	4	0.933	4E-05	0.0368	100

Table 5.8 - cmap analysis showing top 10 compounds for each cell line sharing instances with SFA expression signature

5.3 Using Metabolic Profiling to Determine the Mechanism of Action of SFA

In other unbiased orthogonal approach to understand the mechanism of action of SFA, I undertook the analysis of metabolite profiles in cells treated in the presence or absence of SFA. The motivation was to see if SFA could be exerting its effect through modulating certain metabolic pathways. In addition, our experimental data have suggested that SFA does not act directly on guanosine biosynthesis pathway as it did not inhibit the enzymatic function of IMPDH. Metabolic profiling would help validate this finding, and perhaps offer more insight into the mechanism of action of SFA.

To prepare samples for metabolite profiling, K562 cells were treated with DMSO or 1μM SFA for 0, 12, 24 and 48 hours. Cellular metabolites were extracted with 80% MeOH, dried using a speedvac and stored at -80^{o}C until samples were submitted to Beth Israel Deaconess Medical Center Mass Spectrometry core for processing.

The raw data consisted of peak areas for each detected metabolite. Since the peak area integrated TIC values do not represent absolute concentrations of the metabolites, they had been used only for relative quantification across different sample conditions. Individual peak areas were median normalized to the median of peak areas across all the samples. The fold change for each metabolite that was detected by MS at each treatment time point was computed by obtaining the ratio of SFA versus DMSO treatment data. Metabolite set enrichment analysis (MSEA), an analysis analogous to GSEA, was used to identify important as well as small but coordinated metabolite changes among a group of related metabolites[14].

Tables 5.9 and 5.10 show a list of metabolites that were up and down regulated at specific time points over a 48 hour period respectively (relative those of DMSO

treated cells). The cut off for up/down regulated metabolites was arbitrarily determined to be an increase/decrease of more than 1.5 fold.

Time (hr)	Metabolite	FC	p-value
0	Acetyllysine	1.76	0.053
	trans, trans-farnesyl diphosphate	1.57	0.048
12	riboflavin	2.43	0.025
	N6-Acetyl-L-lysine	1.94	0.009
24	α-ketoglutarate	1.59	0.009
	cytosine	1.58	0.035
48	D-gluconate	6.26	0.003
	hypoxanthine	5.65	0.003
	6-phospho-D-gluconate	4.85	0.013
	guanine	2.70	0.008
	dUMP-nega	2.65	0.004
	inosine	2.50	0.034
	D-sedoheptulose-1-7-phosphate	2.42	0.003
	dephospho-CoA-posi	2.04	0.031
	fructose-1,6-bisphosphate	2.02	0.034
	O8P-O1P	1.95	0.010
	NADH	1.85	0.015
	D-glyceraldehdye-3-phosphate	1.74	0.030
	2-hydroxygluterate	1.59	0.010
	coenzyme A-posi	1.54	0.009
	valine	1.52	0.009
	Phosphorylcholine	1.51	0.014

Table 5.9 - Metabolites that are up regulated upon SFA treatment at indicated time points, FC>1.5

Based off the list of up regulated metabolites, metabolic changes observed in the first 24 hours of SFA treatment were minimal (Table 5.9). After 48 hours, I observed more metabolic changes. When this list of metabolites at 48 hours was subjected to MSEA, I found that pathways involving glucose metabolism (such as pentose phosphate pathway and glycolysis) were being modulated (Figure 5.4). Consistent with

our finding that SFA did not inhibit the enzymatic function of IMPDH2, we did not observe any accumulation of metabolites involved in guanosine biosynthesis (in particular IMP) although in retrospect, metabolite profiling of cells treated with MPA would have been a good positive control experiment.

Time (hr)	Metabolite	FC	p-value
0	N.A		
12	CMP	0.66	0.0126
	Carbamoyl phosphate	0.65	0.0158
	AMP	0.63	0.0192
	CDP-ethanolamine	0.62	0.0209
	UDP-D-glucose	0.62	0.0133
	GMP	0.50	0.0487
	2-oxo-4-methylthiobutanoate	0.43	0.0208
24	2-dehydro-D-gluconate	0.66	0.0171
	4-aminobutyrate	0.58	0.0250
	dAMP	0.58	0.0286
	dTTP-nega	0.56	0.0233
	Carbamoyl phosphate	0.56	0.0051
	dTMP-nega	0.55	0.0370
	CDP-ethanolamine	0.52	0.0010
48	malate	0.65	0.0073
	serine	0.65	0.0104
	aspartate	0.62	0.0018
	fumarate	0.57	0.0261
	pyridoxine	0.57	0.0386
	2-keto-isovalerate	0.56	0.0123
	Maleic acid	0.56	0.0109
	succinate	0.54	0.0118
	Methylmalonic acid	0.53	0.0307
	L-arginino-succinate	0.48	0.0004
	NADP+_posi	0.48	0.0045
	NADP+_nega	0.47	0.0431
	nicotinamide	0.46	0.0234
	glycolate	0.34	0.0002

Table 5.10 - Metabolites that are down regulated upon SFA treatment at indicated time points, FC<0.66

Figure 5.4

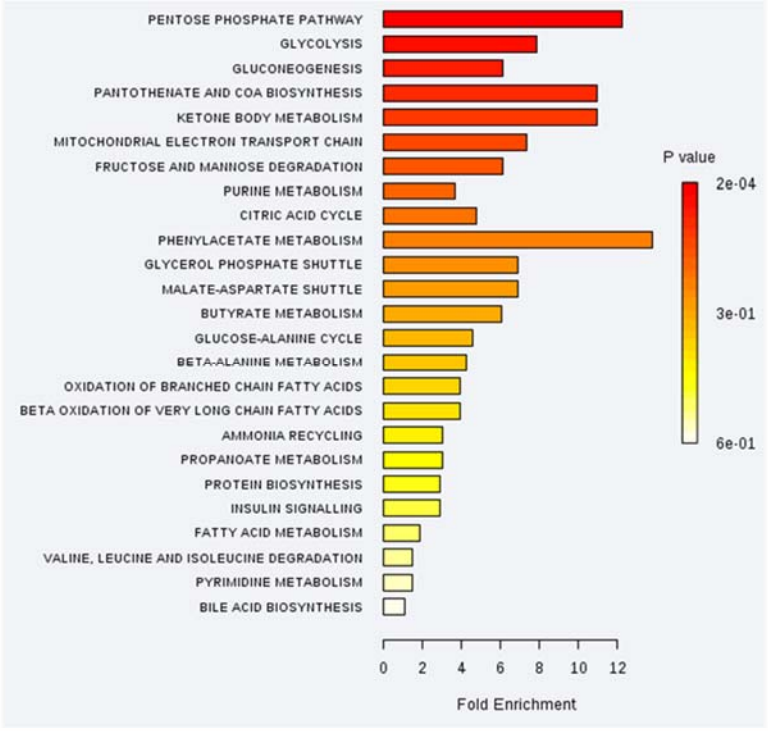

	Metabolite Set	Total	Hits	Expect	P value	Holm P	FDR	Details
	PENTOSE PHOSPHATE PATHWAY	18	4	0.327	1.87E-4	0.015	0.015	View
	GLYCOLYSIS	21	3	0.382	0.00532	0.42	0.204	View
	GLUCONEOGENESIS	27	3	0.491	0.011	0.854	0.204	View
	PANTOTHENATE AND COA BIOSYNTHESIS	10	2	0.182	0.0128	0.984	0.204	View
	KETONE BODY METABOLISM	10	2	0.182	0.0128	0.984	0.204	View
	MITOCHONDRIAL ELECTRON TRANSPORT CHAIN	15	2	0.273	0.0283	1.0	0.377	View
	FRUCTOSE AND MANNOSE DEGRADATION	18	2	0.327	0.0399	1.0	0.435	View
	PURINE METABOLISM	45	3	0.818	0.0435	1.0	0.435	View
	CITRIC ACID CYCLE	23	2	0.418	0.0626	1.0	0.557	View
	PHENYLACETATE METABOLISM	4	1	0.0727	0.0709	1.0	0.567	View
	GLYCEROL PHOSPHATE SHUTTLE	8	1	0.145	0.137	1.0	0.914	View
	MALATE-ASPARTATE SHUTTLE	8	1	0.145	0.137	1.0	0.914	View
	BUTYRATE METABOLISM	9	1	0.164	0.153	1.0	0.941	View
	GLUCOSE-ALANINE CYCLE	12	1	0.218	0.199	1.0	1.0	View
	BETA-ALANINE METABOLISM	13	1	0.236	0.214	1.0	1.0	View
	OXIDATION OF BRANCHED CHAIN FATTY ACIDS	14	1	0.255	0.228	1.0	1.0	View
	BETA OXIDATION OF VERY LONG CHAIN FATTY ACIDS	14	1	0.255	0.228	1.0	1.0	View
	AMMONIA RECYCLING	18	1	0.327	0.284	1.0	1.0	View
	PROPANOATE METABOLISM	18	1	0.327	0.284	1.0	1.0	View
	PROTEIN BIOSYNTHESIS	19	1	0.345	0.297	1.0	1.0	View
	INSULIN SIGNALLING	19	1	0.345	0.297	1.0	1.0	View
	FATTY ACID METABOLISM	29	1	0.527	0.418	1.0	1.0	View
	VALINE, LEUCINE AND ISOLEUCINE DEGRADATION	36	1	0.655	0.491	1.0	1.0	View
	PYRIMIDINE METABOLISM	36	1	0.655	0.491	1.0	1.0	View
	BILE ACID BIOSYNTHESIS	49	1	0.891	0.604	1.0	1.0	View

Figure 5.4 – Metabolite Set Enrichment Analysis of Up Regulated Metabolites Upon SFA Treatment in K562 Cells. Results from MSEA summarizing the matched metabolite sets ranked by their P values at 48hr SFA treatment of K562 cells. Metaboanalyst2.0 was used to perform this analysis (Reference 23).

Interestingly, there were more metabolites that appeared to be down regulated (Table 5.10). Strikingly, carbamoyl phosphate and CDP-ethanolamine were two metabolites that showed consistent, time dependent depletion (12 and 24 hour time point), bolstering our confidence that these metabolite levels could be altered upon SFA treatment (Table 5.10). Carbamoyl phosphate is a metabolic intermediate of the urea cycle as well as one of the substrates utilized in the first committed step in *de novo* pyrimidine biosynthesis. It is catalyzed by carbamoyl phosphate synthetase (CPS) from one molecule of bicarbonate, two molecules of ATP and one molecule of either ammonia or glutamine[15]. In humans, there are two CPS isozymes – CPS I is found primarily in the mitochondria of hepatocytes and is employed by the urea cycle as well as CPSII, a cytosolic enzyme that is involved in de novo pyrimidine synthesis. CDP-ethanolamine is a high energy intermediate involved in phosphatidylethanolamine (PE) synthesis[16]. PEs are phospholipids crucial for membrane architecture and integrity.

MSEA was performed on down regulated metabolites at 48 hour time points (Figure 5.5). Interestingly, I observed that SFA seemed to affect pathways involved in pyrimidine and aspartate metabolism, as well as the urea cycle. Inspection of metabolites down regulated at 48hours indicated other urea cycle metabolites such as L-arginino-succinate, and to some extent urea (p value was slightly above the cut off of 0.05) were down upon SFA treatment (Table 5.10, data not shown). Since not all the urea cycle intermediates (e.g. ornithine, citrulline) were represented, it was difficult to conclude that SFA modulates the urea cycle. It is even more puzzling given the fact that the urea cycle is a metabolic pathway predominant in liver cells. Thus the mechanism connecting urea cycle modulation and cell cycle arrest remains unclear. The depletion

of carbamoyl phosphate suggests that SFA could be modulating some targets upstream of this metabolite and efforts are underway to investigate and confirm this finding. One caveat of interpreting the MSEA data is that the analyses were performed on the 48 hour time point dataset, thus we might have missed the acute effects of the drug. Based on this preliminary metabolomics study, it is safest to assert that SFA, through some unknown mechanism, affects carbamoyl phosphate and CDP-ethanolamine levels.

Figure 5.5

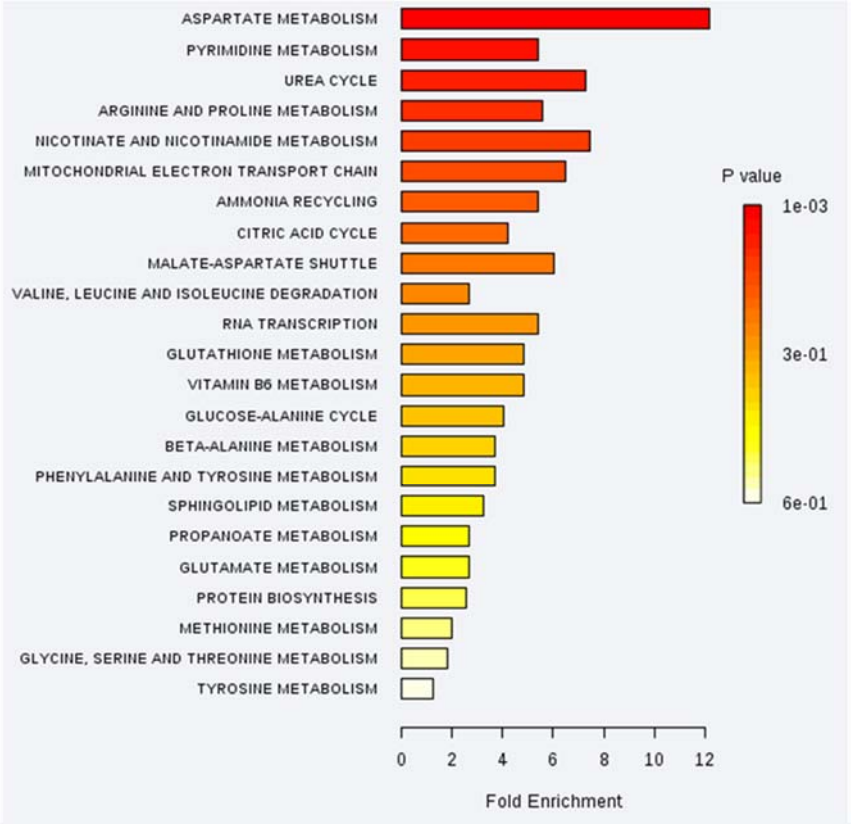

	Metabolite Set	Total	Hits	Expect	P value	Holm P	FDR	Details
	ASPARTATE METABOLISM	12	3	0.247	0.00143	0.114	0.114	View
	PYRIMIDINE METABOLISM	36	4	0.742	0.00485	0.383	0.178	View
	UREA CYCLE	20	3	0.412	0.00668	0.521	0.178	View
	ARGININE AND PROLINE METABOLISM	26	3	0.536	0.0141	1.0	0.282	View
	NICOTINATE AND NICOTINAMIDE METABOLISM	13	2	0.268	0.0273	1.0	0.437	View
	MITOCHONDRIAL ELECTRON TRANSPORT CHAIN	15	2	0.309	0.0359	1.0	0.478	View
	AMMONIA RECYCLING	18	2	0.371	0.0504	1.0	0.576	View
	CITRIC ACID CYCLE	23	2	0.474	0.0784	1.0	0.784	View
	MALATE-ASPARTATE SHUTTLE	8	1	0.165	0.154	1.0	1.0	View
	VALINE, LEUCINE AND ISOLEUCINE DEGRADATION	36	2	0.742	0.167	1.0	1.0	View
	RNA TRANSCRIPTION	9	1	0.185	0.172	1.0	1.0	View
	GLUTATHIONE METABOLISM	10	1	0.206	0.189	1.0	1.0	View
	VITAMIN B6 METABOLISM	10	1	0.206	0.189	1.0	1.0	View
	GLUCOSE-ALANINE CYCLE	12	1	0.247	0.222	1.0	1.0	View
	BETA-ALANINE METABOLISM	13	1	0.268	0.239	1.0	1.0	View
	PHENYLALANINE AND TYROSINE METABOLISM	13	1	0.268	0.239	1.0	1.0	View
	SPHINGOLIPID METABOLISM	15	1	0.309	0.27	1.0	1.0	View
	PROPANOATE METABOLISM	18	1	0.371	0.315	1.0	1.0	View
	GLUTAMATE METABOLISM	18	1	0.371	0.315	1.0	1.0	View
	PROTEIN BIOSYNTHESIS	19	1	0.392	0.33	1.0	1.0	View
	METHIONINE METABOLISM	24	1	0.495	0.398	1.0	1.0	View
	GLYCINE, SERINE AND THREONINE METABOLISM	26	1	0.536	0.423	1.0	1.0	View
	TYROSINE METABOLISM	38	1	0.783	0.555	1.0	1.0	View

Figure 5.5 – Metabolite Set Enrichment Analysis of Down Regulated Metabolites Upon SFA Treatment in K562 Cells. Results from MSEA summarizing the matched metabolite sets ranked by their P values at 48hr SFA treatment of K562 cells. Metaboanalyst2.0 was used to perform this analysis (Reference 23).

5.4 Using Antibody Arrays to Identify Proteins and Pathways Modulated by SFA

Antibody array screening is another unbiased approach to discover key factors and pathways that could be related to a drug's mechanism of action without the need to perform multiple immunoprecipitations and western blots. Toward this end, two different types of antibody arrays were used to identify proteins that could be modulated by SFA – a human phospho-kinase array (R&D Systems) and PathScan Th1/Th2/Th17 cytokine antibody array (Cell Signaling Technologies).

Since many kinases are involved in pathways of cellular proliferation, we first used a Human Phospho-Kinase Array Kit (R&D Systems) as a tool to rapidly and simultaneously detect the relative levels of phosphorylation of a panel of kinase phosphorylation sites. In this assay, capture and control antibodies have been immobilized on nitrocellulose membranes. HCT116 cells were serum starved for 48 hours and pre-treated with SFA or DMSO for 2 hours before restimulation with FBS for 30 minutes. Cells were harvested and the cell lysates obtained from SFA or DMSO treatment were incubated overnight with the membrane array. The membranes were rinsed to eliminate unbound proteins and subsequently incubated with a cocktail of biotinylated detection antibodies that produced a signal proportional to the amount of protein bound at each spot after streptavidin-HRP and chemiluminescent detection reagents were added. There was no observable difference in kinase phosphorylation pattern between the SFA and DMSO treatment arrays (Figure 5.6A).

Figure 5.6

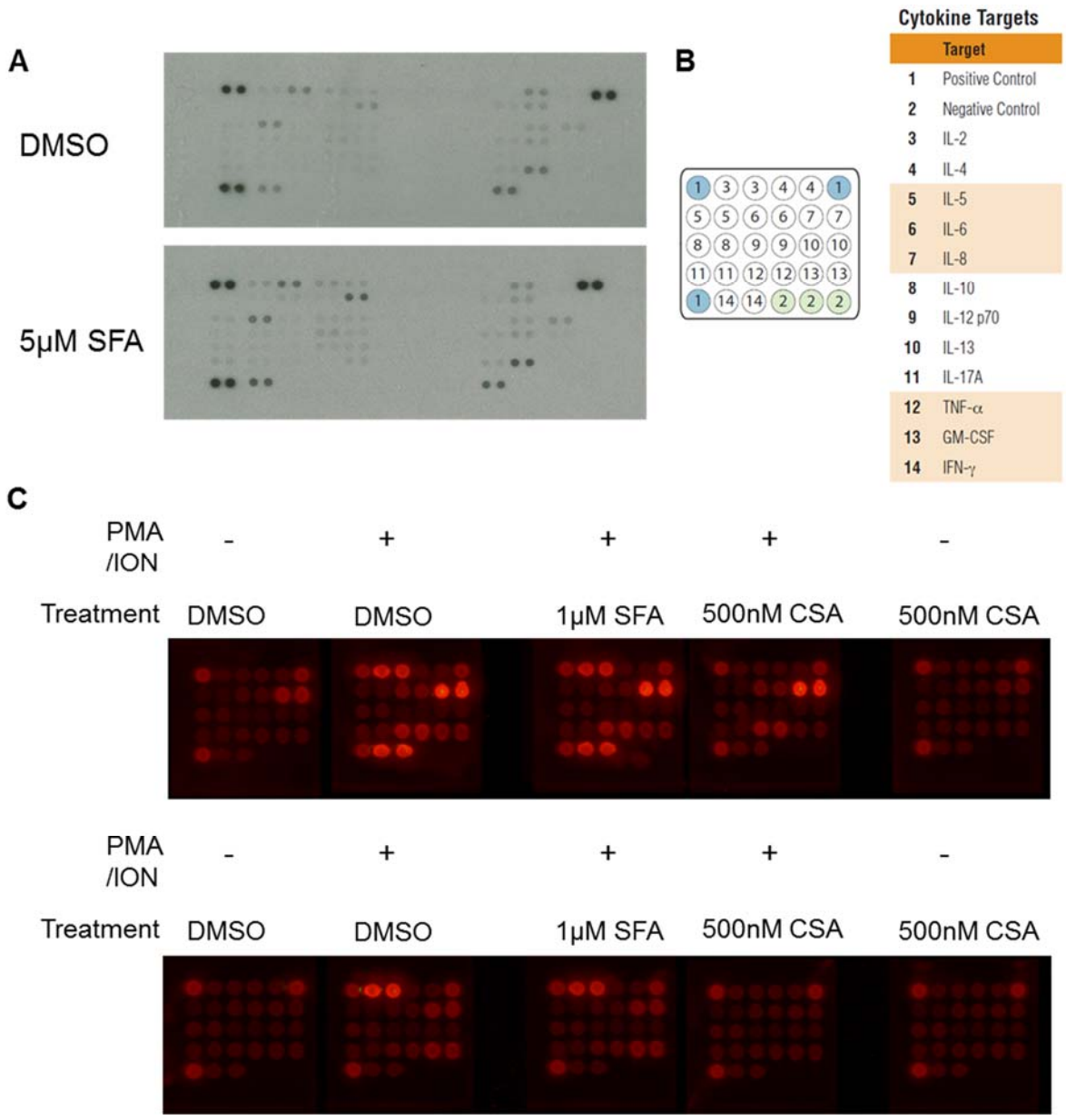

Figure 5.6 – Antibody Arrays to Identify Proteins Modulated by SFA. (A) HCT-116 were serum starved for 2 days, pretreated with 5μM SFA or DMSO and restimulated with FBS for 30 minutes. Cell lysates were collected and analyzed using a human phospho-kinase array kit. The coordinates of the target/control proteins can be found in the Appendix of the instruction manual (Proteome Profiler Array, ARY003B, R&D Systems) (B) Coordinates of the PathScan® Th1/Th2/Th17 cytokine antibody array (Cell Signaling Technologies #13124). Figure adapted from the data sheet of this product. (C) Human (i) PBMCs and (ii) Jurkat cells were stimulated with PMA/ION and co-treated with DMSO, SFA or CSA for 24hrs before supernatant collection. Supernatants were analyzed using the PathScan® Th1/Th2/Th17 cytokine antibody array kit (Cell Signaling Technologies #13124) and images were acquired with LI-COR® Biosciences Odyssey® imaging system.

Going back to study the immunosuppressive origins of SFA, I investigated SFA's effect on cytokine expression in peripheral blood mononuclear cells (PBMCs) and Jurkat cells. For this, I used a cytokine antibody array that allows the simultaneous detection of twelve unique extracellular signaling molecules. Briefly, PBMCs/Jurkats were stimulated with phorbol myristate acetate (PMA) and ionomycin (ION) prior to addition of SFA, DMSO (negative control) and CSA (positive control). The media was collected and centrifuged 24 hours later. The supernatant was diluted and applied to array for overnight incubation. The downstream steps were similar to what was described earlier with the human phospho-kinase array. Cytokines are secreted signaling molecules critical for cell to cell communication, regulating a wide variety of immune response such as inflammation and cellular proliferation. Immunophilin-binding immunosuppressants are known to modulate the production of cytokines in immune cells. CSA inhibits IL-2 production by suppressing IL-2 transcription via the inhibition of calcineurin[17]. SFA has been reported to potently inhibit IL-12p70 production in human dendritic cells and that this effect is exclusive to SFA among other immunophilin-binding immunosuppressants[18]. Stimulation of PBMCs with PMA and ION led to a striking increase in IL-8, IL-2, IFN-γ and to a smaller extent TNF-α (Figure 5.6C, top panel). Addition of CSA to PMA/ION stimulated PBMCs suppressed IL-2 and IFN- γ production whereas SFA did not seem to affect cytokine production in PMA/ION stimulated PBMCs (Figure 5.6C, top panel). A similar result was also observed for PMA/ION stimulated Jurkat cells where only CSA affected IL-2 production (Figure 5.6C, bottom panel).

Although the antibody arrays provided a rapid method for screening proteins that may offer mechanistical clues to distinguish between SFA treated and untreated states,

we did not gain any further insight from this front. For the phospho-kinase screen, factors like duration of drug treatment, serum starvation and stimulation and perhaps cell lines would affect the results immensely since the acute effects of signaling are observed over a very narrow window of time. There could also be other kinase phosphorylation sites that were not represented in the array. This same explanation holds true for the cytokine antibody array. While the cytokine antibody array confirmed CSA's ability to inhibit IL-2 production, there was no new insight into the bioactivity of SFA. Suppression of IL-12 production was neither observed in PBMCs nor in Jurkats as basal expression of IL-12 in these cells was undetectable/low regardless of PMA/ION stimulation. Since dendritic cells are the primary producers of bioactive IL-12, it is possible that SFA's capacity at IL-12 suppression is not observable in the lines we tested[19].

5.5 Conclusions

This chapter examined other hypothesis guided mechanism-of-action studies as well as unbiased approaches toward SFA target identification in the hope to connect the function of the CBS domains of IMPDH2 with the biological effect of SFA. The discovery that dmIMPDH is a transcription factor prompted us to undertake a series of studies to investigate the possibility that PPIA-SFA is inhibiting this moonlighting function of IMPDH2. This transcription factor role of dmIMPDH was found to reside in the CBS domain of this evolutionary conserved enzyme. Notably, we found that the PPIA-SFA engages the CBS domains of IMPDH2. However, we had little success in demonstrating that PPIA-SFA is modulating the DNA binding function of IMPDH2. Gel mobility shift

assays showed that hIMPDH2 binds to ssDNA, but provided no evidence that PPIA-SFA could inhibit IMPDH2-ssDNA interaction. Immunofluoresence experiments showed that hIMPDH2 was largely localized to the cytoplasm regardless of SFA or stress treatment with H_2O_2 in Jurkat cells.

Unbiased approaches with gene expression profiling provided clues that SFA could be modulating the NFκB and GADD45 pathways and efforts are underway to investigate how SFA is affecting these pathways. A more comprehensive analysis of the transcriptome with additional samples (cells treated with multiple doses and time points), preferably with RNA-seq, may offer a more granular insight into the mechanism of action of SFA. cmap analysis of transcriptome signature of K562 cell lines treated with SFA suggested a mechanism of action similar to cardiac glycosides, which are Na^+/K^+-ATPase inhibitors. The lack of consistency in data across the gene expression signature three cell lines from the cmap analysis was concerning, although it is not inconceivable that SFA could have a different mechanism of action in different cell lines. Metabolomics data confirmed that SFA did not impact guanosine biosynthesis although it was difficult to extract additional new insights to the mechanism of action of SFA based on this preliminary metabolic profiling study. Last but not least, antibody arrays tested to date did not yield any new mechanistic insights into the biology of SFA. Moving forward, it could be worthwhile testing antibody arrays of different pathways.

5.6 Concluding Remarks and Future Directions

My doctoral thesis described efforts and progress toward investigating the mechanism of action of macrocyclic natural product Sanglifehrin A. To gain insight into the molecular mechanism of SFA, we enlisted a variety of target identification and validation approaches. For the first time, we demonstrate that IMPDH2 is an intracellular target of PPIA-SFA binary complex. This interaction is highly isoform specific and has been validated by qualitative and quantitative mass spectrometry. We also found through SPR that SFA exhibits an exceptionally high affinity for PPIA with K_d of approximately 0.2nM. This finding challenges the conclusions based off CSA competition experiments – that SFA exerts its effect independent of PPIA, although it remains to be determined if IMPDH2 is the only target. Moreover, whether PPIA is causally involved in SFA's action remains to be discerned. The formation of the ternary complex does not inhibit the dehydrogenase function of IMPDH2 but rather, it modulates cell proliferation through the interaction with the CBS domain of IMPDH2. Through the creation of a series of chimeric IMPDHs, we identified residues I192 and E214 on the CBS domain as necessary for PPIA-SFA interaction. SAR studies with the macrocyclic core of SFA confirmed that while retaining binding to PPIA, this macrocyclic fragment exhibited marked loss in its anti-proliferative effect, and not surprisingly, loss in IMPDH2 engagement. Having brought to light the relationship between PPIA, SFA and IMPDH2, we employed CRISPR/Cas9 system to knockout IMPDH2 in cells. Rescue with a wild-type IMPDH2 construct in IMPDH2 knockout cells restored sensitivity to SFA at 100nM but not with the I192V/E214D double mutant IMPDH2 construct, suggesting that the CBS domain could have a previously unappreciated function in cell proliferation,

and possibly through T-cell signaling although the mechanism by which the CBS domains of IMPDH2 modulate cell growth remains to be elucidated. Unbiased methods we undertook towards understanding the mechanism of action of SFA has not led to much insight.

Nonetheless, our findings present exciting avenues to use SFA as a probe to understand complex biochemical pathways in the cellular milieu. IMPDH2 was found to bind specifically to PPIA-SFA but evidence for PPIA's causal involvement in SFA's action is lacking. The resistance to SFA in PPIA knockout cell lines (by CRISPR) would provide the most compelling evidence for a cyclophilin-dependent model for SFA's action. If a PPIA-dependent model holds true, the next question to address would be whether a dimer of PPIA is essential for mediating the effects of SFA. A PPIA mutant that retains binding to SFA but does not dimerize in the presence of SFA would be essential to address that question. Based on the crystal structure of the PPIA-SFA dimer, we speculate that the mutagenesis of W121 and R148 on PPIA could impair the PPIA-SFA dimer interactions that are mediated by the protein portions of PPIA. In support of a model where the dimeric PPIA-SFA is the biologically active species mediating the effect of SFA, we would expect a PPIA mutant that binds SFA but does not dimerize to exhibit resistance upon SFA treatment when overexpressed in PPIA knockout cell lines. If the effect of SFA turns out to be independent of PPIA, target identification effort by direct immobilization of SFA on a solid support using PPIA-depleted lysates would provide the most straightforward method to identify potential SFA targets. Figure 5.7 outlines the possible mechanism of actions of SFA. To investigate the mechanism of action of SFA from an unbiased standpoint, I propose

performing additional gene expression profiling experiments with multiple SFA dose and/or with different treatment periods. The novel pathways to be uncovered will provide substantial fodder for future study.

Figure 5.7

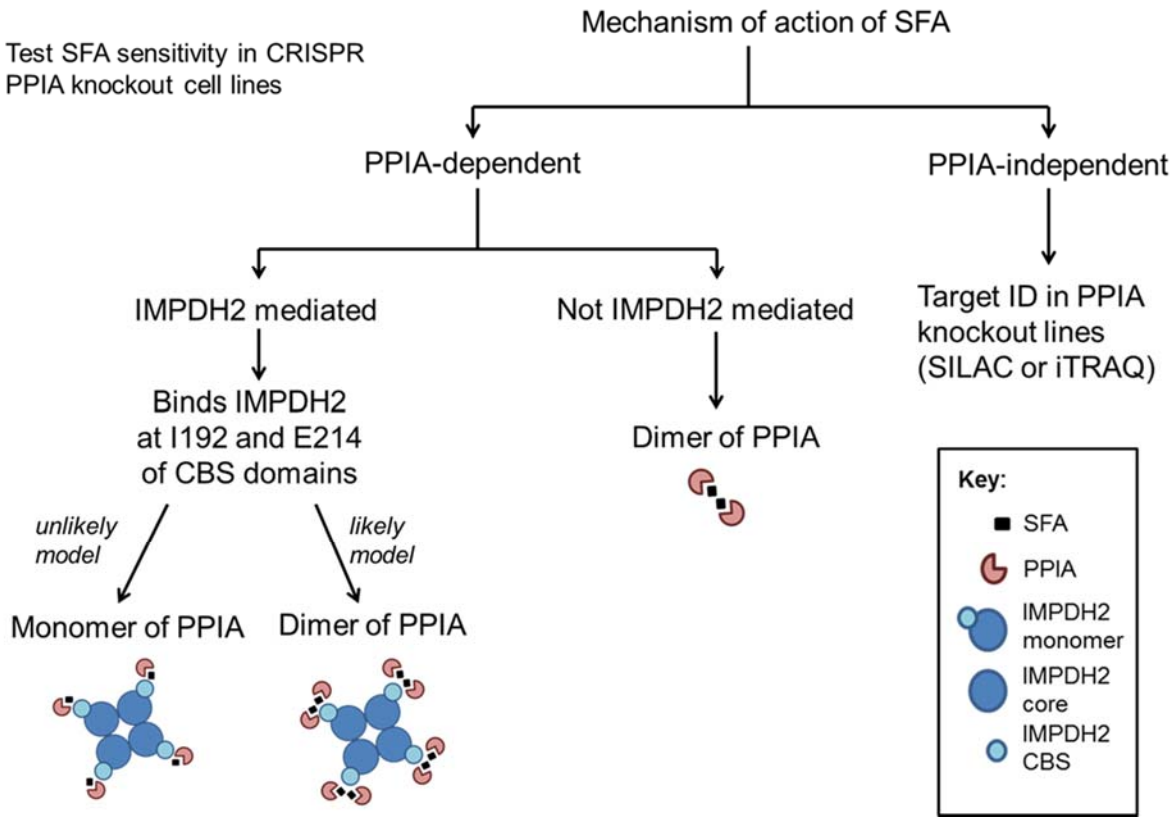

Figure 5.7 – Outline of Possible Mechanisms of Action for SFA.

Macrocyclic natural products have traditionally proven to illuminate fascinating aspects of signaling pathways, and address “undruggable” targets in the clinic. I have faith that by unearthing these powerful class of compounds and exploiting their unique features bestowed by Nature, we will find transformative medicines that can impact the lives of patients with diseases that are at present untreatable.

Experimental Procedures

Gel Mobility Shift Assays

EMSAs were performed using Pierce LightShift® Chemiluminescent EMSA kit. A 6% DNA retardation gel (Life Technologies) was pre-electrophoresed for 90 minutes. Binding reactions (20µl) containing 1x binding buffer, 50ng/µl poly-dIdC, 1nM of biotinylated Mlc2 ssDNA and IMPDH2 were incubated at 4^{o}C for 90 minutes. For IMPDH2 binding to ssDNA, final concentrations of 5µM, 10µM and 15µM were used. For competition EMSA, final concentrations of 15µM IMPDH2, 15µM PPIA and 25µM/250µM SFA (or volume matched DMSO) were used. Binding reactions were resolved by pre-electrophoresed gel at 5mA for 2 hours in the cold room until the bromophenol blue dye has migrated three-quarters down the length of the gel. A nylon membrane (Pierce) was soaked in 0.5x TBE for 10 minutes. The gel, nylon membrane, blotting paper were sandwiched with sponges in an electrophoretic transfer unit (Novex, Life Technologies) filled with 0.5x TBE and transferred at 380mA for 75mins. Transferred DNA on the membrane was crosslinked to the membrane using a hand-held UV lamp equipped with 254nm bulbs for 5 minutes. The membrane was blocked with 20ml blocking buffer and incubated for 15 minutes with gentle shaking followed by another 15 minutes incubation with conjugate/blocking buffer. The membrane was washed 4 times for 5 minutes each in 20ml of 1x wash buffer and rinsed in 30ml of substrate equilibration buffer for 5 minutes with gentle shaking. Substrate working solution was prepared and membrane was allowed to immerse in it for 5 minutes without shaking. The membrane was exposed in a film cassette and developed. Buffers used in this protocol were provided in the LightShift® Chemiluminescent EMSA kit

(Pierce). The oligonucleotides used in this assay were biotinylated at the 5' end (synthesized by Eurofins MWG Operon) with sequences as follows:

Mlc2 (TOP-CT)
– 5' CCCTCTTCCTTGGTCTTCTTCTTCTTAACCTTCTTCTTCT 3'

Mlc2 (BOTTOM-AG)
– 5' AGAAGAAGAAGGTTAAGAAGAAGAAGACCAAGGAAGAGGG 3'

Cell Culture Information

PBMCs (ATCC No. PSC-800-011), human cancer cell lines K562 (a gift from the Saghatelian lab ATCC No. CCL-243) and Jurkat (ATTC No. TIB-152) were cultured in RPMI-1640 medium (Gibco/Life Technologies); HEK-293 cells (ATCC No. CRL-1573), HeLa (ATCC No. CCL-2) and HCT 116 (ATCC No. CCL-243) were maintained in Dulbecco's Modified Eagle Medium (Gibco/Life Technologies). All culture media were supplemented with 10% fetal bovine serum (FBS, Gibco/Life Technologies, Carlsbad, CA, USA), 100 units/mL penicillin and 100 units/mL streptomycin (Gibco/Life Technologies).

Immunofluorescence Experiments

Jurkat cells were grown in 24 well plates, each well containing 5 x 10^5 cells in 450µl media. Cells were treated with a final concentration of 5µM SFA or DMSO 12 hours prior to cell fixation. For stress treatment, H_2O_2 was added 12 hours prior to cell fixation at 1mM. Glass chamber slides (Lab-Tek 4 well glass chamber slides) were coated with an excess of poly-L-lysine (0.01% solution, Sigma-Aldrich) for 10 minutes at room temperature. Poly-L-lysine solution was aspirated and coverslips were allowed to dry completely. After treatment, cells were centrifuged at 400 x *g* for 5 minutes and

resuspended in 200µl PBS. The cell suspension was added to the dried, treated glass chamber slides, incubated at room temperature for 10 minutes before excess cell suspension was aspirated. The chambers were rinsed once with PBS and the chamber surfaces were covered completely by 4% paraformaldehyde solution for 20 minutes. The chambers were washed twice with 400µl of ice cold PBS and incubated with PBS containing 1% Triton X-100 for 10 minutes. Cells were washed in 400µl of 1x PBS thrice for 5 minutes. The coverslips were placed cells-side-up in a petri dish and rinsed once with PBS + 0.1% Triton X-100 (PBS-T). Cells were covered with 400µl blocking buffer (NGS-PBS-T; 10% Goat serum (Sigma-Aldrich), 0.1% Triton-X100, 0.05% Tween-20 in PBS) for 2 hours at room temperature. After blocking, cells were incubated (or co-incubated) with either anti-IMPDH2 (Abcam Ab129165, 1:250) or anti-PPIA antibodies (Abcam Ab58144, 1µg/ml) in NGS-PBS-T overnight at 4^{o}C. Cells were washed with PBS-T three times for 5 minutes each wash, incubated with secondary antibodies (Alexa Fluor 594 Goat Anti-mouse IgG and Alexa Fluor 488 Goat Anti-rabbit IgG, 5µg/ml) in NGS-PBS-T for 1 hour at room temperature, washed three times with PBST and sealed with Vectashield mounting medium with DAPI (Vector Laboratories, #H-1500). Images were taken with the MS-18 Olympus FV300 Laser Scanning Confocal at Harvard's LISE building G04.

RNA isolation and RT-qPCR

Total RNA was purified from cell lines using the Aurum Total RNA Mini Kit (Biorad) and normalized with nuclease-free water for reverse transcription. For qPCR analysis, 2ug of total RNA was reverse transcribed into cDNA using iScript Advanced cDNA Synthesis Kit (Biorad). qPCR analysis was then performed using Taqman probes (Life Technologies, see table below), Taqman Gene Expression Master Mix (Applied Biosystems/Life Technologies) and CFX Connect Real-Time PCR Detection instrument (Biorad) in accordance to the manufacturer's protocol. Each target was run in triplicate using 12.5ng of cDNA template per 10µl PCR reaction, and expression levels were normalized to human hypoxanthine-guanine phosphoribosyltransferase (HPRT) or glyceraldehyde 3-phosphate dehydrogenase (GAPDH).

Target	Taqman Probe ID
GAPDH	Hs02758991_g1
HPRT	Hs02800695_m1
E2F1	Hs00153451_m1
RB	Hs01078066_m1

Microarray

Cultured HeLa cells (~3 x 10^5 cells in 2ml complete media) were seeded in 6 well plates and incubated overnight. K562 and Jurkat cells (~1 x 10^6 cells in 2ml complete media) were seeded in 6 well plates. Cells were treated with 1µM SFA/DMSO for 16 hours. Total RNA was purified from cell lines using the RNeasy Mini Kit (Qiagen) following the manufacturer's protocol. RNA was eluted with 35µl RNase free water (Life Technologies)

and quantitated using Nanodrop (ThermoScientific). mRNA samples were submitted to the Microarray Core Facility at Dana Farber Cancer Institute where the samples were examined for degradation by a bioanalyzer (Agilent 2100) and processed on a 3' IVT HG-U133 plus 2.0 Affymetrix array. The data was analyzed on the software, GenePattern and Connectivity Map (Broad Institute).

Targeted liquid-chromatography mass spectrometry (LC/MS/MS)

LC/MS/MS based metabolomics analysis was performed according to previous published methods[20,21]. 3.75 x 10^5 K562 cells were seeded in each well of a 6 well plate and treated with 1μM SFA or DMSO for 0, 12, 24 or 48 hours. Cells were harvested after treatment by centrifuging at 750 x *g* for 5 minutes at room temperature. The media was removed and metabolites were extracted in 80% (v/v) methanol at -80^{o}C. Cells were gently vortexed and incubated in the -80^{o}C freezer for 30 minutes. Insoluble material in lysates was centrifuged at 14,000 x *g* for 15 minutes and the resulting supernatant was evaporated using a refrigerated speed vac. Samples were submitted to Beth Israel Deaconess Medical Center Mass Spectrometry core for LC/MS/MS. Samples were resuspended using 20 μL LC/MS grade water. 10 μL was injected and analyzed using a 5500 QTRAP triple quadrupole mass spectrometer (AB/SCIEX) coupled to a Prominence HPLC system (Shimadzu) using selected reaction monitoring (SRM) of a total of 292 endogenous water soluble metabolites for analyses of samples. Some metabolites were targeted in both the positive and negative ion mode for a total of 292 SRM transitions. ESI voltage was +5,000 V in the positive ion mode and −4,500 V in the negative ion mode using positive/negative switching. The dwell time was 4ms per

SRM transition, and the total cycle time was 1.82 sec producing 9-12 data points per metabolite peak. Samples were delivered to the MS using hydrophilic interaction chromatography (HILIC) using a 3.6 mm internal diameter × 10 cm Amide XBridge column (Waters) at 300 µL/min. Mobile phase gradients were run starting from 85% buffer B (LC/MS grade acetonitrile) to 35% buffer B from 0–3 min; 35% buffer B to 0% buffer B from 3–12 min; 0% buffer B held from 12–17 min; 0% buffer B to 85% buffer B from 17–18 min; and 85% B held for 7 min to re-equilibrate the column. Buffer A was comprised of 20 mM ammonium hydroxide and 20 mM ammonium acetate in 95:5 water:acetonitrile (pH=9.0). Peak areas from the total ion current for each metabolite SRM transition were integrated using MultiQuant v2.0 software (AB/SCIEX). MSEA was performed using MetaboAnalyst2.0[22,23].

Antibody Arrays

Human phospho-kinase array (R&D Systems)

Approximately 80% confluent HCT 116 cells, grown in 6 well plates, were serum-starved for 48hrs with media containing 0.1% FBS. After serum starvation, cells were treated with DMSO/5µM SFA for 2 hours and stimulated with complete media (10% FBS) for 30 minutes. Lysate samples were prepared for array analysis in accordance to manufacturer's instructions. Chemiluminescence intensities were detected using a ChemiDoc™ XRS+ imaging system (Bio-Rad) with Image Lab™ software (Bio-Rad).

PathScan Th1/Th2/Th17 cytokine antibody array (Cell Signaling Technologies #13214).

PBMCs were thawed according to manufacturer's protocol. 1.5 x 10^6 Jurkat and PBMCs were seeded in each well of a 6-well plate in 2ml complete RPMI media. For positive

control cytokine stimulation, cells were treated with 750 ng/ml ION (Sigma-Aldrich) and 25 ng/ml PMA (Sigma-Aldrich) at final concentration. SFA and CSA were added at 1μM and 500nM, with volume matched DMSO as a negative control. Cells were incubated for 24 hours before the supernatants were collected and analyzed on a cytokine antibody array (Cell Signaling Technologies) in accordance to the manufacturer's protocol. The images of the arrays were acquired using LI-COR® Biosciences Odyssey® imaging system.

References

1. Kozhevnikova, E. N. *et al.* Metabolic enzyme IMPDH is also a transcription factor regulated by cellular state. *Mol. Cell* **47,** 133–9 (2012).

2. Dimova, D. K. & Dyson, N. J. The E2F transcriptional network: old acquaintances with new faces. *Oncogene* **24,** 2810–2826 (2005).

3. McLean, J. E. *et al.* Inosine 5'-monophosphate dehydrogenase binds nucleic acids in vitro and in vivo. *Biochem. J.* **379,** 243–51 (2004).

4. Mortimer, S. E. *et al.* IMP dehydrogenase type 1 associates with polyribosomes translating rhodopsin mRNA. *J. Biol. Chem.* **283,** 36354–36360 (2008).

5. Biswas, A. K. & Johnson, D. G. Transcriptional and nontranscriptional functions of E2F1 in response to DNA damage. *Cancer Res.* **72,** 13–17 (2012).

6. DeGregori, J. & Johnson, D. G. Distinct and Overlapping Roles for E2F Family Members in Transcription, Proliferation and Apoptosis. *Curr. Mol. Med.* **6,** 739–748 (2006).

7. Zhu, J. W. *et al.* E2F1 and E2F2 determine thresholds for antigen-induced T-cell proliferation and suppress tumorigenesis. *Mol. Cell. Biol.* **21,** 8547–8564 (2001).

8. Subramanian, A., Tamayo, P., Mootha, V. K., Mukherjee, S. & Ebert, B. L. Gene set enrichment analysis : A knowledge-based approach for interpreting genome-wide. *Proc Natl Acad Sci U S A* **102,** 15545–15550 (2005).

9. Palchaudhuri, R. & Hergenrother, P. J. Transcript Profiling and RNA Interference as Tools To Identify Small Molecule Mechanisms and Therapeutic Potential. *ACS Chem. Biol.* **6,** 21–33 (2011).

10. Lamb, J. *et al.* The Connectivity Map : Using Gene-Expression Signatures to Connect Small Molecules, Genes, and Disease. *Science (80-.).* **313,** 1929–1935 (2006).

11. Zhang, L. H., Youn, H. D. & Liu, J. O. Inhibition of cell cycle progression by the novel cyclophilin ligand sanglifehrin A is mediated through the NFkappa B-dependent activation of p53. *J. Biol. Chem.* **276,** 43534–40 (2001).

12. Prassas, I. & Diamandis, E. P. Novel therapeutic applications of cardiac glycosides. *Nat. Rev. Drug Discov.* **7,** 926–935 (2008).

13. Chen, D., Song, M., Mohamad, O. & Yu, S. Inhibition of Na+/K+-ATPase induces hybrid cell death and enhanced sensitivity to chemotherapy in human glioblastoma cells. *BMC Cancer* **14,** 716 (2014).

14. Xia, J. & Wishart, D. S. Web-based inference of biological patterns, functions and pathways from metabolomic data using MetaboAnalyst. *Nat. Protoc.* **6,** 743–760 (2011).

15. Holden, H. M., Thoden, J. B. & Raushel, F. M. Carbamoyl phosphate synthetase: An amazing biochemical odyssey from substrate to product. *Cell. Mol. Life Sci.* **56,** 507–522 (1999).

16. Gibellini, F. & Smith, T. K. The Kennedy pathway-de novo synthesis of phosphatidylethanolamine and phosphatidylcholine. *IUBMB Life* **62,** 414–428 (2010).

17. Schreiber, S. L. & Crabtree, G. R. The mechanism of action of cyclosporin A and FK506. *Immunol. Today* **13,** 136–142 (1992).

18. Steinschulte, C., Taner, T., Thomson, a. W., Bein, G. & Hackstein, H. Sanglifehrin A, a Novel Cyclophilin-Binding Immunosuppressant Blocks Bioactive IL-12 Production by Human Dendritic Cells. *J. Immunol.* **171,** 542–546 (2003).

19. Banchereau, J. *et al.* Immunobiology of Dendritic Cells. *Annu. Rev. Immunol.* **18,** 767–811 (2000).

20. Locasale, J. W. *et al.* Phosphoglycerate dehydrogenase diverts glycolytic flux and contributes to oncogenesis. *Nat. Genet.* **43,** 869–874 (2011).

21. Shyh-Chang, N. *et al.* Influence of Threonine Metabolism on S-Adenosylmethionine and Histone Methylation. *Science .* (2012). doi:10.1126/science.1226603

22. Xia, J., Psychogios, N., Young, N. & Wishart, D. S. MetaboAnalyst: A web server for metabolomic data analysis and interpretation. *Nucleic Acids Res.* **37,** 652–660 (2009).

23. Xia, J., Mandal, R., Sinelnikov, I. V., Broadhurst, D. & Wishart, D. S. MetaboAnalyst 2.0-a comprehensive server for metabolomic data analysis. *Nucleic Acids Res.* **40,** 1–7 (2012).